EXPRESSION AND FUNCTION OF THE ATYPICAL CHEMOKINE RECEPTOR CCRL1 IN THE THYMUS

by

Beth Lucas

A thesis submitted to
The University of Birmingham
for the degree of
DOCTOR OF PHILOSOPHY

School of Immunity and Infection
College of Medical and Dental Sciences
The University of Birmingham
August 2014

ACKNOWLEDGEMENTS

I would firstly like to thank both of my supervisors, Antal Rot and Graham Anderson, for their inspiration, guidance and enthusiasm throughout the four years of this PhD. It was Graham who introduced me to the world of thymus research during my second year of undergraduate studies, and this experience motivated me to pursue my interests and embark upon a PhD project in this area.

I can honestly say, that through all the ups and downs, scientific and otherwise, I have never regretted the decision to undertake this PhD. This is almost entirely due to the friends I have made, and the people I have had the pleasure of meeting along the way. Such people include members of the Rot lab, especially Poonam Kelay for welcoming me into the group and being a great friend throughout, and Maria Ulvmar, for always offering detailed scientific help and advice whenever needed. I can certainly say that all members of the Anderson group, particularly Andrea White, have made for a fantastic workplace, not only by their readiness to offer help and lend reagents, but also by their readiness to have a cuppa or go for after-work drinks!

I would like to thank the friends I have made on the fourth floor of the IBR, especially Sarah Cook, who have made the last few years so enjoyable.

Thank you to my family, especially my mom, who has always supported me, especially during the not-so-good days of this PhD! Also, my partner Hayden, for being encouraging and patient with me whilst writing this thesis, and for talking science with me whenever I've needed to get ideas straight.

Completing my PhD has been an immensely rewarding experience, so thank you everybody!

ABSTRACT

Thymus colonisation and thymocyte positioning are mediated by interactions involving CCR7 and CCR9 and their respective ligands CCL19/CCL21 and CCL25. These chemokines also interact with the atypical receptor CCRL1, which is expressed in the thymus and has recently been reported to play an important role in normal abT-cell development. Our study has mapped CCRL1 expression within the adult and embryonic thymus, and shows that CCRL1 is expressed within the thymic cortex, at the subcapsular zone, and surrounding vessels at the corticomedullary junction. We have used flow cytometry to show CCRL1 expression predominantly by cortical thymic epithelial cells, but also by a small population of medullary thymic epithelial cells and by a subset of mesenchymal cells. We show, using CCRL1 deficient mice, that CCRL1 suppresses thymocyte progenitor entry into the thymus, and influences the intrathymic positioning of double negative thymocytes. Nevertheless, we have shown that CCRL1$^{-/-}$ mice have no major perturbations in T-cell populations at different stages of thymic differentiation and development. Overall, this study characterises the expression of CCRL1 in key thymic microenvironments, but argues against a major role for CCRL1 in normal thymus development and function.

TABLE OF CONTENTS

TABLE OF FIGURES

TABLE OF TABLES

LIST OF ABBREVIATIONS

Aire	autoimmune regulator
APC	allophycocyanin (flow cytometry)
APC	antigen presenting cell
APECED	autoimmune polyendocrinopathy-candidiasis-ectodermal dystrophy
BCA	bicinchoninic acid
BCR	B cell receptor
BM	bone marrow
BSA	bovine serum albumin
CCL	CC-chemokine ligand
CCR	CC-chemokine receptor
CCX-CKR	Chemocentryx chemokine receptor
CD	cluster of differentiation
cDC	conventional dendritic cell
cDNA	complementary DNA
CLP	common lymphoid progenitor
CMJ	corticomedullary junction
COOH	carboxyl
cTEC	cortical thymic epithelial cell
CX3CL	CX3C-chemokine ligand
CX3CR	CX3C-chemokine
CXCL	CXC-chemokine ligand
CXCR	CXC-chemokine receptor

Cy	Cyanine
DAPI	4,6-diamidino-2-phenylindole
DARC	Duffy antigen receptor for chemokines
DC	dendritic cell
DKO	double knockout
DMEM	Dulbecco's Modified Eagle Medium
DMSO	Dimethyl sulfoxide
DN	double negative
DNA	deoxyribonucleic acid
DP	double positive
E	embryonic day
EDTA	ethylenediaminetetraacetic acid
ELISA	enzyme-linked immunosorbent assay
EpCAM-1	epithelial cell adhesion molecule 1
ER	endoplasmic reticulum
ETP	early thymic progenitors
FACS	fluorescence activated cell sorting
FCS	fetal calf serum
FITC	fluorescein isothiocyanate
Foxp3	forkhead box P3
FSC	forward scatter
GAG	glycosaminoglycan
GDP	guanosine diphosphate
GFP	green fluorescent protein

Gp38	glycoprotein 38
GTP	guanosine triphosphate
Het	heterozygous
HEV	high endothelial venule
Hi	high
HSA	heat stable antigen
HSC	haematopoietic stem cell
ICAM-1	intercellular adhesion molecule-1
ICAM-2	intercellular adhesion molecule-2
Ig	immunoglobulin
iLN	inguinal lymph node
iSP	immature single positive
Int	intermediate
iNKT	invariant natural killer T cell
KAR	killer activatory receptor
kD	kilodaltons
KIR	killer inhibitory receptor
KO	knockout
Lin	lineage
LN	lymph node
Lo	low
LPS	lipopolysaccharide
MACS	magnetically activated cell sorter
MAdCAM	mucosal vascular addressin cell adhesion molecule

MBL	mannose binding lectin
MHC	major histocompatibility complex
mTEC	medullary thymic epithelial cell
mRNA	messenger RNA
NC	neural crest
NH_2	amino
NK	natural killer
PAMPS	Pathogen Associated Molecular Patterns
PBS	phosphate buffered saline
PCR	polymerase chain reaction
pDC	plasmacytoid dendritic cell
PDGFR	platelet derived growth factor receptor
PE	phycoerythrin
PI3K	phosphatidylinositol-3 kinase
PIP3	phosphatidylinositol-3,4,5-trisphosphate
plt	paucity of lymph node T cells
PNAd	peripheral-node addressins
PRR	pattern recognition receptor
Rag-1	Recombination – activating gene-1
Rag2	Recombination – activating gene-2
RANK	receptor activator NF-κB
RANKL	RANK ligand
RNA	ribonucleic acid
RPMI	Roswell Park Memorial Institute-1640 medium

RTE	recent thymic emigrant
RT-PCR	reverse transcriptase polymerase chain reaction
SCZ	subcapsular zone
SEM	standard error of the mean
SMA	smooth muscle actin
SP	single positive
SSC	side scatter
TCR	T cell receptor
TEC	thymic epithelial cell
Tep	thymic epithelial cell line
tDC	thymic dendritic cell
tFRC	thymic fibroblastic reticular cell
Tg	transgenic
TLR	Toll like receptor
Treg	Regulatory T cell
VCAM	vascular cell adhesion molecule 1
WT	wildtype
XCL	XC-chemokine ligand
XCR	XC-chemokine receptor

CHAPTER 1: GENERAL INTRODUCTION

1.1 The Immune System

The immune system is a complex network of cells and molecules, each with specialised roles for protection against infection and disease. Physical barriers such as the skin and mucosal membranes provide the initial defence against infection, and reflexes such as sneezing and coughing prevent microbial pathogens from adhering to host tissue – a vital process if a pathogen is to colonise the host. In addition, the immune system has developed to provide two fundamentally different responses, which come into play if the initial defences are compromised: the innate and adaptive immune system.

1.1.1 The Innate Immune System

The innate immune system acts immediately once barrier defence mechanisms are breached. It exists to provide early defence, and to alert the adaptive immune system of danger. A defining feature of the innate system is a consistent and rapid response irrespective of previous exposure to the infective agent (Delves and Roitt, 2000). The innate immune response involves the recognition of conserved features of pathogens. These conserved features are known as Pathogen Associated Molecular Patterns (PAMPs) e.g. liposaccharide, a component of gram-negative bacteria. Pattern Recognition Receptors (PRRs) are widely expressed by leukocytes and recognise such PAMPs. Recognition of PAMPs by PRRs allows the innate immune system to distinguish between self and non-self (Medzhitov and Janeway, 2000). Toll like receptors (TLRs) are a class of PRRs and interaction of TLRs with their cognate ligands activates an intracellular signalling cascade leading to the

release of inflammatory cytokines and chemokines (Basset et al., 2003, Kumar et al., 2009).

Ligation of PRRs expressed by macrophages leads to their activation. This causes the release of inflammatory mediators which are responsible for vasodilation and the recruitment of neutrophils and monocytes from the circulation into the tissue (Galli et al., 2011). This rapid influx of cells is known as inflammation and is characterised by the four Latin words *calor, dolor, rubor*, and *tumor* (heat, pain, redness, and swelling).

In addition, macrophages express Fc and complement receptors; this allows phagocytosis of cells that are coated in antibody or complement. The function of complement includes the release of inflammatory mediators, pathogen opsonisation and removal by phagocytes, and the formation of the Membrane Attack Complex, which assembles to form a membrane-spanning pore, thus killing the pathogen (Basset et al., 2003).

1.1.2 The Adaptive Immune System

Typically the adaptive immune response takes several days to develop but has two striking advantages over the innate immune response. Firstly, when a pathogen is encountered by the adaptive immune system, immunological memory is generated, which allows the generation of a faster response should the pathogen be re-encountered. Secondly, the adaptive response is much more specific than the innate response due to the vast repertoire of receptors expressed by cells of the

adaptive immune system. As with the innate immune system, the adaptive immune system is comprised of a variety of cell types that are generated from haematopoietic stem cells (HSCs) in the bone marrow (Delves and Roitt, 2000).

1.1.3 Haematopoiesis

HSCs are self-renewing cells responsible for the long-term generation of all blood-cell lineages. HSCs comprise approximately 0.01% of nucleated cells in the bone marrow (BM) and express Thy 1, c-Kit and Sca-1 and lack expression of the lineage committed markers B220, Gr-1, Ter119, CD3, CD4, CD5, CD8 and CD11b (Rolink et al., 2006). HSCs give rise to multipotent progenitors (MPPs), which are not capable of self-renewal, but have full lineage differentiation potential. MPPs further differentiate into either lymphoid primed multipotent progenitor cells (LPMPs), or common myeloid progenitors (CMPs). LPMPs become common lymphoid progenitors (CLPs) and give rise to lymphocytes and NK cells. CMPs produce granulocyte-monocyte progenitors and megakaryocyte-erythrocyte progenitors and form cells of the myeloid lineage, as well as erythrocytes and platelets (Cedar and Bergman, 2011).

1.1.4 Antigen Presentation to T cells

The adaptive immune response is generated most effectively by professional antigen presenting cells (APCs) such as dendritic cells (DCs). Immature DCs continually sample the environment in peripheral tissues, and preferentially home to sites of inflammation due to secretion of inflammatory chemokines during an innate

immune response. Once a ‘danger signal’ is encountered, either in the form of damaged self or PAMPs, DCs mature to become professional APCs (Delves and Roitt, 2000). DC maturation is characterised by the upregulation of the costimulatory molecules CD80 and CD86. Once in this form, DCs migrate to secondary lymphoid tissue where they present antigen to T cells via major-histocompatibility-complex (MHC) molecules. There are two main classes of MHC molecules: class I and class II. The mechanism by which the antigen is processed and presented is different for each class of MHC molecule.

1.1.5 Antigen Presentation via MHC Class I

MHC class I (MHC-I) is expressed by almost all nucleated cells and is responsible for the presentation of endogenously derived peptides. Firstly, endogenous cytosolic proteins are converted to short peptides by the proteasome. These peptides are then transported to the endoplasmic reticulum (ER) where they form complexes with MHC-I with help from a ‘loading complex’. Once assembled, the peptide-MHC complex is transported from the ER to the cell membrane (Blum et al., 2013). Although MHC-I is usually expressed on all nucleated cells, exceptions include some virally infected cells or cells that have undergone malignant transformation. Cytotoxic CD8 T cells recognise peptides in association with MHC-I molecules via their T cell receptor (Delves and Roitt, 2000). In addition to T cells, NK cells recognise MHC-I by their killer inhibitory receptors (KIR). NK cells also express killer activating receptors (KAR), which bind to stress-related molecules e.g. MICA. If the KAR is engaged, the NK cell will kill the target cell, however, this signal can be overridden by the inhibitory signal produced when the KIR bind MHC-I. This proves

very useful in eliminating abnormal cells that have down regulated MHC-I expression, for example tumour cells (Delves and Roitt, 2000).

1.1.6 Antigen Presentation via MHC class II

MHC class II (MHC-II) molecules present peptides derived from exogenous proteins, and their expression is a unique feature of professional APCs. Antigens are internalised by endocytosis and are transported to the MHC-II compartment where they are processed by cathepsins and loaded onto MHC-II molecules. The assembled complex is exported to the cell membrane, where CD4 T cells are able to recognise the bound peptides (Blum et al., 2013).

1.1.7 CD4 T Cells

1.1.7.1 Conventional CD4 T cells

CD4 T cells are largely cytokine-secreting helper cells, and the type of cytokine secreted by these cells allows them to be categorised into different conventional T helper (Th) subsets. Th1 cells secrete cytokine including IL-2 and IFNγ, whereas Th2 cells secrete cytokine including IL-4, 5, 6 and 10 but not IL-2 or IFNγ. The production of cytokine by Th1 cells facilitates cell-mediated immunity by the activation of macrophages and antigen-specific cytotoxic CD8 T cells, whereas Th2 cells primarily help B cells to produce antibody (Zhou et al., 2009). Additional subsets of CD4 T cells exist, for example Th17 cells, which secrete IL-17, IL-17F, IL-21, IL-6 and IL-23. Th17 cells have been implicated in autoimmune disease such as rheumatoid arthritis and psoriasis (Korn et al., 2009).

1.1.7.2 Regulatory T cells

In addition to conventional Th cells, a subset of regulatory T (Treg) cells exist. Treg are characterised by their expression of the transcription factor Forkhead Box P3 (Foxp3), and can develop in the thymus (natural, nTreg), or in the periphery (inducible, iTreg). Generation of nTreg in the thymus is thought to require high avidity TCR engagement during CD4 T cell development (Bensinger et al., 2001), while peripheral iTreg are generated from activated conventional CD4 T cells, favoured by stimulation with IL-2 and TGF-β, in the absence of IL-6 (Bettelli et al., 2006, Curotto de Lafaille and Lafaille, 2009). The activation of Treg occurs in an antigen-specific manner, however once activated they can supress T cells bearing different specificities (Thornton and Shevach, 2000). The regulatory mechanisms used by Treg include the secretion of inhibitory cytokines, such as IL-10, IL-35 and TGF- β. In addition, Tregs can interact with APCs, which in turn reduces subsequent interactions between the APC and conventional T cells. (Tang and Bluestone, 2008). Another proposed regulatory mechanism of Treg is the release of granzyme B and perforin to induce direct killing, although this has only been shown *in vitro* (Grossman et al., 2004).

1.1.8 CD8 T Cells

CD8 T cells directly kill virally infected cells. This is achieved through the presentation of viral peptide in the context of MHC-I and the subsequent binding of specific CD8 T cells. Once bound, CD8 T cells release pore-forming perforin, which allows granzyme to enter and induce apoptosis in the target cell. In addition, Fas ligand expressed by CD8 T cells is able to ligate Fas molecules expressed by the target cell; this activates intracellular caspases and induces apoptosis. Like CD4 T cells, CD8 T cells also produce cytokines, including TNFα and IFNγ, which activate macrophages and recruit them to the site of inflammation (Zhang and Bevan, 2011).

1.1.9 The T Cell Receptor (TCR)

The TCR is vital for the activation of T cells. The majority of T cells express αβ TCR, however a small population express γδ chains instead. The α and β chains of the TCR are comprised of a constant and variable region, which are spliced together during T cell development in the thymus. The variable region undergoes gene rearrangement and produces a diverse array of TCRs with different specificities. The variable region of the α chain consists of variable (V), and junctional (J) gene segments, whereas the β chain consists of diversity (D), in addition to V and J (Turner et al., 2006).

Very few T cells are specific for a given antigen, however they are capable of producing 10^{15} TCR variable regions. This is achieved by a recombination process, which modifies the variable-region genes by cutting and pasting the gene segments using nucleases and ligases. This process is subject to splicing inaccuracies, which

also increase diversity (Nemazee, 2006). In addition, the enzyme ‘terminal deoxyribonucleotidyltransferase’ adds additional nucleotides before ligation, thereby increasing diversity further (Cabaniols et al., 2001). Recombination–activating genes (*Rag-1* and *Rag-2*) encode two of the enzymes involved in this process, and defects in these genes results in immunodeficiency due to the lack of mature lymphocytes with functional TCRs (Schwarz et al., 1996, Mombaerts et al., 1992).

TCR-peptide-MHC interaction results in clonal selection and expansion of the activated T cell, thereby mounting a specific immune response. Most immune responses involve several clones (and are therefore termed polyclonal), because even simple antigens will bear many epitopes. Although the TCR can distinguish between similar antigens, molecular mimicry can occur. This is when an antigen receptor, such as the TCR, recognises unrelated antigens due to an identical epitope, or an epitope of similar shape or charge being presented. Autoimmune disease, for example psoriatic arthritis can be an outcome of such phenomenon (Cusick et al., 2012).

1.2 Chemokines

Chemokines are small proteins (8-12kDa) required for the directional movement of cells between and within tissues. They have a variety of roles in the immune system including immune organ development, response to infection and wound healing. The majority of chemokines are secreted from the cell with the exception of CX3CL1 and CXCL16, which are tethered to the extracellular surface by mucin-like stalks. Although these chemokines are tethered, they can be cleaved by proteases allowing them to behave like other soluble chemokines (Allen et al., 2007). The tertiary structure of chemokines are similar, however their amino acid sequence can vary considerably. In addition to the structural classification (discussed below), chemokines can also be categorised based on their functional properties. 'Inflammatory chemokines' are those upregulated during an inflammatory response to allow the recruitment of cells to areas of pathological insult. On the other hand, 'homeostatic chemokines' are constitutively expressed to allow the homeostatic migration of cells to lymphoid tissues or other organs (Allen et al., 2007, Rossi and Zlotnik, 2000). These classification systems are not mutually exclusive as certain homeostatic chemokines can be upregulated during inflammation where they are able to recruit lymphocytes and promote the formation of ectopic lymphoid structures (Hjelmstrom et al., 2000, Barone et al., 2005).

1.2.1 Structural Classification of Chemokines: Systematic Nomenclature

The chemokine superfamily is divided into four groups based on the relative position of amino acid residues within a conserved cysteine motif at the N terminus of the protein: CXC, CC, XC, and CX3C. In CXC chemokines, the first two cysteines are

separated by one amino acid, whereas in CC chemokines both cysteines are adjacent. XC chemokines lack the first and third cysteine residue and CX3C chemokines have three amino acids between the first two cysteine residues (Allen et al., 2007, Rossi and Zlotnik, 2000).

1.2.2 Interaction of Chemokines With Glycosaminoglycans

Glycosaminoglycans (GAGs) are long, linear, polysaccharide chains that are highly charged (Tanaka et al., 1993a). They are abundantly expressed by endothelial cells, and are able to bind chemokines thus allowing chemokine presentation on the endothelial cell surface. This immobilisation of chemokines promotes transendothelial migration of leukocytes allowing their entry into tissues (Tanaka et al., 1993a, Rot, 1992). GAGs can differentially regulate chemokines that possess similar binding specificities. An example of this is seen with the CCR7 ligands, CCL19 and CCL21. CCL21 has an extended C-terminal tail, not present in CCL19 (Nagira et al., 1997). Truncation of this C terminal prevents its immobilisation to the lumen of HEVs and as a result prevents the extravasation of lymphocytes (Stein et al., 2000). In addition, matrix-bound CCL21 causes cell adhesion and migration but cleavage of its C terminal tail, causes it to behave more like CCL19, causing cell migration but not adhesion (Schumann et al., 2010). In addition to GAGs, transendothelial cell migration can be regulated by DARC (discussed later).

1.2.3 Chemokine Induced Transendothelial Leukocyte Migration

One of the most studied roles of chemokines is in the movement of leukocytes from blood into lymphoid tissue. Naïve T cells exit the blood into lymph nodes via high endothelial venules (HEVs). This is a multistep process involving chemokine mediated activation, firm arrest and transendothelial migration. HEV express peripheral-node addressins (PNAd), which bind to L-selectin (CD62L) expressed by the T cell. This interaction allows T cells to attach to HEVs, resulting in cell rolling due to the shear forces of blood flow. CCR7 on the rolling lymphocytes binds to CCL19 and/or CCL21 that are immobilised by GAGs on the HEV luminal surface. This induces a conformational change of integrin molecules expressed by the lymphocyte, allowing the T cell to bind firmly to ICAM-1 and ICAM-2 (or MAdCAM in the instance of mesenteric lymph node and Peyer's Patches.) This arrest allows the lymphocyte to transmigrate through the endothelial cell layer, either between the endothelial cells (paracellular) or by piercing through the endothelial cell itself (transcellular) (Forster et al., 2008). The central role of chemokines in this process was shown *in vitro* using pertussis toxin (PTX) which had no affect on leukocyte rolling, but did inhibit leukocyte arrest (Bargatze and Butcher, 1993).

1.2.4 Chemokine Receptors

Chemokine receptors form part of the rhodopsin family of G protein coupled receptors (GPCR). They have seven membrane spanning α-helices, with an extracellular amino terminus, and an intracellular carboxyl terminus. An important feature of GPCR is a DRY motif at the cytoplasmic border of the second intracellular loop. This motif is important for G protein activation (Oldham and Hamm, 2008). The

structure of the chemokine receptor is outlined in Figure 1**.** Importantly, ‘atypical’ chemokine receptors have been described that are not able to activate G proteins. These receptors are described in detail later in this chapter.

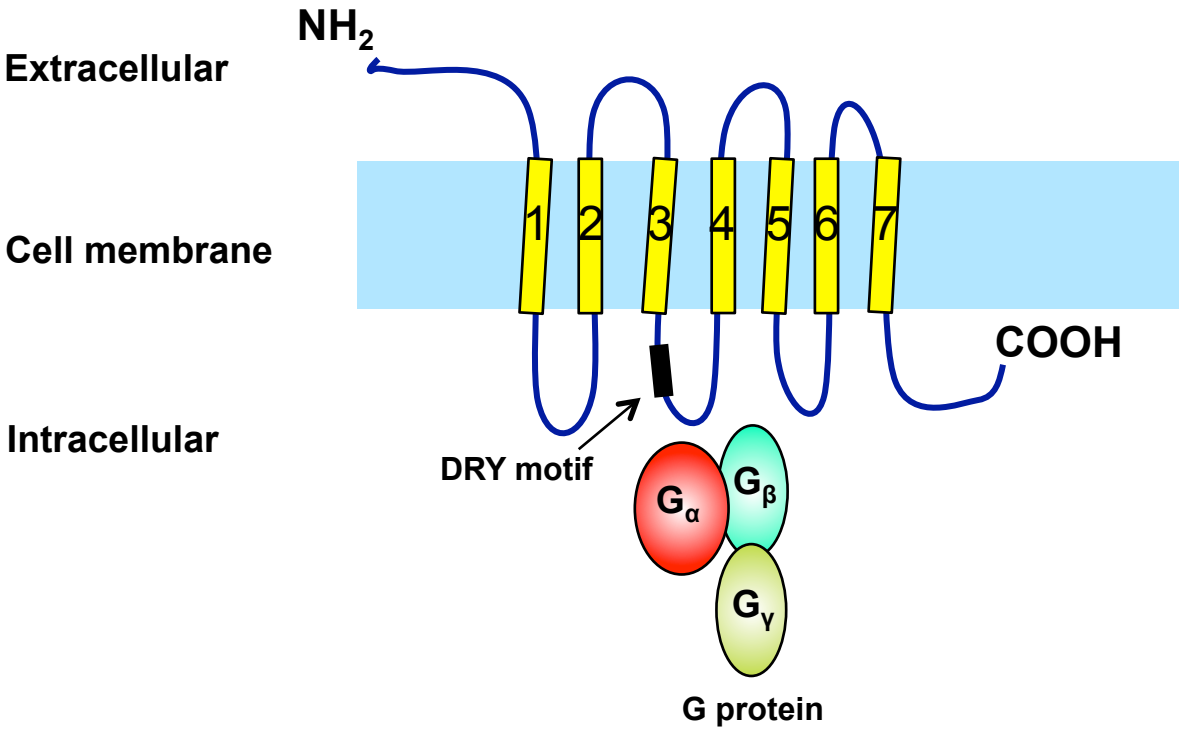

Figure 1. The Structure of the Classical Chemokine Receptor.

The classical chemokine receptor has seven membrane spanning domains (numbered 1-7), an extracellular amino (NH_2) terminus, and intracellular carboxyl (COOH) terminus. The DRY motif is located within the second intracellular loop of the receptor, and is involved in G protein coupling. The carboxyl terminus contains serine and/or tyrosine residues that are phosphorylated by G protein coupled receptor kinases, leading to receptor desensitisation.

1.2.5 GPCR Signalling

GPCR signalling involves the transmission of a signal via the activation of heterotrimeric G proteins. In the case of chemokine receptors, this initial signal is chemokine ligand binding. The heterotrimeric G protein consists of three subunits: Gα, Gβ, Gγ. In humans, there are 21 Gα subunits 6 Gβ subunits, and 12 Gγ subunits. G proteins are divided into four groups based on the structure of Gα: $G\alpha_s$, $G\alpha_i$, $G\alpha_q$ and $G\alpha_{12}$. (Cotton and Claing, 2009, Oldham and Hamm, 2008).

GDP bound to Gα renders the receptor inactive. Upon chemokine ligation, a conformational change causes the release of guanosine diphosphate (GDP) from Gα, this allows the formation of a stable complex between the receptor and G protein. This interaction is destabilised by guanosine triphosphate (GTP) binding to Gα. This allows Gα and Gβγ subunits to interact with downstream signalling targets. Gα is comprised of a GTPase domain that hydrolyses GTP to GDP thus terminating signal transduction (Cotton and Claing, 2009).

Chemokine receptors signal through $G\alpha_i$ to mediate cell migration. Treatment with PTX irreversibly uncouples all isoforms of $G\alpha_i$ and blocks downstream signalling pathways. This feature has been an invaluable tool for chemokine biologists in deciphering the role of chemokines and their receptors in mediating immunological events (Cotton and Claing, 2009, Oldham and Hamm, 2008).

Polarisation is a prerequisite for cell migration. This means that the front of the cell (leading edge) has different molecular processes to the back of the cell (uropod).

Cell migration is mediated by the polymerisation of F-actin at the leading edge and myosin II–mediated contraction at the uropod. In addition, other proteins that regulate the cytoskeleton e.g. the Arp2/3 complex are differentially localised between the leading edge and uropod (Chung et al., 2001). The maintenance of cell polarity is mediated by signalling through positive feedback loops. Members of the Rho family of small proteins, e.g. Rac and cdc42, have been shown to regulate reorganisation of the cytoskeleton during migration (Allen et al., 1998, Chung et al., 2000). In addition, the Wiskott-Aldrich syndrome protein (WASP), and related proteins (N-WASP and Scar), interact with the Arp2/3 complex to drive branched actin polymerisation (Chung et al., 2001, Millard et al., 2004).

Phosphatidylinositol-3 kinase (PI3K) activation occurs upon the activation of most chemokine receptors, however, this is not an absolute requirement for T cell migration (Ward, 2006). The role of PI3K in T cell migration has been studied using p110γ KO mice (p110γ is a catalytic isoform of PI3K). T cells from these mice were impaired in their ability to migrate in response to CCL19, CCL21 and CXCL12. Interestingly, B cell migration was unaffected in these mice, suggesting that B and T cells mediate their migration via different signalling pathways (Reif et al., 2004)

1.3 The Thymus

The thymus is a primary lymphoid organ found in all vertebrates and is located in the central compartment of the thoracic cavity, above the heart and behind the sternum (Boehm, 2008). It is an encapsulated 3-dimensional structure composed of haematopoietic and stromal cells, which provide the necessary signals for T cell development (Alves et al., 2009). Early studies in the 1960's by J. F. Miller were the first to show the immunological function of the thymus. One such study showed that mice thymectomised at birth had increased mortality rates compared to sham-thymectomised controls unless antibiotics were administered, suggesting that thymectomised mice were more susceptible to infection (Miller, 1961). In addition, Miller also showed the tolerogenic function of the thymus. This was achieved by thymectomising CBA.T6T6 mice at birth, transplanting a C57Bl/6 thymus and subsequently transplanting skin grafts from either a syngeneic (C57Bl/6) or allogeneic (BALB/c) donor. These mice accepted the C57Bl/6 skin but rejected the BALB/c skin, suggesting that the transplanted thymus was responsible for the acquisition of tolerance (Miller, 1962). Since then, a wealth of research has provided insight into the mechanisms involved in the effective production of fully competent, self-tolerant T cells.

1.3.1 Colonisation of the Thymus

HSC are not present within the thymus, and therefore T cell development is dependent on the constant recruitment of progenitor cells to the thymus (Donskoy and Goldschneider, 1992). Progenitor cells are recruited from different sources in the prenatal and postnatal mouse. During embryonic development, progenitor cells are derived from the yolk sac, aorta-gonad-mesonephros region, placenta and fetal liver whereas postnatal progenitor cells are derived from the BM (Mikkola and Orkin, 2006).

During pre-vascularisation embryogenesis, progenitor cells migrate directly into the thymic anlage from the surrounding mesenchyme. Once the vasculature has developed progenitor cells enter the thymus by blood vessels at the corticomedullary junction (CMJ). Lymphoid progenitor cells can be detected in the thymus at week 7-8 in human gestation and embryonic day (E) 11.5 (E11.5) in murine thymus (Calderon and Boehm, 2011). Lymphoid progenitor cells give rise to early thymic progenitors (ETPs). ETPs have an extremely limited ability to self-renew therefore constant recruitment of progenitor cells is vital for T cell development; this is thought to occur in periodic waves approximately every four weeks in adult mice (Foss et al., 2001).

One study characterised the vascular adhesion molecules that may be involved in the recruitment of progenitor cells to the adult thymus. This study used mice that were 5 and 9 weeks old (peak of progenitor homing), and mice that were 4 and 7 weeks old (refractory period of progenitor homing). Analysis of the thymi from these

mice by immunohistochemistry revealed expression of PNAd, VCAM-1 and ICAM-1 by post capillary venules at the CMJ. Expression of vascular adhesion protein 1 (VAP-1) was limited to fewer vessels at the CMJ, and medullary vessels were VAP-1 negative. Interestingly, PNAd expression fluctuated temporally, with highest expression during peak progenitor homing, and lower expression during refractory periods, suggesting that PNAd may play a role in progenitor cell recruitment (Lepique et al., 2003).

Chemokine receptor-ligand interactions are responsible for the homing of haematopoietic progenitors to the embryonic thymus. The chemokines CCL21, CCL25 and CXCL12 are expressed by the thymic anlage, and CCL21 and CXCL12 are expressed by the perithymic mesenchyme (Calderon and Boehm, 2011, Liu et al., 2006, Bleul and Boehm, 2000). At E12.5 the receptors for these chemokines (CCR7, CCR9 and CXCR4) can be detected on $CD45^+$ cells isolated from the perithymic mesenchyme (Jenkinson et al., 2007a). The role for chemokines in the homing of progenitors cells to the embryonic thymus has been shown by several experiments using genetically modified mice. A recent report used combinations of CCR7, CCR9 and CXCR4 deficient mice to investigate the involvement of these chemokine receptors. It was shown that at E12.5, the CCR9 KO mouse had reduced numbers of $CD45^+$ cells within the thymus but not around parathyroid. In contrast, the E12.5 CCR7 KO mouse had an absence of $CD45^+$ cells around the parathyroid, in addition to a reduction of $CD45^+$ cells within and around thymus. Analysis of the E12.5 CXCR4 KO thymus revealed a similar distribution of $CD45^+$ cells to WT controls. At E12.5, CCR7, CCR9, CXCR4 triple KO mice has a complete absence of

$CD45^+$ cells in and around the thymus and parathyroid. This suggests that all three chemokine receptors contribute to progenitor homing to the embryonic thymus. The triple KO thymus continued to have reduced cellularity at E17.5, suggesting these chemokines are also important in the recruitment of progenitor cells, post vascularisation (Calderon and Boehm, 2011).

The influence of chemokines in the colonisation of the adult thymus is less clear. One study showed that the reduction of thymocytes in the CCR7/CCR9 double knockout (DKO) embryo is resolved by postnatal day 1 and hypothesises that this is due to compensatory proliferation of thymocytes and subsequent seeding of the thymus by blood vessels at the CMJ in a CCR7/CCR9 independent manner (Liu et al., 2006). A more recent study shows that the adult CCR7/CCR9 DKO has reduced frequencies of ETP but similar frequencies of total thymocytes compared to WT controls due to compensatory proliferation of DN3 thymocytes (Krueger et al., 2010). This suggests that homing to the adult thymus is dependent, in part, on CCR7 and CCR9, but that absolute thymocyte cellularity is unaffected in DKOs due to compensatory mechanisms.

1.3.2 Heterogeneity Within the DN1 Population

Several studies have shown that thymus seeding progenitor cells are not T lineage committed and can give rise to cells belonging to the lymphoid and myeloid lineage. The most immature thymocytes are termed DN1 thymocytes and are defined as $CD25^-CD44^{hi}$. These thymocytes are located at the perimedullary cortex – a narrow region of the cortex adjacent to the medulla (Petrie and Zuniga-Pflucker, 2007). This

is a heterogeneous population and can be subdivided into five groups (a-e) based on expression of CD24 and CD117. In addition to surface phenotype, these cells also differ based on their proliferative capacity, with DN1e cells having a relatively lower proliferative capacity compared to DN1a-d. When seeded onto culture plates containing a monolayer of OP9 cells, DN1a and DN1b cells express NK1.1 whereas DN1c and DN1d show expression of CD19, indicative that cells of the DN1 population can give rise to cells of the NK and B cell lineage (Porritt et al., 2004). In addition to the lymphoid lineage, thymic progenitor cells show myeloid potential in the form of mast cell and DCs (Shen et al., 2003, Taghon et al., 2007). Moreover, studies using RAG-1/Cre X Rosa26YFP mice show YFP^+ expression by thymic granulocytes, suggesting they have a history of *Rag1* expression and are therefore derived from ETPs (De Obaldia et al., 2013).

Notch signalling has been implicated in T lineage commitment. In mammals, four notch homologues exists (Notch 1-4) which interact with five ligands expressed by thymic epithelial cells (TECs): Jagged 1, Jagged 2, Delta-like ligand 1 (DLL1), DLL3 and DLL4 (Radtke et al., 2013, Jenkinson et al., 2006). Early evidence for the role of Notch signalling in T lineage commitment was provided by the inducible inactivation of Notch-1 in newborn mice. These mice showed a block in T cell development, and an accumulation of B cells within the thymus (Radtke et al., 1999). On the other hand, a more recent study suggests the T/B lineage is determined prior to entry to the thymus. $CD45^+$ cells were sorted from E12 fetal liver, perithymic mesenchyme and thymic epithelium, and cultured on OP9 stromal cells in the presence of IL-7. Purified $CD45^+$ precursors from fetal liver gave rise to B cells, whereas precursor

cells from the thymic mesenchyme and epithelium did not (Harman et al., 2005). This provides evidence that loss of B cell potential occurs prior to interaction with notch ligand in the thymus.

1.3.3 Early Intrathymic T Cell Development

The phenotypic changes of thymocytes during DN development are complemented by intrathymic migration. DN1 thymocytes acquire the expression of CD25 and CD117 and efficiently transit to downstream DN2 thymocytes. There are still some cells with NK and myeloid potential in this population, but most are T lineage committed (Rolink et al., 2007, Porritt et al., 2004). DN2 thymocytes are located at the inner cortex where they upregulate *Rag* expression and begin to rearrange TCRγ and TCRδ chains. Stem cell factor (SCF), a cytokine that binds CD117, is expressed in this area of the cortex, and is partly responsible for the proliferation of $CD117^+$ DN2 thymocytes. DN2 thymocytes downregulate expression of CD44 and CD117 to become DN3 thymocytes, and they migrate through the outer cortex to the SCZ along $VCAM^+$ stromal cells (Petrie and Zuniga-Pflucker, 2007). Potential for alternative lineages is lost at this stage; therefore DN3 thymocytes are fully committed to becoming αβ or γδ T cells (Chi et al., 2009). IL-7 signalling is important during this stage of T cell development. OP9-DL1 cells were used to show that transition to the DN3 stage requires high levels of IL-7, but further differentiation past the DN3 stage is favoured by much lower IL-7 concentrations (Huang et al., 2005). The importance of IL-7 production by TECs is seen in IL-7flox-flox FoxN1-Cre mice. Within the thymus of these mice, TECs are unable to produce IL-7, and as a

result have a dramatic reduction in thymocyte cellularity, and a virtually absent γδ T cell population (Shitara et al., 2013). DN3 thymocytes begin to rearrange their TCRβ locus and those which have succeeded in this begin to assemble the TCRβ and pre-TCRα chains to form the pre-TCR complex. Successful expression of the pre-TCR complex allows thymocytes to proceed in their development whereas those thymocytes that have not successfully undergone TCRβ rearrangement die. Pre-TCR^{+} cells dramatically proliferate and downregulate CD44 expression to become DN4 thymocytes. Although these cells downregulate CD44, they rapidly upregulate CD4 and CD8 expression, and for this reason they are also called pre double positive (DP) thymocytes. Pre-DP thymocytes migrate from the SCZ towards the medulla (Petrie and Zuniga-Pflucker, 2007). See Figure 2 for an overview of intrathymic T cell development.

The role of chemokines and their receptors have been implicated in the outward migration of DN thymocytes, such receptors include CXCR4, CCR7 and CCR9. CXCR4 is expressed by ETPs and its ligand, CXCL12, is produced by a subset of cTECs. BM chimeras were generated by transferring donor cells from mice, which have an immature thymocyte-specific deletion of CXCR4, into wild type mice. This model showed that CXCR4 deficient DN thymocytes were unable to migrate outwards from the CMJ and were arrested in early DN development (Plotkin et al., 2003). In addition, CCR7 and its ligands CCL19 and CCL21 influence this outwards migration. This is seen by the accumulation of DN2 thymocytes at the CMJ in plt (Paucity of lymph node T cells) and CCR7 KO mice. (Misslitz et al., 2004). Plt mice have a spontaneous mutation resulting in the genomic deletion of the CCL21 gene

(*Scya21a*), and the CCL19 gene (*Scya19*). As a result, plt mice do not express CCL19 or CCL21 in lymphoid organs, but do express CCL21 in lymphatic endothelium, albeit at reduced levels (Mori et al., 2001). Experiments using CCR9 KO mice have shown that signalling via this receptor is also important for migration of DN thymocytes to the subcapsular zone (SCZ). In these mice, $CD25^+$ DN thymocytes are dispersed throughout the cortex rather than being localised at the SCZ (Benz et al., 2004).

1.3.4 Selection of the αβTCR Repertoire

Newly generated $TCR\alpha\beta^{low}CD4^+CD8^+$ DP thymocytes are subject to stringent selection events within the thymus. DP thymocytes interact via their TCR with peptide-MHC complexes expressed by cTECs. If these interactions are low affinity, thymocytes receive survival signals and further differentiate into SP thymocytes. This enrichment of 'useful' T cells is known as positive selection and only occurs in 1-5% of thymocytes successfully pass through this process. If the TCR-peptide-MHC interactions are high affinity, these potentially autoreactive thymocytes are induced to undergo apoptosis. This is known as negative selection (Takahama, 2006, Petrie and Zuniga-Pflucker, 2007).

Cortical DP thymocytes upregulate CCR7 and migrate to the medulla where CCR7 ligands (CCL19 and CCL21) are expressed. The cortex to medulla migration of thymocytes is dependent on CCR7 and CCR9. An *in vitro* culture system using thymic slices showed that CCR7 deficient SP thymocytes exhibit disorientation compared to WT SP thymocytes which show directional bias towards the medulla

(Ehrlich et al., 2009). CCR9 has also been implicated in cortex to medulla migration of thymocytes via PlexinD1. PlexinD1 is a transmembrane glycoprotein and the receptor for semaphorin3E. PlexinD1 is expressed at high levels by DP thymocytes but has reduced expression by SP thymocytes and semaphorin3E is localised within the thymic medulla (Takamatsu et al., 2010). Using a transwell migration assay, semaphorin 3E-Fc was capable of inhibiting CCR9 mediated migration of positively selected $CD69^+$ thymocytes. Moreover, the thymus from PlexinD1 KO embryos has a disorganised structure, with no clear cortical/medullary demarcation (Choi et al., 2008). This study shows that semaphorin3E represses CCR9/CCL25 signalling, which would normally keep thymocytes within the cortex, thus allowing thymocytes to migrate towards the medulla.

1.3.5 Thymocyte Maturation

SP thymocytes spend approximately 12 days in the medulla before being exported to the periphery (Scollay and Godfrey, 1995). SP thymocytes were originally thought to be fully mature, ready to leave the thymus in an orderly 'first in – first out' or random fashion. However, recent studies have shown a developmental pathway of SP thymocytes within the medulla, and continued development of recent thymic emigrants (RTE) in the periphery. SP thymocytes undergo four developmental stages during their maturation within the medulla. They can be divided into four subsets, SP1 ($6C10^+CD69^+$), SP2 ($6C10^-CD69^+$), SP3 ($CD69^-Qa2^-$), and SP4 ($CD69^-Qa2^+$) (Li et al., 2007). These phenotypic changes are accompanied by the additional deletion of potentially autoreactive thymocytes. The expression of tissue-restricted antigens by mTEC is in part dependent on the transcription factor

autoimmune regulator (Aire). Aire deficiency leads to autoimmune polyendocrinopathy-candidiasis-ectodermal dystrophy (APECED), and a similar condition in mice (Anderson et al., 2002). A recent publication used a system of RelB KO embryonic thymus lobes grafted under the kidney capsule of WT mice to show the effects of an mTEC deficient environment on T cell development. These experiments showed that the medullary microenvironment is not an absolute requirement for the maturation of conventional SP thymocytes, but is required for the maturation of $Foxp3^{-}CD25^{+}$ Treg precursors into $Foxp3^{+}$ $CD25^{+}$ Tregs (Cowan et al., 2013).

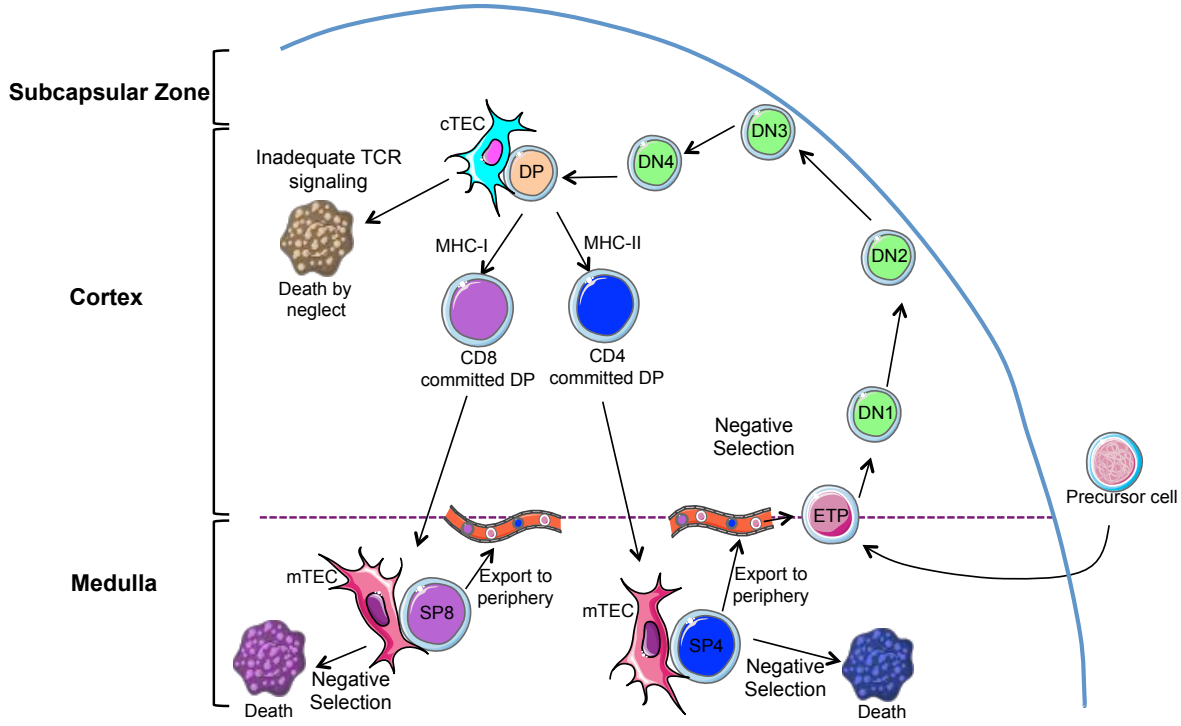

Figure 2. An Overview of Intrathymic T Cell Development.

Haematopoietic precursor cells arise in the bone marrow and enter the thymus by blood vessels at the corticomedullary junction (CMJ). Once inside the thymus they are known as early thymic progenitors (ETP). ETP begin their outward migration from the CMJ and become double negative (DN) thymocytes. DN thymocytes migrate to the subcapsular zone (SCZ) before rearranging their TCRβ chain. Following successful gene rearrangement, DN thymocytes upregulate CD4 and CD8 to become double positive (DP) thymocytes. Developing DP thymocytes interact with cortical thymic epithelial cells (cTEC) associated with self-antigen in the context of MHC-I or MHC-II. Inadequate T cell receptor (TCR) signalling results in cell death by neglect, whereas intermediate levels of TCR signalling results in survival signals. Thymocytes that successfully pass through this selection process migrate to the medulla, where they interact with self-antigen presented by medullary thymic epithelial cells (mTEC). High affinity binding of thymocytes to self-antigen results in pro-apoptotic signalling, to ensure removal of potentially autoreactive thymocytes (negative selection). SP thymocytes continue their maturation within the medulla before leaving the thymus by blood vessels at the corticomedullary junction (CMJ).

1.3.6 Additional Mechanisms of Negative Selection

In addition to mTEC, thymic dendritic cells (DC) contribute to the deletion of autoreactive thymocytes during negative selection. Three populations of thymic DC exist, plasmacytoid (p)DC, Sirpα$^-$ conventional (c)DC, and Sirpα$^+$ cDC. The chemokine XCL1 is produced by mTEC, and its receptor, XCR1 is expressed by thymic DCs. Work from Takahama's lab recently showed that the expression of XCL1 by mTEC is AIRE dependant, and an absence of XCL1 production results in the disrupted positioning of thymic DCs across the CMJ. The correct positioning of DCs was shown to be vital for the induction of central tolerance, as thymocytes from XCL1 KO mice caused autoimmunity when transferred into athymic nude mice (Lei et al., 2011).

Thymic pDCs are a migratory DC subset and are involved in the transport of peripheral antigen to the thymus for presentation to developing thymocytes. Moreover, use of CCR9 KO mice showed that CCR9 controls the homing of pDCs to the thymus, In addition, using a TCR transgenic system, it was shown that antigen-loaded pDCs were effective at deleting antigen-specific SP thymocytes. This data showed that pDCs were capable of inducing central tolerance in a CCR9 dependant fashion (Hadeiba et al., 2012). Sirpα$^-$ cDCs are not migratory, instead these cells are generated intrathymically. Using langerin-GFP reporter mice, it was shown that Sirpα$^-$ cDCs arise within the DN1c population of cells described by Petrie and colleagues, but not amongst ETP (Luche et al., 2011, Porritt et al., 2004). This suggests that Sirpα$^-$ cDCs are generated from a separate DC precursor cell. Unlike Sirpα$^-$ cDCs which are generated intrathymically and are located within the thymic

medulla, Sirpα^{+} cDCs are a migratory subset and are positioned within the cortex and perivascular areas. Baba and colleagues used CCR2 KO mice, which have a reduction in Sirpα^{+} cDCs, to show a role for these DCs in the presentation of blood-borne antigen to developing thymocytes during negative selection (Baba et al., 2009).

The thymus also contains a small population of B cells that play a role during negative selection. Experiments using RAG2pGFP Tg mice suggest that these B cells arise within the thymus from *Rag2* expressing progenitor cells (Perera et al., 2013). In addition, parabiosis studies of congenic CD45.1 and CD45.2 mice show minimal circulation of B cells through the thymus (Perera et al., 2013). Thymic B cells have a unique phenotype compared to peripheral B cells, they express higher levels of MHC-II, CD80 and CD86, and are capable of presenting self antigen to mediate negative selection of autoreactive T cells (Perera et al., 2013, Frommer and Waisman, 2010). The influence of chemokines on the thymic B cell population is not clear, however CCR7 KO mice have a reduction in this population of cells (Akirav et al., 2011).

1.3.7 Export to the Periphery

The mechanisms for thymocyte egress from the thymus are still not fully clear, however several molecules have been implicated both in neonatal and adult mice. SP thymocytes upregulate the transcription factor Kruppel-like factor (KLF) 2 and as a result, target genes including sphingosine-1-phosphate receptor-1 (S1P1) and CD62L are also upregulated (Zachariah and Cyster, 2010). The concentration of the S1P1 ligand, S1P, is high in serum and low in the thymus, thereby creating an S1P gradient allowing mature thymocytes to egress. In addition to S1P in the serum, S1P is produced by neural crest pericytes which ensheathe thymic blood vessels. Specific deletion of S1P production by such pericytes has been shown to dramatically impair thymic export (Zachariah and Cyster, 2010). CD69 is transiently upregulated on SP thymocytes following TCR engagement. Interestingly S1P1 KO mice fail to downregulate CD69 expression on SP thymocytes, and treatment with the S1P1 agonist FTY720 results in the downregulation of CD69 on thymocytes. Moreover, constitutive expression of CD69 by thymocytes inhibits their egress from the thymus, therefore suggesting this molecule has a role in egress from the thymus (Love and Bhandoola, 2011).

CCR7 KO and plt neonatal mice have a reduction in peripheral T cell numbers, indicating a role for CCR7 in thymocyte egress. Thymocyte egress in adult mice seems to be CCR7 independent as these abnormalities are restored to normal levels after the neonatal stage (Ueno et al., 2004). Moreover, an *in vitro* system which used FTOC thymus lobes, cultured in the presence or absence of chemokines showed a highly significant increase in thymic export in the presence of CCL19

compared to several other chemokines, including the alternative CCR7 ligand, CCL21 (Ueno et al., 2002). This study also used neutralising antibodies and showed that blockade of CCL19 reduced the number of T cells in peripheral blood of newborn mice, whereas CCL21 did not, providing further evidence for the role of CCL19 in thymocytes egress (Ueno et al., 2002). See Figure 3 for an overview of the involvement of chemokines and their receptors in T cell development.

The identification of recent thymic emigrants (RTE) as a population distinct from the bulk peripheral T cells is an important factor when studying thymic egress. RTE were first identified by injecting fluorescein isothiocyanate (FITC) into the thymus of mice, and isolating $FITC^+$ T cells from the periphery (Berzins et al., 1999). This technique has several caveats, including the short half-life of FITC, and the inadvertent labelling of recirculating T cells. Recently, the use of RAG2p-GFP Tg mice, in which the *Rag2* promoter drives the expression of GFP, has been used to identify RTE. In these mice, the GFP signal remains, even once the *Rag* gene is switched off, thereby labelling RTE as GFP^+. This model has an additional advantage of allowing young GFP^{hi} RTE to be distinguished from older GFP^{lo} RTE. RTE undergo a maturation process in the periphery characterised by the downregulation of CD24, D3, CTLA-4 and PD-1, and the upregulation of Qa2, CD45RB, Ly6C, IL-7Rα, and CD28 (Fink, 2013, Boursalian et al., 2004).

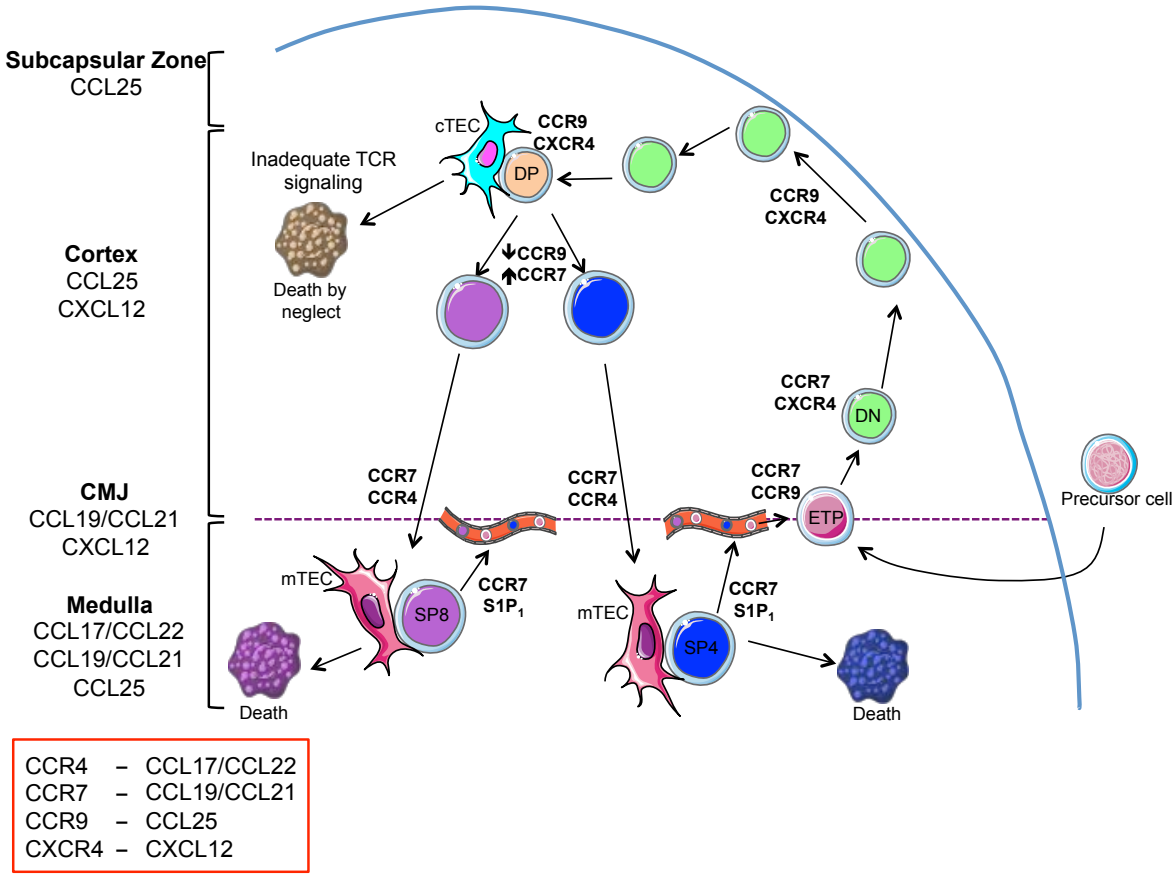

Figure 3. The Involvement of Chemokines and Chemokine Receptors in T Cell Development

The recruitment of early thymic progenitors (ETP) from the vasculature into the thymus is dependant on the expression of CCR7 and CCR9. During the development of double negative (DN) thymocytes, downregulation of CCR7 expression, and upregulation of CCR9 and CXCR4 occurs. This mediates the outward migration of DN thymocytes towards the subcapsular zone (SCZ). Upon reaching the double positive (DP) stage, thymocytes express high levels of CCR9 and CXCR4. Following selection events within the cortex, developing thymocytes express CCR7 and CCR4 and downregulate the expression of CCR9 to allow the migration of single positive (SP) thymocytes into the thymic medulla. Fully mature SP thymocytes upregulate the expression of sphingosine-1-phosphate receptor ($S1P_1$), in addition to CCR7, to mediate their egress into the periphery.

1.4 Thymic Stroma

Optimal thymic microenvironments for T cell development are created by the thymic stroma. Thymic stroma consists of primarily EpCAM-1 positive TEC, but also a population of EpCAM-1 negative cells which are comprised of mesenchymal cells, endothelial cells and fibroblasts.

1.4.1 Thymic Epithelial Cells

During positive and negative selection events, developing thymocytes interact with peptide-MHC complexes on TECs. cTEC express MHC-I and MHC-II, and mediate positive selection. Mice deficient in Thymus Specific Serine Protease (TSSP) or cathepsin L have shown the importance of these proteases in the positive selection of SP4 thymocytes (Nakagawa et al., 1998, Viret et al., 2011, Gommeaux et al., 2009). Selection of CD8 T cells by cTEC requires the thymoproteasome subunit β5T (Nitta et al., 2010). The majority of self-peptides presented by TEC are derived from endogenous proteins, due to their poor ability to phagocytose. TECS exhibit high levels of autophagy and when this process is disrupted, for example in *Atg5* (a gene essential for mammalian macroautophagy) deficient mice, positive selection is impaired, suggesting this is an important mechanism for peptide presentation (Nedjic et al., 2008). cTEC express the markers cytokeratin-8, CD205, Ly51 and β5T. Flow cytometric analysis of cTEC allows the identification of $cTEC^{lo}$ ($CD40^{lo}MHC\text{-}II^{lo}$) and $cTEC^{hi}$ ($CD40^{hi}MHC\text{-}11^{hi}$) cells. mTEC express markers such as cytokeratin-5, UEA-1, CD80, Aire, ERTR5, and lack expression of cTEC specific markers. Like cTEC, mTEC can be divided into $mTEC^{lo}$ ($CD80^{lo}MHC\text{-}II^{lo}$) and

mTEC^{hi} (CD80^{hi}MHC-II^{hi}). A proportion of mTEC^{hi} cells express Aire (Anderson and Takahama, 2012, Gray et al., 2006).

1.4.2 TEC Development

TEC development begins early during embryonic development by the existence of a bipotent cell which can give rise to both cTEC and mTEC lineages. This was shown using a model that involved the isolation of a single TEC from an E12 YFP^{+} mouse. This cell was microinjected into a non-fluorescent host thymus that was then grafted under the kidney capsule of a WT mouse. Analysis of the graft revealed YFP^{+} cells in both the cortex and medulla, elegantly showing the ability of the bipotent TEC to form cTEC and mTEC (Rossi et al., 2006). A recent study further characterised TEC progenitors. This study isolated CD205^{+}CD40^{-} TEC from an E15 thymus to create a reaggreate thymic organ culture that was then grafted under the kidney capsule of a WT mouse. After 6-8 weeks, the graft was analysed and showed the presence of cTEC and mTEC. Moreover, the graft was capable of supporting normal T cell development (Baik et al., 2013). This suggests that TEC expressing CD205, (which was previously thought to be expressed by only those cells in the cTEC lineage), are able to give rise to both cTEC and mTEC lineages. A similar result was shown using β5t-Cre-loxP-GFP mice which showed GFP expression by mTEC, in addition to cTEC, suggesting that β5t must be expressed by TEC progenitors which give rise to both cTEC and mTEC (Ohigashi et al., 2013).

1.4.3 Thymic Mesenchyme

Thymic mesenchyme originates from neural crest (NC) cells, which migrate into the pharyngeal region and surround the third pharyngeal pouch during early embryonic development. Interactions between mesenchymal cells and TEC have been implicated in thymus organogenesis. One study used E12 thymi in which PDGFRα^{+} mesenchyme was removed, or left intact (Jenkinson et al., 2007b). These thymi were subsequently grafted under the kidney capsule of WT mice and harvested 3 weeks later. Analysis of the grafted thymi revealed demarcation of cortical and medullary areas and an ability to support T cell development, irrespective of the presence or absence of PDGFRα^{+} mesenchyme. Interestingly, mesenchyme depleted thymi were hypoplastic suggesting that PDGFRα^{+} mesenchymal cells play a role in the induction of TEC proliferation. The extent to which NC derived cells make a long-lasting contribution to the adult thymus remains poorly understood.

Mesenchymal stromal cells are a broad population of cells. Within the thymus they comprise of the connective tissue forming cells of the capsule and septae, endothelial cells, perivascular cells and fibroblastic cells. Studies have used Sox10-cre Rosa26-YFP mice to label NC derived cells (Muller et al., 2008, Foster et al., 2008). Flow cytometric analysis of the thymus from Sox10-cre Rosa26-YFP adult mice revealed UEA^{-}CD31^{-}EpCAM-1^{-}Ly51^{+} cells that expressed YFP (Muller et al., 2008). Embryonic NC derived cells are PDGFRα^{+}PDGFRβ^{+}, whereas NC derived cells in the adult thymus are PDGFRα^{-}PDGFRβ^{+} (Muller et al., 2008, Foster et al., 2008). Staining of the adult Sox10-cre Rosa26-YFP thymus by both immunofluorescence and flow cytometry shows YFP^{+}αSMA^{+} perivascular cells

(Muller et al., 2008, Foster et al., 2008). High magnification images show that larger vessels at the CMJ coexpress YFP and αSMA whereas cortical capillaries show heterogeneity. Some cortical capillaries show an inner layer of endothelial cells, surrounded by $YFP^{+}\alpha SMA^{-}$ cells, followed by $YFP^{-}\alpha SMA^{+}$ cells, whereas others coexpress YFP and SMA. A third subset of cortical capillaries comprise of only an inner layer of endothelium surrounded by YFP^{+} cells, such capillaries could be surrounded by pericytes of non-NC origin (Muller et al., 2008).

Thymic mesenchyme, in addition to TEC, has been identified as a source of VEGF. Moreover, VEGF-A deletion in TEC results in altered thymic vasculature, suggesting that the thymic mesenchyme may play a role in the formation of thymic vasculature (Muller et al., 2005). A recent study used a combination of Foxn1 mutant, KO and WT mice to specifically address this issue. This study showed that Foxn1 is responsible, in a dose dependent manner, for the generation of thymic vasculature. Moreover, Foxn1 is needed to ensure the generation of a complete capillary network within the thymus, and for tight association between endothelial and perivascular cells (Bryson et al., 2013). This data therefore provides evidence that epithelial-endothelial-mesenchymal cell interactions are vital for the development of a functional thymic vascular network.

1.5 Atypical Chemokine Receptors

Atypical chemokine receptors (ACKRs) are 7-transmembrane receptors that share a similar structure to classical chemokine GPCR. The defining feature of ACKR is the absence or modification of the DRYLAIV domain in the second intracellular loop of the GPCR. This results in a receptor which is able to ligate its cognate chemokine, but unable to couple to G proteins and therefore unable to induce classical chemokine signalling and subsequent cell migration. To date, four atypical chemokine receptors have been recognised and incorporated into the new nomenclature, ACKR1 (Duffy antigen receptor for chemokines, DARC), ACKR2 (D6), ACKR3, (CXCR7), and ACKR4 (CCRL1) (Ulvmar et al., 2011, Nibbs and Graham, 2013) (Bachelerie et al., 2014) Two additional molecules (CCRL2 and C5a complement receptor) await independent confirmation. See Figure 4 for an overview of the atypical chemokine receptor family.

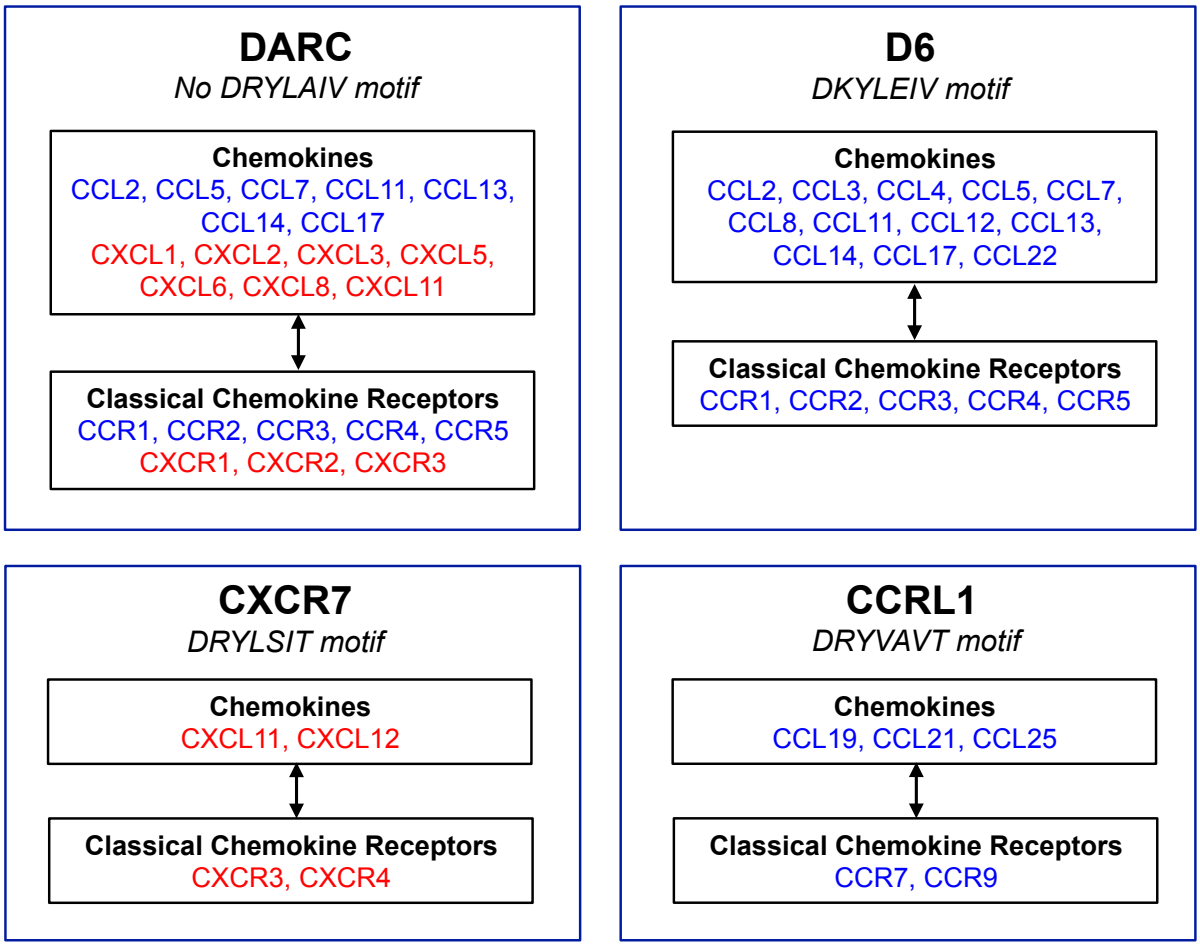

Figure 4. Atypical Chemokine Receptors and Their Ligands.

The chemokines (CCL in blue, CXCL in red), and their interaction with atypical and classical chemokine receptors.

1.5.1 ACKR1, DARC

DARC was initially discovered as the Duffy (fy) blood group antigen. It consists of two major co-dominant alleles, FY*A and FY*B. The antigen was named after R. Duffy, a haemophiliac patient who suffered adverse reactions following blood transfusions. In depth analysis of serum from this patient revealed an 'unusual antibody'. This antibody was specific towards Fyb^{+} erythrocytes (Cutbush and Mollison, 1950).

Interestingly, in addition to Duffy 'positive' homozygous and heterozygous individuals, a third Duffy 'negative' phenotype exists. The majority of individuals of West African ancestry carry the Duffy 'negative' phenotype. The FY*B allele of Duffy 'negative' individuals has a single nucleotide polymorphism within the GATA-1 binding site of erythroid cells (Tournamille et al., 1995). These individuals therefore lack DARC expression by erythrocytes, but retain DARC expression by endothelial cells. Two malarial parasites (*Plasmodium vivax* and *Plasmodium knowlesi*) use DARC to enter erythrocytes (Horuk et al., 1993, Miller et al., 1975). It is believed that the Duffy 'negative' phenotype evolved to protect against infection from *Plasmodium*.

Duffy was designated DARC after it was shown to bind a wide range of inflammatory CC and CXC chemokines (Tournamille et al., 1997, Lee et al., 2003). Erythrocytes lack the cellular machinery needed for endocytosis therefore chemokines bound to erythrocyte DARC remain on the cell surface. For this reason erythrocyte DARC was originally described as a chemokine 'sink' (Darbonne et al., 1991). This theory

was supported when DARC deficient mice were used to show the importance of DARC in reducing circulating levels of inflammatory chemokines and dampening the inflammatory response (Dawson et al., 2000). A recent review proposed a model whereby erythrocyte DARC buffers chemokine levels during homeostatic and inflammatory conditions (Hansell et al., 2011).

In vitro studies using MDCK cells transfected with DARC show the ability of DARC to transport chemokines across cell monolayers (Pruenster et al., 2009). Moreover, in a model of contact hypersensitivity, mice that overexpress endothelial DARC, show enhanced leukocyte migration into the skin (Pruenster et al., 2009). These experiments elegantly show the ability of endothelial DARC to transcytose its chemokine ligands from the baso-lateral to luminal surface, and as a result, enhance leukocyte extravasation.

1.5.2 ACKR2, D6

D6 was first identified in 1997. Competitive radio-ligand binding assays identified it as a receptor with high promiscuity for inflammatory CC chemokines (Nibbs et al., 1997b, Nibbs et al., 1997a). Ligand binding of D6 fails to induce a calcium flux and classical chemokine receptor signalling (Fra et al., 2003). Immunofluorescent staining of HEK293 cells transfected with D6-GFP shows the majority of D6 within the cell. This intracellular localisation of D6 is due to its constitutive recycling to and from the cell surface independent of ligand binding. A recent study has shown that a conserved tyrosine motif in the N terminus is needed for chemokine internalisation and therefore effective chemokine scavenging (Hewit et al., 2014).

Inflammatory disease models in D6 deficient mice highlight a role for D6 in the regulation of the inflammatory response. Carbon tetrachloride induced liver damage in D6 KO mice revealed increased chemokine levels and prolonged liver damage (Berres et al., 2009). Similar phenotypes of D6 KO mice were observed during *Mycobacterium tuberculosis* infection (Di Liberto et al., 2008), and allergen-induced airway disease (Whitehead et al., 2007). Interestingly, expression of D6 by lymphatic endothelial cells allows the clearance of inflammatory CC chemokines to prevent inflammatory leukocytes adhering to these cells. This allows mature $CCR7^{+}$ DCs to sense the CCL21 gradient and enter the lymph node without obstruction (McKimmie et al., 2013).

1.5.3 ACKR3, CXCR7

Comparison of CXCR4 deficient and WT fetal liver cells revealed that surprisingly, CXCL12 bound with similar affinity to both (Burns et al., 2006). This data was the first to suggest the existence of another chemokine receptor for CXCL12. This receptor was identified as CXCR7. CXCR7 KO mice show perinatal lethality implicating CXCR7 in embryogenesis, specifically vasculogenesis and angiogenesis (Sanchez-Martin et al., 2013).

In vitro studies using cells transfected with CXCR4 or CXCR7 revealed interesting data about the binding specificities of CXCR7. Addition of CXCL11 inhibited the binding of CXCL12 to CXCR7 but not CXCR4. Moreover, ligand binding of CXCR7 did not induce calcium flux or cell migration (Burns et al., 2006). As a result, CXCR7 was identified as an ACKR for CXCL11 and CXCL12.

A recent study used pharmacological blockade of CXCR7 and showed its involvement in the regulation of circulating CXCL12 (Berahovich et al., 2014). Additional studies point towards a role for CXCR7 in autoimmunity, as arthritic symptoms were relieved by the administration of CXCR7 antagonists in a mouse model of collagen induced arthritis (Watanabe et al., 2010).

1.5.4. ACKR4, CCRL1

CCRL1, also known as CCX-CKR; **C**hemo**C**entry**x** **C**hemo**k**ine **R**eceptor (in reference to the company that was among the first to clone the receptor), CCR11, and ACKR4, was first identified in 2000 (Gosling et al., 2000, Schweickart et al., 2000). The first publication to describe this molecule showed expression of CCRL1 mRNA by several human tissues. These included non-hematopoietic organs such as heart, kidney, placenta and brain, but also lymphoid tissues, specifically spleen and lymph node. Moreover, CCRL1 mRNA was detected in human T cells and monocyte-derived immature DCs.

HEK293 cells were transfected with human CCRL1 (hCCRL1) to investigate the chemokine binding specificity of this receptor. Radio-ligand binding experiments revealed high affinity binding of CCL19, CCL21 and CCL25 to CCRL1. This study also identified CXCL13 as a lower-affinity ligand of CCRL1. Approximately 80 other chemokines, both human and murine, were assessed and showed no affinity for CCRL1 (Gosling et al., 2000).

In 2002, Townson and Nibbs identified murine CCRL1 (mCCRL1). mCCRL1 shares 85% identity with hCCRL1 and 30-40% identity with other CC chemokine receptors such as CCR7 and CCR9. This study also revealed that mice have one copy of the CCRL1 gene whereas humans have two; one on chromosome 3, and the other on chromosome 6; these genes differ in sequence by three nucleotides (Townson and Nibbs, 2002).

Ligand cross-competition studies showed that similarly to hCCRL1, mCCRL1 exhibits high affinity binding of CCL19, CCL21 and CCL25 without subsequent calcium flux. Binding affinity of mCCRL1 is highest for CCL19, and slightly lower for CCL21 and CCL25. Interestingly, unlike hCCRL1, mCCRL1 does not bind mCXCL13 (Townson and Nibbs, 2002). CCL19, CCL21 and CCL25 were later confirmed as the ligands for CCRL1 in 2007 (Heinzel et al., 2007).

The function of CCRL1 was further assessed *in vitro* using HEK293 cells transfected with hCCRL1. CCL19 was added to cultures of HEK-hCCRL1 and HEK-hCCR7 and the fate of internalised chemokine determined using trichloroacetic acid precipitation, an assay often used to determine chemokine degradation. Cells transfected with hCCRL1 showed an accumulation of CCL19, moreover these cells were capable of degrading high levels of CCL19 compared to control HEK-hCCR7 cells. Furthermore, when in continuous culture with excess CCL19, hCCRL1 transfectants were able to degrade the majority of CCL19 whereas hCCR7 transfectants performed equally to non-transfected controls (Comerford et al., 2006). In keeping with a scavenging function, TEP cells transfected with CCRL1 have been

shown to inhibit the CCL19 and CCL21 migration of BM derived DCs *in vitro* (Ulvmar et al., 2014).

Expression of mCCRL1 was analysed by Townson and Nibbs using Northern blot analysis and RT-PCR. CCRL1 was detected in non-hematopoietic organs as previously described, including heart, testis, and skeletal muscle. mCCRL1 was also detected in the spleen, and at lower levels in Peyer's patches, lymph nodes and peripheral blood. Northern blot analysis of hCCRL1 failed to detect expression by leukocytes, contrary to previous reports (Townson and Nibbs, 2002, Gosling et al., 2000).

One study used CCRL1-eGFP knock in mice to map protein expression of CCRL1 in heterozygous mice, which were phenotypically indistinguishable from WT mice. Flow cytometric analysis confirmed that hematopoietic cells from BM, spleen and lymph nodes do not express CCRL1. Immunofluorescence revealed CCRL1 expression by non-hematopoietic cells within the thymus, intestine, epidermis, and subcapsular sinus of the lymph node. Contrary to previous reports, CCRL1 expression was undetectable in the heart, kidney, spleen and brain (Heinzel et al., 2007). A recent publication has also used these CCRL1-eGFP mice, and a specific anti-CCRL1 antibody, to further characterise the expression of CCRL1 within the lymph node. Here, CCRL1 is expressed by a particular subset of lymphatic endothelial cells that line the outer wall of the subcapsular sinus (Ulvmar et al., 2014).

Given the *in vitro* data showing a role for CCRL1 in chemokine degradation (Comerford et al., 2006), CCRL1-eGFP homozygous mice were used to investigate CCRL1 deficiency *in vivo*. Analysis of the lymph nodes from these mice revealed a reduction in MHC-II^{hi} DCs, but no alteration in the number of MHC-II^{lo} DCs. This suggests a requirement for CCRL1 in steady state homing of DCs to the lymph node via afferent lymphatics. Interestingly, epicutaneous application of FITC normalised the numbers of MHC-II^{hi} DCs in the lymph nodes suggesting that activation of DCs must facilitate additional homing mechanisms to compensate for the lack of CCRL1 (Heinzel et al., 2007). A more recent study has further examined the lymph nodes in resting CCRL1$^{-/-}$ mice by flow cytometry and immunofluorescence. This study revealed an accumulation of CCR7^{+} DCs at the subcapsular sinus, which is coupled with a reciprocal decrease in the number of CCR7^{+} DCs within the lymph node. Immunofluorescent staining of CCL21 in CCRL1$^{-/-}$ lymph nodes revealed disrupted patterning of CCL21 in the subcapsular sinus compared to littermate controls. These experiments show that expression CCRL1 at the subcapsular sinus is necessary to create gradients of CCL21 to allow effective migration of CCR7^{+} DCs into the lymph node (Ulvmar et al., 2014).

Although the evidence favours a scavenging role for CCRL1, there are other functions this ACKR could have. One such function could be the transcytosis of chemokines, similar to endothelial DARC. Over-expression of cavolin-1, a negative regulator of caveolae-mediated endocytosis significantly reduced the ability of HEK-hCCRL1 cells to internalise CCL19 (Comerford et al., 2006). This suggests that CCRL1 uses caveolae to mediate chemokine internalisation, rather than β-arrestin dependent clathrin-coated pits used by classical chemokine receptors. Although

caveolae have been implicated in transcytosis, it is important to note that transcytosis mediated by endothelial DARC is cavolin-1 independent (Zhao et al., 2011). In addition, a more recent study shows the recruitment of β-arrestins by hCCRL1 upon stimulation with CCL19, CCL21 and CCL25 (Watts et al., 2013). These conflicting data on signalling and vesicular involvement downstream of CCRL1 are yet to be clarified. A recent study co-expressed CCRL1 with many different classical chemokine receptors. FRET analysis of cells co-transfected with CCRL1-GFP and CXCR3-Venus showed heteromerisation. In addition, this study showed that co-expression of CCRL1 with CXCR3 resulted in the inhibition of chemotaxis of HEK293 cells in response to CXCL9 and CXCL10, suggesting that CCRL1 may influence the availability of chemokines other than CCR7L and CCR9L via this mechanism (Vinet et al., 2013). The *in vivo* significance this data has not yet been shown.

Consistent with a scavenging function, CCRL1$^{-/-}$ mice have increased levels of CCL21 in the serum (Comerford et al., 2010). The levels of CCL19 and CCL21 in the lymph nodes of CCRL1 deficient mice are less clear, one study reported increased levels of both chemokines in lymph nodes from CCRL1$^{-/-}$ mice, however a more recent study found no difference in the level of either chemokine, using the same strain of CCRL1$^{-/-}$ mice (Comerford et al., 2010, Ulvmar et al., 2014). Further analysis of CCRL1$^{-/-}$ mice using a model of MOG induced experimental autoimmune encephalitis (EAE) has implicated CCRL1 in CD4 T cell differentiation and the kinetics of the immune response. This study showed that CCRL1$^{-/-}$ mice have an earlier onset of EAE with more severe symptoms. In depth analysis of lymph nodes

during EAE revealed fewer $CCR6^+$ CD4 T cells within the $CCRL1^{-/-}$. In contrast, the spleen of $CCRL1^{-/-}$ mice had increased cellularity, specifically of $CCR6^+$ T cells. During EAE, $CCRL1^{-/-}$ mice also had fewer Th1 cells per Th17 cell in the spleen and spinal cord, along with increased levels of IL-23 in the spleen. IL-23 causes differentiation of Th17 cells, leading to the conclusion that CCRL1 plays a role in the suppression of Th17 responses. Administration of anti-CCL21 neutralising antibodies during the time course of EAE delays the onset of disease in $CCRL1^{-/-}$ mice compared to WT, therefore suggesting that CCRL1 mediates its effects in this model via CCL21 (Comerford et al., 2010).

ACKRs, including CCRL1, have been implicated in cancer. These studies primarily show a reduced ACKR expression in cancer tissue compared to healthy tissue (Zhu et al., 2013, Zeng et al., 2011, Feng et al., 2009). All studies correlate a lack of ACKR co-expression (DARC, D6 and CCRL1) with lymph node metastasis and poor survival (Feng et al., 2009, Hou et al., 2013, Zeng et al., 2011, Zhu et al., 2013). The effect of CCRL1 expression alone on cancer development has not been clearly addressed, however low CCRL1 expression has been correlated with lymph node metastasis (Feng et al., 2009). Many questions in this area of research are yet to be answered.

1.5.5 CCRL1 in Thymus Function

Heinzel and colleagues carried out the first detailed analysis of CCRL1 within the thymus. Using CCRL1-eGFP mice, they mapped thymic expression of CCRL1. Immunofluorescence was used to show expression of CCRL1 exclusively by TEC, specifically perivascular epithelial cells of the CMJ and medulla, and subcapsular epithelial cells. This method revealed no GFP^+ cells within the thymic cortex. $ERTR7^+$ fibroblasts were negative for GFP, as were tomato lectin stained endothelial cells. Flow cytometric analysis confirmed expression of CCRL1 by only EpCAM-1^+ TECs. cTEC were identified by flow cytometry using the marker CDR-1; these cells expressed intermediate levels of GFP. Flow cytometry excluded CCRL1 expression from the population of UEA-1^+ mTEC (Heinzel et al., 2007). More recent publications have confirmed that thymic expression of CCRL1 is primarily cTEC (Bunting et al., 2013, Rode and Boehm, 2012, Ribeiro et al., 2013), however the latest report showed intermediate levels of CCRL1 expression by $CD80^+$ mTEC in the postnatal thymus (Ribeiro et al., 2014). Analysis of the embryonic thymus revealed CCRL1 expression from E13.5 by TEC of the SCZ (Heinzel et al., 2007), this was confirmed using flow cytometry in a more recent publication (Ribeiro et al., 2014).

The thymus from WT, heterozygous and homozygous CCRL1-eGFP mice were analysed to assess thymic function (Heinzel et al., 2007). This study reported no defect in T cell development in the absence of CCRL1. Thymus cellularity and proportions of DN, SP and DP thymocytes were unaltered. Thymocyte proliferation and apoptosis were similar in WT and CCRL1-$^{GFP/GFP}$ mice. Distribution of $CD25^+$

DN thymocytes was assessed in the CCRL1 $^{GFP/GFP}$ thymus, and was comparable to those in WT mice. In addition, the number of $CD4^+CD69^+CD62L^-$ RTEs were reported as normal in CCRL1 $^{GFP/GFP}$ mice. Combined, these results suggested CCRL1 was not needed for postnatal thymus function. Analysis of the early embryo (E12.5 and E13.5) showed similar numbers of $CD45^+$ cells in the WT and CCRL1 $^{GFP/GFP}$ thymus. These findings indicate that CCRL1 is not needed for the recruitment of progenitor cells to the embryonic anlagen. Overexpression of CCRL1 by $Foxn1^+$ TEC reduces the thymus cellularity in the embryo (Heinzel et al., 2007), suggesting that CCRL1 may play a role in the recruitment of progenitor cells to the embryonic thymus but in the absence of CCRL1, a compensatory mechanism is in place.

The most detailed analysis of CCRL1 in the thymus was recently reported by Bunting and colleagues (Bunting et al., 2013). They describe the $CCRL1^{-/-}$ thymus as dramatically larger with increased cellularity compared to WT counterparts. They report a disrupted architecture of the $CCRL1^{-/-}$ thymus, containing fewer, but significantly larger medullary areas. Flow cytometric analysis of the $CCRL1^{-/-}$ thymus revealed increased proportions of SP4 thymocytes. Within the SP thymocyte population, there were higher proportions of $CD69^+CD62L^-$ immature thymocytes. Analysis of the localisation of $CD25^+CD44^+$ DN thymocytes revealed an accumulation of these cells within the medulla. Pixel analysis of CCL25 staining in WT mice showed a reduction from the cortex inwards towards the medulla, suggestive of a chemokine gradient. This gradient is lost in the $CCRL1^{-/-}$ thymus, and is presumably responsible for the accumulation of DN thymocytes within the

medulla. Analysis of chemokine levels by ELISA shows a reduction in CCL19 and CCL25 in the CCRL1$^{-/-}$ thymus, this finding is less intuitive considering the role of CCRL1 as a scavenging receptor. It is argued the reduction in chemokine levels is the product of altered chemokine production due to an increased number of mTEC. In addition, *in vitro* analysis of thymic lobes treated with CCL19 results in increased egress of CD69^{+}CD62L^{-} CD4 and CD8 T cells. This increase in RTE is also reported *in vivo* by increased proportions of CD3^{+}CD4^{+}CD44^{-}CD69^{-}CD24^{+} cells in the spleen. Moreover, analysis of the CCRL1$^{-/-}$ spleen revealed increased proportions of CD3^{+}CD4^{+}CD8^{+} peripheral DP cells, suggesting that DP thymocytes are leaking out of the thymus. Aged (8-10 month) CCRL1$^{-/-}$ mice showed spontaneous autoimmunity that resembles Sjögren's syndrome. This was characterised by immune infiltrate into the submandibular salivary gland and liver. This autoimmune phenotype was proposed to be mediated by autoreactive T cells generated due to defective thymic function in the absence of CCRL1 (Bunting et al., 2013).

Several studies have used CCRL1 as a tool to probe thymus function. One such study crossed IL-7-YFP and CCRL1-GFP reporter mice and showed that within the TEC compartment, IL-7^{+} cTECs express high levels of CCRL1. In addition, a proportion of IL-7^{-}CCRL1^{+} cTECs were also identified, suggesting the potential use of CCRL1 as a marker of cTEC heterogeneity (Ribeiro et al., 2013). These dual reporter mice have been used more recently to show that cTEC acquire expression of CCRL1 after E12.5 of gestation and by E18.5 of gestation, all CCRL1^{hi} TEC are IL-7^{+} as seen in the postnatal thymus (Ribeiro et al., 2014). Development of CCRL1^{+} cTEC was blocked in the severely lymphopenic Rag2$^{-/-}$IL2rg$^{-/-}$ strain of mouse,

suggesting that cTEC maturation is regulated by crosstalk between TEC and immature thymocytes. This study also identified a population of CCRL1^{int} CD80^{+} mTEC; these cells are not present during embryogenesis, but are clearly visible 5 days after birth. CCRL1^{int} mTEC are rare in Rag2$^{-/-}$ thymi, but were found to be restored in Rag2$^{-/-}$-Marilyn TCR Tg mice, suggesting that the development of CCRL1^{int} mTEC is closely linked with T cell selection (Ribeiro et al., 2014). Another study used CCRL1-DTR mice to selectively ablate the cTEC compartment. These experiments revealed a sexually dimorphic ability of cTECs to regenerate, a mechanism linked to androgen receptor expression within the TEC compartment (Rode and Boehm, 2012).

Collectively, although the above studies indicate CCRL1 expression by thymic stroma, the precise expression pattern is unclear. Moreover, given conflicting reports of the thymic phenotype in CCRL1 deficient mice, the role of this molecule in thymus development and function remains controversial. Thus a major goal of this thesis is to investigate the expression pattern of CCRL1 within the thymus, and determine the effect of CCRL1 expression on thymic function.

THESIS AIMS

As discussed in this introduction, the sequential stages of T cell development have been well described. However, the precise involvement of the atypical chemokine receptor, CCRL1, in these processes is yet to be fully elucidated.

The general aims and objectives of this thesis are as follows:

- To map the expression of CCRL1 within the embryonic and adult thymus
- To identify the cell type(s) which express CCRL1
- To study the role of CCRL1 in sequential stages of T cell development, using two different strains of CCRL1 deficient mice

CHAPTER 2: MATERIALS AND METHODS

2.1 Mice

Timed matings were obtained by placing a male mouse into a cage with one or two female mice. The presence of a vaginal plug was designated as day zero of gestation (E0). This method made it possible to identify the exact age of mice used in this study. Adult mice were 8-10 weeks old. Details of mouse strains used in this thesis are in Table 1.

Table 1. Mouse strains

Mouse Strain	CD45 Isotype	Source
C57Bl/6	CD45.2	Harlan
BoyJ	CD45.1	BMSU
CCRL1$^{-/-}$	CD45.2	R. Nibbs, University of Glasgow (Comerford et al., 2010)
CCRL1-eGFP	CD45.2	T. Boehm, Max Plank Institute (Heinzel et al., 2007)
Plt	CD45.2	BMSU (Mori et al., 2001)
RAG2pGFP	CD45.2	BMSU (Boursalian et al., 2004)
CCL25$^{-/-}$	CD45.2	BMSU

2.2 Isolation of Cells From Primary Tissue

2.2.1 Tissue Isolation

Lymphoid tissue was dissected using forceps and scissors and placed in Roswell Park Memorial Institute (RPMI)-1640 media (Sigma). Tissue was cleaned of blood and surrounding connective tissue using forceps, before subsequent processing. [redacted] Embryos were removed from the uterus and washed in phosphate buffered saline (PBS). Placentas and amniotic sacs were removed from the uterus and the embryos were placed in RPMI. Thymic lobes were then dissected from the thoracic tree of the embryo using fine forceps.

2.2.2. Isolation of Haematopoietic Cells

Haematopoietic cells from the adult thymus were obtained by mincing the thymic lobes with sharp scissors in eppendorfs containing 1mg/ml collagenase D and 0.2mg/ml DNase in RPMI. Eppendorfs were placed in a thermomixer at 37°C for 30 minutes. Disaggregation was aided by gentle pipetting of the cells. The enzymatic reaction was stopped by the addition of 1mM EDTA in RPMI-1640 containing 10% heat inactivated fetal calf serum (FCS) (Invitrogen). Cell suspensions were filtered through a 70μm cell strainer (BD).

Haematopoietic cells were isolated from embryonic thymic lobes by placing the lobes in eppendorfs containing 1mg/ml collagenase D (Roche) and 0.2mg/ml DNase (Roche). Eppendorfs were incubated in a thermomixer at 37°C for 15 minutes. A

single cell suspension was obtained by gentle pipetting. The enzymatic reaction was stopped as described above.

Haematopoietic cells were isolated from spleen and lymph nodes by gently forcing the tissue through a 70µm cell strainer (BD) and rinsing thoroughly with FACS buffer. FACS buffer consisted of Ca^{2+} and Mg^{2+} free PBS, supplemented with 0.3mM EDTA (Sigma), and 1% bovine serum albumin (BSA) (Sigma).
Spleen samples were centrifuged at 350g for 10 minutes, and the subsequent cell pellet treated with 2ml ACK red blood cell lysis buffer (Invitrogen) for 5 minutes at 4°C. Splenocytes were then washed with 20ml RPMI containing 10% FCS.

Blood was acquired from either the tail vein, or from the heart in a terminal procedure, into tubes containing an appropriate volume of 100mM EDTA. Blood was red blood cell lysed by the addition of an appropriate volume of BD Pharm Lyse buffer (BD). Samples were incubated with this buffer at room temperature for 5 minutes before being washed with 20ml RPMI containing 10% FCS.

All single cell suspensions were centrifuged at 350g for 10 minutes at 4°C and then resuspended in an appropriate volume of FACS buffer. All cells were counted using Count Bright Absolute Counting Beads (Invitrogen).

2.2.3 Isolation of Stromal Cells

Embryonic thymic lobes were suspended in 0.25% trypsin (Sigma) diluted in 0.02% EDTA and incubated at 37°C for 10-20 minutes (exact timing of incubation

depended on age of embryo). Complete disaggregation was ensured by gentle pipetting until a single cell suspension was observed. Enzyme activity was quenched by adding an equal volume of RPMI containing 10% FCS followed by centrifugation at 400g for 10 minutes at 4°C.

Stromal cells were isolated from the adult thymus by mincing the tissue with sharp scissors followed by enzymatic digestion with liberase (Roche) and 0.2mg/ml DNase for 30 minutes at 37°C in a thermomixer. After 15 minutes the proportion of media containing free cells was removed and replaced with fresh enzyme mix. The reaction was stopped by the addition of 1mM EDTA in RPMI containing 10% FCS and the resulting cell suspension was filtered through a 70μm cell strainer. Cells were centrifuged at 350g for 10 minutes at 4°C. Cell pellets were resuspended in an appropriate volume of FACS buffer and cells were counted using Count Bright Absolute Counting Beads.

2.3 Surface Staining of Cells for Flow Cytometry

Cells from WT or CCRL1-GFP thymi were surface stained using for flow cytometry using the same protocol. Cell suspensions were incubated with purified anti-CD16/32 (eBioscience) for 15 minutes, and then an appropriate volume of cells were transferred into a 96 well v-bottom plate and pelleted by centrifugation at 350g for 4 minutes at 4°C. The supernatant was flicked off and cells were resuspended in 50-100μl of primary antibody diluted in FACS buffer (volume of antibody was dependent upon number of cells to be stained). Cells were incubated for 30 minutes

at 4°C and then washed twice with 200µl FACS buffer. During anti-CCR7 staining, cells were incubated with the primary antibody cocktail at 37°C for 30 minutes.

Once staining was complete, cells were washed and resuspended in an appropriate volume of FACS buffer and transferred to FACS tubes. An LSRFortessa was used to collect the data and FlowJo software was used for analysis. See Table 2 for details of antibodies used for flow cytometry. Cells stained with each antibody individually were used for compensation, and a combination of unstained cells or fluorescence minus one were used to set gates where appropriate.

Table 2. Antibodies Used for Flow Cytometry.

Target antigen and conjugate	Clone	Source	Working dilution
CD45.2 AlexaFluor-700	104	ebioscience	1:200
CD45 PE-Cy7	30-F11	ebioscience	1:500
CD45.1 eFluor-450	A20	ebioscience	1:50
CD4 Brilliant Violet-605	RM4-5	Biolegend	1:200
CD4 PerCP-Cy5.5	RM4-5	BD	1:600
CD4 eFluor450	RM4-5	ebioscience	1:100
CD3 PerCP	145-2C11	BD	1:50
CD8α Brilliant Violet-510	53-6.7	Biolegend	1:200
CD8α V500	53-6.7	BD	1:200
CD8α APC	53-6.7	ebioscience	1:600
CD44 PE-Cy7	IM7	ebioscience	1:1000
CD25 FITC	PC61	BD	1:500
CD25 APC	PC61.5	ebioscience	1:1000
TCRβ APC-eFluor-780	H57-5	ebioscience	1:100
TCRγδ PE	GL3	ebioscience	1:600
CD69 PerCP-Cy5.5	H1.2F3	ebioscience	1:100

Target antigen and conjugate	Clone	Source	Working dilution
CD62L APC	MEL-14	ebioscience	1:1000
CD19 PE-Cy7	1D3	ebioscience	1:600
B220 FITC	RA3-6B2	ebioscience	1:400
CD11c eFluor450	N418	ebioscience	1:50
Lineage cocktail eFluor450 CD3, B220, CD11b, TER-119, Ly-G6	17A2, RA3-6B2, M1/70, TER-119, RB6-8C5	ebioscience	1:15
CD117 PerCP-eFluor-710	2B8	ebioscience	1:70
CCR7 PE	4B12	ebioscience	1:50
CCR9 PerCP-eFluor710	CW-1.2	ebioscience	1:500
TER-119 AlexaFluor-700	TER-119	Biolegend	1:100
EpCAM PerCP-eFluor710	G8.8	ebioscience	1:1000
Ly51 PE (used to define cortex)	BP-1	BD	1:1000
CD31 PE-Cy7	390	ebioscience	1:600
Podoplanin eFluor660	8.1.1	ebioscience	1:400
MHC-II (I-A/I-E) AlexaFluor-700	M5/114.15.2	ebioscience	1:200
CD80 Brilliant Violet 421	16-10A1	Biolegend	1:200
Foxp3-eFluor450	FJK-16s	ebioscience	1:100
AIRE AlexaFluor488	5H12	ebioscience	1:100

2.4 Staining of Intracellular Antigens for Flow Cytometry

The staining protocols used to detect intracellular antigens varied depending on i) the antigen being detected, and ii) whether preservation of GFP was needed.

Detection of Aire was always performed in conjunction with IC fixation buffer (eBioscience). Once surface staining was complete, cells were incubated with 200µl IC fixation buffer for 30 minutes at room temperature. Cells were then washed twice in 200µl 1x perm buffer (eBioscience). Anti-Aire-488 was diluted in 1x perm buffer, and then added to cells. Cells were incubated at 4°C for 20 minutes, then washed twice in 1x perm buffer, before being resuspended in FACS buffer. Aire staining was only performed on WT cells, therefore preservation of GFP was not needed.

If preservation of GFP was not needed, then detection of Foxp3 was performed using a Foxp3 staining kit in accordance with manufacturer's instructions (eBioscience). Briefly, following surface staining, cells were incubated with 200µl fixation/permeabilisation working solution for 30 minutes at room temperature. Cells were then washed twice in 200µl 1x perm buffer Anti-Foxp3-efluor450 was diluted in 1x perm buffer and added to cells. Cells were incubated at 4°C for 20 minutes, then washed twice in 1x perm buffer, before being resuspended in FACS buffer.

If preservation of GFP was needed, then detection of Foxp3 was performed using a BD Cytofix/Cytoperm kit (BD). Following surface staining, cells were incubated in 200µl Cytofix/Cytoperm solution for 30 minutes at room temperature. Cells were then washed twice in 200µl 1x perm/wash buffer. Anti-Foxp3-efluor450 was diluted

in 1x perm/wash buffer and added to cells. Cells were incubated at 4°C for 20 minutes, then washed twice in 1x perm/wash buffer, before being resuspended in FACS buffer.

2.5 Magnetic Activated Cell Sorting

Cell suspensions from digested adult thymus were depleted of $CD45^+$ haematopoietic cells to increase the proportion of stromal cells, for stromal cell analysis by flow cytometry. This was achieved using the cell separation system from Miltenyi biotech according to manufacturer's instructions. Briefly, cells were incubated with anti-CD45 microbeads (10µl of beads per 10^6 cells) at 4°C for 15 minutes. Cells were then washed using FACS buffer and resuspended in the appropriate volume of FACS buffer. Cell suspensions were added to LD columns that had been pre-washed with FACS buffer. Columns were rinsed with at least 5ml FACS buffer, and the flow-through collected.

2.6 Tissue Sectioning and Fixation

Non-GFP tissue was embedded in OCT compound (Fisher Scientific) and frozen using dry ice. The block of tissue was then transferred to a cryostat where it equilibrated to -20°C. Tissue was mounted on a metallic cryostat chuck using OCT compound. The cryostat was used to cut 8µm sections, which were collected, onto either multi-spot or superfrost glass slides (Fisher Scientific). Sections were dried at room temperature for one hour before fixation in acetone (Sigma) at 4°C for 20

minutes. Fixed tissue sections were allowed to dry for 5 minutes at room temperature and were then stored at -20°C until use.

GFP tissue was fixed prior to freezing. This was achieved by incubating the tissue in a solution of 2-4% PFA containing 10% sucrose (Sigma) for 4 hours at 4°C. Tissue was then washed in 20% sucrose overnight at 4°C and then embedded in OCT compound and frozen on dry ice. Tissue was sectioned as described above, but was collected onto only superfrost slides, and then stored at -80°C until use.

2.7 Immunofluorescent Labelling of Frozen Sections

Sections were removed from storage and left at room temperature to thaw within grip seal bags. Staining buffer consisted of PBS containing 10% FCS and 0.5% Tween-20 (Sigma). Once thawed, sections were blocked for 20 minutes using 10% serum obtained from the species in which the secondary antibody was raised. Serum was diluted using staining buffer. Serum was blotted off and the area surrounding each section was dried using tissue. 50-70µl of primary antibody mix or staining buffer only (for control sections) was added to each section. The volume added depended on the area to be covered. All steps were performed in the dark and at room temperature. Sections were incubated with the primary antibody for 1 hour, and then washed for 15 minutes in staining buffer. Any secondary and tertiary antibodies needed were applied using the same method but incubation periods were reduced to 30 minutes. Control sections were treated with no primary but all subsequent antibodies. GFP was detected using anti-GFP antibody. Details of all antibodies used for immunofluorescence in Table 3 and Table 4.

Stained slides were submerged in F4',6-diamidino-2-phenylindole (DAPI, 300nM in distilled water, Invitrogen) for 20 seconds, followed by three 20 second washes in PBS. Slides were mounted with Prolong Gold (Invitrogen) and a cover slip was added and sealed using clear nail varnish. Slides were left to dry at room temperature overnight and then stored at -20°C. Images were acquired using a Zeiss LSM 510 Meta, or Zeiss LSM 710 Zen confocal microscope. Image analysis was performed using Zeiss AIM image analysis software, ZenLite and ImageJ.

Table 3. Antibodies Used for Immunofluorescent Staining of Murine Tissue.

Target antigen and conjugate	Clone	Source	Working dilution
CD45 biotin	30-F11	ebioscience	1:200
EpCAM AF-647	G8.8	ebioscience	1:100
CD8β biotin	H35-17.2	ebioscience	1:200
CD25 FITC	PC61	BD	1:500
CD31 biotin	390	ebioscience	1:100
CD205 AF-488 (used to define cortex)	205yekta	eBioscience	1:100
β5T	Polyclonal	MBL International	1:100
Keratin-5 (used to define medulla)	Polyclonal	Covance	1:1000
Keratin-8 (used to define cortex)	KS8.7	Progene	1:10
Pan-cytokeratin FITC	C-16	Sigma	1:600
α-SMA Cy3	1A4	Sigma	1:400
CCRL1	C16	Santa Cruz	1:50
CD25 APC	PC61.5	ebioscience	1:1000
Podoplanin supernatant		A. Farr*	1:10

Target antigen and conjugate	Clone	Source	Working dilution
Pan-endothelial cell antigen	MECA-32	BD	1:100
CD31	MEC 13.3	BD	1:100
CD49f (integrin α 6) biotin	GoH3	ebioscience	1:100
Fibronectin	Polyclonal	Millipore	1:100
Laminin	LAM-89	Sigma	1:1000
ER-TR7 supernatant		W. van Ewijk**	1:10

AF, AlexaFluor
* Grown from a hybridoma cell line, gift from Andy Farr, University of Washington
** Grown from a hybridoma 1:2 cell line, gift from W. van Ewijk, Leiden University, Netherlands

Table 4. Secondary Antibodies Used for Immunofluorescence.

Reactivity and conjugate	Host	Source	Working dilution
Anti goat IgG AF647	Donkey	Invitrogen	1:100
Anti goat IgG AF488	Donkey	Invitrogen	1:200
Anti goat IgG AF555	Donkey	Invitrogen	1:400
Anti rabbit IgG AF647	Donkey	Invitrogen	1:100
Anti rabbit IgG AF488	Donkey	Invitrogen	1:200
Anti rabbit IgG AF555	Donkey	Invitrogen	1:400
Anti rat IgG AF546	Donkey	Invitrogen	1:400
Anti rat IgG AF555	Donkey	Invitrogen	1:400
Anti rat IgG AF647	Chicken	Invitrogen	1:100
Anti rat IgM AF594	Goat	Invitrogen	1:500
Anti FITC AF488	Rabbit	Invitrogen	1:200
Anti rabbit FITC	Goat	Southern Biotech	1:100
Anti hamster IgG biotin	Rabbit	Invitrogen	1:200
Anti mouse IgG2b AF488	Goat	Invitrogen	1:200
Anti mouse IgG2b AF555	Goat	Invitrogen	1:200
Anti GFP AF488	Rabbit	Invitrogen	1:200
Anti GFP	Goat	Abcam	1:400

Reactivity and conjugate	Host	Source	Working dilution
Streptavidin 647	-	Invitrogen	1:100
Streptavidin 488	-	Invitrogen	1:200
Streptavidin 555	-	Invitrogen	1:1000

AF; AlexaFluor, GFP; green fluorescent protein

2.8 Preparation of Human Thymus for Immunofluorescence

Human thymus tissue was obtained from young children undergoing cardiac surgery. Tissue was washed in PBS, and cut into small pieces (approx. 1cm^3) and frozen using dry ice. Cryosections were generated and sections were stained using the same methods described for murine tissue. Details of antibodies used for the detection of human antigens can be found in Table 4.

Table 4. Antibodies Used for Immunofluorescent Staining of Human Thymus.

Target antigen and conjugate	Clone	Source	Working dilution
CD4 FITC	RPA-T4	ebioscience	1:100
CD8a biotin	HIT8a	ebioscience	1:100
EpCAM biotin (used to define medulla)	1B7	ebioscience	1:100
CD205 AF647 (used to define cortex)	HD30	Biolegend	1:100
CCRL1	13E11	J. Chiba*	1:200
CD31	JC70	ebioscience	1:200

* Gift from J. Chiba, Department of Biological Science and Technology, Tokyo University of Science, Japan (Takatsuka et al., 2011)

2.9 Genotyping of CCRL1$^{-/-}$ and CCRL1-eGFP mice

2.9.1 Extraction of DNA

Ear clips from mice were placed in autoclaved eppendorfs, and 75µl of lysis buffer (25mM NaOH, 0.2mM EDTA in RNAse free water) was added to each sample. Eppendorfs were incubated at 95°C for 30 minutes and were subsequently neutralised using an equal volume of 40mM Tris-HCl. Samples were then thoroughly vortexed and kept at 4°C until use.

2.9.2 Genotyping

A 10µl PCR mix was made which contained all appropriate primers (20µM), MyTaq Red Mix (Bioline), and water. This mix was combined with 2µl DNA in 96 well PCR plates (4titude). PCR reactions were carried out in an Eppendorf Thermocycler. Details of the primers used are summarised in Table 5 and Table 6.

Genotyping of CCRL1$^{-/-}$ mice required the following PCR conditions: 5 mins (94°C), followed by 37 cycles of 15 seconds (94°C), 30 seconds (55°C), 45 seconds (72°C), then 72°C for 10 minutes. Genotyping of CCRL1-GFP mice required the following PCR conditions: 5 mins (95°C), followed by 29 cycles of 30 seconds (95°C), 30 seconds (55°C), 1 minute 30 seconds (72°C), then 72°C for 10 minutes.

At the end of each PCR, samples were kept at 4°C until being run on agarose gels. 1.5% agarose gels containing 1x SybrSafe (Invitrogen) were cast. Once the gel had set, combs were removed and the gel was submerged in an electrophoresis tank

containing 1x bionic buffer (Sigma). 10µl of PCR product was loaded into each well and gels were run at 80V until clear separation of bands was visible. 100bp or 1kb DNA ladder (Invitrogen) was included on the gel to allow the sizes of the PCR products to be determined. Product visualisation was achieved using GeneSnap software.

Table 5. Primers Used for Genotyping CCRL1$^{-/-}$ Mice.

Primer	Primer sequence
11com5	TGC TGG TGA GCT CTG GGT TC
11wt5	AAT CGC CAC AAC TAC GGA GTT C
3'IRES	CCC TAG ATG CAT GCT CGA CG

Table 6. Primers Used for Genotyping CCRL1-GFP Mice.

Primer	Primer sequence
P1	TAG GAT TTA GTG ACT AAG AGC
P2	CAC ACA CAG GCA ACA GAT CC
P3	TGA ACT TGT GGC CGT TTA CGT C

2.10 Phenotyping of RAG2pGFP Mice

20-40µl of blood was obtained from the tail vein in tubes containing 100µl 100mM EDTA. Red blood cells were lysed using BD Pharm Lyse buffer as described previously, and the subsequent cell suspension was analysed by flow cytometry using an LSRFortessa. The presence of GFP^{+} cells confirmed RAG2pGFP heterozygous or homozygous mice.

2.11 Quantitation of Chemokine Levels

2.11.1 Preparation of Samples for Chemokine Measurement

The thymus was weighed and immersed in 500µl homogenisation solution (Tissue Protein Extraction Reagent (Pierce) containing 1 Complete Protease Inhibitor Cocktail tablet (Roche) per 10ml). The tissue was homogenised (OMNI International) in this solution. The resulting protein lysate was transferred into eppendorfs and centrifuged at 10,000g for 5 minutes at 4°C and the supernatants removed for analysis. The total protein content of the lysate was determined using a BCA protein assay kit (Pierce) according to manufacturer's instructions and using serial dilutions of BSA (Merck Millipore) as standards.

2.11.2 ELISA

CCL19, CCL21 and CCL25 levels were measured using DuoSet ELISA kits (R&D Systems), according to manufacturer's instructions. All steps of the ELISA were carried out at room temperature. ELISA plates (Nunc, Thermo Scientific) were coated with 100µl capture antibody and left overnight (1µg/ml anti-CCL25, 2µg/ml anti-CCL19, 4µg/ml anti-CCL21). Plates were then washed 3 times with PBS containing 0.05% Tween-20 (Sigma) using a multichannel pipette, and blocked with 300µl reagent diluent (1% BSA in PBS) for 1 hour. Standards were prepared following manufacturer's instructions. Plates were washed and 100µl detection antibody was added to each well (600ng/ml anti-CCL25, 100ng/ml anti-CCL19, 50ng/ml anti-CCL21). Plates were incubated for 2 hours and washed as before. 100µl streptavidin-HRP diluted to 1:200 was added to each well and incubated for

20 minutes in the dark. Plates were washed and 100µl substrate solution (R&D Systems) was added to each well. Plates were incubated in the dark for 20 minutes. 50µl 1M HCl (Sigma) was added to each well and the OD read at 450nm. A standard curve was generated using GraphPad Prism software and from this, the sample chemokine concentrations were calculated.

2.12 Generation and Maintenance of TEP-CCRL1

2.12.1 TEP-CCRL1 Generation

TEP cells (Tanaka et al., 1993b) were retrovirally transfected with CCRL1 by Kyoko Nakamura at the University of Birmingham.

2.12.2 Maintenance of TEP-CCRL1 cells

TEP-CCRL1 cells were cultured in Dulbecco's modified Eagles medium (DMEM) (Sigma) with 10% FCS, 2mM L-glutamine (Sigma), penicillin and streptomycin (Sigma). Cells were passaged every 2-3 days once 80% confluency was achieved. To passage cells, all media was removed from the 75cm^2 culture flask (Corning) and cells were rinsed with PBS. Adherent cells were then treated with TrypLE Express (Invitrogen) at a volume of 1ml/25cm^2 surface area. After this process, cells were examined using an inverted microscope to ensure all cells were detached. TrypLE Express was then inactivated by the addition of culture media and the resulting cell suspension was transferred to a 15ml tube. Cells were pelleted via centrifugation at 200g for 6 minutes at room temperature. Pelleted cells were either resuspended in

warm culture media, and transferred to new culture flasks for further use, or were frozen (see below).

2.12.3 Cryopreservation of Cells

Cell pellets were resuspended in culture media containing 10% Dimethyl Sulphoxide (DMSO, Sigma) and transferred to a 1ml cryovial (Nunc, Thermo Scientific) which was placed in a Nalgene Mr Frosty freezing container (Sigma), precooled to 4°C. The freezing container was then transferred to -80°C to allow a 1°C/minute cooling rate. Once frozen, vials were transferred to liquid nitrogen for long-term storage.

2.13 Transmigration Assay

The 5µm-pore polycarbonate filters (Corning) of 6.5mm diameter cell culture inserts were coated with murine collagen IV (BD Biosciences, Oxford, UK) for 4 hours at room temperature. Inserts were rinsed twice with PBS to remove excess collagen, and were then transferred to 12 well plates containing 600µl cell culture media (as described previously). TEP-CCRL1 or TEP-GFP cells were seeded onto the filter in 100µl (at a concentration of $2x10^4$cells/insert), and were left to grow for two days. One hour before the assay, the medium in the bottom wells was changed to RPMI + 2% FCS + chemokine or RPMI + 2% FCS alone. Thymocytes were isolated by forcing the tissue through a 70µm cell strainer and the final cell concentration adjusted to $1x10^6$ cells/ml RPMI + 2% FCS. Cell culture media was removed from the upper well and replaced with 100µl cell suspension. Plates were incubated for 3 hours at 37ºC with 5% CO_2. After incubation, the plate was put on ice, the inserts removed and EDTA (Sigma-Aldrich) was added to the wells at 5nM to detach any

cells which had adhered to the bottom of the well. Cells from the lower chamber were counted and stained as previously described.

2.14 Generation of Irradiation Bone Marrow Chimeras

Baytril was used as an antibiotic and was added to drinking water of recipient mice one week prior to irradiations. Mice were [redacted] irradiated with two separate doses of 5.5Gy. Bone marrow cells were harvested from the femur and tibia of donor mice. Between 2-6x10^6 cells were injected i.v per mouse. Congenic CD45.1 and CD45.2 mice were used to allow the identification of host and donor cells.

2.15 Human Thymus Tissue

Human thymus tissue was obtained from children (usually aged between 1-4 years) undergoing cardiac surgery. Samples are acquired from the University of Birmingham Human Biomaterials Resource Centre (application number 12-110).

CHAPTER 3: EXPRESSION OF CCRL1 WITHIN THE THYMUS

3.1 Introduction and Aims

CCL19, CCL21, and CCL25, and their classical chemokine receptors, CCR7 and CCR9, are heavily involved in T cell development. They have been implicated in the recruitment of progenitor cells, cortex to medulla migration of SP thymocytes, cortex to subcapsular migration of DN thymocytes, and the export of mature T cells. CCRL1 expression by perivascular TECS and subcapsular epithelial cells has been described (Heinzel et al., 2007); however the detailed phenotype of these cells remains unknown. In addition, $CCRL1^{+}$ TEC have been described in the E13.5 thymus (Heinzel et al., 2007). Despite this initial description, follow-up studies have not addressed expression of CCRL1 within the thymus during ontogeny.

In view of this, the focus of this chapter was to characterise the expression of CCRL1 within the thymus. Thus the aims were as follows:

- To establish methods of CCRL1 detection
- To identify the thymic microenvironments in which CCRL1 is expressed
- To identify the cell type(s) which express CCRL1
- To determine the expression of CCRL1 within the thymus during ontogeny

3.2 Results

3.2.1 Establishing Methods for Measuring CCRL1 Expression In Situ

To determine expression of CCRL1 within the thymus it was necessary to establish reliable methods of detection. At the time this project commenced, very few anti-CCRL1 antibodies were commercially available, and none had been used in the literature. Expression of CCRL1 protein had only been shown using CCRL1-GFP reporter mice generated by Heinzel *et al* (Heinzel et al., 2007*)*. This publication detected GFP expression by 4% paraformaldehyde (PFA) fixation of tissues, followed by slow-freezing and the cutting of relatively thick (18μm) sections. Although this allowed the detection of GFP, the thick sections did not give an optimal resolution for imaging (Heinzel et al., 2007).

Our aim was to optimise and compare the use of anti-CCRL1 antibody and CCRL1-GFP reporter mice for the detection of CCRL1 in the thymus. To test the antibody approach, sections of WT and $CCRL1^{-/-}$ thymus were generated and stained with the anti-CCRL1 antibody (following the immunofluorescence staining protocol described in the Materials and Methods chapter of this thesis). $CCRL1^{+}$ cells were detected in the WT thymus but not in the $CCRL1^{-/-}$ thymus (Figure 5). Low levels of staining were present in the $CCRL1^{-/-}$ thymus, however this staining was determined as non-specific, as it was visually distinct from the CCRL1 staining in the WT thymus. Next, we assessed the detection of GFP in the CCRL1-GFP reporter thymus. To do this, thymi from CCRL1-GFP and WT mice were fixed in 4% and 2% PFA, and sections generated. Sections wre stained using anti-GFP, and upon imaging, GFP^{+} cells were detected in CCRL1-GFP thymi (fixed in 2% and 4% PFA),

and importantly, no GFP^+ cells were detected in the WT thymus (Figure 6). Moreover, these cells were in similar locations to those detected using the anti-CCRL1 antibody. Interestingly, more $CCRL1^+$ cells were detected using the CCRL1-GFP reporter thymus compared to CCRL1 detection using the antibody, and possible reasons for this are discussed later in this thesis.

Detection using CCRL1-GFP reporter mice revealed much higher sensitivity than the antibody, whilst maintaining specificity. The main disadvantage to this system is the PFA fixation process, which is necessary to detect GFP. PFA cross-links antigens and can render them unrecognisable to antibody detection. For this reason, we fixed CCRL1-GFP tissue in 2% PFA, rather than the 4% used by Heinzel *et al.* This resulted in the same sensitivity and specificity of GFP detection as 4% PFA fixation (Figure 6). Both systems of CCRL1 detection were tested for use in flow cytometry, however only CCRL1-GFP mice yielded successful results. We have used CCRL1-GFP mice to map CCRL1 expression where possible, however in certain situations, where PFA fixation was not compatible with the use of particular antibodies, detection of CCRL1 was by anti-CCRL1 antibody. A list of antibodies that were tested in conjunction with 2% PFA fixation can be found in Table 7.

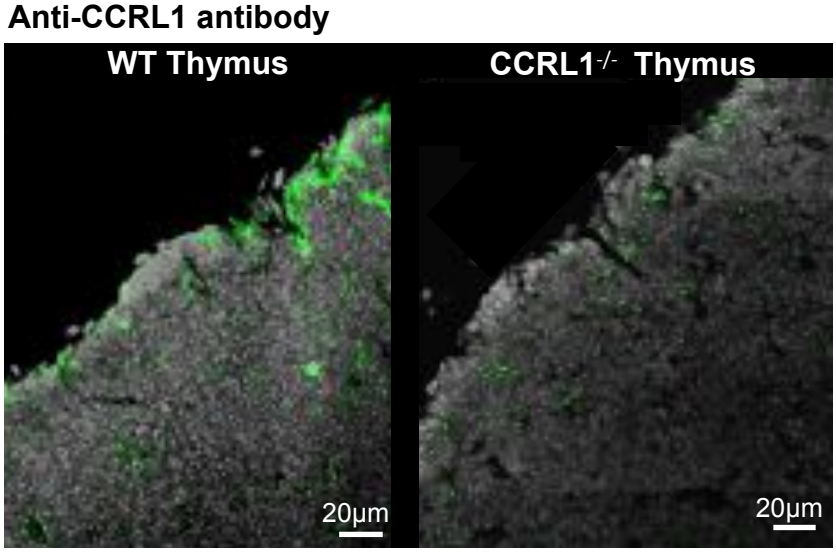

Figure 5. Sensitivity and Specificity of Anti-CCRL1 Antibody in Adult Thymus.

The thymus from adult WT and CCRL1$^{-/-}$ mice was frozen, and cryosections generated. Sections were stained with anti-CCRL1 antibody. Staining shown is representative of at least three experiments.

A

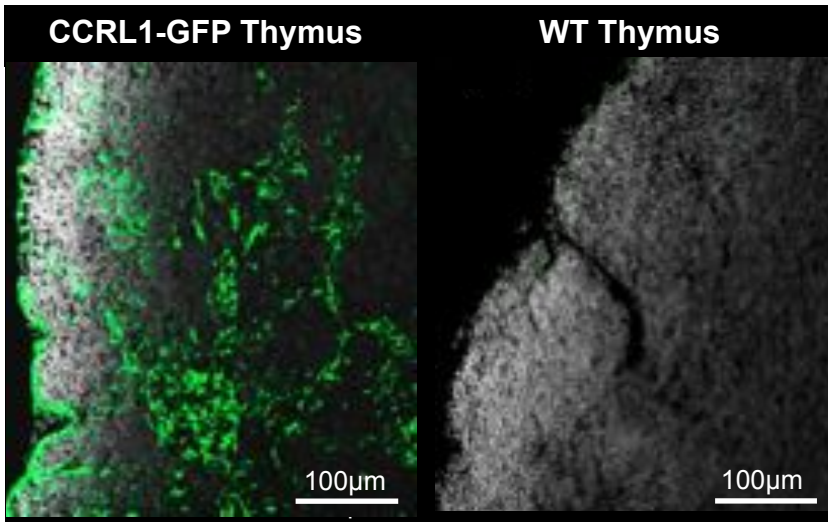

B

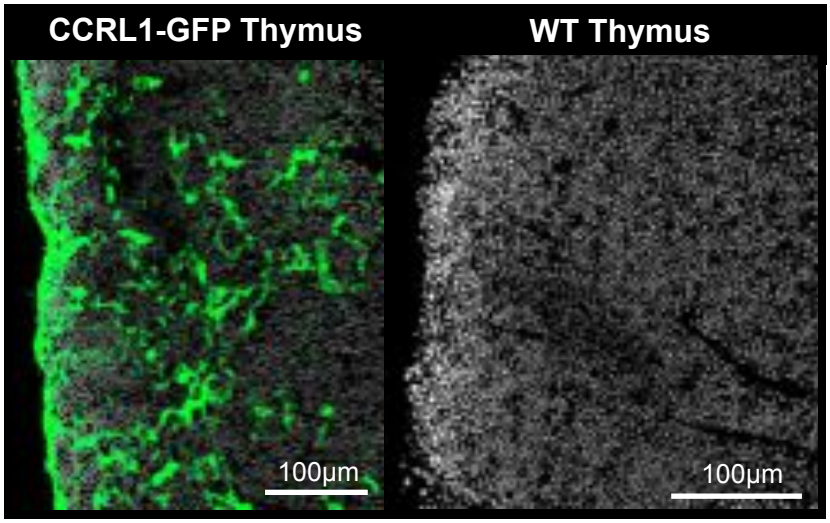

Figure 6. Sensitivity and Specificity of CCRL1-GFP Reporter Mice.

Adult CCRL1-GFP and WT thymi were fixed in 4% (A) and 2% PFA (B) and then frozen. Cryosections were generated, stained with DAPI and anti-GFP, and images were acquired. Images are representative of staining from at least three experiments.

Table 7. Antibodies Tested on Thymus Tissue Treated With 2% PFA

Antibody	Primary Antibody Dilution	Secondary Antibody	Secondary Antibody Dilution	Successful Staining
PDGFRβ biotin	1:100	SA 555	1:1000	Yes
Keratin-8 biotin	1:100	SA 555	1:1000	No
CD80 biotin	1:100	SA 555	1:1000	No
CD31 biotin	1:100	SA 555	1:1000	Yes
CD205 biotin	1:100	SA 555	1:1000	Yes
ERTR7 (rat)	1:10	Anti-rat 555	1:500	No
Podoplanin (hamster)	1:10	Anti-hamster 594	1:500	Yes
CD31 (rat)	1:100	Anti-rat 555	1:500	No
NG2 (rabbit)	1:100	Anti-rabbit 555	1:500	No
MECA-32 (rat)	1:100	Anti-rat 555	1:500	Yes
Keratin-5 (rabbit)	1:1000	Anti-rabbit 555	1:500	No
MTS10 (rat)	1:10	Anti-rat IgM 594	1:500	No
B5t (rabbit)	1:100	Anti-rabbit 555	1:500	No
αSMA Cy-3	1:200	N/A	N/A	Yes
CD25 PE	1:200	N/A	N/A	No
UEA-1 biotin	1:100	SA 555	1:1000	No
VEGFR3 (rat)	1:100	Anti-rat 555	1:500	No
Integrin-α6 biotin	1:100	SA 555	1:1000	Yes
ICAM biotin	1:100	SA 555	1:1000	Yes

Antibody	Primary Antibody Dilution	Secondary Antibody	Secondary Antibody Dilution	Successful Staining
CCRL1 (goat)	1:50	Anti-goat 555	1:500	No
ERTR5 (rat)	1:1000	Anti-rat IgM 594	1:500	No
CD4 647	1:200	N/A	N/A	Yes
CD8β biotin	1:200	SA 555	1:1000	Yes
CD45 biotin	1:200	SA 555	1:1000	Yes
Fibronectin (rabbit)	1:100	Anti-rabbit 555	1:500	Yes
Laminin (rabbit)	1:1000	Anti-rabbit 555	1:500	Yes
CD248 (rabbit)	1:400	Anti-rabbit 594	1:500	Yes
Pan-keratin FITC	1:600	N/A	N/A	No

3.2.2 CCRL1 is Expressed Within the Adult Thymus

Following successful detection of CCRL1, we determined the location of CCRL1 expression within the adult thymus using both anti-CCRL1 antibody and CCRL1-GFP reporter mice. Firstly, sections of WT adult thymus were stained with antibodies against CD4, CD8, and CCRL1. This allowed the identification of thymic cortex and medulla, based on the restricted distribution of DP and SP thymocytes respectively. Expression of CCRL1 was detected by cells at the thymic capsule (Figure 7A), within the cortex (Figure 7B), and surrounding the vasculature at the CMJ (Figure 7C). Co-staining was not visible between CCRL1 and CD4, however few cells appeared to co-express CCRL1 and CD8 within the cortex (Figure 7B). We next performed similar staining on sections from CCRL1-GFP thymi, this time using anti-GFP, rather than anti-CCRL1, and show CCRL1 expression at the capsule (Figure 8A), within the cortex (Figure 8B), and surrounding vasculature at the CMJ (Figure 8C), as in WT mice. CCRL1 expression, determined using this more specific method of detection, revealed no co-expression between CCRL1 and either CD4 or CD8.

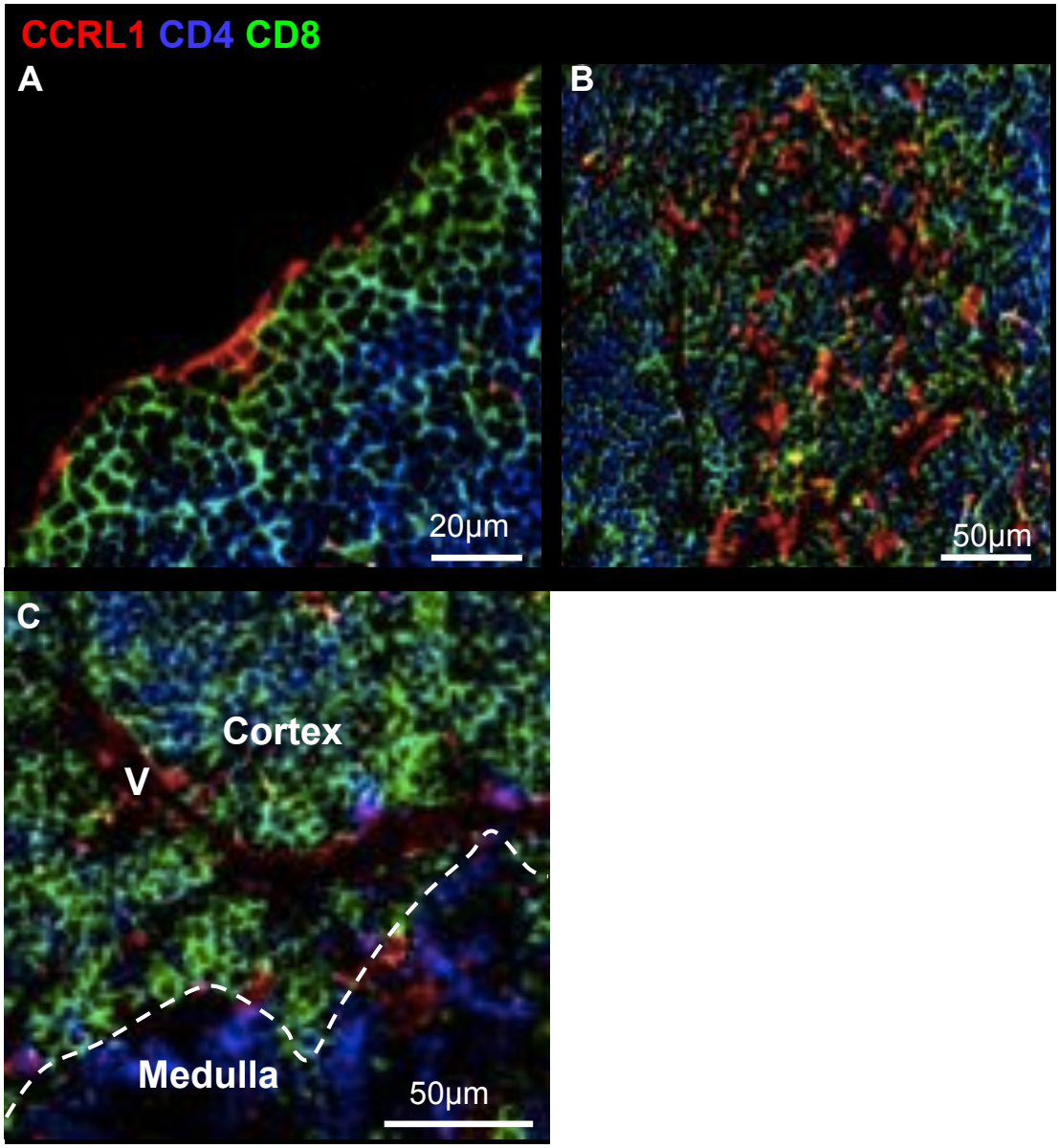

Figure 7. Staining of WT Thymus Using Anti-CCRL1 Antibody.

Cryosections of adult WT thymus were stained for CD4, CD8 and CCRL1. CCRL1 expression (red) is observed by cells at the thymic capsule (A), within the cortex (B), and surrounding vessels (labelled 'V') at the corticomedullary junction (C). A minimum of 3 mice were analysed, similar expression patterns were seen.

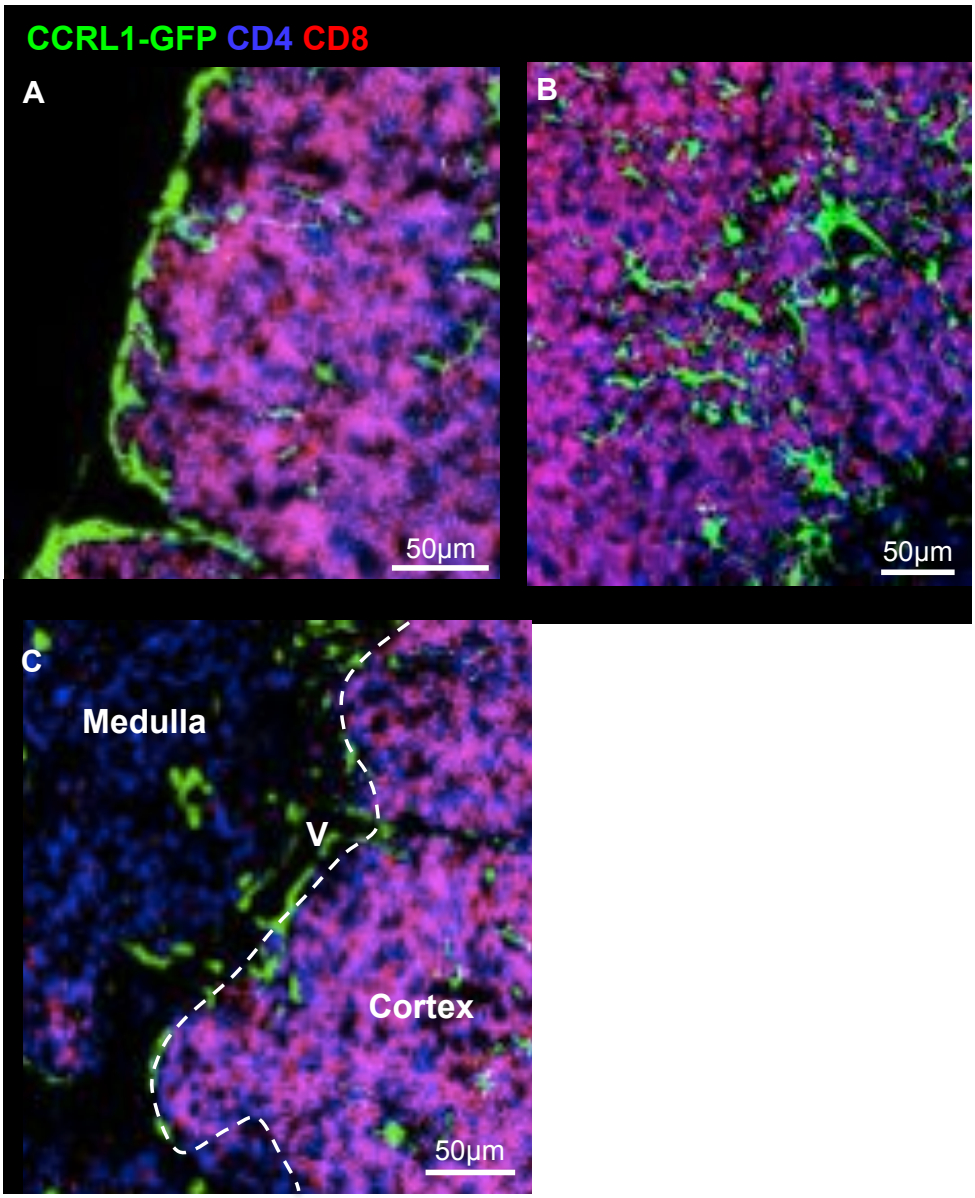

Figure 8. Staining of CCRL1-GFP Adult Thymus.

Adult CCRL1-GFP thymi were fixed in 2% PFA and then frozen. Cryosections were stained for CD4, CD8, and anti-GFP. CCRL1 expression (green) is readily observed by cells at the thymic capsule (A), within the cortex (B), and surrounding vessels at the corticomedullary junction (C). 'V' indicates vessel. A minimum of 3 mice were analysed, similar expression patterns were seen.

3.2.3 CCRL1 is Expressed by Non-Haematopoietic Cells

The thymus is home to several different types of haematopoietic cells, including thymocytes, B cells, and DCs. Our initial CCRL1 detection, using anti-CCRL1 antibody, revealed possible co-expression between CCRL1 and CD8, although this was not reproduced when CCRL1-GFP reporter mice were used. This co-expression of CCRL1 and CD8 may represent the non-specific staining, visible in the $CCRL1^{-/-}$ thymus using this method of detection. Nevertheless, it was important to determine whether CCRL1 was expressed by haematopoietic cells within the thymus. To achieve this, we used CCRL1-GFP reporter mice in conjunction with immunofluorescence (as previously described) and stained thymus sections for CD45 (a haematopoietic marker) (Figure 9A). No co-staining was visible between CD45 and CCRL1, suggesting that thymic expression of CCRL1 is restricted to non-haematopoietic cells. To verify this, thymi from CCRL1-GFP mice were digested to generate a cell suspension consisting of both haematopoietic and non-haematopoietic cells. The resulting cell suspension was stained for CD45 and EpCAM (epithelial cell adhesion molecule, expressed by TEC). Analysis of these cells by flow cytometry showed expression of CCRL1 by $CD45^-$ cells, but not by $CD45^+$ cells (Figure 9B). WT thymi were stained alongside, GFP expression by $CD45^+$ and $CD45^-$ cells were used to set the gate for the detection of GFP.

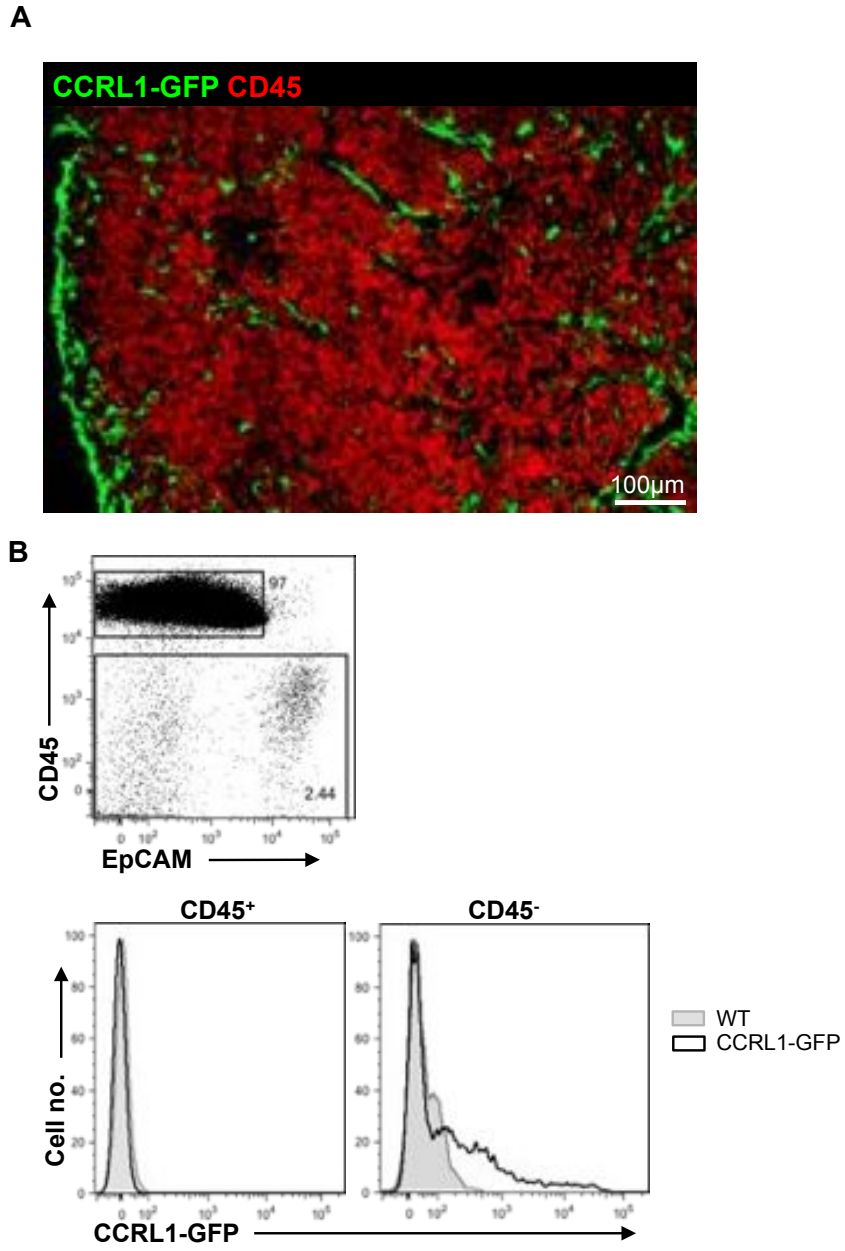

Figure 9. CCRL1 is Expressed by Non-Haematopoietic Cells.

Adult CCRL1-GFP thymi were fixed in 2% PFA and then frozen. Cryosections were stained for CD45 (red). Co-staining was not observed between CCRL1 (green) and CD45 (red) (A). Adult CCRL1-GFP thymi were digested and cells stained for CD45 and EpCAM. Histograms show CCRL1 expression by $CD45^+$ and $CD45^-$ cells from WT and CCRL1-GFP thymi (B). A minimum of 10 mice were analysed, similar expression patterns were seen.

3.2.4 CCRL1 is Expressed by Thymic Epithelial Cells

CCRL1 expression by TEC has previously been described by others (Heinzel et al., 2007, Bunting et al., 2013). We confirmed expression of CCRL1 by TEC using flow cytometry and immunofluorescence. CCRL1-GFP thymi were digested, and the resulting cell suspension was stained for CD45 and EpCAM as before. Flow cytometric analysis revealed CCRL1 expression by 26% of total TECs (mean value) (Figure 10A, C). We further characterised CCRL1 expression by TEC by including Ly51 (a marker specific for cTEC) to allow the identification of cTEC ($Ly51^+$) and mTEC ($Ly51^-$) by flow cytometry. WT thymi were stained alongside, and GFP expression within each population from WT thymi was used to set the gate for the detection of GFP^+ cells (Figure 10B). Quantitative analysis showed that CCRL1 was expressed by approximately 15.2% (mean value) of mTEC and significantly more cTEC (mean: 58.4%, p=<0.0001) (Figure 10D).

TEC were also identified using immunofluorescence by staining thymus sections from CCRL1-GFP reporter mice with antibodies against keratin-8 and CD205, to identify cTEC (Figure 11A), and keratin-5 to identify mTEC (Figure 11B). Co-staining was visible between CCRL1-GFP and both keratin-8 and CD205, thus confirming CCRL1 expression by cTEC. GFP^+ cells were not detected within the keratin-5^+ areas of the thymus, despite the detection of $CCRL1^+$ cells within the $Ly51^-$ mTEC population by flow cytometry. Possible reasons for this discrepancy are later discussed.

Analysis of TEC compartments by flow cytometry allows the use of additional markers to distinguish between immature TEC (TEC^{lo}), and mature TEC (TEC^{hi}). The thymus from CCRL1-GFP mice was digested and cTEC and mTEC identified as previously show. mTEC were further analysed based on their expression of MHC-II and CD80. MHC-$II^{lo}CD80^{-}$ ($mTEC^{lo}$), and MHC-$II^{hi}CD80^{+}$ ($mTEC^{hi}$) were assessed for CCRL1-GFP expression. cTEC were also analysed based on their expression of MHC-II and CD40, and expression of CCRL1 was determined by $cTEC^{lo}$ (MHC-$II^{lo}CD40^{-}$) and $cTEC^{hi}$ (MHC-$II^{hi}CD40^{+}$) populations. WT thymi were stained alongside, and GFP expression within each population from WT thymi was used to set the gate for the detection of GFP^{+} cells. (Figure 12). Quantitative analysis of CCRL1 expression by these populations showed low levels of CCRL1 expression by both mTEC populations (median: 15.2% of $mTEC^{lo}$, 6.3% of $mTEC^{hi}$). Interestingly, CCRL1 expression by $mTEC^{lo}$ was significantly higher than the expression by $mTEC^{hi}$ ($p=0.0041$) (Figure 13A). Expression of CCRL1 by cTEC was consistently higher than by mTEC, and interestingly CCRL1 expression by $cTEC^{lo}$ was also significantly higher than expression by $cTEC^{hi}$ ($p=0.0262$). (Figure 13B).

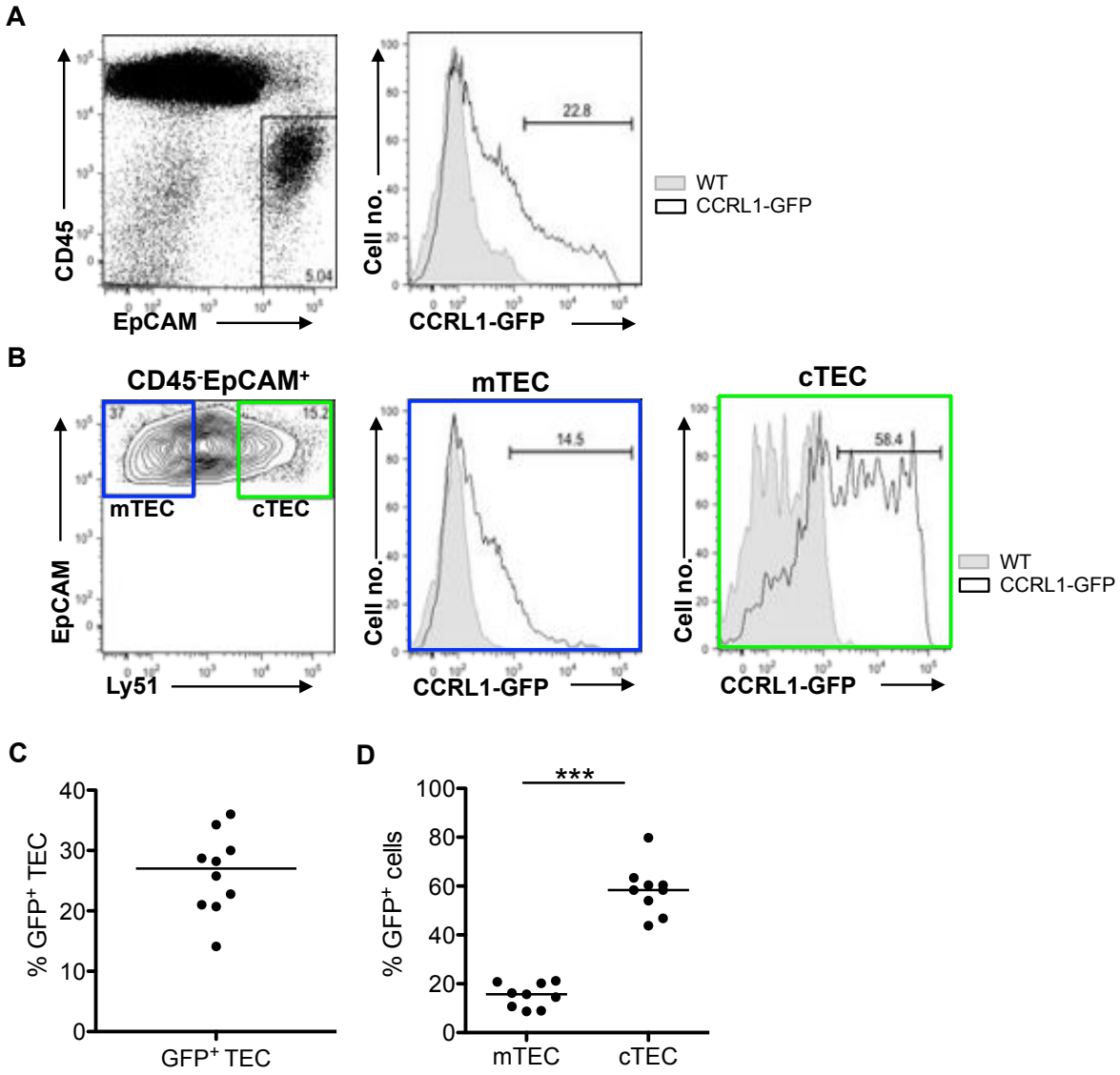

Figure 10. CCRL1 Expression by Thymic Epithelial Cells is Detectable by Flow Cytometry.

Adult CCRL1-GFP thymi were digested and stained for flow cytometry. CCRL1 is expressed by $CD45^{-}EpCAM^{+}$ cells (A). Staining with Ly51 allowed the identification of mTEC and cTEC. CCRL1 was expressed by $Ly51^{-}$ mTEC and $Ly51^{+}$ cTEC (B). Quantitation of GFP expression by total TEC ($CD45^{-}EpCAM^{+}$) n=10 mice (C). Quantitation of GFP expression by mTEC and cTEC n=9 mice (D). Statistical analysis performed (D'Agostino-Pearson followed by t test). ****p<0.0001.*

A

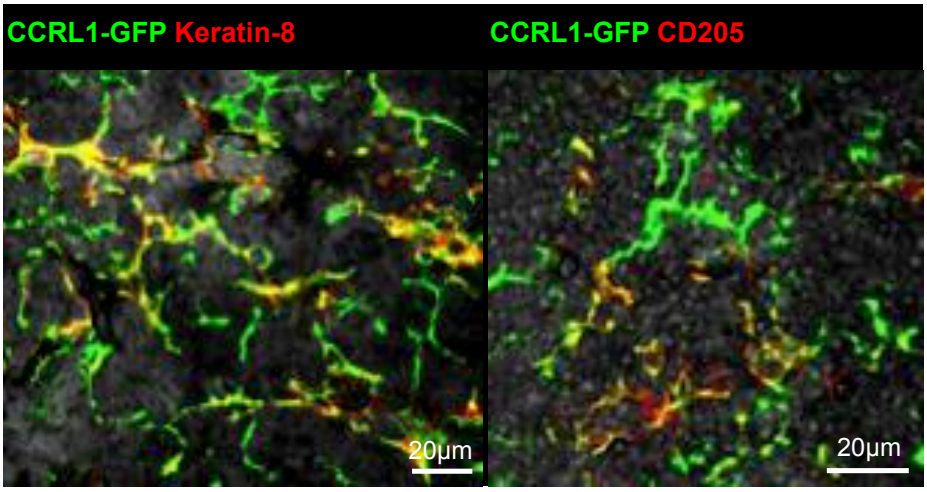

B

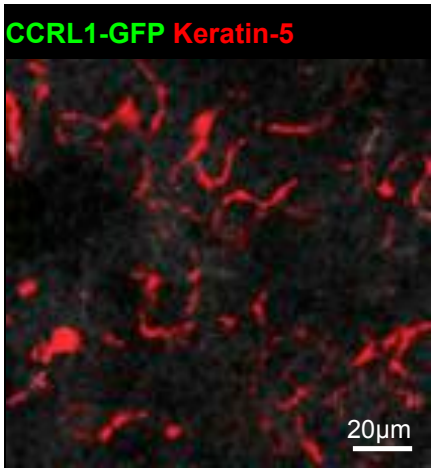

Figure 11. CCRL1 Expression by Thymic Epithelial Cells is Detectable by Immunofluorescence.

Adult CCRL1-GFP thymi were fixed in 2% PFA and then frozen. Cryosections were stained for keratin 8 (red), and CD205 (red), in conjunction with anti-GFP (green). Co-expression was visible between both keratin-8 and CD205, and CCRL1 (A). Sections were also stained for keratin 5 (red), and anti-GFP (green) to identify mTEC, however co-expression was not observed (B). A minimum of 3 mice were analysed, similar expression patterns were seen.

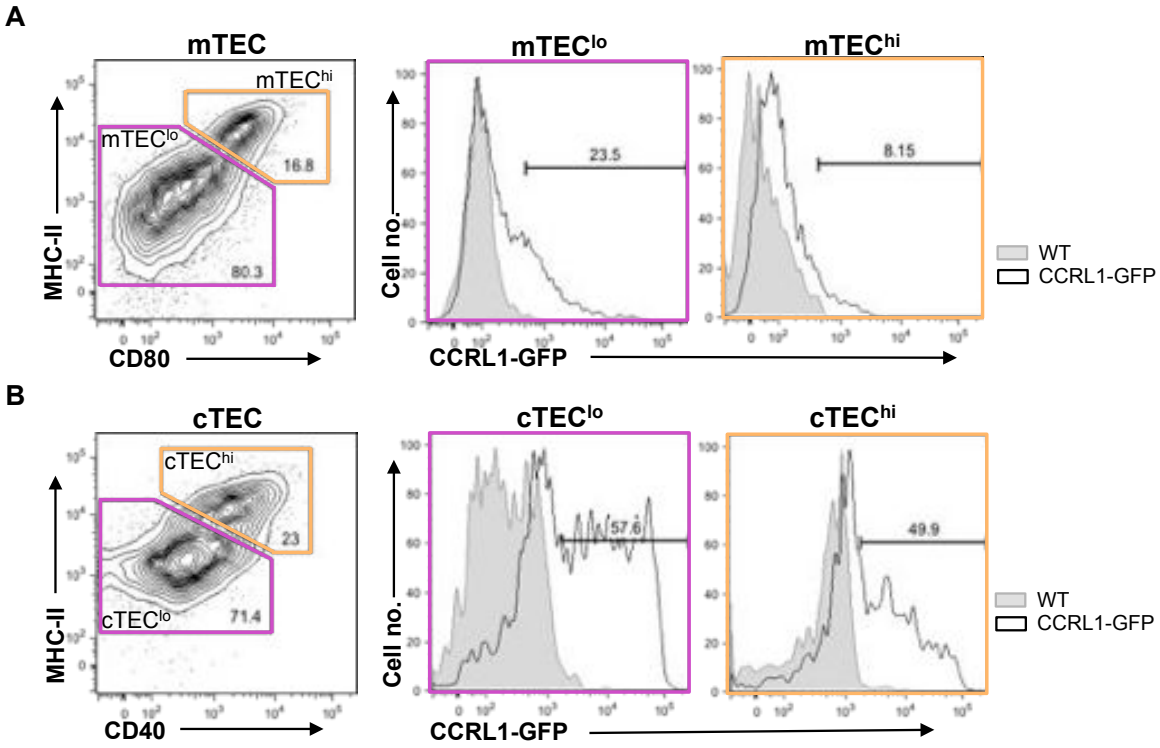

Figure 12. Differential CCRL1 Expression by Defined Populations of Thymic Epithelial Cells.

Adult CCRL1-GFP thymi were digested and stained for flow cytometry. $CD45^-$ $EpCAM^+$ cells were first gated, then mTEC were gated as $Ly51^-$, and cTEC were gated as $Ly51^+$ prior to the analysis shown. $mTEC^{hi}$ and $mTEC^{lo}$ were gated based on the expression of MHC-II and CD80 (A). $cTEC^{hi}$ and $cTEC^{lo}$ were gated based on the expression of MHC-II and CD40 (B). CCRL1 expression by each population in CCRL1-GFP and WT thymi is shown in overlay histograms. Staining was repeated on 7 mice with similar expression patterns.

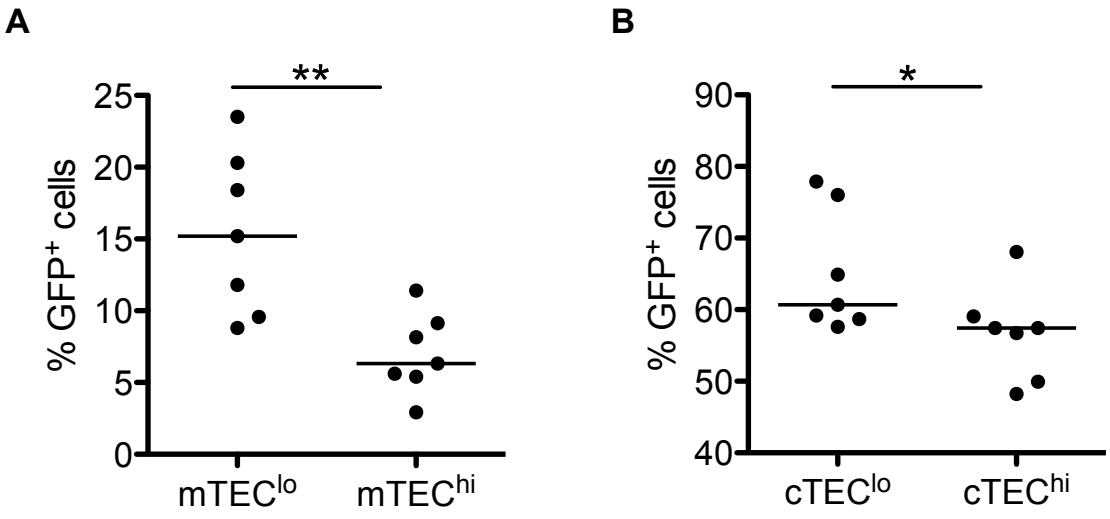

Figure 13. CCRL1 Expression by Populations of mTEC and cTEC.

Quantitation of CCRL1-GFP expression by $mTEC^{lo}$ and $mTEC^{hi}$ (A), and $cTEC^{lo}$ and $cTEC^{hi}$ (B). n=7 mice. Statistical analysis performed (Man Whitney). ***p<0.01, *p<0.05.*

3.2.5 CCRL1 is Expressed by a Population of EpCAM Negative Stromal Cells

Although TEC comprise a high proportion of stromal cells within the thymus, a heterogeneous population of $EpCAM^-$ cells exist. CCRL1 expression by $EpCAM^-$ cells within the thymus was determined using CCRL1-GFP mice. $EpCAM^-Ly51^+$ cells have been described; these are mesenchymal cells of neural crest origin within the adult thymus (Muller et al., 2008). $EpCAM^-podoplanin^+$ cells have also been described, and are termed thymic fibroblastic reticular cells (tFRC) (Fuertbauer et al., 2013).

We digested the thymus of CCRL1-GFP mice and stained for Ly51 and podoplanin for analysis by flow cytometry. Expression of Ly51 and podoplanin by $CD45^-EpCAM^-$ $TER\text{-}119^-$ cells revealed three populations, $Ly51^+podoplanin^-$, $Ly51^-podoplanin^-$ and $Ly51^{int}podoplanin^+$ (Figure 14A). Expression of CCRL1 by each of these populations was determined, using a WT thymus to set the gate for detection of GFP^+ cells (Figure 14B). Quantitative analysis showed GFP expression by 22% of $Ly51^{int}podoplanin^+$ cells (median value). This was significantly higher than expression by $Ly51^+podoplanin^-$ ($p=0.0079$) and $Ly51^-podoplanin$ ($p=0.0079$) cells (Figure 14C).

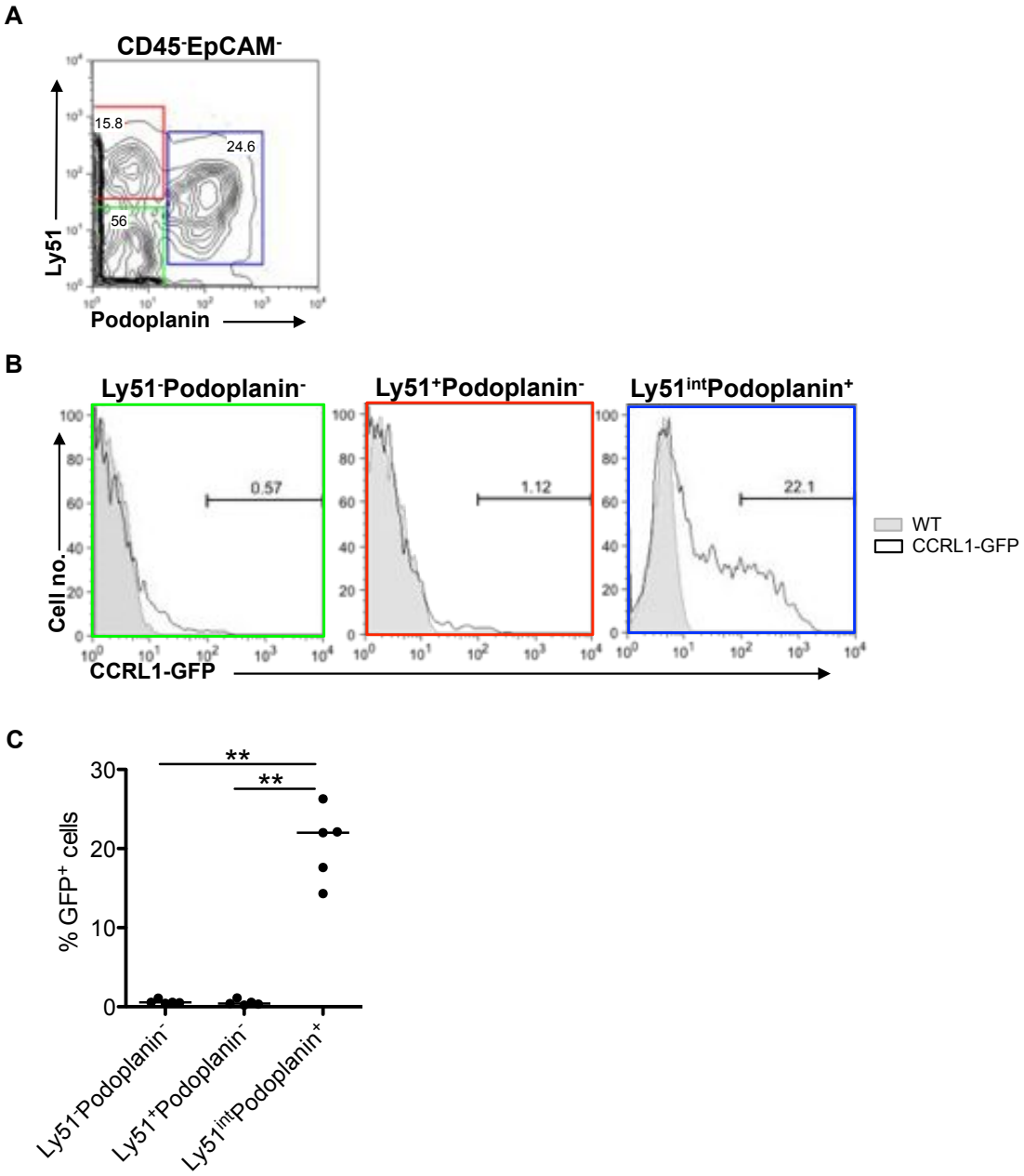

Figure 14. CCRL1 is Expressed by a Population of EpCAM Negative Cells.

Adult CCRL1-GFP thymi were digested and stained for flow cytometry. CD45$^-$ EpCAM$^-$TER-119$^-$ cells were first gated prior to the analysis shown. Three populations of cells are identified based on the expression of Ly51 and podoplanin (A). CCRL1 expression on each of these subsets in WT and CCRL1-GFP mice is shown in overlay histograms (B). Quantitation of CCRL1-GFP expression by thymic mesenchymal populations (C) n=5 mice. Statistical analysis performed (Man Whitney). ***p<0.01.*

3.2.6 CCRL1 Expression Surrounding Vasculature Does Not Map to Endothelial Cells or Basal Membrane Proteins

Initial confocal images of the thymus from CCRL1-GFP mice revealed CCRL1 expression surrounding vessels at the CMJ. We stained sections of CCRL1-GFP and WT thymi with a wide array of markers to identify the phenotype of these cells. First, we stained endothelial cells using the markers CD31 (Figure 15A) and MECA-32 (Figure 15B). Both markers revealed $CCRL1^+$ cells surrounding the endothelial cells, however high resolution images reveal an absence of co-staining between CCRL1 and either endothelial cell marker. To further analyse expression of CCRL1 in relation to CD31, ZenLite Software was used to generate a profile of the distance between the two fluorophores (Figure 15C). Although there was some overlap, the peak intensity of CCRL1 and CD31 were distinct, confirming that CCRL1 and CD31 were in close proximity but were not co-expressed by the same cell. Due to the close proximity of $CCRL1^+$ cells and endothelial cells, we next determined whether CCRL1 was expressed by the basal lamina or basement membrane associated with the thymic vasculature. To achieve this, CCRL1-GFP thymi were stained for laminin to identify the basal lamina (Figure 16A). $CCRL1^+$ cells were in close proximity but co-expression was not observed. This was confirmed using ZenLite software as before, to show the distance between peak intensities for laminin and CCRL1 (Figure 16B). CCRL1-GFP thymi were also stained for fibronectin to identify the extracellular matrix proteins associated with the basement membrane (Figure 17A). Similar to the other markers, $CCRL1^+$ cells were in close proximity to $fibronectin^+$ cells, but co-localisation was not detected (Figure 17B).

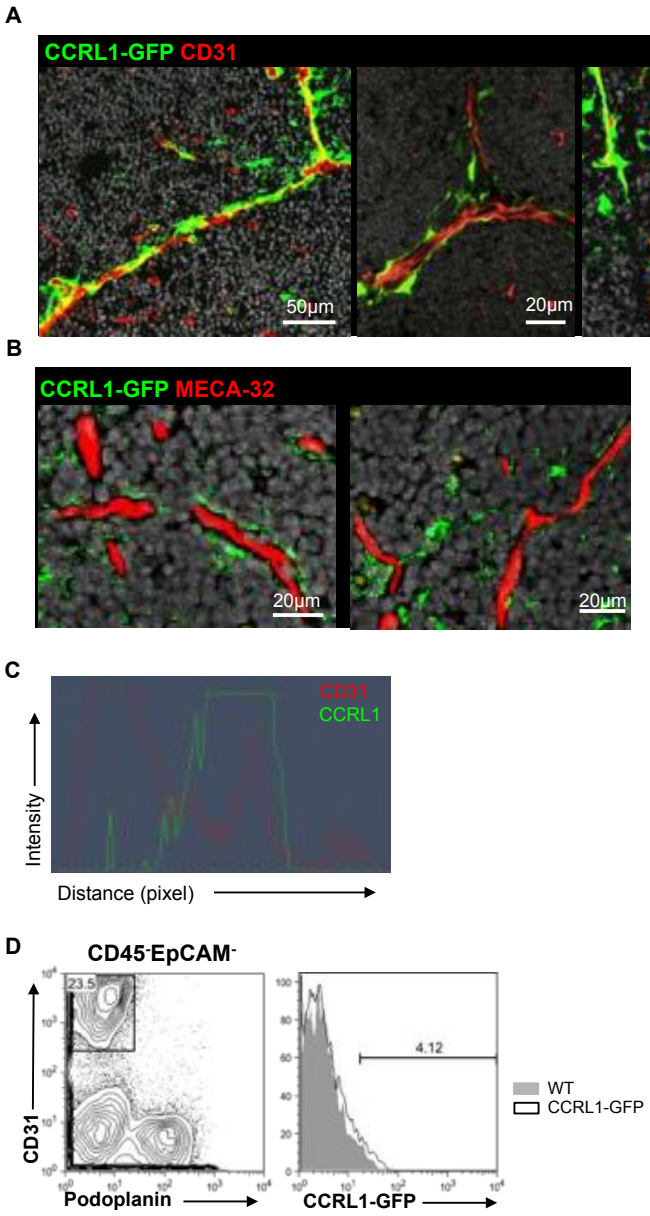

Figure 15. CCRL1 is Not Expressed by Endothelial Cells.

Adult CCRL1-GFP thymi were fixed in 2% PFA and then frozen. Cryosections were stained for CD31 (red) (A), and MECA-32 (red) (B), in conjunction with anti-GFP (green). No co-localisation is visible between CCRL1 (green) and either CD31 or MECA-32. Distance between the two fluorophores was determined using Zeiss Zen software, which shows no co-expression between CCRL1 (green) and CD31 (red) (C). CCRL1 expression was determined on $CD31^{+}podoplanin^{-}$ endothelial cells by flow cytometry (D). A minimum of 3 mice were analysed and similar expression patterns were seen.

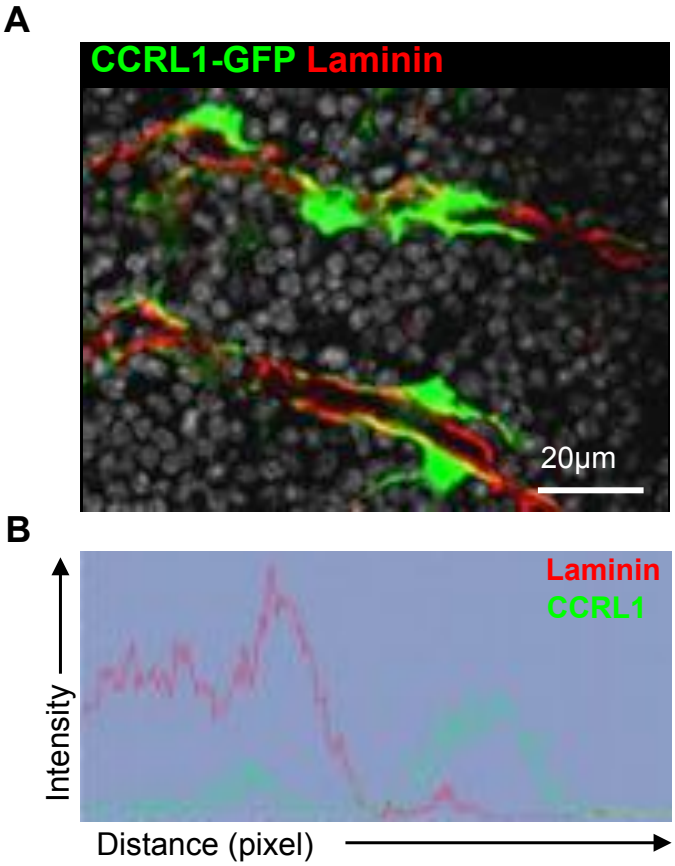

Figure 16. CCRL1 is Not Expressed by the Basal Lamina of Thymic Blood Vessels.

Adult CCRL1-GFP thymi were fixed in 2% PFA and then frozen. Cryosections were stained for laminin (red), and anti-GFP (green) (A). Distance between the two fluorophores was determined using Zeiss Zen software, which shows no co-expression between CCRL1 (green) and laminin (red) (B).

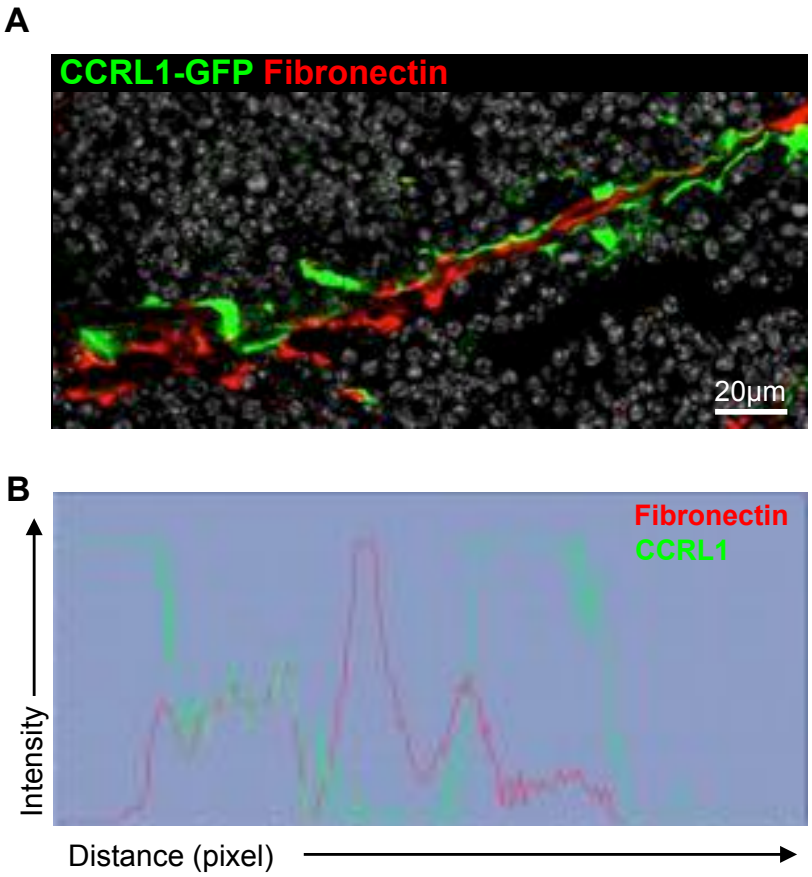

Figure 17. CCRL1 is Not Expressed by Extracellular Matrix Proteins Surrounding Blood Vessels.

Adult CCRL1-GFP thymi were fixed in 2% PFA and then frozen. Cryosections were stained for fibronectin (red), and anti-GFP (green) (A). Distance between the two fluorophores was determined using Zeiss Zen software, which shows no co-expression between CCRL1 (green) and fibronectin (red) (B).

3.2.7 CCRL1 Expression Surrounding Vasculature Does Not Map to Pericytes

Pericytes are cells that line the outer surface of endothelial cells. The expression of CCRL1 by cells surrounding endothelial cells, rather than expression by the endothelial cells themselves, suggested CCRL1 may be expressed by pericytes. The thymus from CCRL1-GFP mice was sectioned and was stained for αSMA, which is expressed by vascular smooth muscle cells of thymic arterioles, but is undetectable surrounding capillaries of the adult thymus (Odaka, 2009). $CCRL1^+$ cells were visible surrounding $αSMA^+$ pericytes of a vessel close to the CMJ (Figure 18A). A cross-section of a larger vessel showed CCRL1 expression by cells lining the outer surface of $αSMA^+$ cells, rather than co-expression between CCRL1 and αSMA (Figure 18B), suggesting that $CCRL1^+$ cells are located at the outer surface of pericytes.

Sections of CCRL1-GFP thymus were also stained for CD248 (endosialin). CD248 is a mesenchymal stromal cell marker expressed within the thymus by pericytes (Lax et al., 2012). Similarly to αSMA, this staining revealed the location of $CCRL1^+$ cells surrounding the outer surface of $CD248^+$ pericytes. Interestingly, this staining combination revealed heterogeneity in the thymic blood vessels. Some vessels were surrounded by a layer of $CD248^+$, followed by a layer of $CCRL1^+$ cells, whereas some vessels were surrounded with only $CCRL1^+$ or $CD248^+$ cells (Figure 19A). Absence of co-localisation between CCRL1 and CD248 was verified using ZenLite software (Figure 19B).

A

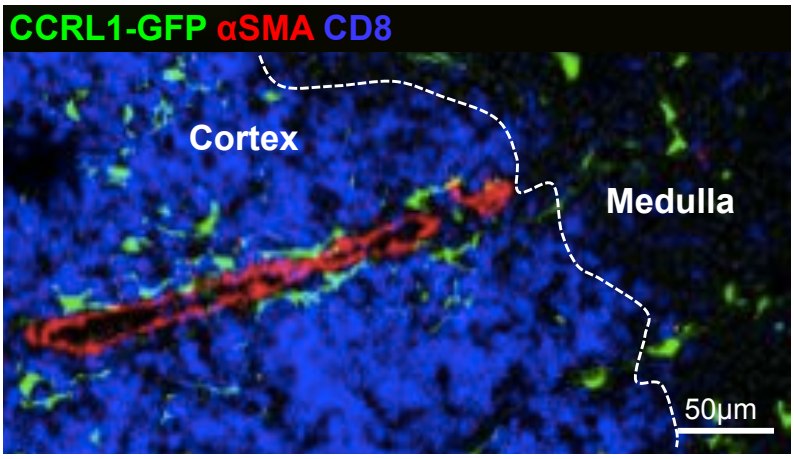

B

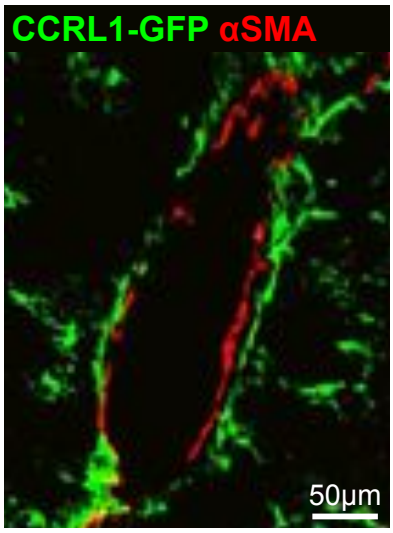

Figure 18. CCRL1 is Not Expressed by αSMA$^+$ Pericytes.

Adult CCRL1-GFP thymi were fixed in 2% PFA and then frozen. Subsequent cryosections were stained for αSMA (red), CD8 (blue), and anti-GFP (green) (A). CCRL1 expression surrounding αSMA$^+$ cells can be at the CMJ. A cross section of a larger vessel clearly shows CCRL1 is expressed by cells that line the outer surface of αSMA$^+$ pericytes, no co-localisation is visible (B). A minimum of 3 mice were analysed and similar expression patterns were seen.

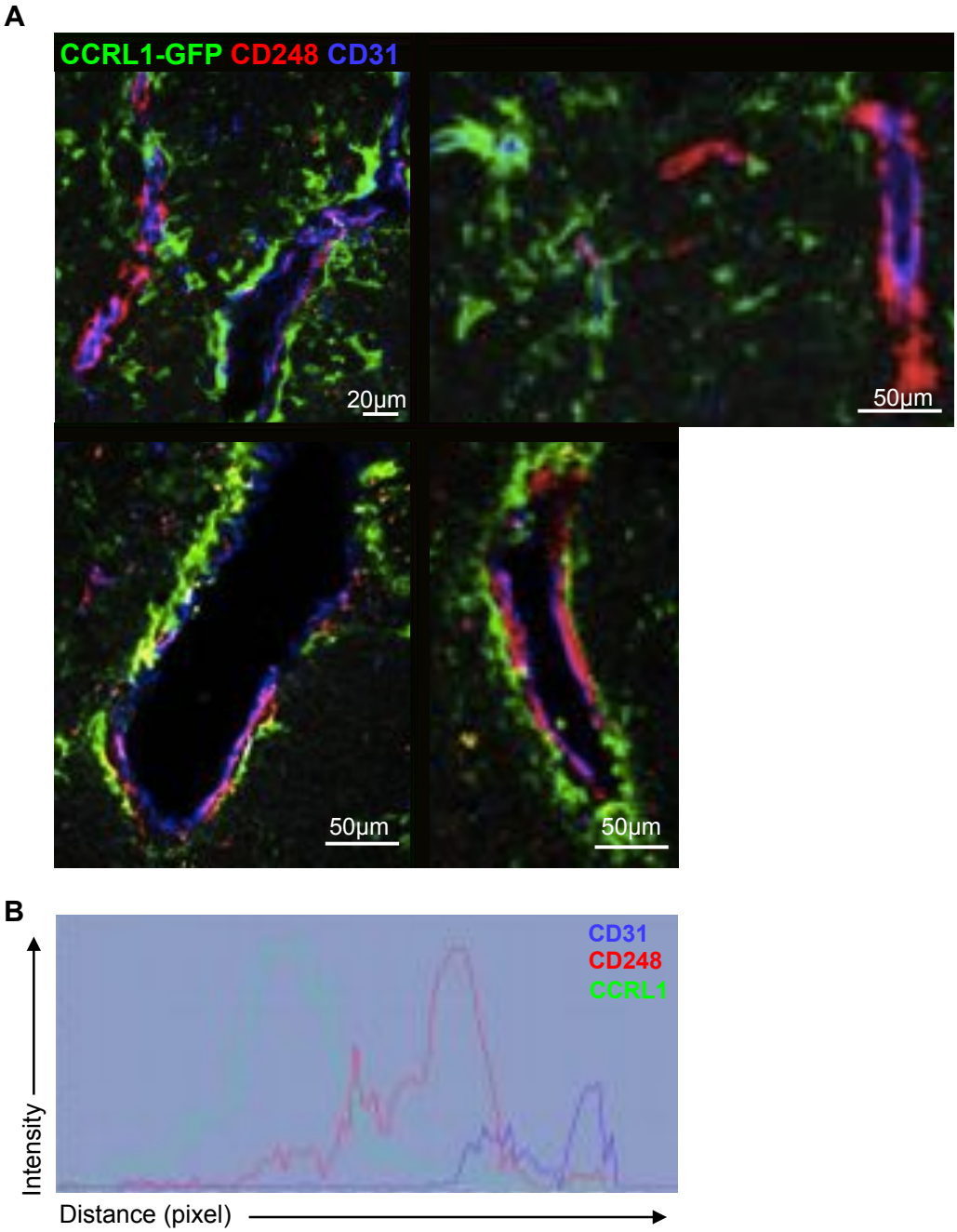

Figure 19. CCRL1 is Not Expressed by CD248^{+} Pericytes.

Adult CCRL1-GFP thymi were fixed in 2% PFA and frozen. Cryosections were stained for CD248 and CD31. CCRL1 is expressed by cells surrounding CD248^{+} pericytes or is surrounding vessels which lack CD248^{+} pericytes (A). Distance between the two fluorophores was determined using Zeiss Zen software, which shows no co-expression between CCRL1 (green) and CD248 (red) (B). A minimum of 3 mice were analysed and similar expression patterns were seen.

3.2.8 CCRL1 Expression Surrounding Thymic Vasculature is by Podoplanin$^+$ PDGFRβ$^+$ TEC

We described a population of CCRL1$^+$ cells surrounding endothelial cells at the CMJ, which were negative for pericyte markers. Although the specific expression of CCRL1 surrounding the vessels doesn't fit with wide-spread TEC localisation, it was important to determine whether these CCRL1$^+$ cells were TEC. To achieve this, cryosections of WT adult thymus were stained for CCRL1, pan-keratin and CD31 to identify CCRL1 expression in relation to TEC and endothelial cells (Figure 20A, B). Pan-keratin staining was not compatible with PFA fixation, hence WT thymus and anti-CCRL1 antibody were used in this instance. Co-staining of CCRL1 and pan-keratin was visible surrounding CD31$^+$ endothelial cells (Figure 20C). Due to the localisation of these vessels at the CMJ, we next determined whether these CCRL1$^+$ TEC expressed keratin-8 or keratin-5 (markers typically associated with cTEC and mTEC respectively) (Figure 21). Vessels were identified based on DAPI staining, and at these locations CCRL1 co-stained with keratin-8 but not keratin-5, indicative of CCRL1 expression by cTEC.

Additional staining was performed on sections from CCRL1-GFP thymi using antibodies against podoplanin and GFP (Figure 22A). This revealed co-staining of CCRL1 and podoplanin by cells surrounding vessels (Figure 22B). Podoplanin is a 38kDa glycoprotein expressed by many cell types including podocytes of the kidney, lymphatic endothelial cells, and fibroblastic reticular cells (FRCs). In the thymus, podoplanin is expressed by thymic FRCs, predominately within the medulla. The importance of podoplanin in the development of nTreg has been shown using

podoplanin deficient mice. In addition, analysis of CCL21 localisation within the podoplanin deficient thymus revealed CCL21 staining scattered within the cortex, whereas in WT mice CCL21 staining was restricted to the medulla (Fuertbauer et al., 2013). These experiments show the contribution of podoplanin to CCL21 compartmentalisation within the thymus. Thymus sections from CCRL1-GFP mice were also stained for PDGFRβ, a receptor with expression limited to cells surrounding thymic blood vessels within the thymus (Odaka, 2009) (Figure 23A). This showed co-staining of CCRL1 with PDGFRβ (Figure 23B), suggestive of a population of CCRL1^{+} podoplanin^{+} PDGFRβ^{+} cTEC surrounding CMJ vasculature.

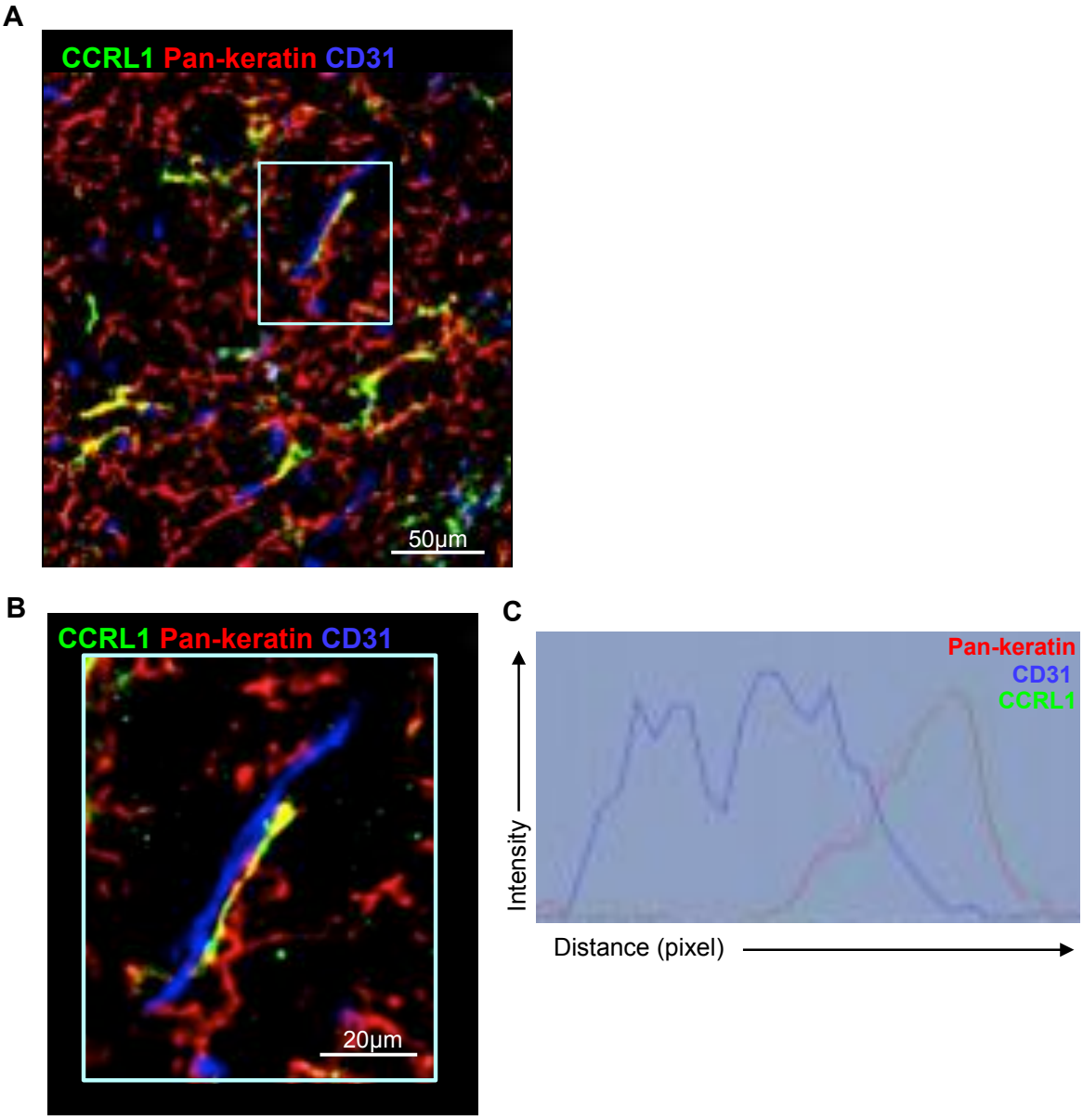

Figure 20. CCRL1 Expression Surrounding Vessels is by a Population of TEC.

Adult WT thymi were frozen and subsequent cryosections stained for CCRL1 (green), pan-keratin (red), and CD31 (blue) (A). Co-localisation of pan-keratin and CCRL1 surrounding the vasculature is highlighted in the enlarged inset (B), and is verified using ZenLite software (C).

A

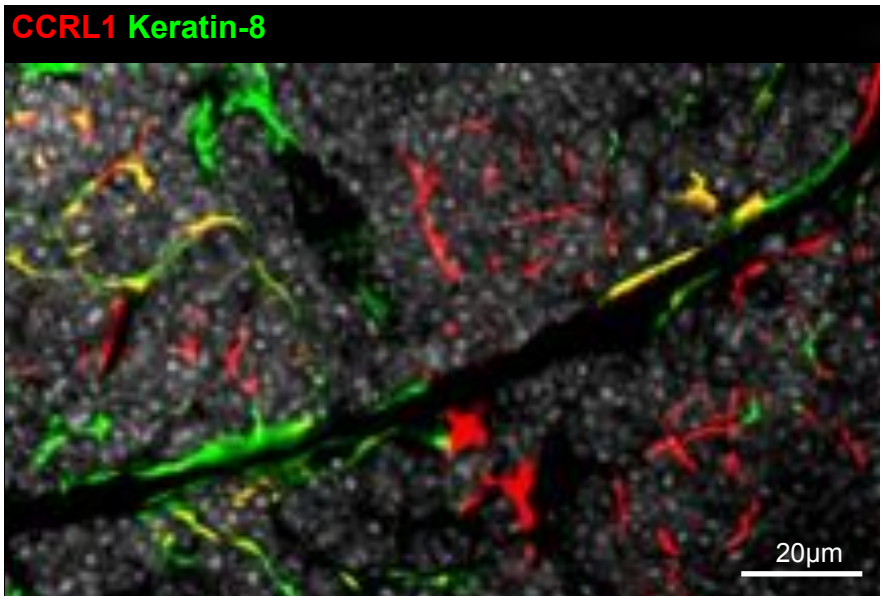

B

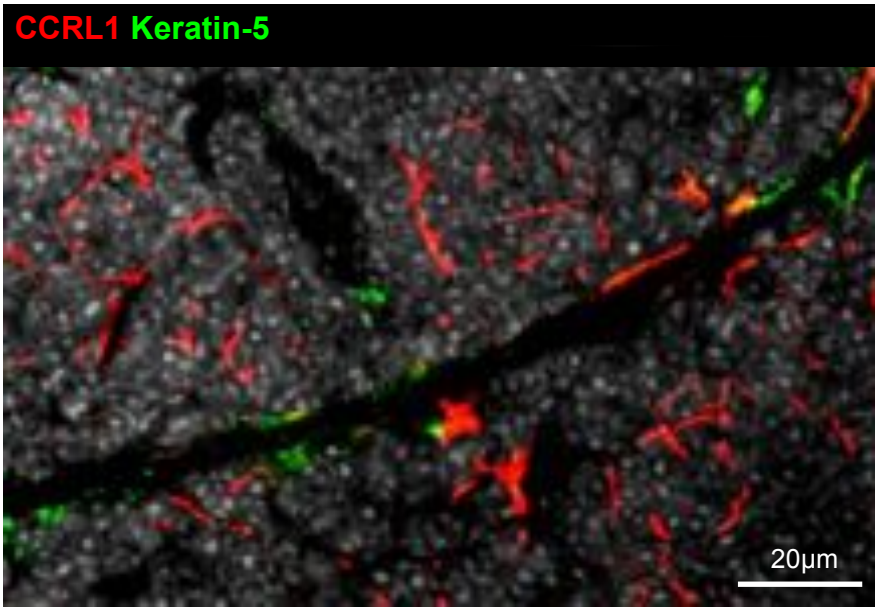

Figure 21. CCRL1^{+} TEC Surrounding Vessels Express Keratin-8.

Cryosections of WT thymus were stained with keratin-8 (green), (A) and keratin-5 (B) to identify cTEC and mTEC, respectively. CCRL1 (red) is expressed by keratin-8^{+} cells surrounding the vasculature. Co-localisation is not visible between keratin-5 and CCRL1.

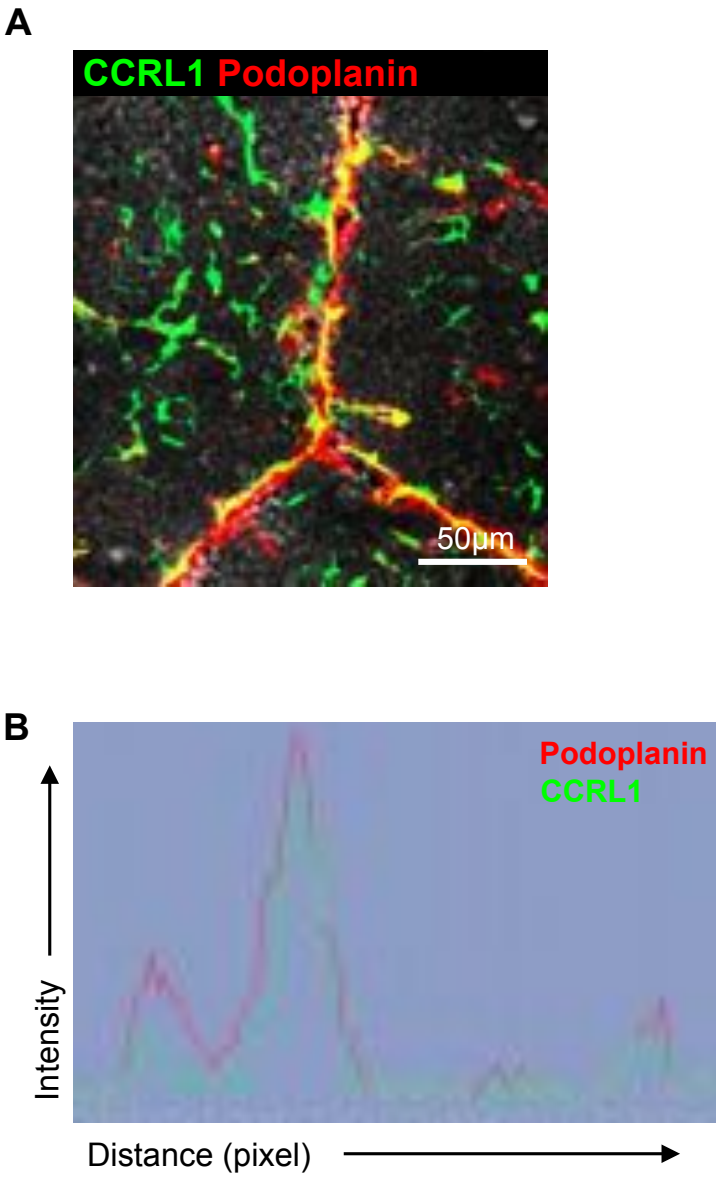

Figure 22. CCRL1^{+} TEC Surrounding Thymic Blood Vessels are Podoplanin^{+}.

Adult CCRL1-GFP thymi were fixed in 2% PFA and then frozen. Cryosections were stained for podoplanin (red) and anti-GFP (green) (A). Distance between the two fluorophores was determined using Zeiss Zen software, which shows co-expression between CCRL1 (green) and podoplanin (red) (B). A minimum of 3 mice were analysed and similar expression patterns were seen.

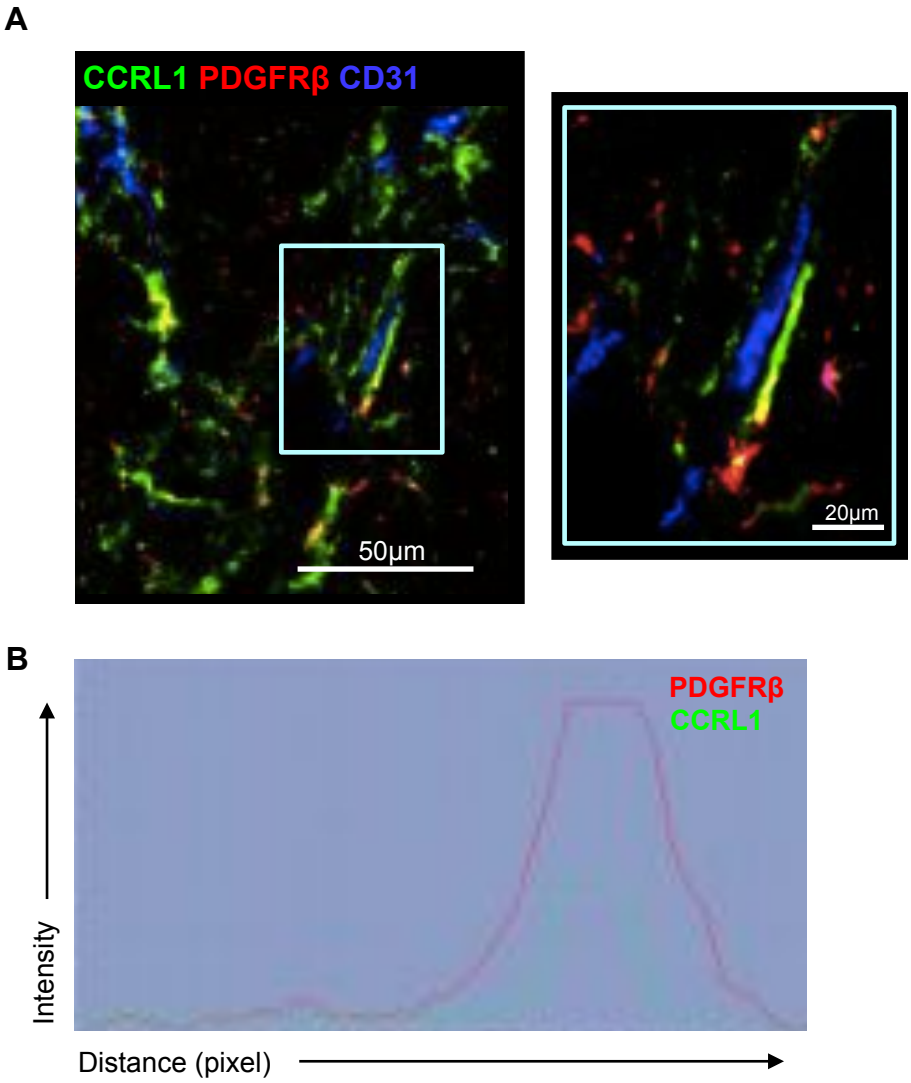

Figure 23. CCRL1^{+} TEC surrounding vessels are PDGFRβ^{+}.

Adult CCRL1-GFP thymi were fixed in 2% PFA and then frozen. Cryosections were stained for PDGFRβ (red), CD31 (blue), and GFP (green) (A). Co-expression of CCRL1 and PDGFRβ was verified using Zeiss Zen software (B).

3.2.9 Podoplanin^{+} cTEC at the Thymic Capsule Express CCRL1

Initial examination of CCRL1 expression within the thymus revealed expression of CCRL1 by CD45^{-} stromal cells at the thymic capsule. To further characterise these cells, cryosections of WT thymi were stained with anti-CCRL1 in conjunction with antibodies against ERTR7 (a marker of thymic reticular fibroblasts) (Figure 24A) and CD248 (a marker of fibroblasts and pericytes) (Figure 24B). Co-localisation was not visible between ERTR7 and CCRL1, and CCRL1^{+} cells were in close proximity to CD248^{+} cells. Further analysis using ZenLite software showed no co-staining of CCRL1 and CD248 (Figure 24C). WT thymus sections were also stained for CCRL1 in conjunction with CD205 (Figure 25A) and podoplanin (Figure 25B). Clear co-staining is visible between CCRL1 and both these markers thus identifying CCRL1^{+} cells at the thymic capsule as podoplanin^{+} cTEC.

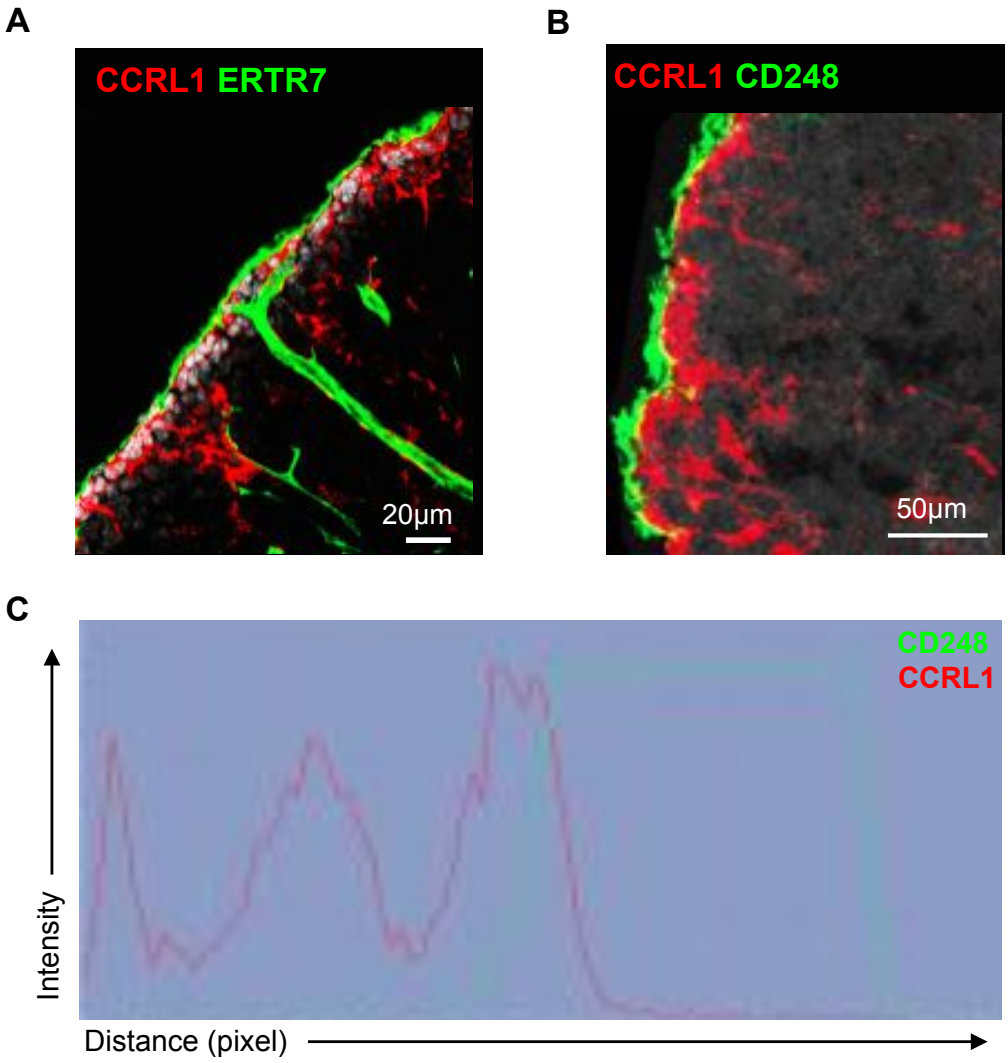

Figure 24. CCRL1 Expression at the Thymic Capsule Does Not Map With ERTR7 or CD248 Expression.

Cryosections of WT thymi were stained for CCRL1 (red), in conjunction with ERTR7 and CD248 (green) (A). No co-localisation is visible between CCRL1 and either of these markers. Absence of co-localisation between CCRL1 and CD248 was verified using Zeiss Zen software (C). A minimum of 3 mice were analysed and similar expression patterns were seen.

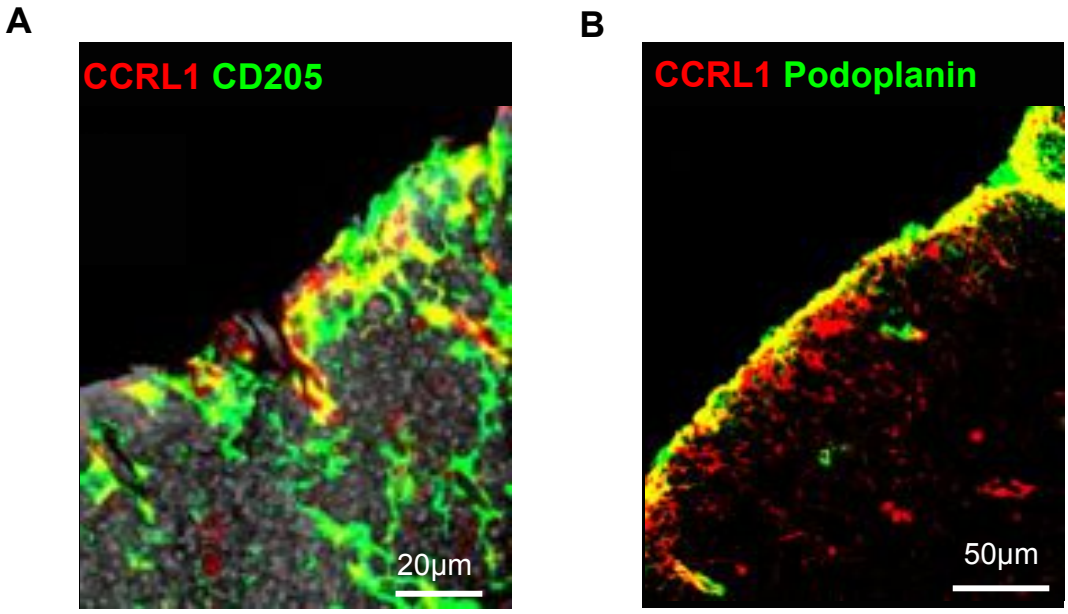

Figure 25. CCRL1 Expression at the Thymic Capsule is by a Population of Podoplanin^{+} cTEC.

Cryosections of WT thymi were stained for CCRL1 (red), in conjunction with CD205 (A) and podoplanin (B). Co-localisation is visible between CCRL1 and both of these markers. A minimum of 3 mice were analysed and similar expression patterns were seen.

3.2.10 CCRL1 is Expressed by TEC in the Embryonic Thymus From E13

CCRL1 expression has previously been described within the E13 thymus (Heinzel et al., 2007) therefore we systematically mapped the thymic expression of CCRL1 during ontogeny.

Embryonic TEC development can be analysed by flow cytometry, using the markers CD40 and CD205. At E12 the thymus contains only $EpCAM^{+}CD40^{-}$ TEC, which can be split into two populations, $CD205^{-}$ and $CD205^{+}$ (Baik et al., 2013). The $CD40^{-}CD205^{-}$ population declines in size during embryonic development, and by E17, very few cells have this phenotype (Baik et al., 2013). $CD40^{-}CD205^{+}$ cells were thought to be immature cTEC, however these cells have since been shown to have mTEC lineage potential (Baik et al., 2013). Further maturation of the TEC population involves continual upregulation of CD40. $CD40^{+}CD205^{+}$ cells are thought to be fully mature cTEC. Between E14 and E15 a population of $CD40^{+}CD205^{-}$ cells emerge; these cells are the start of the mTEC population, a population that increases in size during late embryonic and neonatal development (Baik et al., 2013). We have used the cTEC marker Ly51, as a surrogate for CD205, along with CD40, to allow the identification of these TEC populations.

Thymi from E12 CCRL1-GFP mice were digested and stained for CD45, EpCAM, Ly51, and CD40 for analysis by flow cytometry. Expression of CCRL1 by $CD45^{-}EpCAM^{-}$ mesenchymal cells was negligible. In addition, CCRL1 was undetectable on all $EpCAM^{+}$ TEC populations (Figure 26A). To confirm this observation, thymi from E12 WT mice were frozen and cryosections were generated. Sections were

stained for CCRL1 and pan-keratin (Figure 26B). CCRL1 expression was not detectable by any cells within the E12 thymus.

E13 CCRL1-GFP thymi were analysed using the same method of flow cytometry (Figure 27A, B), and immunofluorescence (Figure 27C). No $CCRL1^+$ cells were detectable in the $EpCAM^-CD45^-$ thymic mesenchyme population. Analysis of the E13 TEC compartment by flow cytometry revealed two populations of cells ($CD40^-Ly51^-$, and $CD40^-Ly51^+$). Expression of CCRL1 was detected in both of these populations of cells (mean: 7.9% of $CD40^-Ly51^-$, and 11.6% of $CD40^-Ly51^+$). Immunofluorescence analysis of E13 WT thymi stained with anti-CCRL1 showed few $CCRL1^+$ cells at the periphery of the thymic anlagen, however CCRL1 did not co-stain with pan-keratin.

Flow cytometric analysis of the E14 thymus revealed multiple TEC populations ($CD40^-Ly51^-$, $CD40^-Ly51^+$, $CD40^{int}Ly51^+$, $CD40^{hi}Ly51^+$, and $CD40^{hi}Ly51^-$) (Figure 28A). CCRL1 was expressed by a relatively high proportion of $CD40^-Ly51^-$ cells (mean: 49%), and $CD40^-Ly51^+$ cells (mean: 69%). A small population of the maturing cTEC ($CD40^{int}Ly51^+$) express CCRL1 (mean: 33% of cells). Within the E14 thymus the emergence of the mTEC population was visible ($CD40^{hi}Ly51^-$), however no $CCRL1^+$ cells were detected within this population (Figure 28B). CCRL1 expression was significantly upregulated on $CD40^-Ly51^+$ cells compared to $CD40^-Ly51^-$ cells ($p=0.0006$), and was significantly downregulated at every subsequent stage of TEC development. Analysis of the E14 thymus by immunofluorescence showed CCRL1 expression by many cells at the periphery of the thymus (Figure

29C). No co-localisation was detectable between CCRL1 and pan-keratin, and the possible reasons for this are discussed later in this chapter.

Flow cytometric analysis of the E15 thymus revealed a significant upregulation of CCRL1 expression between transition of $CD40^{-}Ly51^{-}$ cells to $CD40^{-}Ly51^{+}$ cells ($p=0.0286$). CCRL1 was expressed by 53.2% of $CD40^{-}Ly51^{-}$ cells, 87.3% of $CD40^{-}Ly51^{+}$ cells, 82.9% of $CD40^{int}Ly51^{+}$ cells, and 41.4% of $CD40^{hi}Ly51^{+}$ cells (mean values). The emerging mTEC population ($CD40^{hi}Ly51^{-}$) expressed much lower levels of CCRL1 compared to $CD40^{hi}Ly51^{+}$ cells (mean: 8.2% of cells, $p=0.0286$) (Figure 29B). Immunofluorescence of the E15 thymus also revealed much greater expression of CCRL1 than seen at earlier developmental stages. The location of CCRL1 expression was also altered from earlier developmental stages; at E15 CCRL1 is expressed throughout the thymus rather than being localised at the periphery (Figure 29C). Some co-staining is detected between CCRL1 and pan-keratin.

Analysis of the E17 thymus by flow cytometry showed a similar expression pattern of CCRL1 as in the E15 thymus (Figure 30A). Here, CCRL1 was expressed by 97.6% of $CD40^{-}Ly51^{+}$, 94.8% of $CD40^{lo}Ly51^{+}$, and 95.6% of $CD40^{int}Ly51^{+}$ cells (mean values). Expression of CCRL1 by mature cTEC ($CD40^{hi}Ly51^{+}$) was significantly reduced compared to $CD40^{int}Ly51^{+}$ cells (mean: 82%, $p=0.0135$), and expression by $CD40^{hi}Ly51^{-}$ mTEC was further reduced compared to $CD40^{hi}Ly51^{+}$ cells (mean: 6.4%, $p=0.0009$) (Figure 30B).

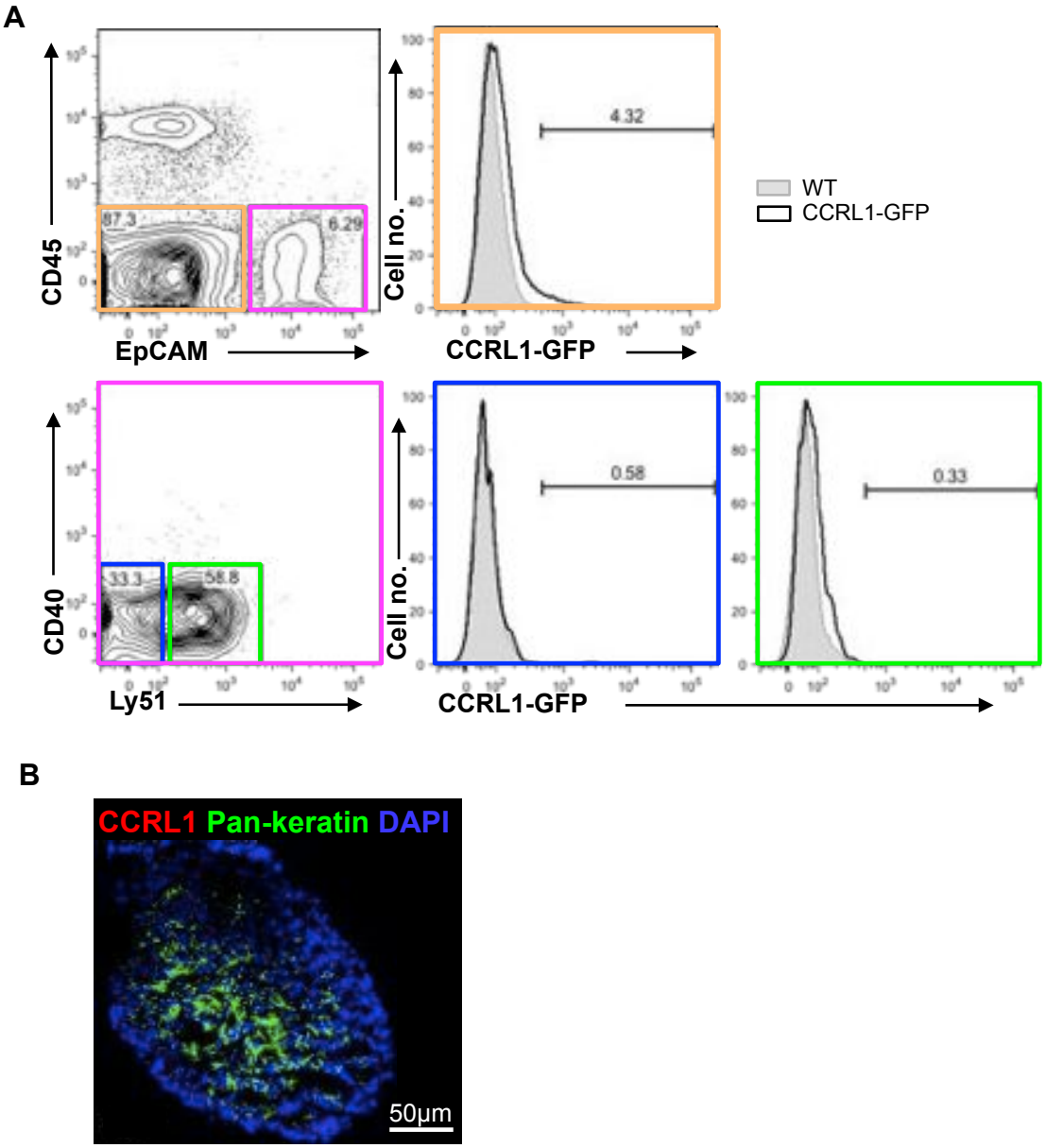

Figure 26. CCRL1 is Not Expressed Within the E12 Thymus.

E12 thymi from CCRL1-GFP mice were digested and stained for flow cytometry. Live cells were gated prior to the analysis shown. Overlaid histograms show GFP expression in WT and CCRL1-GFP mice. CCRL1 expression is not detected in $CD45^{-}EpCAM^{-}$ cells, $CD45^{-}EpCAM^{+}CD40^{-}Ly51^{-}$ or $CD45^{-}EpCAM^{+}CD40^{-}Ly51^{+}$ cells (A). Cryosections of E12 WT thymi were stained for CCRL1 (red), in conjunction with pan-keratin (green) and DAPI (blue) (B). No $CCRL1^{+}$ cells were visible within the E12 thymus. Immunofluorescence staining is representative of at least three thymi.

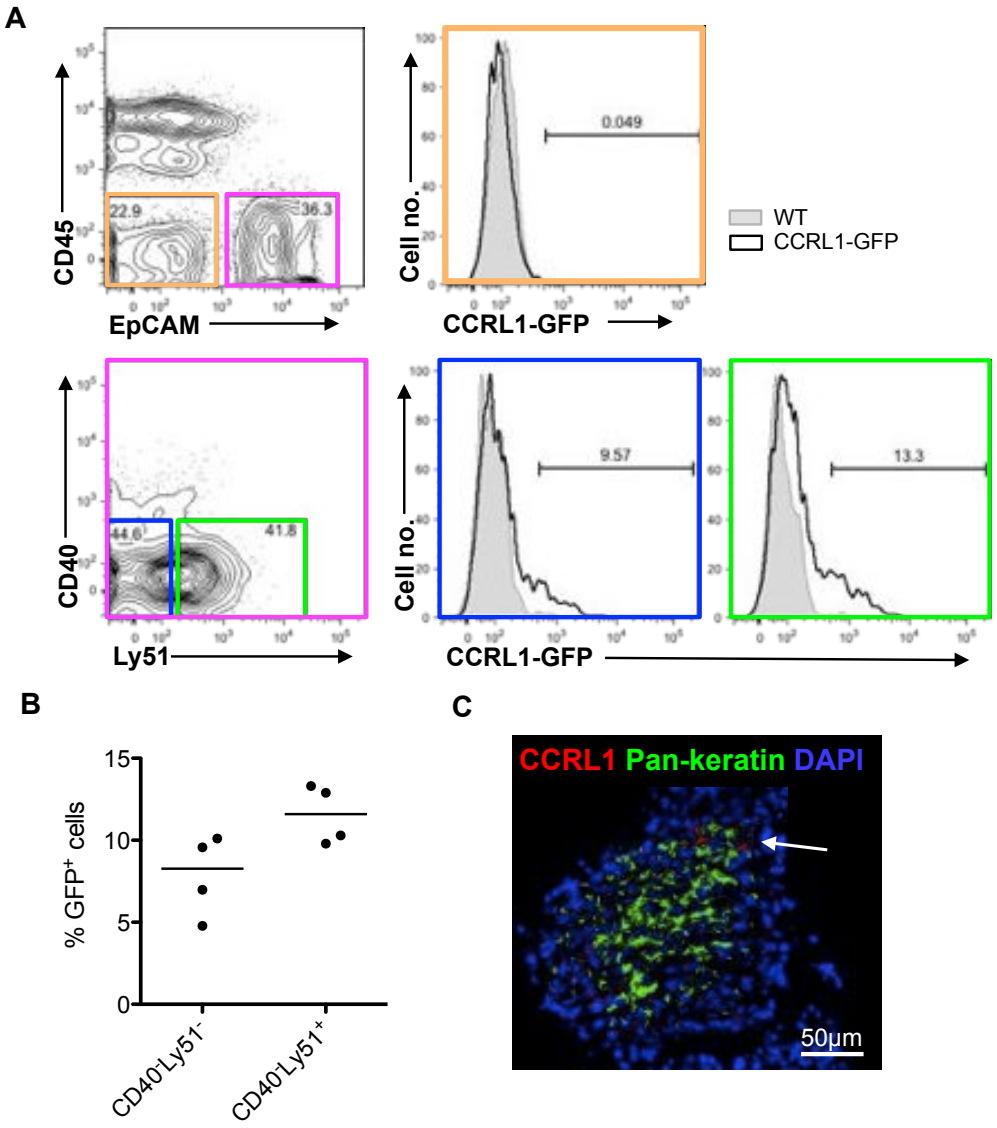

Figure 27. CCRL1 is Expressed by TEC Within the E13 Thymus.

E13 thymi from CCRL1-GFP mice were digested and stained for flow cytometry. Live cells were gated prior to the analysis shown. Overlaid histograms show GFP expression in WT and CCRL1-GFP mice. CCRL1 expression is not detected in $CD45^-EpCAM^-$ cells. $CD45^-EpCAM^+CD40^-Ly51^-$ and $CD45^-EpCAM^+CD40^-Ly51^+$ cells reveal a population of $CCRL1^+$ cells (A). Quantitation of GFP expression by TEC (B) n=4. Cryosections of E13 WT thymi were stained for CCRL1 (red), in conjunction with pan-keratin (green) and DAPI (blue) (B). Few $CCRL1^+$ cells were visible within the E13 thymus (shown with white arrow). Immunofluorescence staining is representative of at least three thymi.

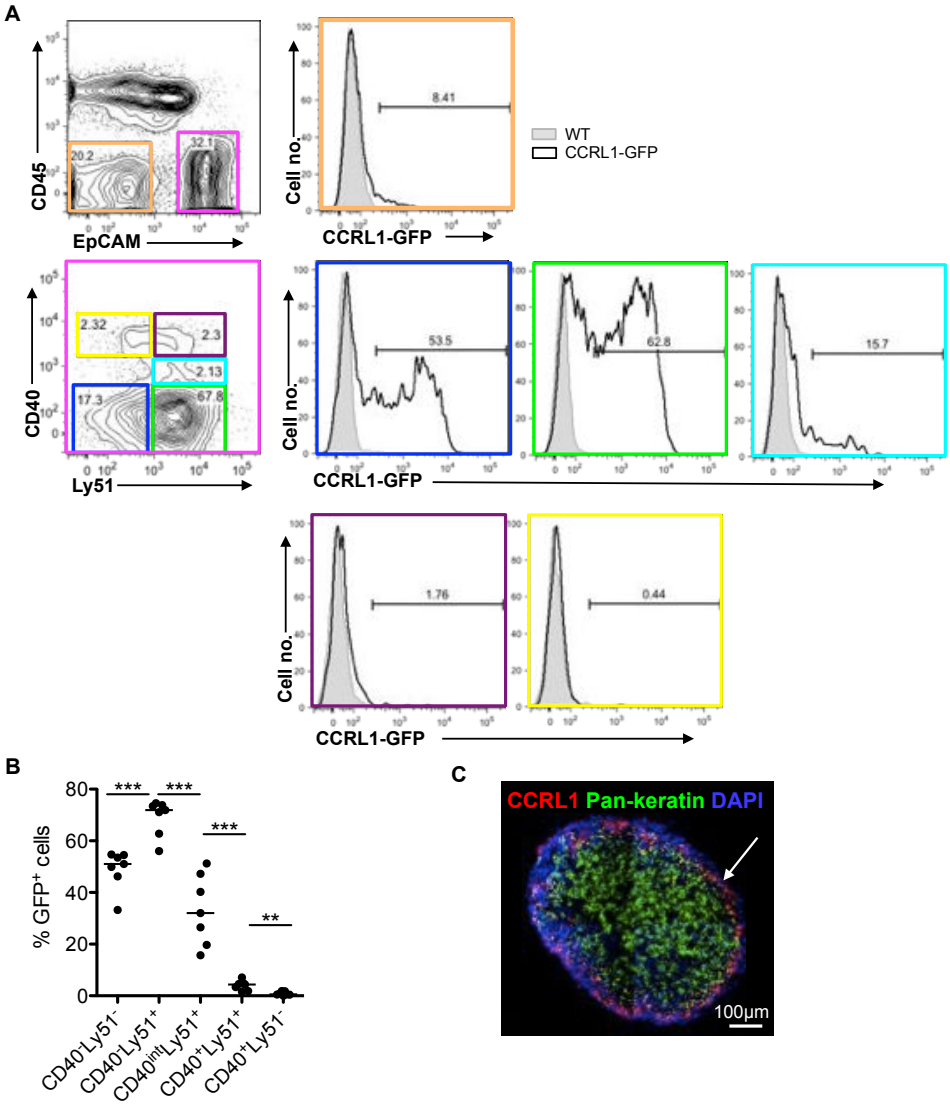

Figure 28. CCRL1 is Expressed by Immature cTEC at E14.

E14 thymi from CCRL1-GFP mice were digested and stained for flow cytometry. Live cells were gated prior to the analysis shown. Overlaid histograms show GFP expression in WT and CCRL1-GFP mice. CCRL1 expression is detected in a small proportion of $CD45^{-}EpCAM^{-}$ cells. $CD45^{-}EpCAM^{+}CD40^{-}Ly51^{-}$ and $CD45^{-}EpCAM^{+}CD40^{-}Ly51^{+}$ cells reveal expression of CCRL1 (A). Quantitation of GFP expression by TEC (B) n=7 **p=<0.01, ***p=<0.001*. Cryosections of E14 WT thymi were stained for CCRL1 (red), in conjunction with pan-keratin (green) and DAPI (blue) (B). $CCRL1^{+}$ cells were visible at the subcapsular region of the E14 thymus (shown with white arrow). Immunofluorescence staining is representative of at least three thymi.

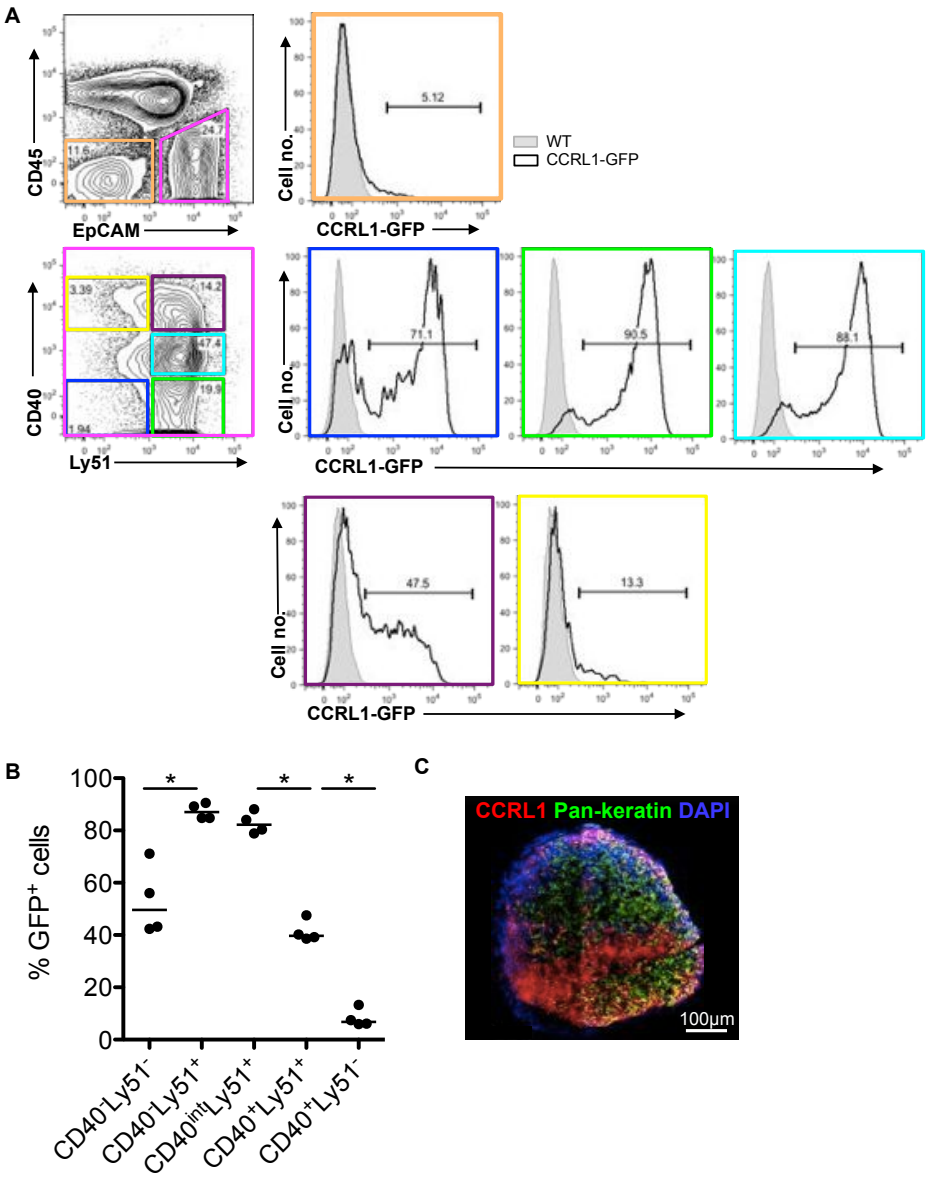

Figure 29. CCRL1 is Expressed by Immature and Mature cTEC at E15.

E15 thymi from CCRL1-GFP mice were digested and stained for flow cytometry. Live cells were gated prior to the analysis shown. Overlaid histograms show GFP expression in WT and CCRL1-GFP mice. $CD45^{-}EpCAM^{+}CD40^{-}Ly51^{-}$, $CD45^{-}EpCAM^{+}CD40^{-}Ly51^{+}$, $CD45^{-}EpCAM^{+}CD40^{int}Ly51^{+}$ and $CD45^{-}EpCAM^{+}CD40^{+}Ly51^{+}$ cells reveal expression of CCRL1 (A). Quantitation of GFP expression by TEC (B) n=4 *$p<0.05$*. Cryosections of E15 WT thymi were stained for CCRL1 (red), in conjunction with pan-keratin (green) and DAPI (blue) (C). $CCRL1^{+}$ cells were visible throughout the E15 thymus. Immunofluorescence staining is representative of at least three thymi.

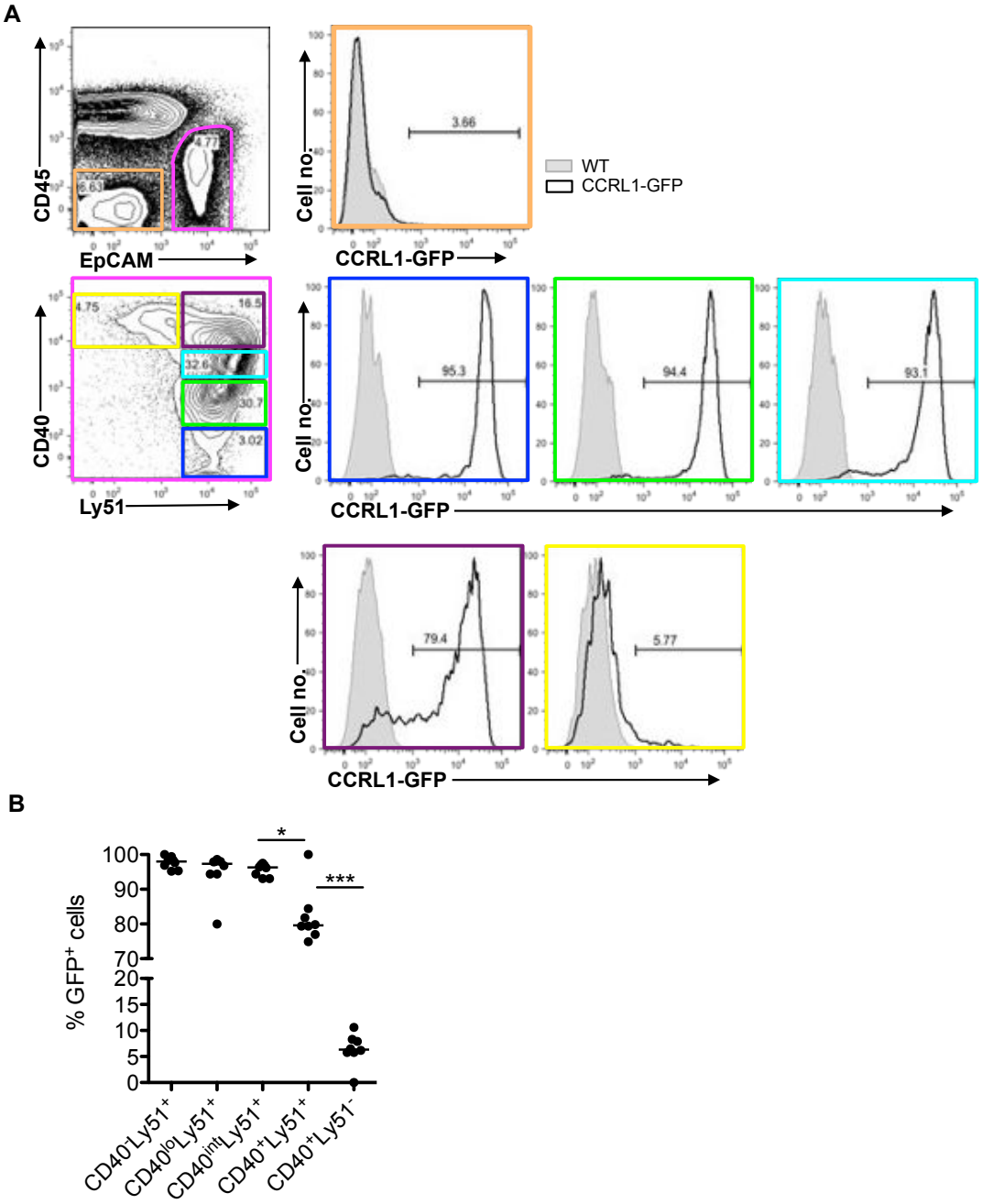

Figure 30. CCRL1 is Highly Expressed by all cTEC at E17.

E17 thymi from CCRL1-GFP mice were digested and stained for flow cytometry (A). Overlaid histograms show GFP expression in WT and CCRL1-GFP mice. Live cells were gated prior to the analysis shown. $CD45^{-}EpCAM^{+}CD40^{-}Ly51^{-}$, $CD45^{-}EpCAM^{+}CD40^{lo}Ly51^{+}$, $CD45^{-}EpCAM^{+}CD40^{int}Ly51^{+}$ and $CD45^{-}EpCAM^{+}CD40^{+}Ly51^{+}$ cells reveal expression of CCRL1. Quantitation of GFP expression by TEC (B) n=8 *$p<0.05$, ***$p<0.001$*

3.2.11 CCRL1 Is Expressed Within The Human Thymus

Expression of CCRL1 was determined within the human thymus using an anti-human CCRL1 antibody in conjunction with immunofluorescence (Takatsuka et al., 2011). Human thymus tissue was acquired from young children undergoing cardiac surgery. The human thymus was cut into small pieces (approx. $1cm^2$) and frozen. 8μm cryosections were generated from the frozen tissue, and sections were stained for CD4 and CD8, in conjunction with CCRL1, to determine cortex and medulla (Figure 31A). CCRL1 expression is detected primarily within the thymic medulla (based on the location of SP4 and SP8 thymocytes). In the murine thymus, CCRL1 expression was not found within the medulla by immunofluorescence, therefore it was vital to confirm this unusual expression pattern in the human thymus. To achieve this, sections of human thymus were stained with antibodies against EpCAM (to identify mTEC), and CD205 (to identify cTEC) (Figure 31B). This staining revealed $CCRL1^+$ cells located within the $EpCAM^+$ thymic medulla, particularly associated with structures that appear to be Hassall's Corpuscles. Few $CCRL1^+$ cells were also detected within the cortex, close to the CMJ. Co-staining was not visible between CCRL1 and either EpCAM or CD205. CCRL1 expression close to the CMJ prompted us to determine whether CCRL1 was expressed surrounding vessels in the human thymus, as in the mouse thymus. We therefore stained sections of human thymus for CD31 and CCRL1 to determine if the expression pattern was similar (Figure 31C). This staining combination revealed $CCRL1^+$ cells surrounding $CD31^+$ endothelial cells.

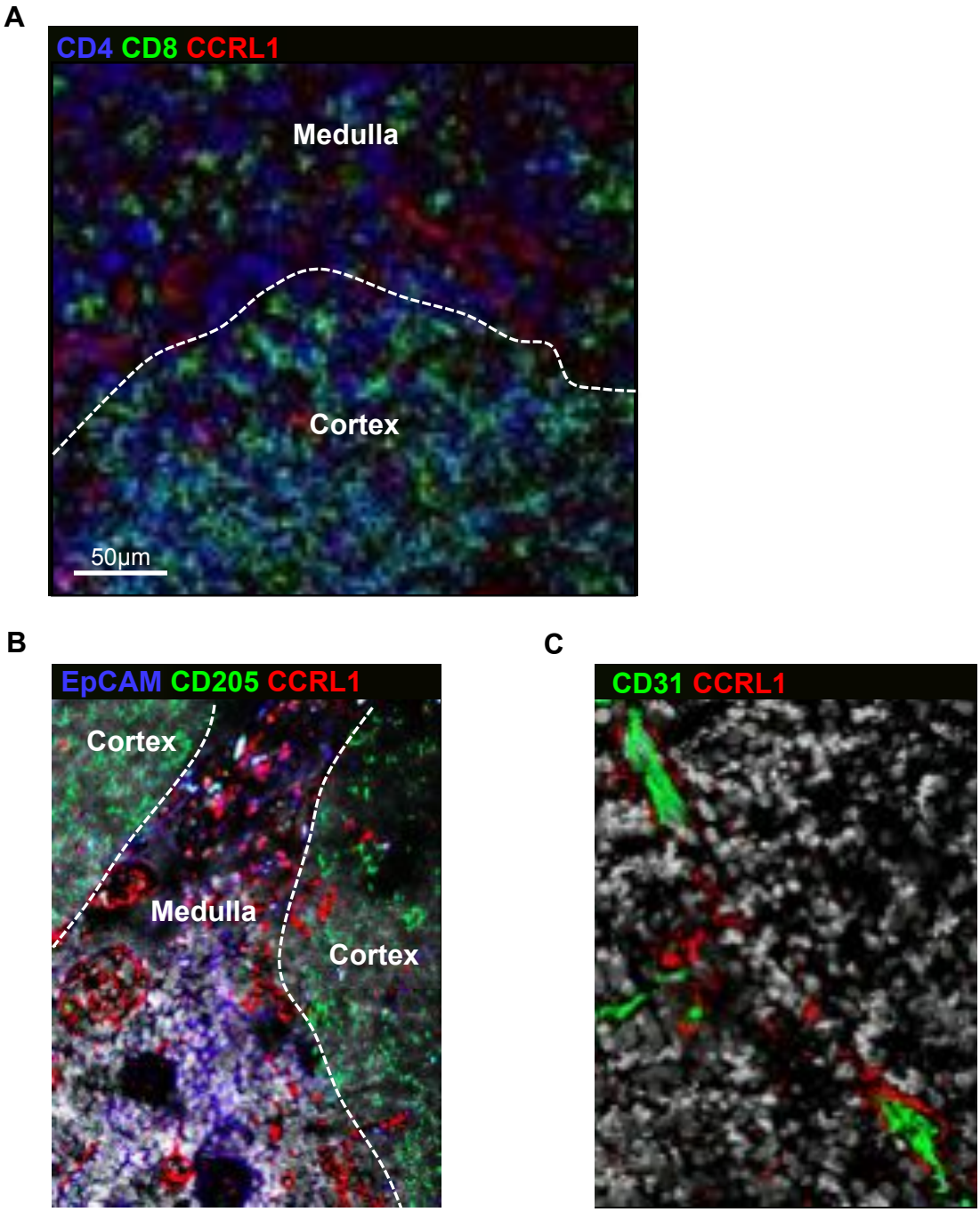

Figure 31. CCRL1 is Expressed Within the Human Thymus.

Human thymi were frozen and cryosections generated. Sections were stained for CCRL1 in conjunction with CD4 and CD8 (A), EpCAM and CD205 (B), and CD31 (C). CCRL1 is expressed within the thymic medulla, and surrounding $CD31^+$ endothelial cells. Image representative of one experiment.

3.3 Discussion

3.3.1 CCRL1 is Expressed by TEC

This chapter described a detailed analysis of CCRL1 expression within the adult and embryonic thymus. We have identified CCRL1 expressing cells using both anti-CCRL1 antibody, and CCRL1-GFP reporter mice. It is important to note that CCRL1 detection using the antibody will show expression of CCRL1 protein, whereas detection using CCRL1-GFP reporter mice will show CCRL1 gene activity. If expression of CCRL1 is highly regulated at the protein level, there will be discrepancies in the expression of CCRL1 using both methods of detection. We have shown that detection of CCRL1 by both approaches gives a similar expression pattern, however the anti-CCRL1 antibody gives a much weaker expression profile compared to CCRL1-GFP reporter mice. In addition to abundance of CCRL1 protein, other reasons for this comparatively weaker detection of CCRL1 may be due to a working dilution of the primary or secondary antibody that is too low, or a poor ability of the secondary antibody to recognise and bind the primary antibody. The anti-CCRL1 antibody was tested at different concentrations, with additional amplification staining steps, and in conjunction with different secondary antibodies. The protocol that gave the optimal balance between specificity and sensitivity was used for all anti-CCRL1 antibody detection in this thesis.

We have used flow cytometry and immunofluorescence to show that $CD45^+$ cells within the thymus do not express CCRL1; this is in agreement with several publications (Bunting et al., 2013, Rode and Boehm, 2012, Heinzel et al., 2007). Expression of CCRL1 by thymic epithelial cells (TEC) has previously been detected

using immunofluorescence, flow cytometry and real time PCR of sorted cell populations (Bunting et al., 2013, Rode and Boehm, 2012, Heinzel et al., 2007). Interestingly, our flow cytometric analysis of thymi from CCRL1-GFP mice shows CCRL1 expression by approximately 60% of Ly51$^+$ cTEC whereas a similar analysis of these mice by Heinzel *et al* showed CCRL1 expression by all CDR-1$^+$ (Ly51) cTECs (Heinzel et al., 2007). In keeping with our data, selective ablation of cTEC by CCRL1-DTR transgenic mice does not affect some small clusters of keratin-8$^+$ cTEC, thus providing additional evidence that not all cTEC express CCRL1 (Rode and Boehm, 2012).

Our study shows expression of CCRL1 by a population of mTEC using flow cytometry but not immunofluorescence. This is in contrast to the report by Heinzel *et al*, where flow cytometry revealed a lack of CCRL1 expression by all UEA-1$^+$ mTECs. Furthermore, ablation of CCRL1$^+$ TEC by the CCRL1-DTR system leaves the mTEC population intact, suggesting that, in agreement with Heinzel *et al,* CCRL1 is not expressed by mTEC (Rode and Boehm, 2012). Despite this, a recent publication using CCRL1-GFP reporter mice identified intermediate levels of CCRL1 expression by a population of mTEC in the postnatal thymus (Ribeiro et al., 2014). The fact that we can detected CCRL1 expression by mTEC using only flow cytometry may be due to the lower sensitivity of immunofluorescence (Basiji et al., 2007). Our flow cytometric analysis identified mTEC as EpCAM$^+$Ly51$^-$, therefore it is possible that some CCRL1$^+$ cTEC which may express lower levels of Ly51 could be included in this gate. To further assess CCRL1 expression by cTEC and mTEC we stained for CD40, CD80 and MHC-II to allow the division of cTEC and mTEC into

mature and immature populations, moreover, inclusion of CD80 allows the positive identification of at least some mTEC. CCRL1 expression by each population was determined by flow cytometry and revealed expression of CCRL1 by both immature and mature cTEC and mTEC. CCRL1 detection by mature mTEC (MHC-II^{hi}CD80^{hi}), suggest that this is true expression by mTEC, rather than contamination within the gate by cTEC, and is in agreement with the recent publication by Ribeiro *et al*.

3.3.2 CCRL1 is Expressed by Thymic Mesenchyme

Thymic stroma consists of mesenchymal cells and TEC. The mesenchymal population within the thymus is poorly defined, however a population of EpCAM^{-} Ly51^{+} cells of neural crest origin have been described (Muller et al., 2008). CCRL1 expression by different populations of thymic mesenchymal cells have been investigated by others using real time PCR. Rode and colleagues sorted EpCAM^{-} Ly51^{+} cells and detected minimal expression of CCRL1, while Bunting *et al* sorted bulk non-epithelial non-endothelial (EpCAM^{-}CD31^{-}) cells and detected higher levels of CCRL1 transcript than those expressed by CD45^{+} cells (Bunting et al., 2013, Rode and Boehm, 2012).

We determined expression of CCRL1 within the mesenchymal population by flow cytometry using CCRL1-GFP reporter mice. We showed CCRL1 expression by a population of EpCAM^{-}Ly51^{int}podoplanin^{+} cells. This population of cells has been shown by others to produce retinoic acid, which is needed for the regulation of TEC expansion (Sitnik et al., 2012). Our flow cytometric analysis of the thymic mesenchyme showed that the majority of podoplanin^{+} cells express intermediate

levels of Ly51, therefore this population is likely to include the recently described podoplanin^{+} thymic fibroblastic reticular cells (tFRCs) (Fuertbauer et al., 2013). We show CCRL1 expression by approximately 20% of Ly51^{int}podoplanin^{+} cells, which may account for the low levels of CCRL1 transcript shown by Bunting *et al* in EpCAM^{-}CD31^{-} cells. Despite our ability to detect CCRL1 expression by this population using flow cytometry, we were unable to confirm expression of CCRL1 by mesenchymal cells using immunofluorescence. We have detected few cells, which are negative for pan-keratin by immunofluorescence, however like EpCAM, pan-keratin may not stain all TEC when using immunofluorescence. Moreover, we were unable to combine pan-keratin staining with the use of CCRL1-GFP reporter mice. CCRL1^{+} mesenchymal cells express podoplanin, however many TEC also express podoplanin, therefore this cannot be used as a definitive marker for either population. We would need to further characterise the CCRL1^{+} mesenchymal population by flow cytometry to identify additional markers that could be used to identify these same cells using immunofluorescence, in order to obtain information regarding their intrathymic location.

3.3.3 CCRL1 is Expressed by Perivascular and Subcapsular TEC

Heinzel *et al* first described CCRL1 expression by cells surrounding tomato lectin stained endothelial cells within the thymus. This article concluded that these cells were TEC based on the expression of EpCAM by all CCRL1-GFP^{+} cells (Heinzel et al., 2007). We confirmed CCRL1 expression by perivascular cells, but further identified these cells as PDGFRβ^{+}podoplanin^{+} cTEC. Podoplanin^{+} epithelial cells associated with thymic vasculature have previously been described (Farr et al.,

1992), however PDGFRβ expression described within the thymus has been limited to mesenchymal cells (Odaka, 2009). As a result, this population of cTEC is not described in the literature, therefore it would be necessary to show co-expression of PDGFRβ with TEC-specific markers.

CD248 is a pericyte-specific mesenchymal stromal cell marker within the thymus that regulates blood endothelial vessel formation (Lax et al., 2012). We have shown that CCRL1 is not expressed by $CD248^{+}$ pericytes. Interestingly our staining revealed CD248 is commonly expressed surrounding vessels which are not surrounded by CCRL1 and vice-versa. This heterogeneity in vascular structures may point towards differences in function of these vessels. In addition, we have confirmed the expression of CCRL1 by subcapsular cTECs described by Heinzel *et al* (Heinzel et al., 2007). Moreover, we further characterised these cells based on their expression of podoplanin.

3.3.4 CCRL1 is Expressed Within the Thymus During Ontogeny

The expression of CCRL1 by TEC has been described in the embryonic thymus (Heinzel et al., 2007, Ribeiro et al., 2014). In agreement with Heinzel *et al,* we could not detect any $CCRL1^+$ cells within the E12 thymus by confocal microscopy or flow cytometry, but were able to detect $CCRL1^+$ cells at the periphery of the thymic anlagen by E13.5 of gestation. By E14, the thymus had a clear population of $CCRL1^+$ cells surrounding the entire periphery, and flow cytometric analysis identified these cells as $CD40^-Ly51^-$ and $CD40^-Ly51^+$. Widespread CCRL1 expression was visible in the E15 thymus, however Heinzel *et al* reported that at this stage of gestation, CCRL1 expression was limited to subcapsular regions (Heinzel et al., 2007). Flow cytometric analysis of the E15 thymus showed high expression by immature and mature cTEC. This data is in agreement with Ribeiro *et al*, who described the progressive acquisition of CCRL1 by cTEC during E12.5-E15.5 of gestation. By E17, we showed expression of CCRL1 by the majority of immature $CD40^{-/low}$ cTEC, and $CD40^+$ mature cTEC.

It is interesting to note that within the E17 thymus, considerably more cTEC express CCRL1 at higher levels, than within the adult thymus. The gates for GFP^+ cells in both adult and embryonic thymi were set based on the GFP level in the same population of cells from WT mice of the same age. Background levels of GFP, as determined by levels in WT mice, are lower in the embryonic stromal cell populations compared to those from the adult. This may account for an underestimation of the proportion of GFP^+ cells in the adult thymus, as it would suggest that adult WT stromal cells have increased auto-fluorescence.

Interestingly, CCRL1 expression detected by immunofluorescence did not reveal co-staining with pan-keratin, whereas flow cytometric analysis clearly identified these cells as $EpCAM^{+}$. Flow cytometric analysis of CCRL1 expression in the embryonic thymus used CCRL1-GFP mice, whereas immunofluorescence analysis used anti-CCRL1 antibody. The discrepancies in the data produced by both methods is likely due to the different sensitivities of both methods as discussed earlier in this chapter.

Although still not fully clear, the developmental programme of TEC during embryogenesis has recently been revised and shows that $CD205^{+}$ TEC, (a marker commonly associated with cTEC) can give rise to mature mTEC (Baik et al., 2013). It is clear that during this pathway CCRL1 is downregulated, thus providing evidence that this molecule is expressed by precursors to both mTEC and cTEC lineages, however CCRL1 expression is maintained primarily within cTEC populations.

3.3.5 CCRL1 Has a Distinct Expression Pattern in The Human Thymus

CCRL1 expression within the human thymus has not previously been determined. For this reason we used an anti-human CCRL1 antibody and show that unlike the murine thymus, CCRL1 is expressed primarily within the medulla. Despite this localisation of CCRL1 expression, immunofluorescence did not reveal co-staining between CCRL1 and EpCAM or CD205, therefore we were unable to conclude that CCRL1 is expressed by TEC. The role of the cortex and medulla in murine and human thymi are similar, therefore there is not an obvious reason for the differential expression of CCRL1. For these reasons, confirmation of CCRL1 expression either using a different CCRL1-antibody or by PCR on sorted populations of cells, would be necessary before drawing conclusions from this data.

It was initially proposed that human CCRL1 binds CXCL13 (Gosling et al., 2000), however follow-up studies have not since mentioned this interaction. Human thymic B cells express CXCR5, the classical chemokine receptor for CXCL13 (Rehm et al., 2009), therefore if CCRL1 scavenges CXCL13, it may play a role in the positioning of B cells within the human thymus. Within the human thymic medulla, epithelial cell structures called Hassall's corpuscles are proposed to aid in the removal of apoptotic cells and the development of Treg (Watanabe et al., 2005). CCRL1 expression is detected on groups of medullary cells which appear to be Hassall's corpuscles based on EpCAM and DAPI staining, however co-staining was not visible, therefore further analysis would be needed to confirm this.

Similarly to the murine thymus, perivascular cells within the human thymus also express CCRL1. Although their positioning would suggest they are TEC, this has not been shown.

To summarise, CCRL1 is expressed solely by stromal cells within the murine thymus. It is expressed primarily by cTEC positioned at the SCZ, by cells surrounding vessels at the CMJ, and by cells scattered throughout the cortex. Expression of CCRL1 by cells surrounding vasculature is maintained in the human thymus, however unlike the murine thymus, CCRL1 is expressed primarily within the human thymic medulla. We have identified CCRL1 expression within the murine embryonic thymus, and have specifically shown the onset of expression at E13 of gestation, where it is expressed by few cells at the periphery. In addition, we have shown that as ontogeny progresses, CCRL1 expression becomes more widespread until the majority of cTEC are $CCRL1^{+}$. Due to the heterogeneous expression of CCRL1 by thymic stromal cell populations, it may be of use as a marker to further study distinct TEC and mesenchymal populations to aid our understanding of thymic stromal cell development and function.

CHAPTER 4: INVESTIGATING THE ROLE OF CCRL1 IN THYMUS DEVELOPMENT AND FUNCTION

4.1 Introduction and Aims

Intrathymic T cell development requires developing thymocytes to migrate within and between specialised thymic microenvironments. This intrathymic migration is mediated by chemokines, in particular CCL19, CCL21 and CCL25, which bind the classical chemokine receptors CCR7 and CCR9, and the atypical chemokine receptor CCRL1. In addition to intrathymic migration, these chemokines are involved in the recruitment of progenitor cells to the embryonic and adult thymus (Krueger et al., 2010, Liu et al., 2006), and the export of mature thymocytes (Ueno et al., 2004, Ueno et al., 2002).

In the previous chapter, I defined the expression of CCRL1 by thymic stroma. Such studies identified expression of CCRL1 by subsets of cTEC and mTEC, in the embryonic and adult thymus. In addition, we identified CCRL1 expression by a population of perivascular TEC, and non-epithelial stromal cells in the adult thymus.

Importantly, analysis of CCRL1 expression specifically identifies three microenvironments of the thymus: the SCZ, the cortex, and the CMJ. The SCZ is implicated in the development of DN thymocytes, and cTEC provide the necessary environment for positive selection. Vasculature at the CMJ is the site for recruitment of progenitor cells and the export of mature T cells into the periphery. Collectively, the expression of CCRL1 within these three microenvironments may suggest its involvement during multiple stages of T cell development.

Conflicting data in the literature leaves the precise role of CCRL1 during T cell development unclear. One study used mice lacking CCRL1 due to homozygous

expression of CCRL1-GFP and determined no major role for CCRL1 within the thymus (Heinzel et al., 2007). However, a more recent study analysed an alternative strain of CCRL1$^{-/-}$ mouse and described severe defects in many stages of T cell development (Bunting et al., 2013).

In view of this, the objective of this chapter is, by building on expression data in the previous chapter, to analyse several stages of T cell development in both strains of CCRL1 deficient mice, compared to WT mice, to determine any potential role for CCRL1 in these processes. Specifically the aims are:

- To determine if populations of DP and SP thymocytes are affected in the CCRL1 deficient thymus.
- To determine if DN thymocyte development is altered in the absence of CCRL1.
- To analyse the recruitment of progenitors to the CCRL1 deficient thymus.
- To determine any alteration in the export of mature T cells from the CCRL1 deficient thymus.

4.2 Results

4.2.1 CCRL1 Inhibits Thymocyte Migration to CCL19 and CCL25 *In Vitro*

In vitro studies have shown that CCRL1 binds the chemokines CCL19, CCL21, and CCL25 and targets them for degradation (Townson and Nibbs, 2002, Comerford et al., 2006). We wanted to determine the effect of CCRL1 on the ability of thymocytes to migrate in response to these ligands. This was achieved using an *in vitro* transmigration assay, similar to the assay used by Ulvmar and colleagues (Ulvmar et al., 2014). Briefly, the thymic epithelial cell line (TEP) (Tanaka et al., 1993b) was retrovirally transfected to express GFP (TEP-GFP), or CCRL1 in conjunction with GFP (TEP-CCRL1) (Figure 32). The expression of GFP was determined using flow cytometry, prior to their use in transmigration assays, to ensure a similar, and relatively high proportion of TEP cells were transfected (75.2% of TEP-GFP, and 63.5% of TEP-CCRL1) (Figure 33). Cell culture inserts with a pore size of 3μm were seeded with TEP-GFP or TEP-CCRL1. Once confluent, the media in the plates was changed to differing concentrations of CCL19 or CCL25. Unfractionated WT thymocytes from adult thymus were added to the upper well and incubated for 3 hours at 37°C.

WT thymocytes added to the CCL19 assay, 'input cells', were stained for CD4, CD8 and CCR7 and analysed by flow cytometry (Figure 34A). In addition the migrated thymocytes were also stained, and representative FACS plots show the analysis of cells that migrated in response to 10nM CCL19 (Figure 34B). It is clear that migrated cells are predominantly $CCR7^+$ SP4 and $CCR7^+$ SP8 thymocytes. The number of thymocytes that migrated in response to 0nM, 1.25nM, 2.5nM, 5nM, 10nM, 20nM

CCL19 in the presence of either TEP-GFP or TEP-CCRL1 are shown (Figure 34C). TEP transfected with CCRL1 appeared to inhibit the migration of thymocytes at concentrations ranging from 1.25-10nM CCL19. At 20nM CCL19, numbers of migrated thymocytes are similar between TEP-GFP and TEP-CCRL1.

The transmigration assay was repeated with varying concentrations of CCL25 (0-180nM) (Figure 35). Migrated thymocytes were stained for CD4, CD8, TCRβ and CCR9 and counted by flow cytometry, and representative FACS plots show cells that have migrated in response to 120nM CCL25 (Figure 35B). It is clear that TEP-GFP and TEP-CCRL1 both result in the migration of the same populations of thymocytes. Comparison between bulk thymocytes that were put into the assay, and specifically those which have migrated, reveal a preferential migration of $CCR9^+$ DP thymocytes. The number of cells that migrated was tallied (Figure 35C). Although similar numbers of cells migrated in response to 20-80nM CCL25, there is a clear reduction in the number of cells that have migrated across the TEP-CCRL1 monolayer in response to 120nM CCL25. At 180nM CCL25, numbers of migrated thymocytes are reduced, and similar between TEP-GFP and TEP-CCRL1.

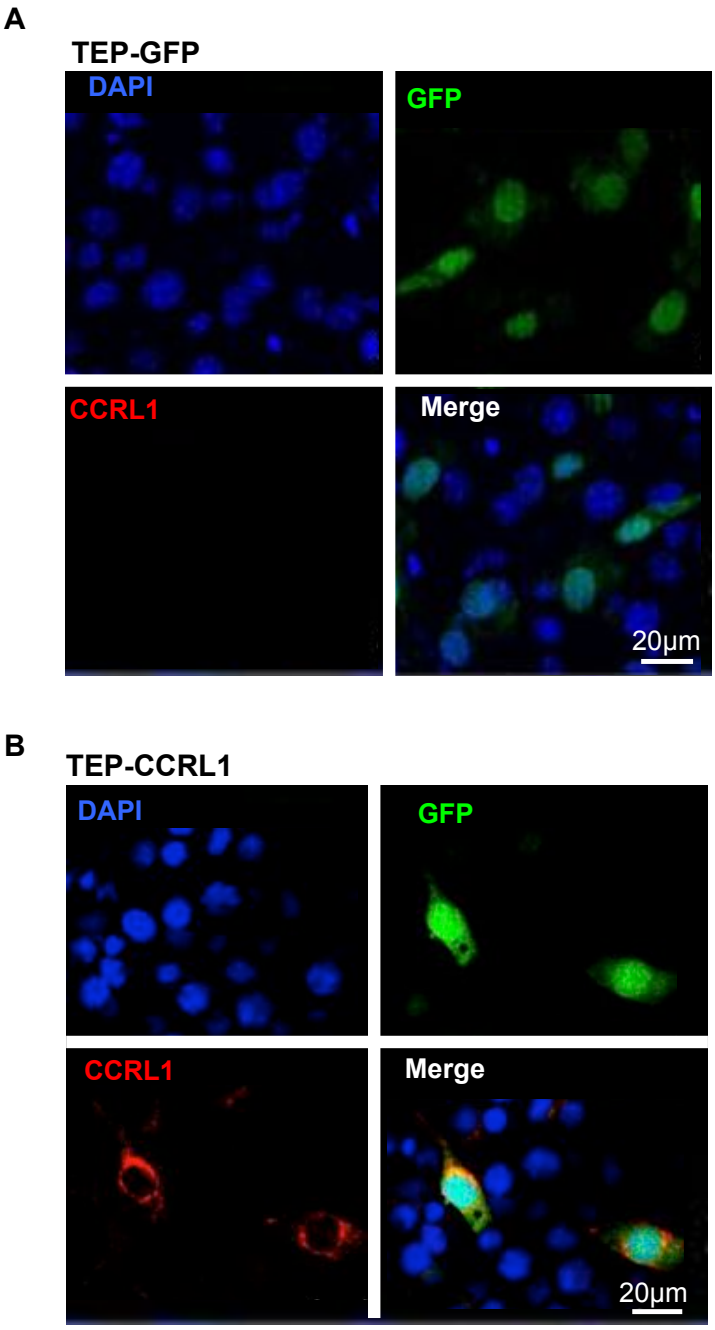

Figure 32. Expression of CCRL1 and GFP by TEP-GFP and TEP-CCRL1

TEP cells transfected with TEP-GFP (A) or TEP-CCRL1 (B) were seeded onto lab-tek chamber slides and cultured overnight at 37°C. The following day, transfected cells were stained for CCRL1 and DAPI and images acquired. Expression of CCRL1 can be seen on TEP cells transfected with TEP-CCRL1 only. GFP^+ cells are present within TEP-GFP and TEP-CCRL1 cells.

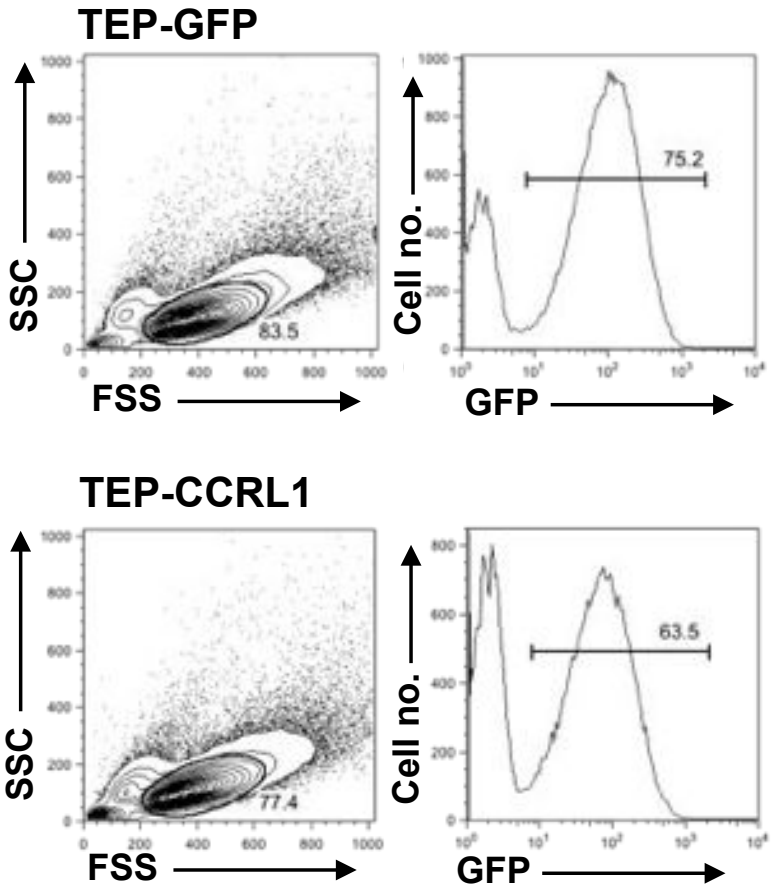

Figure 33. Expression of GFP by TEP-GFP and TEP-CCRL1 by Flow Cytometry

Expression of GFP by TEP-GFP and TEP-CCRL1 were assessed using flow cytometry to determine the proportion of transfected cells, prior to their use in transmigration assays.

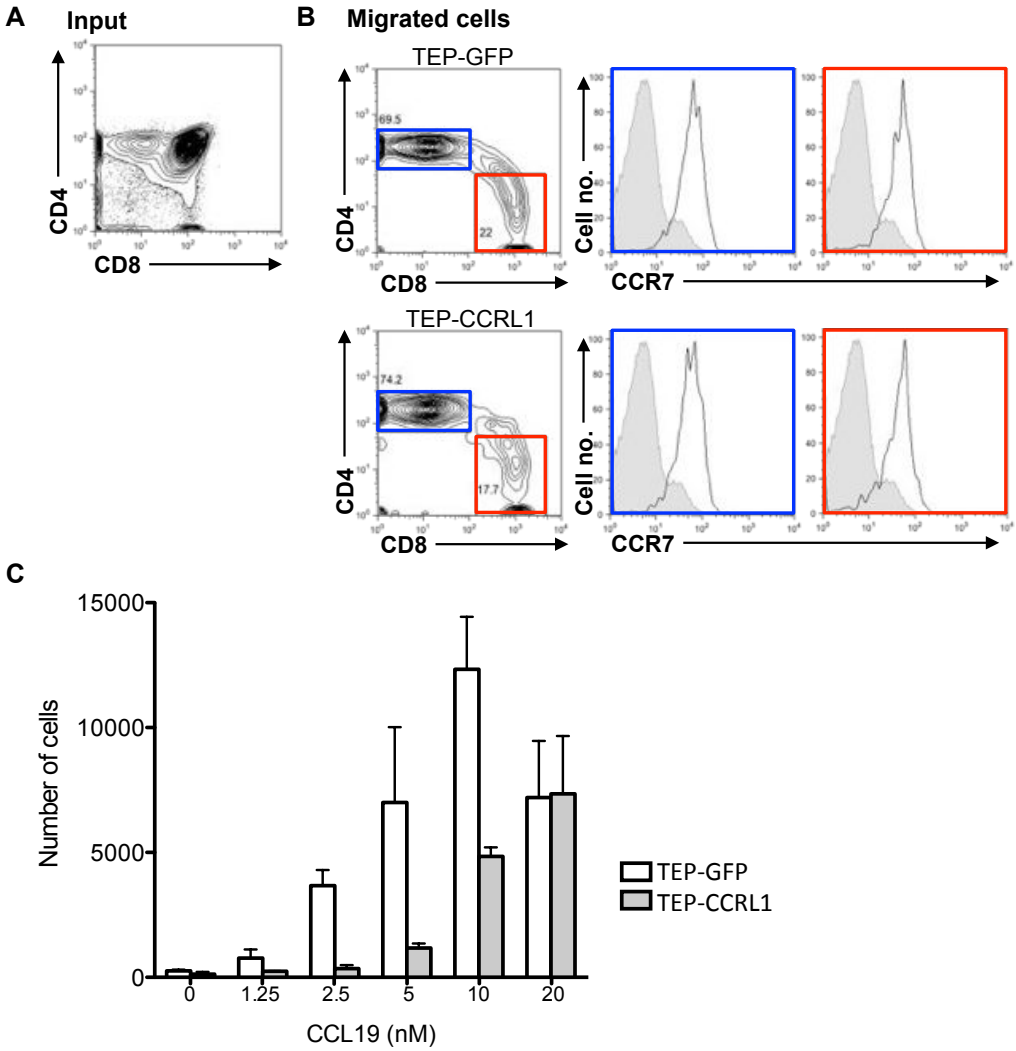

Figure 34. CCRL1 Inhibits Thymocyte Migration in Response to CCL19 *In Vitro*

WT thymocytes were added to a transwell coated with a monolayer of thymic epithelial cells (TEP) transfected with CCRL1 or vector only (GFP). Flow cytometric analysis of the thymocytes added to the assay is shown (A). Migrated thymocytes were stained for CD4, CD8 and CCR7 and analysed by flow cytometry. Grey histograms show CCR7 expression on total thymocytes added to the assay (B). Representative density plots show thymocytes that have migrated in response to 10nM CCL19. The numbers of cells in the lower chemotaxis chamber were counted using counting beads in conjunction with flow cytometry (C). Bars represent the mean, and error bars show the SEM. Each concentration of CCL19 was used in duplicate; therefore no statistical analysis was performed.

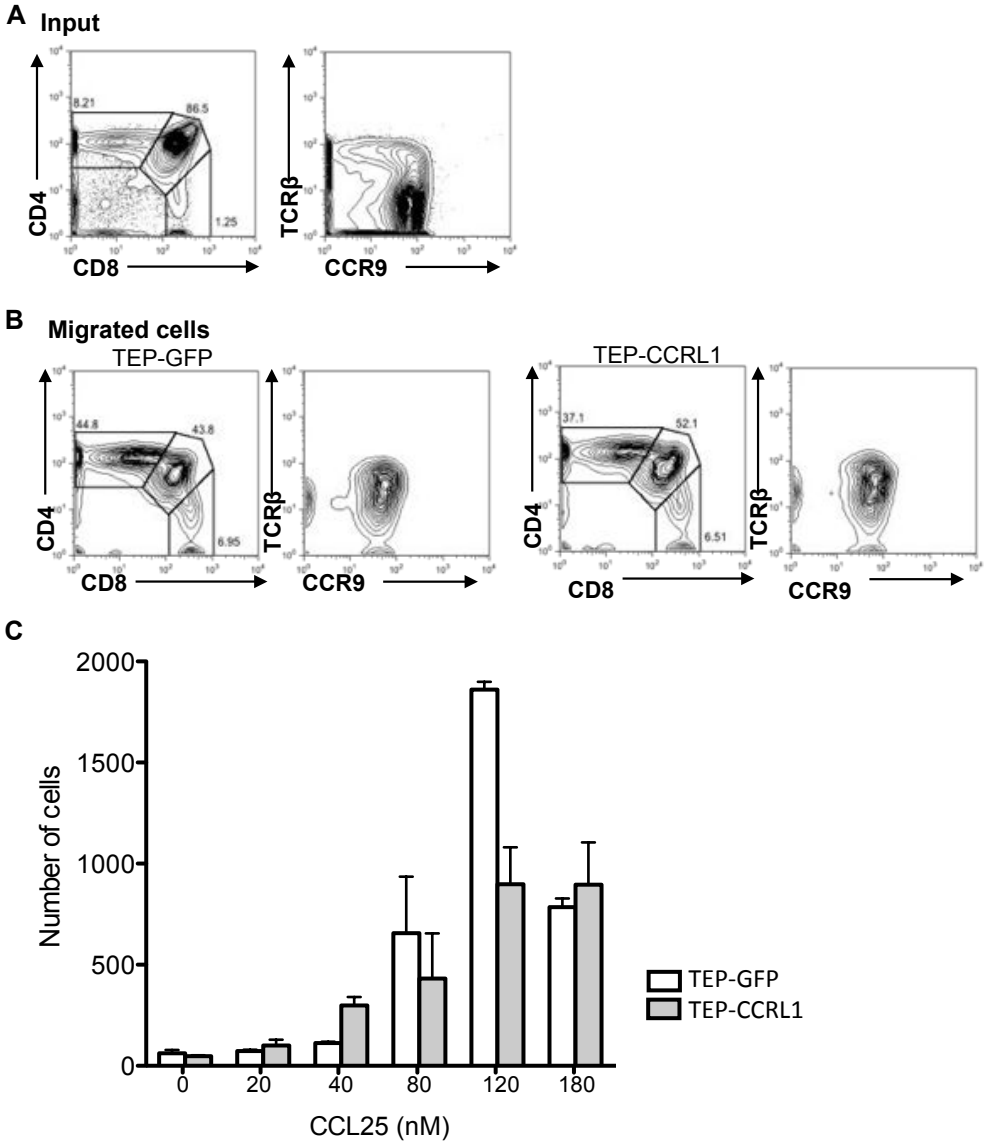

Figure 35. CCRL1 Inhibits Thymocyte Migration in Response to CCL25 *In Vitro*

WT thymocytes were added to a transwell coated with a monolayer of thymic epithelial cells (TEP) transfected with CCRL1 or vector only (GFP). Flow cytometric analysis of the thymocytes added to the assay is shown (A). Migrated thymocytes were stained for CD4, CD8, TCRβ and CCR9 and analysed by flow cytometry (B). Representative density plots show thymocytes that have migrated in response to 120nM CCL25. The numbers of cells in the lower chemotaxis chamber were counted using counting beads in conjunction with flow cytometry (C). Bars represent the mean, and error bars show the SEM. Each concentration of CCL25 was used in duplicate; therefore no statistical analysis was performed.

4.2.2 The CCRL1 Deficient Thymus is of Normal Weight and Cellularity

Our *in vitro* studies have shown the ability of CCRL1 to influence thymocyte migration. Moreover, expression of CCRL1 within the thymus suggests this molecule may play a role in T cell development and thymus function. To gain insight into the potential role of CCRL1 *in vivo,* we carried out a systematic analysis of thymus function in CCRL1 deficient mice.

Two strains of CCRL1 deficient mice have been described; conventional CCRL1$^{-/-}$ and CCRL1-$^{GFP/GFP}$. CCRL1$^{-/-}$ mice were generated by replacing the open reading frame of CCRL1 with a floxed phosphoglycerine kinase (PGK) neomycin cassette (Comerford et al., 2010). It has been reported that these mice have significant defects in thymus function, including increased thymus size and cellularity, and disruptions to the thymic stroma resulting in defective T cell development and the escape of autoreactive T cells, which leads to Sjögren's Syndrome in aged mice (Bunting et al., 2013). The second strain; CCRL1-$^{GFP/GFP}$ knock-in mice, were generated by replacing the N-terminal half of the single coding exon of CCRL1 with an EGFP cassette. Mice homozygous for GFP are CCRL1 deficient. Interestingly, all parameters of thymus function are reported to be normal in these mice (Heinzel et al., 2007). Due to these conflictions, the initial experiments in this chapter use both strains of mice.

Macroscopic examination of the thymus from CCRL1$^{-/-}$ mice showed that it has a similar size and appearance to WT and heterozygous (het) littermate controls (Figure 37A). To allow quantitation of thymus size, thymi from WT, het and CCRL1$^{-/-}$

littermates were dissected from both male and female mice and the weight determined (Figure 37B and Table 8). No statistical difference was found in the weight of the CCRL1$^{-/-}$ thymus from female or male mice compared to littermate controls (Table 10). In addition to thymus weight, the cellularity of the thymus was also determined. To do this, the thymus was digested and absolute cell number tallied using counting beads in conjunction with flow cytometry. The thymus cellularity was similar between all genotypes of the same sex, and no statistical difference was found (Figure 37C, Table 11, Table 12).

The same methods were employed to determine thymus weight and thymus cellularity from CCRL1-$^{GFP/GFP}$ mice to account for any differences in strain of mice (Figure 37D). Thymi from female CCRL1-$^{GFP/GFP}$ mice were of a similar weight and cellularity to thymi from female CCRL1$^{-/-}$ mice (Table 9 and Table 11). Moreover, there was no difference in weight or cellularity of the thymus between WT, het and CCRL1-$^{GFP/GFP}$ (Table 10, Table 12). These experiments show no difference in thymus weight or cellularity in either strain of CCRL1 deficient mice.

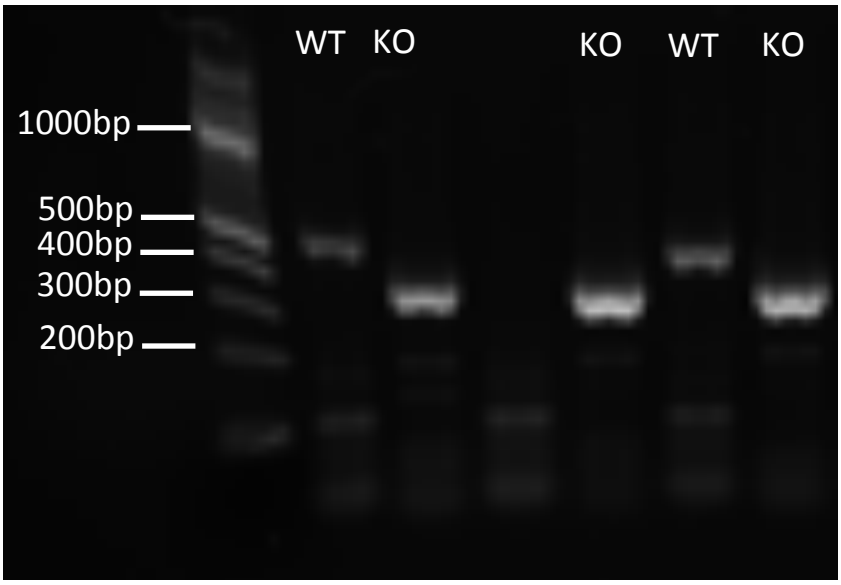

Figure 36. Representative Genotyping of CCRL1$^{-/-}$ Mice.

Image of agarose gel with DNA ladder to indicate size of PCR product. DNA from WT mice is 610bp, and CCRL1$^{-/-}$ mice is 420bp.

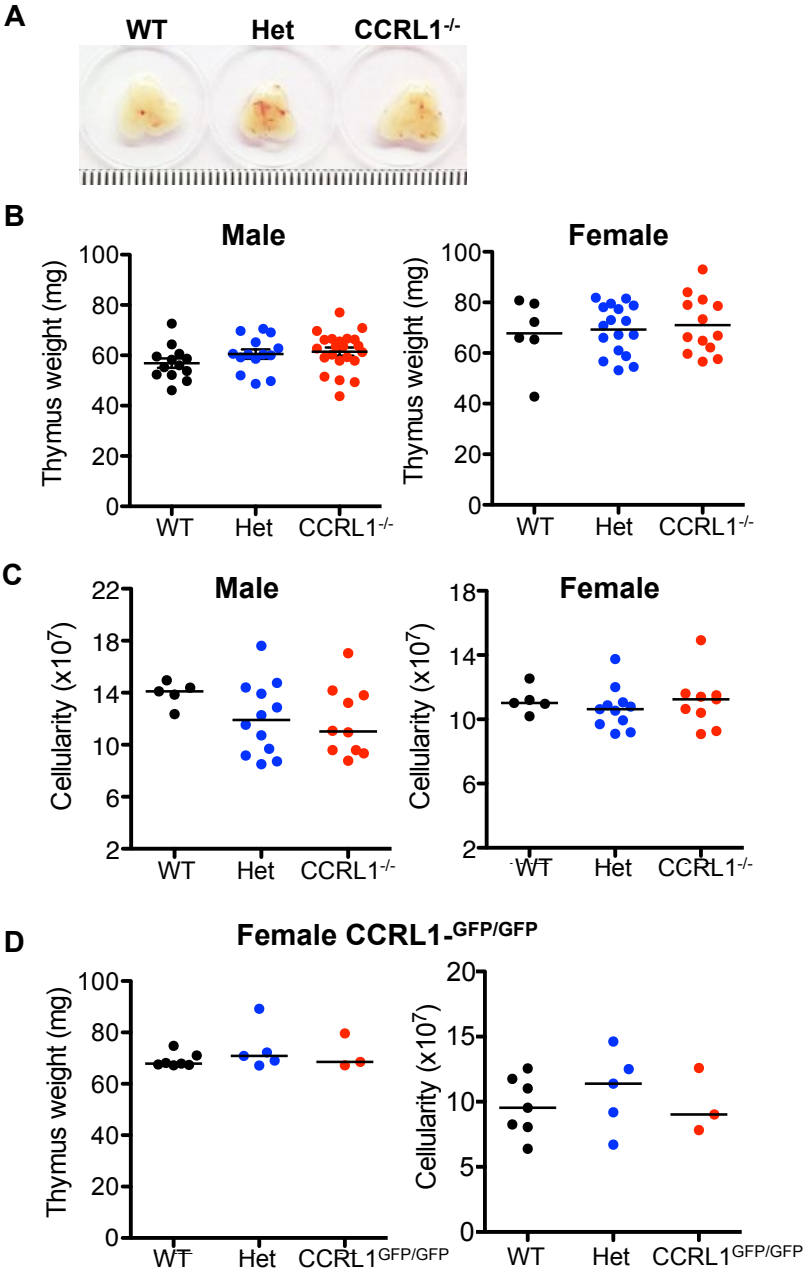

Figure 37. Thymus Weight and Cellularity is Normal in CCRL1 Deficient Mice.

Macroscopic image of WT, het and CCRL1$^{-/-}$ littermate thymi, scale bar shows increments of 1mm (A). The thymus from WT, het and CCRL1$^{-/-}$ mice were weighed (B), and the cellularity calculated by flow cytometry (C). Horizontal bars represent the mean values. Statistical analysis performed (D'Agostino-Pearson followed by t test). The procedure was repeated in CCRL1-$^{GFP/GFP}$ mice (D). Horizontal bars represent the median values. Statistical analysis performed (Mann Whitney). Each point represents one mouse.

Table 8. Thymus Weight in Male and Female CCRL1$^{-/-}$ Mice.

	Female			Male		
	WT (n=6)	Het (n=17)	CCRL1$^{-/-}$ (n=13)	WT (n=13)	Het (n=14)	CCRL1$^{-/-}$ (n=22)
Mean (mg)	67.8	69.3	71.0	56.9	60.5	61.5
SEM	5.66	2.36	3.15	1.88	1.84	1.65

Data expressed as mean and standard error of the mean (SEM).

Table 9. Thymus Weight in Female CCRL1-$^{GFP/GFP}$ Mice.

	Female CCRL1-$^{GFP/GFP}$		
	WT (n=7)	Het (n=5)	CCRL1-$^{GFP/GFP}$ (n=3)
Median (mg)	**67.9**	**70.9**	**68.5**
25th Quartile	67.4	68.1	67.2
75th Quartile	71.0	60.7	79.6

Data expressed as median (bold) with 25th and 75th quartile.

Table 10. Statistical Analysis of Thymus Weight.

	WT vs. Het	WT vs. KO	Het vs. KO
Female CCRL1$^{-/-}$	0.7719	0.5980	0.6602
Male CCRL1$^{-/-}$	0.1837	0.0846	0.6969
Female CCRL1-$^{GFP/GFP}$	0.4318	0.7317	0.7857

p values shown. D'Agostino-Pearson followed by t test was performed for female and male CCRL1$^{-/-}$. Mann Whitney statistical test was used for female CCRL1-$^{GFP/GFP}$. Female CCRL1$^{-/-}$ strain, WT n=6, het n=17, KO n=13. Male CCRL1$^{-/-}$ strain, WT n=14, het n=14, KO n=23. Female CCRL1-$^{GFP/GFP}$ strain, WT n=7, het n=5, KO n=3.

Table 11. Thymus Cellularity in CCRL1$^{-/-}$ and CCRL1-$^{GFP/GFP}$ mouse lines.

		WT (n=5)	Het (n=11)	KO (n=9)
Female CCRL1$^{-/-}$	Median (x 10^8)	**1.102**	**1.064**	**1.124**
	25th Quartile	1.058	0.970	0.984
	75th Quartile	1.187	1.107	1.156
		WT (n=5)	**Het (n=12)**	**KO (n=10)**
Male CCRL1$^{-/-}$	Median (x 10^8)	**1.311**	**1.190**	**1.102**
	25th Quartile	1.411	0.930	0.952
	75th Quartile	1.467	1.429	1.390
		WT (n=7)	**Het (n=5)**	**KO (n=3)**
Female CCRL1-$^{GFP/GFP}$	Median (x 10^8)	**0.954**	**1.139**	**0.903**
	25th Quartile	0.807	0.795	0.783
	75th Quartile	1.176	1.356	1.259

Data expressed as median (bold) with 25th and 75th quartile.

Table 12. Statistical Analysis of Thymus Cellularity in CCRL1$^{-/-}$ and CCRL1-$^{GFP/GFP}$ Mice

	WT vs. Het	WT vs. KO	Het vs. KO
Female CCRL1$^{-/-}$	0.2127	1.000	0.4941
Male CCRL1$^{-/-}$	0.1296	0.0539	0.8691
Female CCRL1-$^{GFP/GFP}$	0.5303	1.000	0.7857

p values shown. No statistical differences are found. D'Agostino-Pearson followed by t test was performed for female and male CCRL1$^{-/-}$. Mann Whitney statistical test was used for female CCRL1-$^{GFP/GFP}$. Female CCRL1$^{-/-}$ strain, WT n=5, het n=11, KO n=9. Male CCRL1$^{-/-}$ strain, WT n=5, het n=12, KO n=10. Female CCRL1-$^{GFP/GFP}$ strain, WT n=7, het n=5, KO n=3.

4.2.3 CCRL1$^{-/-}$ Mice Have a Normal Programme of T Cell Development

CCRL1-/- mice and littermate controls were genotyped as described in the materials and methods, and representative genotyping is shown in Figure 38. To determine any alterations in the populations of thymocytes in the CCRL1$^{-/-}$ thymus compared to control mice, thymi from WT, het and CCRL1$^{-/-}$ mice, were digested and the resulting cell suspension stained for flow cytometry. Antibodies against CD4, CD8 and TCRβ were used to identify DP and SP thymocytes. Representative FACS plots show the gating strategy used (Figure 39A). The proportions and absolute cell numbers of DP and SP thymocytes were determined in male and female littermates (Figure 39B and Figure 39C). These parameters are unchanged in CCRL1$^{-/-}$ mice compared to littermate controls, irrespective of gender (Table 13 and Table 14).

The maturation of SP thymocytes occurs within the medulla and is a well-defined process. Immature SP thymocytes express CD69 and their maturation is accompanied by the upregulation of Qa2 and CD62L (Weinreich and Hogquist, 2008). We determined the maturation status of SP thymocytes in CCRL1$^{-/-}$ and control thymi by staining thymocytes for CD69 and CD62L, in addition to CD4, CD8 and TCRβ (Figure 40A). The proportions of CD69^{+}CD62L^{-} immature, and CD69^{-} CD62L^{+} mature, SP4 and SP8 thymocytes are unaltered in the CCRL1$^{-/-}$ thymus compared to littermate controls (Figure 40B, Figure 40C, and Table 15).

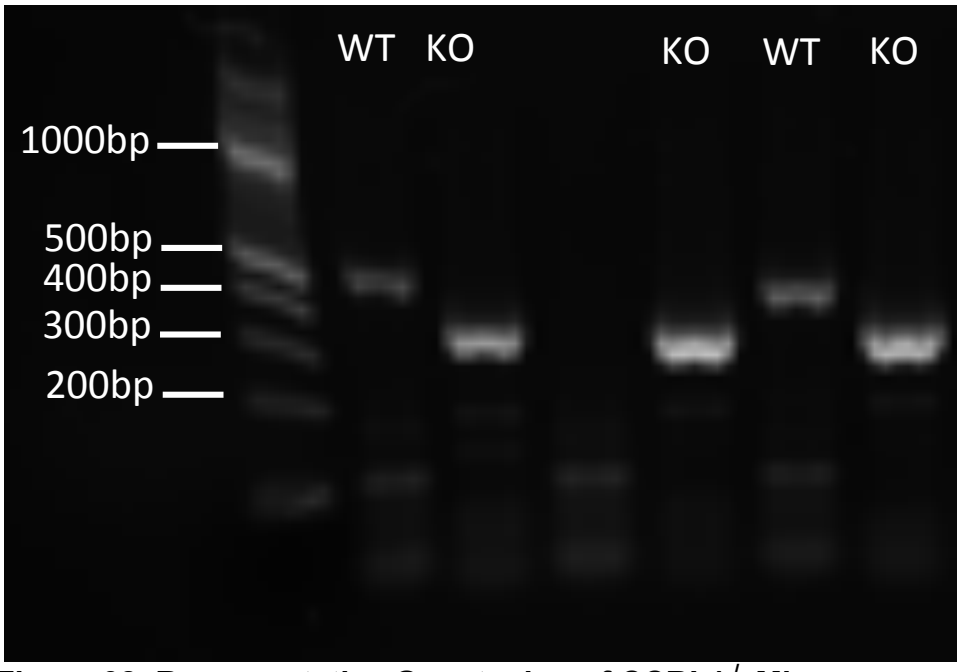

Figure 38. Representative Genotyping of CCRL1$^{-/-}$ Mice.

Image of agarose gel showing PCR products from genotyping WT and CCRL1$^{-/-}$ mice. DNA ladder indicates size of PCR product. WT PCR product is 610bp, CCRL1$^{-/-}$ PCR product is 420bp.

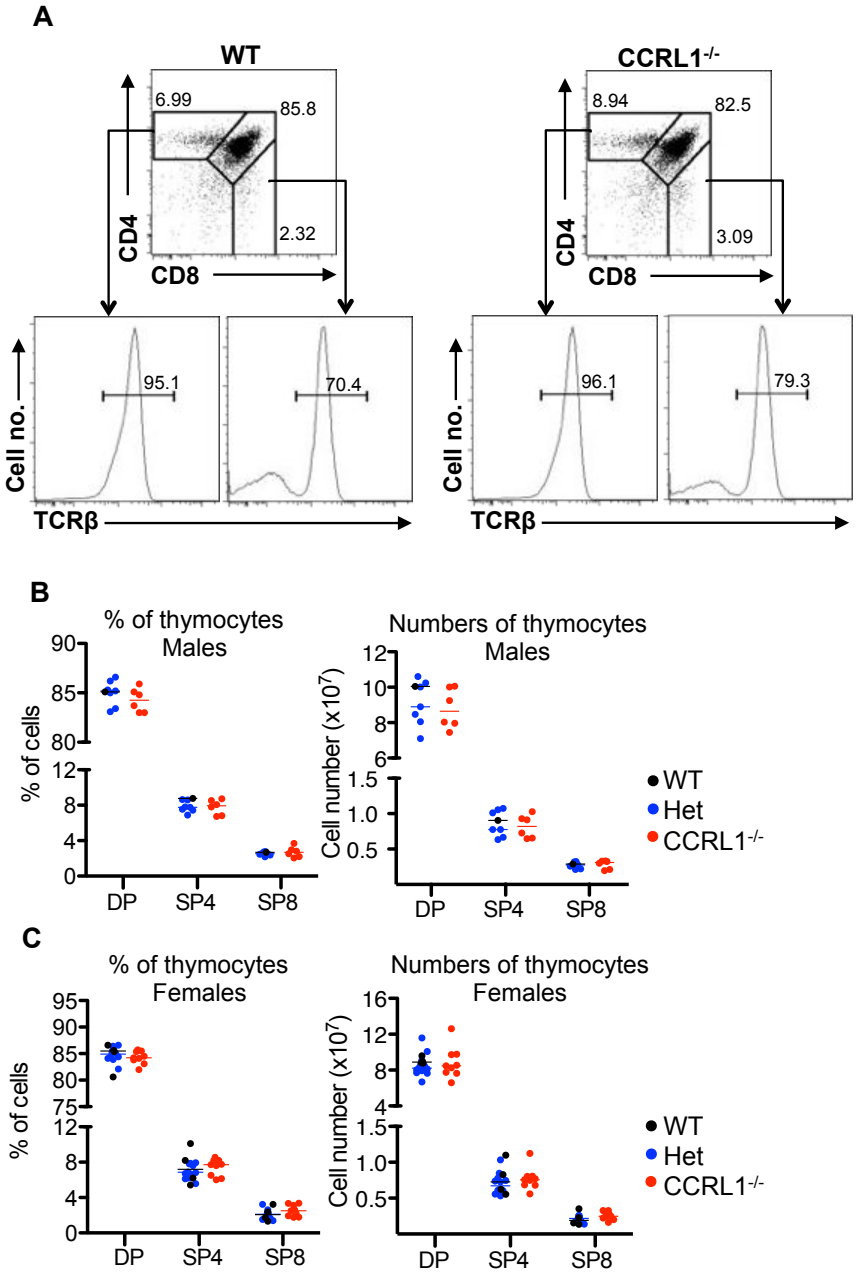

Figure 39. Normal Numbers of DP and SP Thymocytes in CCRL1$^{-/-}$ Mice.

Thymocytes were stained to allow the identification of DP and SP thymocytes by flow cytometry. Live CD45^{+} cells were first gated. DP were identified as CD4^{+}CD8^{+}, SP4 were identified as CD4^{+}CD8^{-}TCRβ^{+}, and SP8 were identified as CD4^{-}CD8^{+}TCRβ^{+} (A). The proportions and absolute cell numbers of DP and SP thymocytes were determined in the male thymus (B), and female thymus (C). Horizontal bars represent the median values. Statistical analysis performed (Mann Whitney). Each point represents one mouse.

Table 13. Statistical Analysis of Proportions of DP, SP4 and SP8 Thymocytes in CCRL1$^{-/-}$ Mice Compared to Littermate Controls

		WT vs. Het	WT vs. KO	Het vs. KO
Female	DP	0.8281	0.6000	0.2132
	SP4	0.8082	1.000	0.3028
	SP8	0.9517	0.3301	0.1768
Male	DP	N/A	N/A	0.2343
	SP4	N/A	N/A	1.000
	SP8	N/A	N/A	0.5380

p values shown. Female WT n=4, het n=12, KO n=9. Male WT n=1, het n=7, KO n=6.

Table 14. Statistical Analysis of the Numbers of DP, SP4 and SP8 Thymocytes in CCRL1$^{-/-}$ Mice Compared to Littermate Controls

		WT vs. Het	WT vs. KO	Het vs. KO
Female	DP	0.1296	0.4140	0.8036
	SP4	0.5853	0.9399	0.1886
	SP8	0.7618	0.4140	0.0817
Male	DP	N/A	N/A	0.6282
	SP4	N/A	N/A	0.6282
	SP8	N/A	N/A	0.5338

p values shown. No statistical differences are found. Mann Whitney statistical test was used for all data. Female WT n=4, het n=12, KO n=9. Male WT n=1, het n=7, KO n=6.

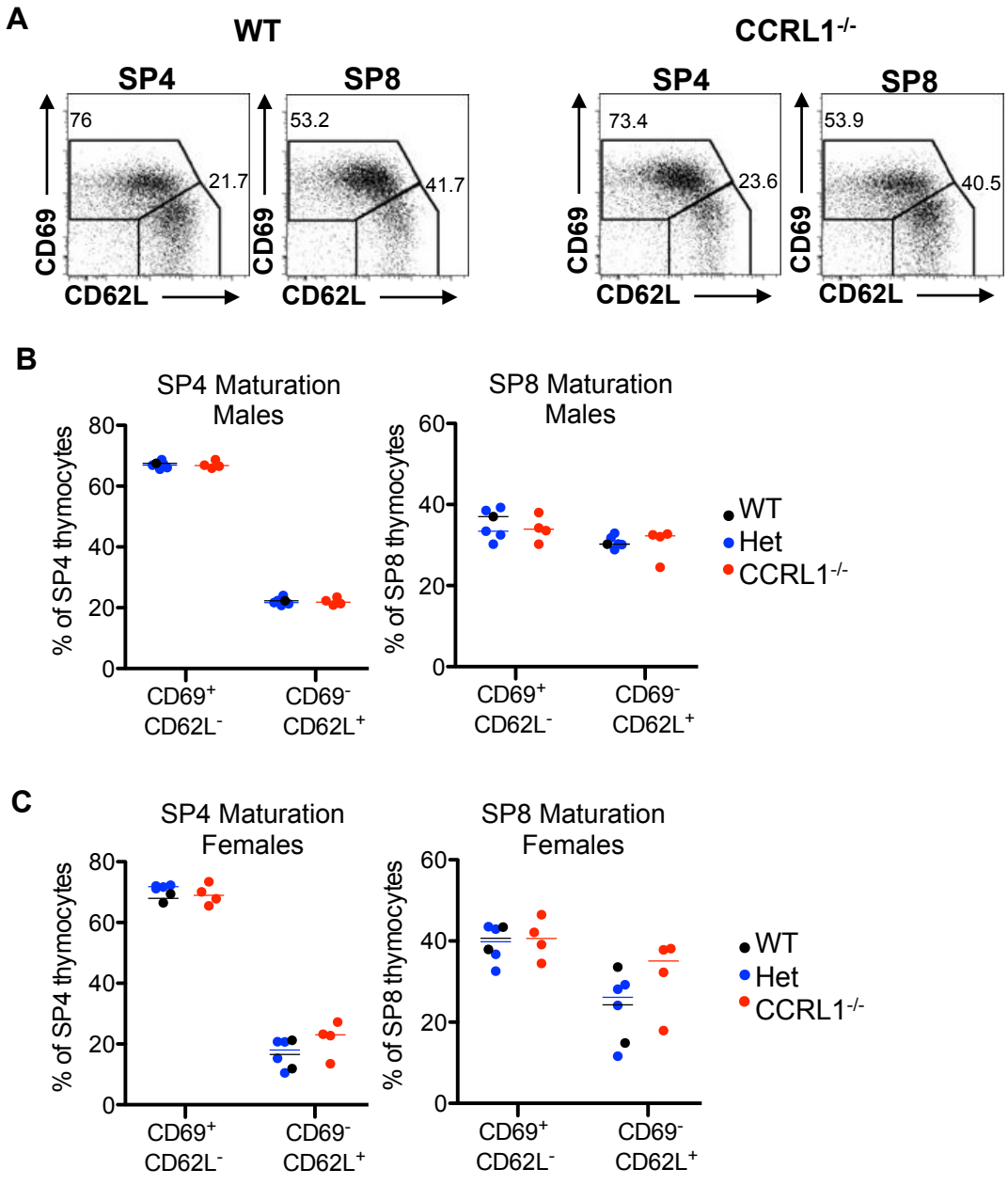

Figure 40. Unaffected SP Thymocyte Maturation in the CCRL1$^{-/-}$ Thymus.

Thymocytes were stained for CD62L and CD69 to allow the identification mature (CD62L^{+}CD69^{-}) and immature (CD62L^{-}CD69^{+}) SP thymocytes by flow cytometry. Representative density plots were gated on live CD45^{+}, CD4/CD8^{+}, TCRβ^{+} cells, before the analysis of CD62L and CD69 expression (A). The proportions and numbers of mature and immature SP thymocytes in the male thymus (B), and female thymus (C) were determined. Horizontal bars represent the median values. Statistical analysis performed (Mann Whitney). Each point represents one mouse.

Table 15. Statistical Analysis of SP Thymocyte Maturation in CCRL1$^{-/-}$ Mice Compared to Littermate Controls.

		Het vs. CCRL1$^{-/-}$	
		SP4	**SP8**
Female	$CD69^{+}CD62L^{-}$	0.3249	0.8857
	$CD69^{-}CD62L^{+}$	0.2000	0.2000
Male	$CD69^{+}CD62L^{-}$	0.9017	1.000
	$CD69^{-}CD62L^{+}$	1.000	0.7302

p values shown. No statistical differences are found. Mann Whitney statistical test was used for all data. Female WT n=2, het n=4, CCRL1$^{-/-}$ n=4. Male WT n=1, het n=5, CCRL1$^{-/-}$ n=4.

4.2.4 Normal Expression of CCR7 and CCR9 by CCRL1$^{-/-}$ Thymocytes

CCRL1 has been shown to scavenge its ligands CCL19, CCL21 and CCL25 *in vitro* (Gosling et al., 2000). Moreover, a recent publication has illustrated the scavenging function of CCRL1 *in vivo*, by showing disrupted CCL21 gradients in the lymph node of CCRL1$^{-/-}$ mice, which resulted in the accumulation of CCR7^{+} DCs in the subcapsular sinus of these mice (Ulvmar et al., 2014). For these reason we analysed the populations of CCR7^{+} and CCR9^{+} thymocytes from CCRL1$^{-/-}$ mice compared to littermate controls.

Populations of DP and SP thymocytes were identified by flow cytometry as previously shown, and then the expression of CCR7 by each population determined. Representative histograms show CCR7 expression by thymocytes from CCRL1$^{-/-}$ and littermate control mice (Figure 41A). Thymocytes from CCR7$^{-/-}$ mice were stained alongside as a negative control to ensure correct positioning of the CCR7 gate. In the littermate control thymus, CCR7 expression was highest on SP thymocytes (mean: 78.7% of SP4 and 73.5% of SP8), whereas expression of CCR7 on DP thymocytes was minimal (mean: 3%). CCR7 expression by the same thymocyte populations from CCRL1$^{-/-}$ mice was comparable to control thymi (mean: 3.2% of DP, 79.2% of SP4, 69.9% of SP8) (Figure 41B). In addition, the median fluorescent intensity (MFI) of CCR7 expression by DP, SP4 and SP8 thymocytes was calculated to determine whether the density of CCR7 expression at the cell surface was influenced by CCRL1 (Figure 41C). There was no statistical difference in the proportion of CCR7^{+} thymocytes, or the CCR7 MFI expression by DP, SP4 or SP8 thymocytes from CCRL1$^{-/-}$ or control mice (Table 15).

Expression of CCR9 by DP and SP thymocytes was also determined by flow cytometry (Figure 42A). In the littermate control thymus, CCR9 was expressed highly by DP thymocytes (mean: 85.5%), but was expressed by fewer SP thymocytes (mean: 42.9% of SP4, 30.3% of SP8). CCR9 expression by CCRL1$^{-/-}$ thymocytes is comparable to thymocytes from littermate control mice (mean: 84.6% of DP, 40.7% of SP4, 28.2% of SP8) (Figure 42B). Moreover, CCR9 MFI was determined on populations of DP, SP4 and SP8 thymocytes, and revealed no significant differences in levels of CCR9 expression by CCRL1$^{-/-}$ thymocytes compared to littermate controls. (Figure 42C, Table 17)

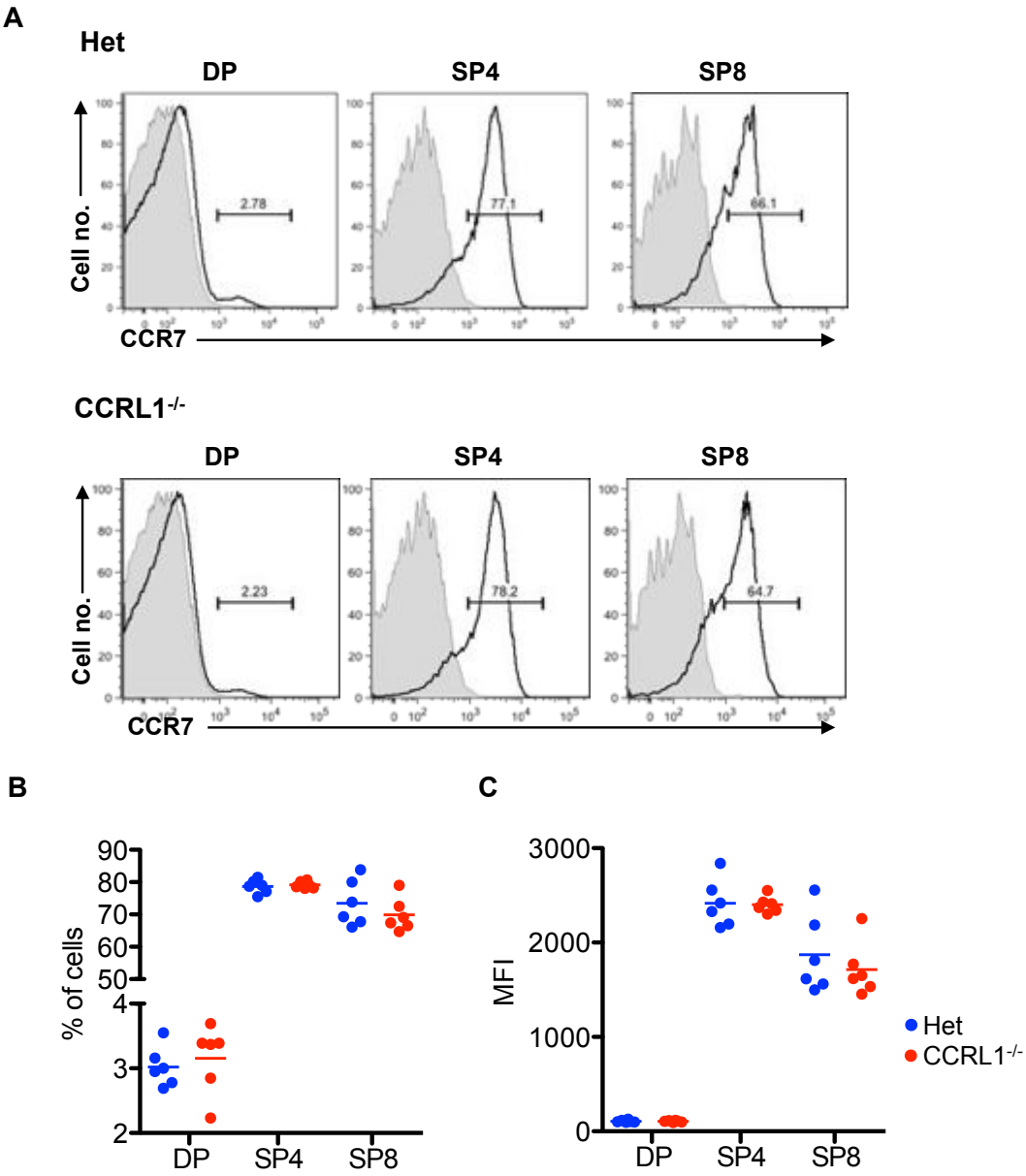

Figure 41. CCR7 Expression by Thymocytes is Unaltered in CCRL1$^{-/-}$ Mice.

Thymocytes were stained for CCR7, and a CCR7$^{-/-}$ thymus was used as a negative control for CCR7 staining (grey solid histogram). DP and SP thymocytes were identified as previously shown. Expression of CCR7 by DP and SP thymocytes was determined (A). The proportion of CCR7^{+} thymocytes (B), and MFI (median fluorescent intensity) of CCR7 expression (C) is shown. Horizontal bars represent the median values. Statistical analysis performed (Mann Whitney). Each point represents one mouse.

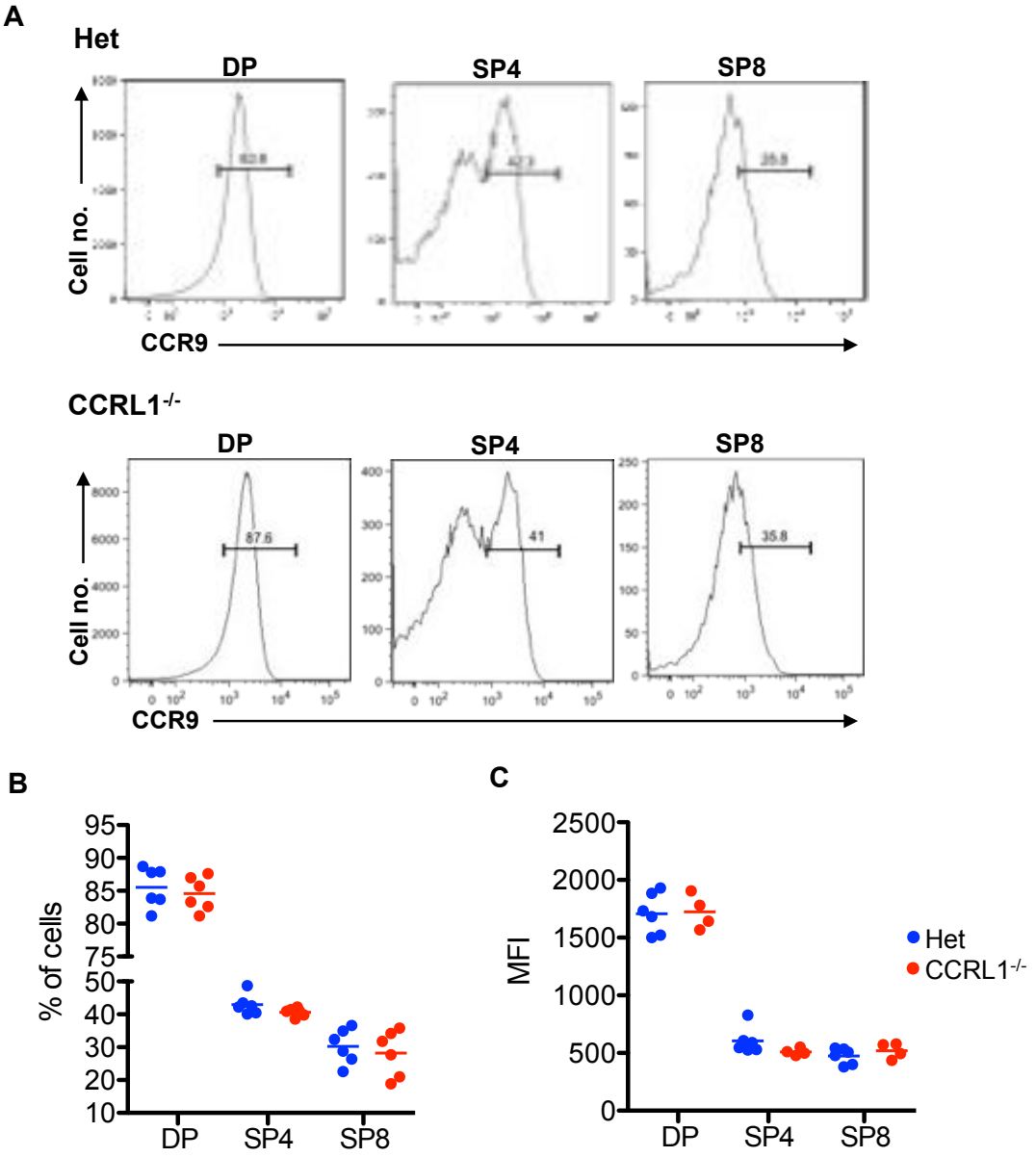

Figure 42. CCR9 Expression by Thymocytes is Unaltered in CCRL1$^{-/-}$ Mice.

Thymocytes were stained for CCR9, and the expression of CCR9 by DP and SP thymocytes was determined (A). DP and SP thymocytes were identified as previously shown. The proportion of CCR9^{+} thymocytes (B), and MFI (median fluorescent intensity) of CCR9 expression (C) is shown. Statistical analysis performed (Mann Whitney). Each point represents one mouse.

Table 16. Statistical Analysis of CCR7 Expression by DP, SP4 and SP8 Thymocytes in CCRL1$^{-/-}$ Mice Compared to Littermate Controls.

	Het vs. CCRL1$^{-/-}$	
	CCR7^{+} cells	**CCR7 MFI**
DP	0.6095	1.000
SP4	1.000	0.9372
SP8	0.6095	0.6991

p values shown, no statistical differences were found.
Mann Whitney statistical test was used for all data. Het n=6, CCRL1$^{-/-}$ n=4.

Table 17. Statistical Analysis of CCR9 Expression by DP, SP4 and SP8 Thymocytes in CCRL1$^{-/-}$ Mice Compared to Littermate Controls.

	Het vs. CCRL1$^{-/-}$	
	CCR9^{+} cells	**CCR9 MFI**
DP	0.3358	0.9143
SP4	0.1488	0.0667
SP8	0.5887	0.3524

p values shown, no statistical differences were found.
Mann Whitney statistical test was used for all data. Het n=6, CCRL1$^{-/-}$ n=4.

4.2.5 Normal Generation of nTreg in the CCRL1$^{-/-}$ Thymus

Within the thymus, interactions between CCR7 and CCR9, and their ligands CCL19/CCL21 and CCL25 respectively, are required for cortex to medulla migration of SP thymocytes (Choi et al., 2008, Ehrlich et al., 2009). Although we have shown no difference in the populations of conventional SP thymocytes in the CCRL1$^{-/-}$ thymus, the medullary microenvironment is vital for the maturation of Treg (Cowan et al., 2013). Due to the potential ability of CCRL1 to influence CCR7 and CCR9 dependent processes, we analysed the maturation of Treg in the CCRL1$^{-/-}$ thymus and littermate controls. This was achieved by staining SP thymocytes for CD69, CD25 and Foxp3 for flow cytometric analysis. Treg precursors were identified as CD69^{+}CD25^{+}Foxp3^{-} whereas mature Treg were identified as CD69^{-}CD25^{+}Foxp3^{+} (Figure 43A). The majority of CD69^{+} SP thymocytes were conventional SP4 thymocytes and therefore lacked expression of CD25 or Foxp3. Although few CD69^{+}CD25^{+}Foxp3^{-} cells were detected in CCRL1$^{-/-}$ and control thymi (mean: 0.73% in het, 0.72% in CCRL1$^{-/-}$), no statistical difference was found (p=0.9944). CD69^{-} CD25^{+}Foxp3^{+} mature Treg accounted for a slightly larger population of CD69^{-} cells (mean: 4.5% in het, 4.3% in CCRL1$^{-/-}$), however no statistical difference was found between CCRL1$^{-/-}$ and littermate control mice (p=0.7861) (Figure 43B). These results show normal maturation of Treg precursors into mature Treg.

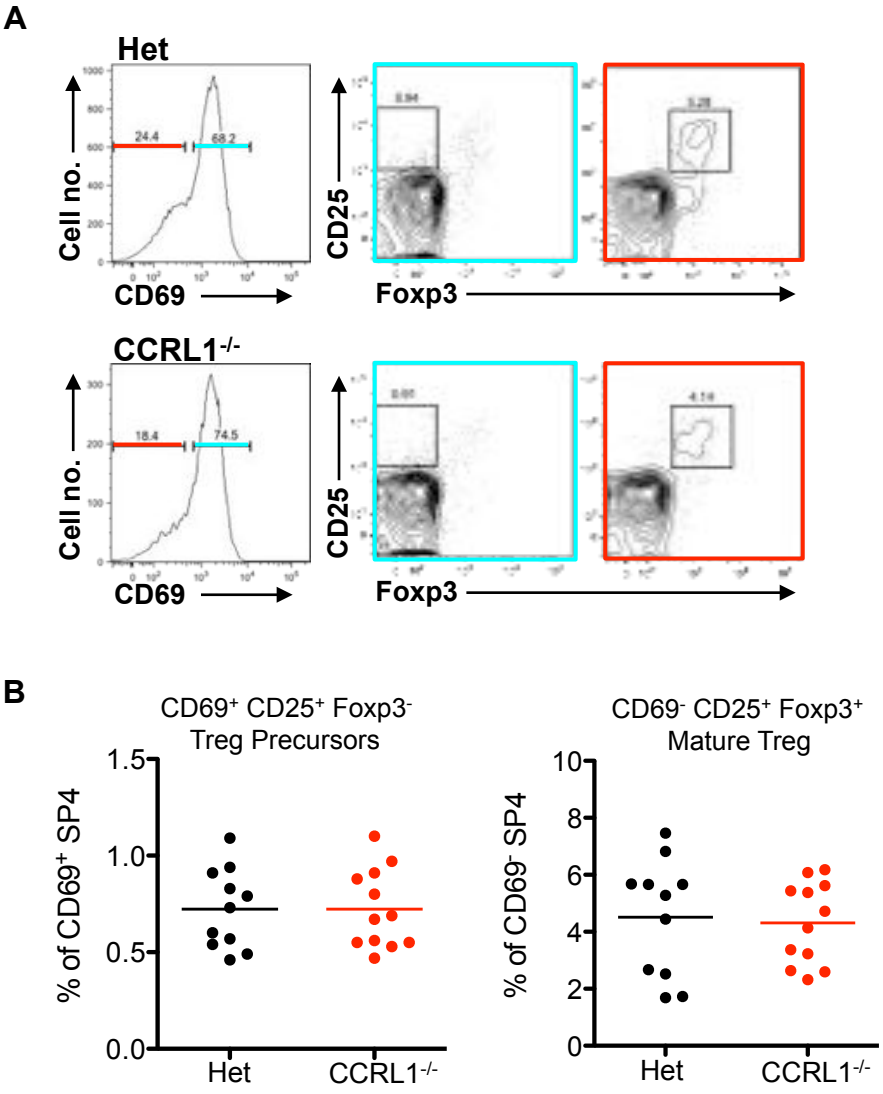

Figure 43. nTreg Development is Normal in the CCRL1$^{-/-}$ Thymus.

Treg precursors and mature Tregs were identified in the thymus based on the expression of CD69, CD25 and Foxp3 by flow cytometry. Cells were first gated as live CD45^{+}CD4^{+}TCRβ^{+}, then Treg precursors were identified as CD69^{+}CD25^{+}Foxp3^{-} whereas mature Treg were identified as CD69^{-}CD25^{+}Foxp3^{+} (A). The proportion of Treg precursors and mature Treg are shown (B). Horizontal bars represent the median values. Statistical analysis performed (Mann Whitney). Each point represents one mouse.

4.2.6 Normal DN Thymocyte Development but Increased ETP in CCRL1$^{-/-}$ Mice

The outward migration of DN thymocytes during their development is dependent on CCR7 and CCR9 mediated signalling (Benz et al., 2004, Misslitz et al., 2004). To determine any potential involvement of CCRL1 in this process, we analysed the proportions and numbers of DN thymocytes in CCRL1$^{-/-}$ and littermate controls. Thymi were digested and thymocytes stained with a panel of markers to allow the identification of DN thymocytes by flow cytometry. DN thymocytes were identified as CD45^{+}lineage^{-}. The markers used to define lineage were, CD3, CD4, CD8, TCRβ, B220, CD11b, CD11c, TER-119, ly-G6. Populations of DN1-4 thymocytes were subsequently identified based on their expression of CD44 and CD25 (Figure 44A). The proportions and absolute cell numbers of DN1 (CD44^{+}CD25^{-}), DN2 (CD44^{+}CD25^{+}), DN3 (CD44^{-}CD25^{+}), and DN4 (CD44^{-}CD25^{-}) thymocytes were determined in thymi from female (Figure 44B), and male (Figure 44C) mice. Proportions and numbers of thymocytes in each DN population were similar between all genotypes, irrespective of gender. There was a significant difference in the number of DN3 thymocytes within the female WT vs. het thymus (p=0.0476) (median: 1.309x10^{6} cells in WT, 1.133x10^{6} cells in het), however no other statistical differences were found (Table 18 and Table 19).

Studies using chemokine receptor deficient mice have shown that the recruitment of progenitor cells to the adult thymus is also dependent on CCR7 and CCR9. (Krueger et al., 2010, Zlotoff et al., 2010, De Obaldia et al., 2013). We determined the proportions and numbers of ETP in the CCRL1$^{-/-}$ thymus compared to littermate controls. ETP were identified by flow cytometry as CD45^{+}lineage^{-}CD25^{-}

$CD44^{+}CD117^{+}$ (Figure 45A). The percentage and number of ETP was determined in thymi from male (Figure 45B) and female (Figure 45C) mice. There is a consistent trend for increased percentages and absolute numbers of ETP in male and female $CCRL1^{-/-}$ thymi compared to littermate controls (Table 20). Proportions of ETP in the male $CCRL1^{-/-}$ thymus were increased to a median of 0.56% from 0.37% of lineage negative cells present in WT/het thymi (p=0.1055). Absolute numbers of ETP in the male $CCRL1^{-/-}$ thymus were also increased and approaching a level of significance (median: 13462 cells in $CCRL1^{-/-}$, 9350 cells in mixed control group, p=0.0667). Proportions of ETP in the female $CCRL1^{-/-}$ thymus were significantly increased from a median of 0.35% of lineage negative cells present in control thymi to a median of 0.69% of lineage negative cells in $CCRL1^{-/-}$ thymi (p=0.0163). Absolute numbers of ETP in the female $CCRL1^{-/-}$ thymus were also increased, but levels of significance not reached (median: 9560 in WT/het, 12366 in $CCRL1^{-/-}$, p=0.2977). See Table 21 for p values.

This data suggests a potential role for CCRL1 in either the recruitment of ETP to the adult thymus, or the production of common lymphoid progenitors (CLP) in the bone marrow (BM). $CD135^{+}CD27^{+}CD127^{+}$ CLP have been described within the BM, and BM chimeras have identified this population of cells as those responsible for a robust and rapid wave of thymopoiesis (Serwold et al., 2009). We identified this population of cells in the BM of $CCRL1^{-/-}$ mice compared to littermate controls using flow cytometry. In our analysis, CLP were identified as $CD45^{+}lineage^{-}$ $CD135^{+}CD27^{+}CD127^{+}$ (Figure 46A). The proportion of CLP in the BM of $CCRL1^{-/-}$ and control mice were very similar (Figure 46B) (median: 31.5% of lineage negative

cells in control, 30.3% of lineage negative cells in CCRL1$^{-/-}$, p=1.000). This result suggested that the production of CLP is unaffected in the CCRL1$^{-/-}$, therefore the increased ETP observed in the CCRL1$^{-/-}$ thymus is more likely to be due to increased recruitment of progenitors from the circulation.

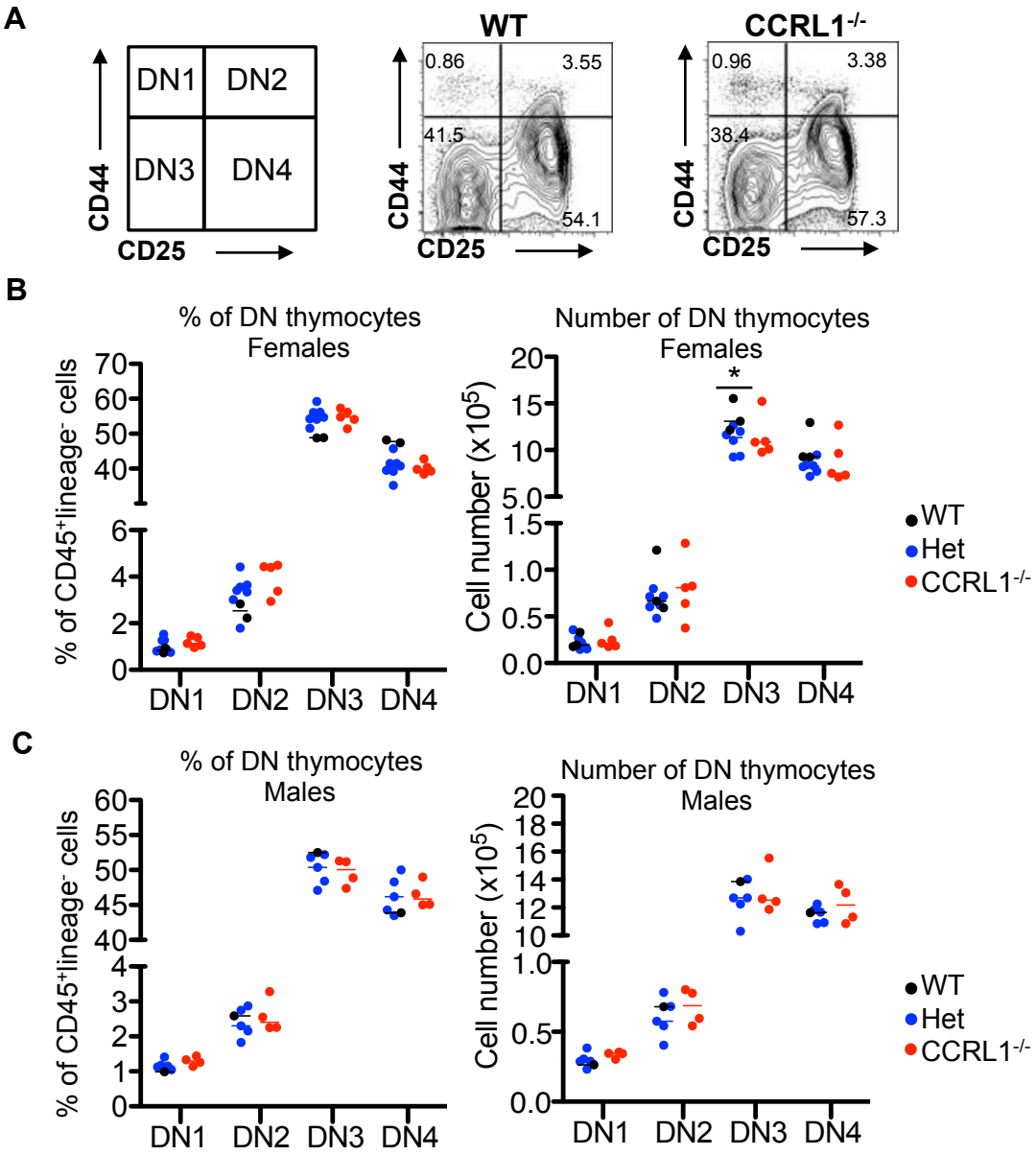

Figure 44. DN Thymocyte Development is Unaffected in CCRL1$^{-/-}$ Mice.

Thymocytes were stained for CD25 and CD44 to allow the identification of DN1 (CD44^{+}CD25^{-}), DN2 (CD44^{+}CD25^{+}), DN3 (CD44^{-}CD25^{+}), and DN4 (CD44^{-}CD25^{-}). Cells were first gated as live CD45^{+}lineage^{-}, prior to the identification of DN1-4 (A). Lineage markers used were CD3, CD4, CD8, TCRβ, B220, CD11b, CD11c, TER-119, ly-G6. The proportions and absolute cell numbers of DN1-4 thymocytes in the female thymus (B), and male thymus (C). Horizontal bars represent the median values. Statistical analysis performed (Mann Whitney). Each point represents one mouse.

Table 18. Statistical Analysis of Proportions of DN Thymocytes in CCRL1$^{-/-}$ Mice Compared to Littermate Controls.

	Het vs. CCRL1$^{-/-}$	
	Female	**Male**
DN1	0.3290	0.2857
DN2	0.3434	0.7302
DN3	1.000	0.9048
DN4	0.7449	0.9048

p values shown, no statistical differences were found.
Mann Whitney statistical test was used for all data.
Female WT n=2, het n=7, CCRL1$^{-/-}$ n=5. Male WT n=1, het n=5, CCRL1$^{-/-}$ n=4.

Table 19. Statistical Analysis of Numbers of DN Thymocytes in CCRL1$^{-/-}$ Mice Compared to Littermate Controls.

		WT vs. Het	WT vs. KO	Het vs. KO
	DN1	0.9048	0.6623	0.7857
Female	**DN2**	0.9048	0.3290	1.000
	DN3	***0.0476***	0.9307	0.1429
	DN4	0.0952	0.9307	0.3929
	DN1	N/A	N/A	0.2857
Male	**DN2**	N/A	N/A	0.5556
	DN3	N/A	N/A	1.000
	DN4	N/A	N/A	0.7302

p values shown. Significant difference highlighted in bold italic type.
Mann Whitney statistical test was used for all data.
Female WT n=3, het n=6, CCRL1$^{-/-}$ n=5. Male WT n=1, het n=5, CCRL1$^{-/-}$ n=4.

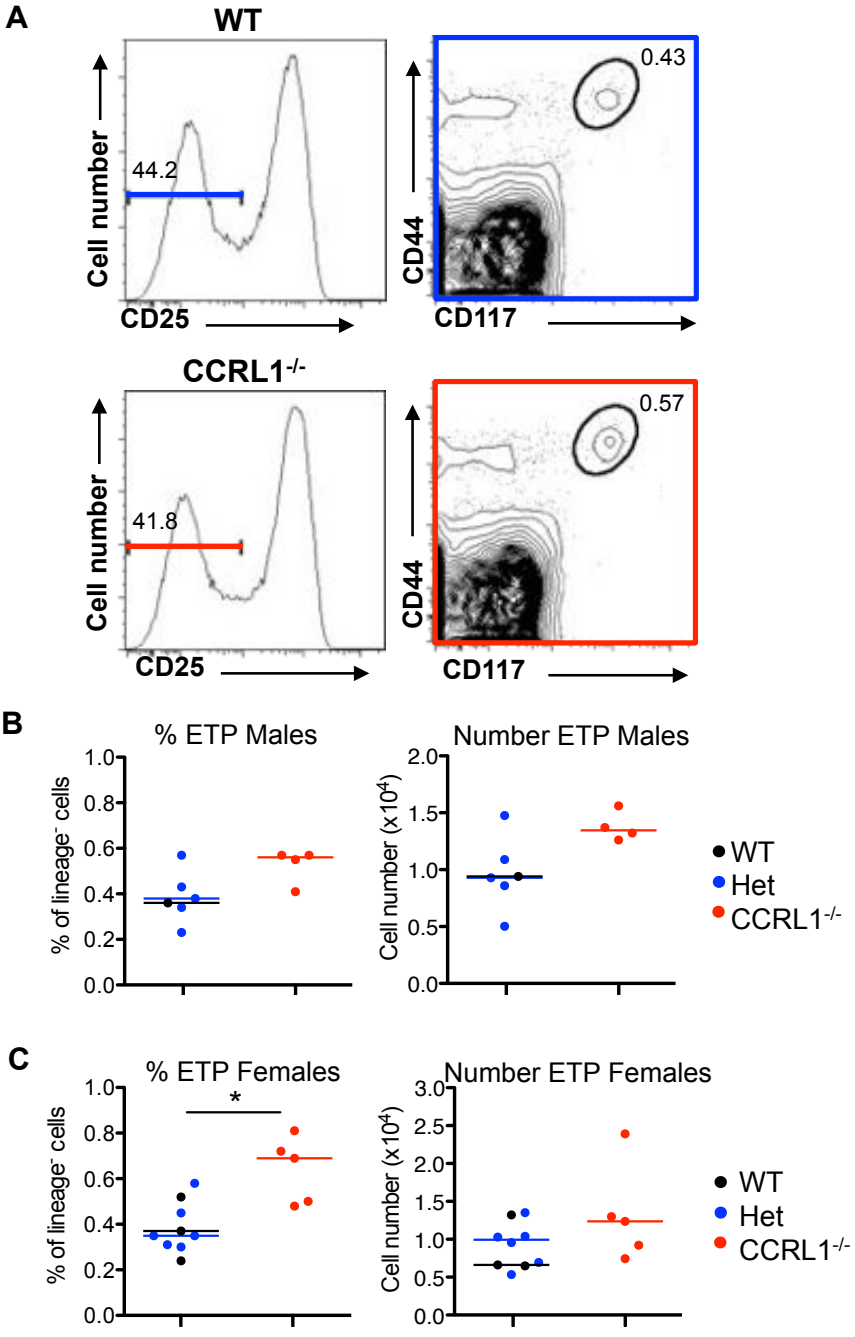

Figure 45. Increased ETP in the CCRL1$^{-/-}$ Thymus.

Thymocytes were stained to allow the identification of ETP by flow cytometry. ETP were identified as CD45^{+}lineage^{-}CD25^{-}CD44^{+}CD117^{+} (A). Lineage markers used were CD3, CD4, CD8, TCRβ, B220, CD11b, CD11c, TER-119, ly-G6. The proportions and absolute cell numbers of ETP in the male (B), and female (C) thymus are shown. Horizontal bars represent the median values. Statistical analysis performed (Mann Whitney) *$p<0.05$. Each point represents one mouse.

Table 20. Proportions of ETP in Male and Female Thymi of CCRL1$^{-/-}$ Mice Compared to Littermate Controls.

		WT	Het	CCRL1$^{-/-}$
Female	Median (%)	**0.37**	**0.35**	**0.69**
	25th Quartile	0.24	0.31	0.49
	75th Quartile	0.52	0.48	0.77
Male	Median (%)	**0.36**	**0.38**	**0.56**
	25th Quartile	0.36	0.29	0.45
	75th Quartile	0.36	0.5	0.57

Data expressed as median (bold) with 25th and 75th quartile.
Female WT n=3, het n=6, CCRL1$^{-/-}$ n=5. Male WT n=1, het n=5, CCRL1$^{-/-}$ n=4.

Table 21. Statistical Analysis of ETP Frequency in CCRL1$^{-/-}$ Mice Compared to Littermate Controls.

		WT vs. Het	WT vs. KO	Het vs. KO
Female	Proportion	0.8969	0.1429	**0.0222**
	Cell number	0.7143	0.3929	0.4286
Male	Proportion	N/A	N/A	0.1706
	Cell number	N/A	N/A	0.1111

p values shown. Statistical differences highlighted in bold italic type.
Mann Whitney statistical test was used for all data.
Female WT n=3, het n=6, CCRL1$^{-/-}$ n=5. Male WT n=1, het n=5, CCRL1$^{-/-}$ n=4.

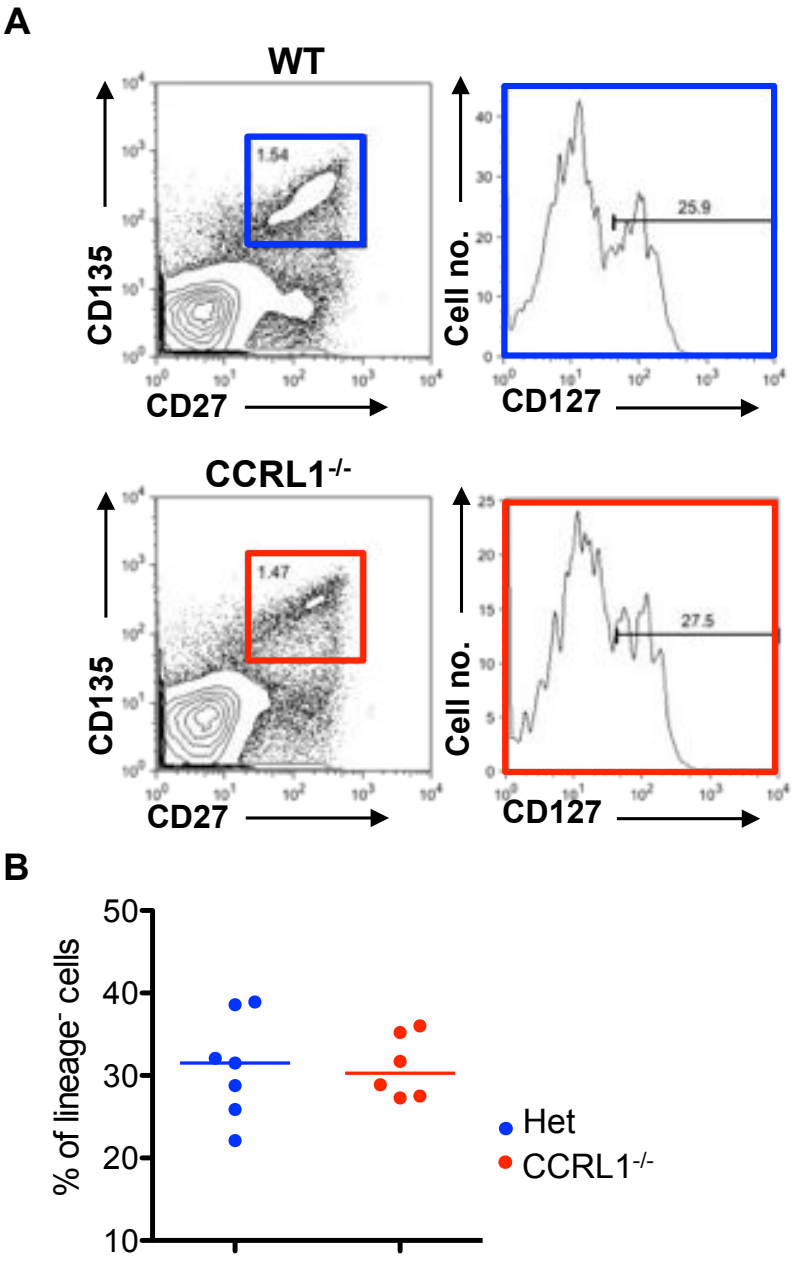

Figure 46. Unaltered Frequency of CLP in the Bone Marrow of CCRL1$^{-/-}$ Mice.

The bone marrow (BM) was stained for flow cytometry to allow the identification of CLP ($CD45^+lineage^-CD135^+CD27^+CD127^+$) (A). Lineage markers used were CD3, CD4, CD8, TCRβ, B220, CD11b, CD11c, TER-119, ly-G6. The proportion of CLP in the BM were determined (B). Horizontal bars represent the median values. Statistical analysis performed (Mann Whitney). Each point represents one mouse.

4.2.7 Increased Frequency of Migratory Sirpα^{+} cDCs in CCRL1$^{-/-}$ Mice

Two subsets of conventional (c) DC are present within the thymus and can be identified by flow cytometry based on the expression of MHC-II, CD11c, CD11b and Sirpα. Sirpα^{-} cDCs are generated within the thymus whereas Sirpα^{+} cDCs are generated extrathymically, and are a migratory subset, which are recruited into the thymus (Luche et al., 2011, Baba et al., 2009). A recent publication identified a reduction in the population of CD8α^{+} Sirpα^{-} resident thymic cDCs from CCR7/CCR9 DKO BM, suggestive of a role for CCR7 and CCR9 in the development or maintenance of this population (De Obaldia et al., 2013). For this reason, we analysed populations of thymic DC in CCRL1$^{-/-}$ and littermate control mice.

We identified resident Sirpα^{-} cDC as MHC-II^{+}CD11c^{+}CD11b^{-}Sirpα^{-}, and Sirpα^{+} cDC as MHC-II^{+}CD11c^{+}CD11b^{+}Sirpα^{+} (Figure 47A). The proportion and number of both subsets of cDCs were quantitated in the CCRL1$^{-/-}$ thymus compared to littermate controls (Figure 47B, C). The percentage of Sirpα^{+} cDCs was significantly increased in the CCRL1$^{-/-}$ thymus (median: 12.4% of MHC-II^{+} cells in het, 17.3% of MHC-II^{+} cells in CCRL1$^{-/-}$, p=0.0012). In addition, the absolute cell number of Sirpα^{+} cDCs was also significantly increased in the CCRL1$^{-/-}$ thymus (median: 121,440 cells in het thymus, 190,545 cells in CCRL1$^{-/-}$ thymus, p=0.0140). There was no difference in the percentage or number of resident Sirpα^{-} cDCs in the CCRL1$^{-/-}$ thymus compared to littermate controls.

In addition to cDC, plasmacytoid (p) DC exist within the thymus. Thymic pDCs are a migratory DC subset responsible for the transport of peripheral antigens to the thymus in a CCR9-dependant manner (Hadeiba et al., 2012). Thymic pDCs were identified as $B220^{+}CD11c^{+}$ cells (Figure 48A), and the proportion and absolute number of these cells calculated (Figure 48B). No statistical difference was found in the percentage ($p=0.3660$) or absolute number ($p=0.2949$) of pDCs between $CCRL1^{-/-}$ and littermate controls.

We next determined the positioning of thymic DCs in $CCRL1^{-/-}$ mice by staining cryosections of WT and $CCRL1^{-/-}$ thymus with CD4, CD8 and CD11c. This allowed the identification of cortex and medulla, using the localisation of DP and SP thymocytes respectively, and allowed identification of total DC based on expression of CD11c. Thymic DCs were localised primarily within the medulla in the WT thymus (Figure 49A), which was comparable to their localisation within the $CCRL1^{-/-}$ thymus (Figure 49B). These results suggest that CCRL1 expression is not needed for the correct positioning of thymic DCs.

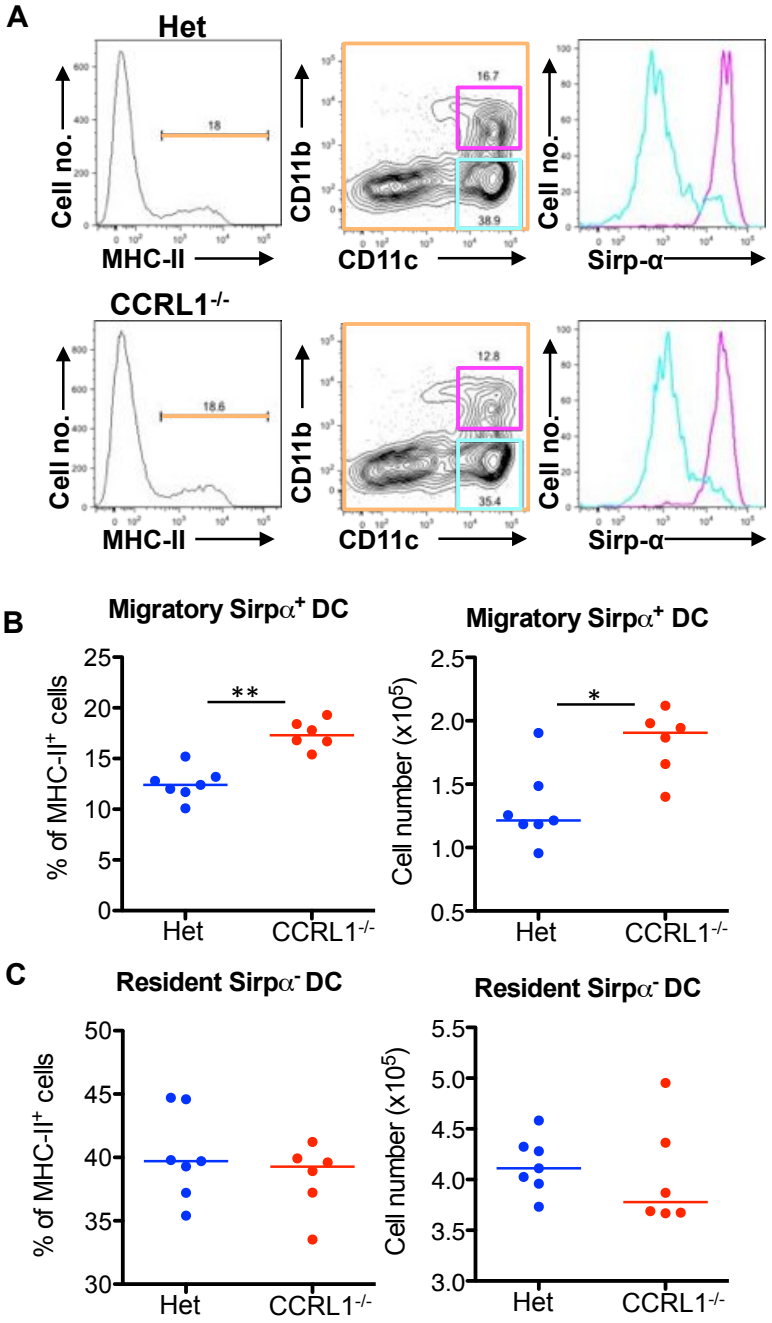

Figure 47. Increased Sirpα$^+$ DCs in the CCRL1$^{-/-}$ Thymus.

Cell suspensions obtained from digested thymi were stained for CD11b and Sirpα to allow the identification of Sirpα$^+$ migratory DC, and Sirpα$^-$ resident DC. Representative density plots were first gated on live cells, prior to the identification of thymic cDC (A). The proportions and absolute cell numbers of migratory and resident thymic DC are shown (B). Horizontal bars represent the median values. Statistical analysis performed (Mann Whitney) ***p<0.001 *p<0.05.* Each point represents one mouse.

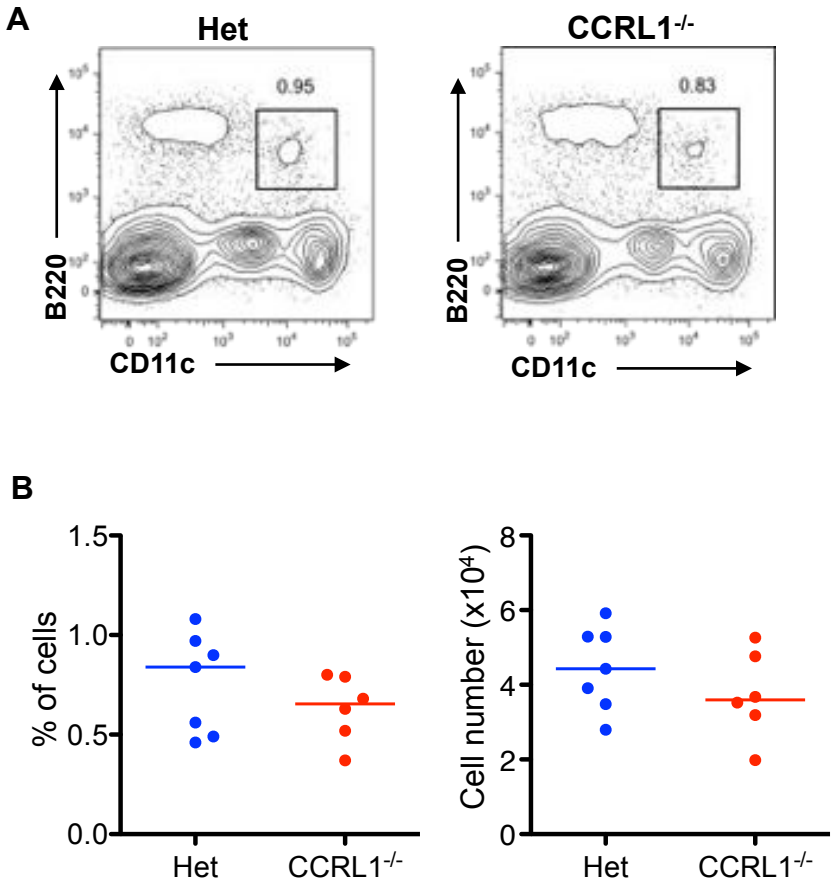

Figure 48. Unaltered Frequency of Thymic Plasmacytoid DC in CCRL1$^{-/-}$ Mice.

Cell suspensions obtained from digested thymi were stained for B220 and CD11c to allow the identification of B220^{+}CD11c^{+} plasmacytoid (p) DC. Representative density plots were first gated on live cells, prior to the identification of pDCs (A). The proportions and absolute cell numbers of pDCs were determined (B). Horizontal bars represent the median values. Statistical analysis performed (Mann Whitney). Each point represents one mouse.

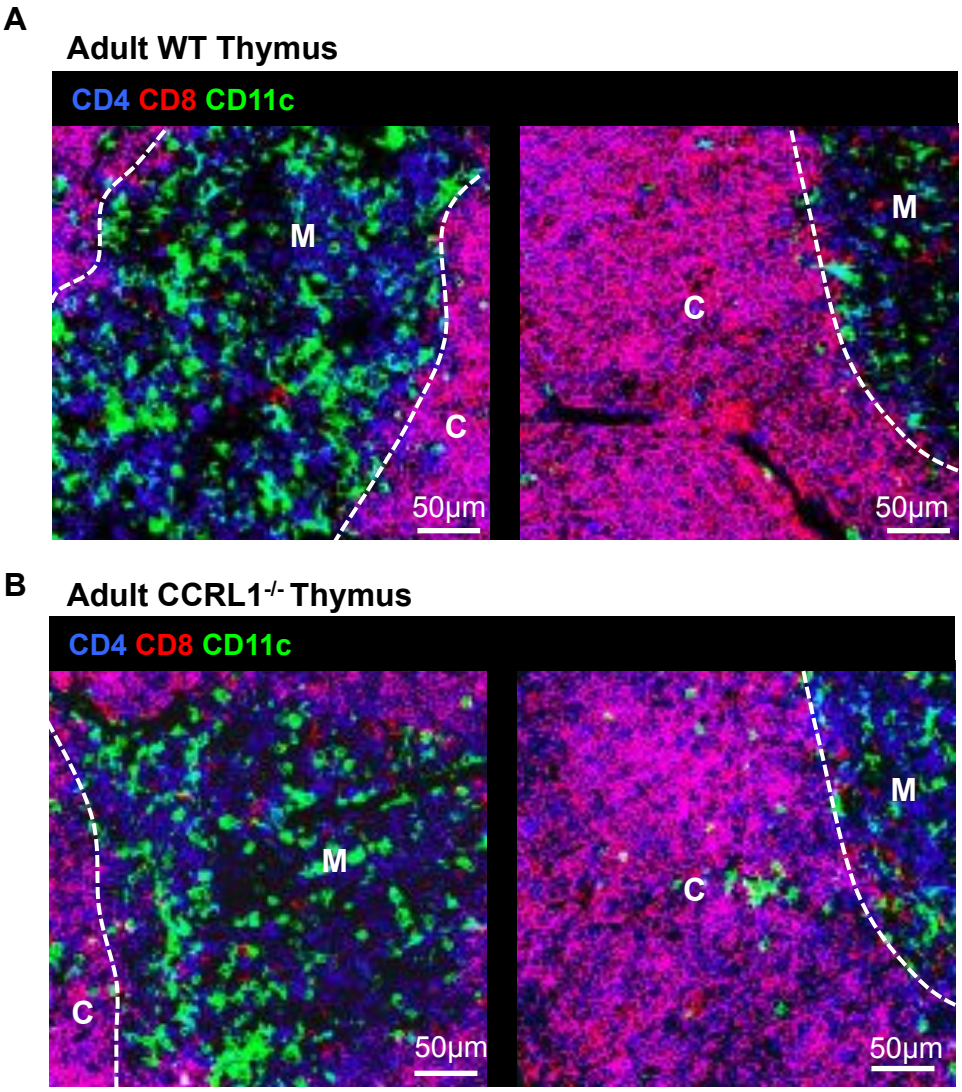

Figure 49. Normal Localisation of Thymic DC in CCRL1$^{-/-}$ Mice.

Adult WT (A) and CCRL1$^{-/-}$ (B) thymi were frozen and sections stained for CD4, CD8 and CD11c. CD11c^{+} DC are localised primarily within the thymic medulla, with some DCs positioned close to the corticomedullary junction. Dashed line shows demarcation between cortex 'C' and medulla 'M'.

4.2.8 Unaltered Frequency of Thymic B Cells in CCRL1$^{-/-}$ Mice

The population of thymic B cells remains largely unstudied, however their role in the presentation of self-antigen in the process of negative selection has been documented (Frommer and Waisman, 2010, Akirav et al., 2011, Perera et al., 2013, Walters et al., 2014). These cells arise from *Rag* expressing progenitor cells within the thymus, however it is not clear whether these progenitor cells would form part of the ETP population we identified using flow cytometry in this study. Experiments using BM chimeras have shown a reduction in thymic B cells from CCR7/CCR9 DKO BM (De Obaldia et al., 2013), suggesting these chemokine receptors could be involved in either the generation of thymic B cells or their transport into the thymus.

Given our data showing increased ETP in the CCRL1$^{-/-}$ thymus, and the possible role of CCR7 and CCR9 in the recruitment of thymic B cell progenitors, we analysed the population of thymic B cells in the CCRL1$^{-/-}$ and littermate control thymus. Thymi were digested and thymic B cells identified by flow cytometry as CD45^{+}CD4^{-}CD8^{-} TCRβ^{-}B220^{+}CD19^{+}. A small population of B cells are detected in control and CCRL1$^{-/-}$ thymi (Figure 50A). The percentage and absolute number of thymic B cells were determined in male and female thymi (Figure 50B, C). There was no difference in the percentage or absolute numbers of B cells in the thymus from male (%, p=0.9048, cell number, p=0.4127) or female (%, p=0.4678, cell number, p=0.3429) CCRL1$^{-/-}$ mice compared to het littermate controls.

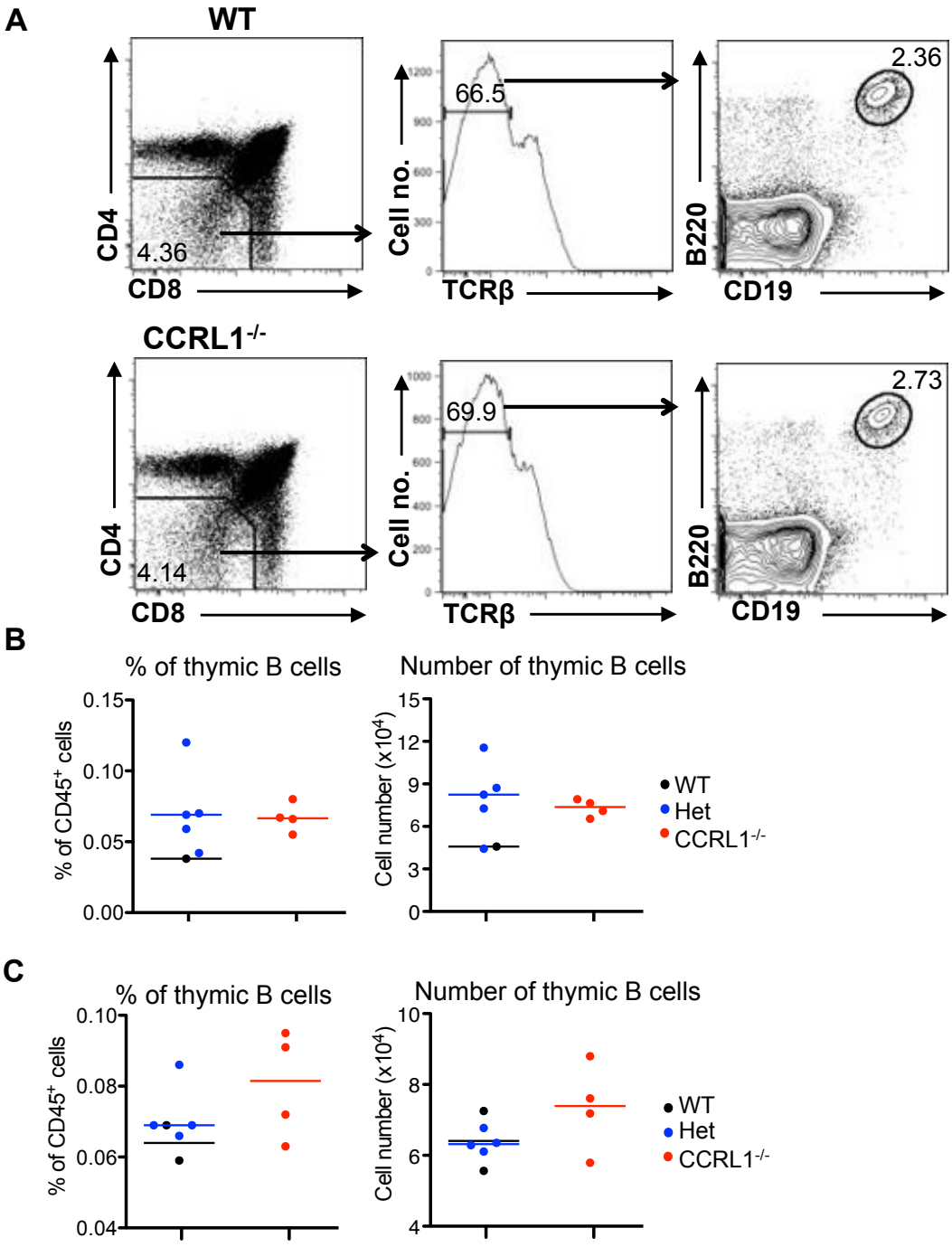

Figure 50. Unaltered Frequency of Thymic B Cells in CCRL1$^{-/-}$ Mice.

Thymic B cells were identified as CD45^{+}CD4^{-}CD8^{-}TCRβ^{-}B220^{+}CD19^{+} (A). The proportions and absolute cell numbers of thymic B cells are shown in the male thymus (B), and female thymus (C). Horizontal bars represent the median values. Statistical analysis performed (Mann Whitney). Each point represents one mouse.

4.2.9 Abnormal Distribution of DN Thymocytes in CCRL1$^{-/-}$ Mice

The outward migration of DN thymocytes, which is accompanied by their development, is mediated by several chemokine receptors. Mice deficient in CXCR4, CCR7 or CCR9 show abnormal localisation of DN thymocytes, however the homing of DN thymocytes to the SCZ is not an absolute requirement for T cell development (Misslitz et al., 2004, Benz et al., 2004, Plotkin et al., 2003). The localisation of DN thymocytes in the CCRL1$^{-/-}$ thymus was determined by staining cryosections of thymi for CD4, CD8 and CD25. CD4 and CD8 identify the thymic cortex and medulla by the distribution of DP and SP thymocytes respectively. CD25 is expressed by DN2 ($CD44^{+}CD25^{+}$) and DN3 ($CD44^{-}CD25^{+}$) thymocytes. Within the adult thymus the following areas were identified: SCZ (50μm from the tissue edge), outer cortex (100μm from the SCZ), mid cortex (any area between the outer cortex and CMJ), and CMJ (50μm into the cortex from the medulla). Representative images of heterozygous and CCRL1$^{-/-}$ thymus showing these areas can be found in Figure 51A. $CD25^{+}$ cells were manually enumerated in each area to determine the number of $CD25^{+}$ cells/mm^2. Three sections were stained from each mouse, and three areas were quantitated per section. The mean of the three areas quantitated was used for all subsequent analysis. Three CCRL1$^{-/-}$ and three control thymi were analysed. $CD25^{+}$ cells were found in greatest density at the SCZ, and at this location there was a significant reduction of these cells in the CCRL1$^{-/-}$ thymus ($p=0.0040$). $CD25^{+}$ cells were also reduced in the CCRL1$^{-/-}$ at the outer cortex ($p=0.0081$). There was no difference in the number of $CD25^{+}$ cells at the cortex or CMJ regions of the CCRL1$^{-/-}$ thymus compared to controls (Figure 51B, Table 22).

A similar quantitation was carried out in the thymus from neonatal mice (2 days old), where the localisation of $CD25^+$ DN thymocytes to the SCZ is more prevalent (Benz et al., 2004). In these younger mice, $CD25^+$ cells at the SCZ (50μm from the tissue edge) and outer cortex (100μm from the SCZ) were identified. A representative image from $CCRL1^{-/-}$ and control thymi, showing these areas can be found in Figure 52A. $CD25^+$ cells were manually enumerated in each area to determine the number of $CD25^+$ cells/mm^2. Three sections were stained from each mouse, and three areas were quantitated per section. Three thymi of each genotype were analysed. Similar to the adult thymus, $CD25^+$ cells were found in greatest density at the SCZ, where there was a significant reduction in the $CCRL1^{-/-}$ thymus ($p=0.0151$). $CD25^+$ cells were not reduced in the neonatal $CCRL1^{-/-}$ thymus at the outer cortex ($p=0.9114$) (Figure 52B, Table 23).

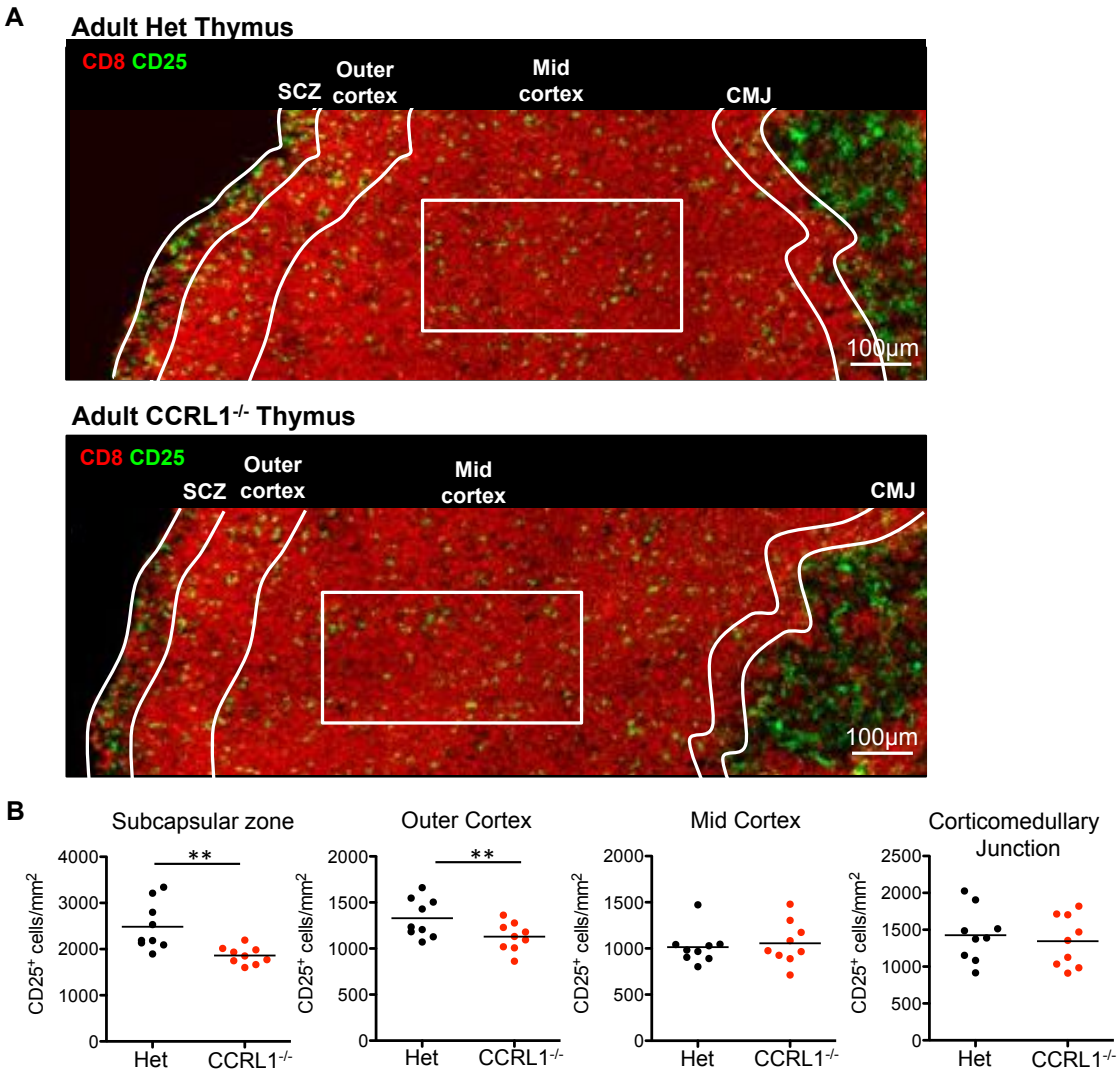

Figure 51. Abnormal Distribution of CD25$^+$ DN Thymocytes in CCRL1$^{-/-}$ Thymi.

Cryosections were stained for CD8 and CD25 and the following areas identified: SCZ (50μm from the tissue edge), outer cortex (100μm from SCZ), mid cortex (any area between outer cortex and CMJ), and CMJ (50μm into the cortex from the medulla) Representative confocal staining of het and CCRL1$^{-/-}$ thymus, with areas to be quantitated identified (A). Scale bar shows 50μm. Cells were manually enumerated to determine the number of CD25$^+$ cells/mm^2 in each area (B). Three sections were stained from each mouse, and three areas were quantitated per section, n=3 mice of each genotype. Each point represents the mean quantitation per section and horizontal bars represent the mean. Statistical analysis performed (Two way ANOVA with Bonferroni post test) ***p<0.01*

A

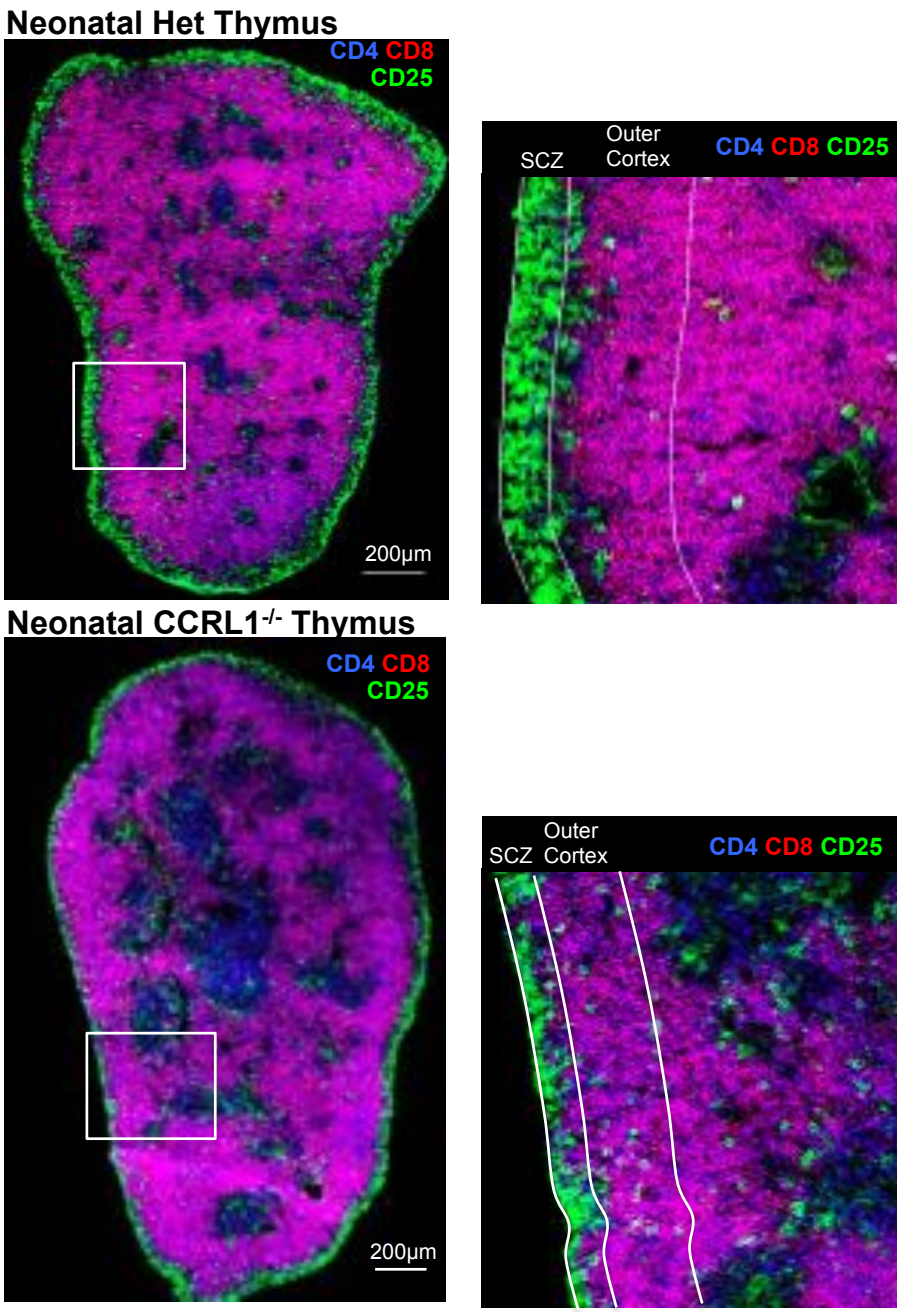
Neonatal Het Thymus
CD4 CD8
CD25
200μm
SCZ
Outer
Cortex
CD4 CD8 CD25
Neonatal CCRL1-/- Thymus
CD4 CD8
CD25
200μm
SCZ
Outer
Cortex
CD4 CD8 CD25

B

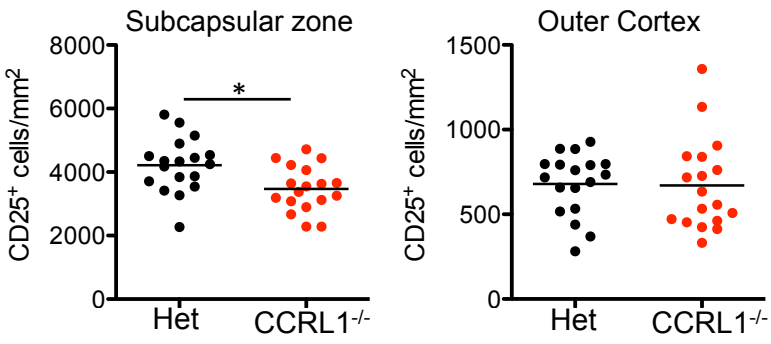
Subcapsular zone
CD25+ cells/mm2
8000
6000
4000
2000
0
*
Het
CCRL1-/-
Outer Cortex
CD25+ cells/mm2
1500
1000
500
0
Het
CCRL1-/-

Figure 52. Abnormal Distribution of CD25^{+} DN Thymocytes at the Subcapsular Zone of Neonatal CCRL1$^{-/-}$ Mice.

Thymi from 2 day old mice was cryosectioned and stained for CD4 CD8 and CD25 and the following areas identified: SCZ (50μm from the tissue edge), and the outer cortex (100μm from SCZ). Representative confocal staining of het and CCRL1$^{-/-}$ thymus, with areas to be quantitated identified is shown. Three sections were stained from each mouse, and two areas were quantitated per section, n=3 mice of each genotype. Each point shows the quantitation per section and horizontal bars represent the mean. Statistical analysis performed (Two way ANOVA with Bonferroni post test) *$p<0.05$*

Table 22. $CD25^+$ cells/mm^2 in the Adult Thymus

	Het		$CCRL1^{-/-}$		Het vs. $CCRL1^{-/-}$
	Mean	SEM	Mean	SEM	P value
SCZ	2486	173.6	1864	62.7	***0.0040***
Outer cortex	1329	69.9	1129	51.2	***0.0081***
Mid cortex	1015	63.3	1057	77.5	0.6872
CMJ	1428	121.0	1347	116.0	0.5690

The mean and SEM of the number of $CD25^+$ cells/mm^2 in the SCZ, outer cortex, mid cortex and CMJ of the $CCRL1^{-/-}$ and het adult thymus. n=3 het, 3 $CCRL1^{-/-}$.
Significant p values are highlighted in bold italic type (two way ANOVA with Bonferroni post test).

Table 23. $CD25^+$ cells/mm^2 in the Neonatal Thymus

	Het		$CCRL1^{-/-}$		Het vs. $CCRL1^{-/-}$
	Mean	SEM	Mean	SEM	P value
SCZ	4219	199.9	3474	168.1	***0.0151***
Outer cortex	680	43.2	671	63.8	0.9114

The mean and SEM of the number of $CD25^+$ cells/mm^2 in the SCZ and outer cortex of the $CCRL1^{-/-}$ and het neonatal thymus. n=3 het, 3 $CCRL1^{-/-}$.
Significant p values are highlighted in bold italic type (two way ANOVA with Bonferroni post test).

4.2.10 Unaltered Levels of CCRL1 Ligand in the CCRL1$^{-/-}$ Thymus

Although the scavenging function of CCRL1 has been shown several times *in vitro*, this has not been consistently reflected by levels of CCRL1 ligand *in vivo*. Analysis of the CCRL1$^{-/-}$ mouse by Comerford and colleagues revealed increased levels of CCL19 and CCL21 in the lymph node of CCRL1$^{-/-}$ mice, however this was not reproduced in the latest analysis of the same mice by Ulvmar *et al* (Ulvmar et al., 2014, Comerford et al., 2010). In addition, analysis by Bunting *et al* revealed reduced levels of CCL19 and CCL25 in the CCRL1$^{-/-}$ thymus, a surprising finding, considering the scavenging role of CCRL1 (Bunting et al., 2013). Due to these conflicting reports, we analysed the levels of CCL19, CCL21 and CCL25 in the thymus of CCRL1$^{-/-}$ and littermate control mice. The levels of these chemokines were determined by ELISA, using thymus tissue from plt and CCL25$^{-/-}$ mice as negative controls for CCL19/CCL25 and CCL25 respectively. There was no significant difference in the levels of CCL19, CCL21 or CCL25 between CCRL1$^{-/-}$ thymi and littermate controls (Figure 53, Table 24).

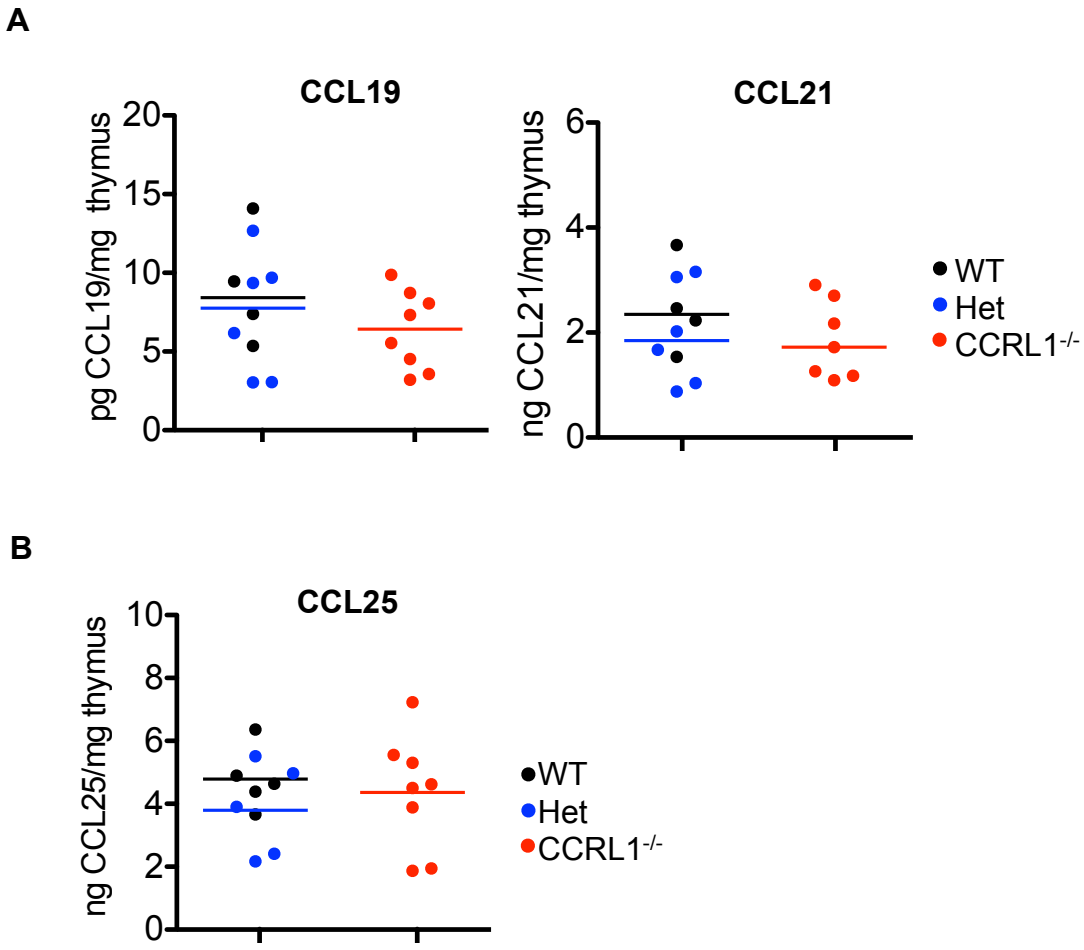

Figure 53. Unaltered Levels of CCR7L and CCR9L in the CCRL1$^{-/-}$ Thymus.

CCR7L and CCR9L were quantified by ELISA analysis. The levels of CCL19 and CCL21 were determined, and the thymus from a plt mouse used as a negative control (A). The level of CCL25 was also determined, using the thymus from a CCL25$^{-/-}$ mouse as a negative control (B). Each point represents one mouse and horizontal bars represent the median. Statistical analysis performed (Mann Whitney).

Table 24. Levels of CCL19, CCL21, and CCL25 in the CCRL1$^{-/-}$ Thymus Compared to Littermate Controls.

					p values		
		WT n=4	**Het n=6**	**KO n=8**	**WT vs. Het**	**WT vs. KO**	**Het vs. KO**
CCL19 pg/mg thymus	Median	**8.423**	**7.766**	**6.429**	0.6095	0.2828	0.8518
	25th	5.866	3.058	3.813			
	75th	12.94	10.44	8.560			
		WT n=4	**Het n=6**	**KO n=7**	**WT vs. Het**	**WT vs. KO**	**Het vs. KO**
CCL21 ng/mg thymus	Median	**2.347**	**1.847**	**1.720**	0.4762	0.3152	1.000
	25th	1.711	0.997	1.175			
	75th	3.366	3.082	2.703			
		WT n=5	**Het n=5**	**KO n=8**	**WT vs. Het**	**WT vs. KO**	**Het vs. KO**
CCL25 ng/mg thymus	Median	**4.641**	**3.907**	**4.562**	0.5476	0.8329	0.8329
	25th	4.022	2.292	2.431			
	75th	5.627	5.243	5.493			

Data expressed as median (bold) with 25th and 75th quartile. p values shown (Mann Whitney statistical test).

4.2.11 Unaltered TEC Populations in the CCRL1$^{-/-}$ Thymus

Recent analysis of the stromal compartment of the CCRL1$^{-/-}$ thymus reported increased numbers of immature mTEC^{lo} and mature mTEC^{hi} (Bunting et al., 2013). We also performed a detailed analysis of the TEC population in CCRL1$^{-/-}$ mice compared to littermate controls. Briefly, thymi were digested and stromal cells enriched by MACS depletion of CD45^{+} cells. Cells were stained for EpCAM to identify total TEC, then Ly51 to distinguish between Ly51^{-} mTEC and Ly51^{+} cTEC. Staining for CD80 and Aire allowed the identification of mature CD80^{+}Aire^{+} mTEC (Figure 54A). The absolute cell number of total TEC was unchanged between CCRL1$^{-/-}$ and het thymi (p=0.3429) (Figure 54B). The proportion and cell number of EpCAM^{+}Ly51^{+} cTEC was also similar between CCRL1$^{-/-}$ and littermate controls (p=0.3429, p-0.3429 respectively) (Figure 54C). The percentage of EpCAM^{+}Ly51^{-} mTEC was similar been CCRL1$^{-/-}$ and control mice (p=0.8857), as was the absolute cell number (p=0.4857). The median proportion of CD80^{+}Aire^{+} mTEC was also similar in CCRL1$^{-/-}$ (7.8%), and het (7.9%) thymi (p=0.8857); this was reflected in absolute cell numbers (p=0.4857) (Figure 54D). In summary, our analysis showed no difference in the percentage or absolute cell number of any TEC population analysed in CCRL1$^{-/-}$ compared to littermate controls.

To determine the localisation of cortical and medullary microenvironments within the CCRL1$^{-/-}$ thymus, we stained sections of WT (Figure 55A) and CCRL1$^{-/-}$ (Figure 55B) thymus for CD205 and TR5 to show cortex and medulla, respectively. This revealed distinct cortical and medullary regions in both WT and CCRL1$^{-/-}$ mice. Moreover,

staining for CD4 and CD8 revealed the correct positioning of DP and SP thymocytes within the cortex and medulla in CCRL1$^{-/-}$ thymus.

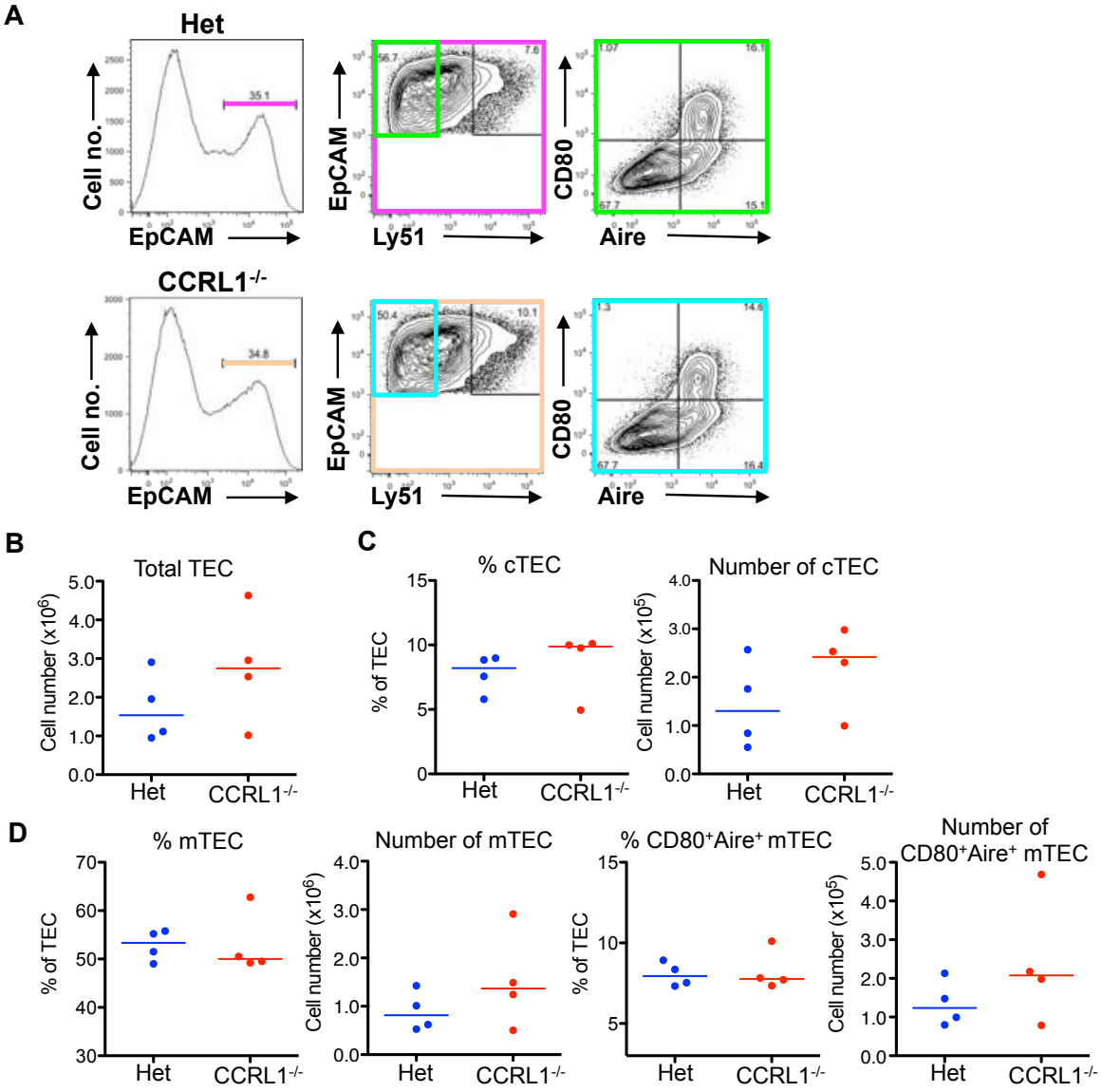

Figure 54. No Alteration in TEC Populations in the CCRL1$^{-/-}$ Thymus.

Thymi were digested and TEC were enriched by depleting CD45^{+} cells using MACS technology. Cells were stained to allow the identification of TEC populations by flow cytometry (A). The absolute number of TEC (B), the proportions and absolute cell numbers of Ly51^{+} cTEC (C), Ly51^{-} mTEC, and CD80^{+}Aire^{+} mTEC (D) are shown. Horizontal bars represent the median values. Statistical analysis performed (Mann Whitney). Each point represents one mouse.

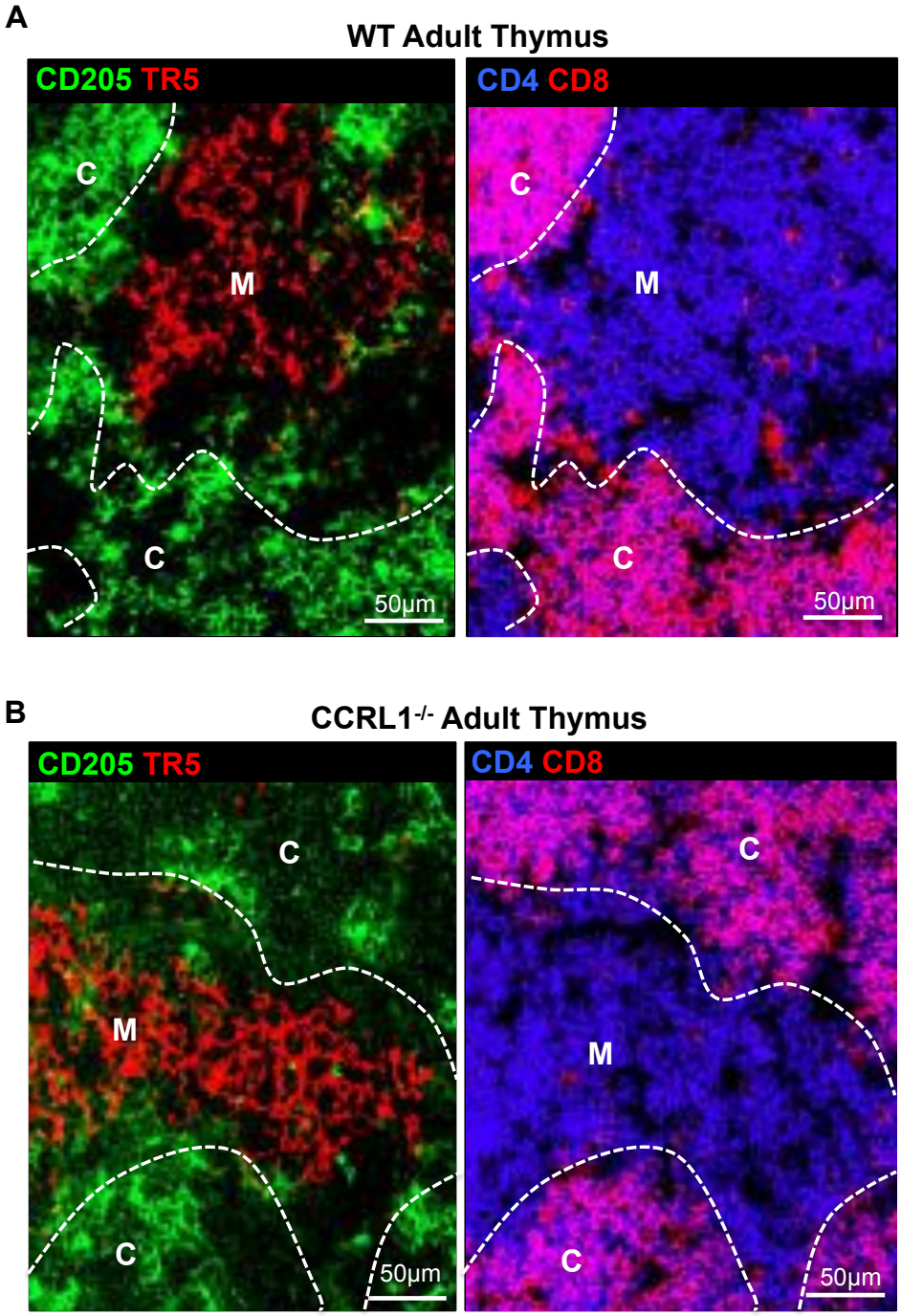

Figure 55. Normal Cortex and Medulla Organisation in CCRL1$^{-/-}$ Mice

Thymus sections from WT (A), and CCRL1$^{-/-}$ (B) mice were stained for CD205 and TR5 to identify cortex 'C' and medulla 'M' respectively. Sections were also stained for CD4 and CD8 to allow the identification of SP and DP thymocytes, and determine their positioning within the thymus with respect to cortical and medullary areas.

4.2.12 Analysis of Irradiation Bone Marrow Chimeras

The data shown so far focuses on the CCRL1$^{-/-}$ thymus under steady-state conditions, and fails to identify a major role for CCRL1. To further this study, we generated irradiation bone marrow (BM) chimeras to determine any involvement of CCRL1 in thymic reconstitution. Two groups of mice were created; CCRL1$^{-/-}$ hosts that were reconstituted with WT BM, and WT hosts that were reconstituted with CCRL1$^{-/-}$ BM. Haematopoietic cells from CCRL1$^{-/-}$ mice were CD45.2 whereas those from WT mice were CD45.1. This allowed the identification of host and donor cells in our analysis.

The thymus from irradiation bone marrow chimeras were harvested 9 weeks post reconstitution, and analysed using flow cytometry. The thymus was digested and thymocytes stained for CD4, CD8 and TCRβ, to allow the identification of DN, DP and SP thymocytes (Figure 56A). The cellularity of the thymus was calculated and showed a significant difference in WT hosts that had received CCRL1$^{-/-}$ BM ($p=0.0303$) (Figure 56B). The proportions of DN, DP, SP4 and SP8 thymocytes were similar in both groups of BM chimeras ($p=0.0732$, $p=0.8705$, $p=0.8708$, $p=0.1490$ respectively). The number of DN thymocytes was significantly different in WT mice that had received CCRL1$^{-/-}$ BM, compared to CCRL1$^{-/-}$ mice that had received WT BM (WT mice reconstituted with CCRL1$^{-/-}$ BM median: 429776 cells, CCRL1$^{-/-}$ mice reconstituted with WT BM median: 319601 cells, $p=0.0051$). Despite this, there was no significant difference in the absolute cell number of DP ($p=0.2020$), SP4 ($p=0.2677$) or SP8 ($p=0.7551$) thymocytes (Figure 56C).

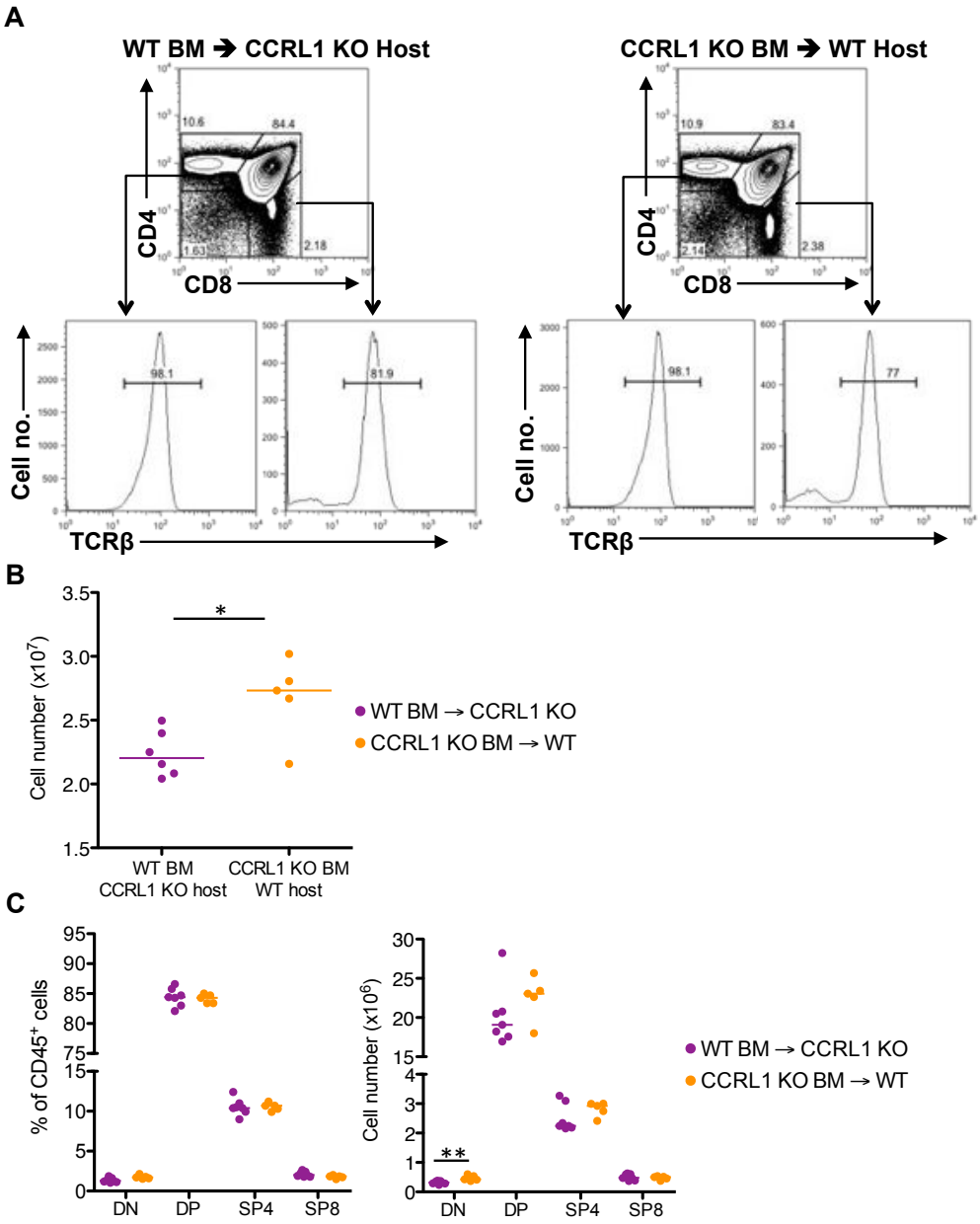

Figure 56. Increased DN Thymocytes in Irradiated WT Hosts, Reconstituted with CCRL1$^{-/-}$ Bone Marrow.

Irradiation bone marrow chimeras were generated and the thymus was analysed by flow cytometry 9 weeks post reconstitution. Thymocytes were stained to allow the identification of DN, DP and SP thymocytes by flow cytometry as previously shown (A). Thymus cellularity was calculated (B), and the proportions and absolute cell numbers of DN, DP and SP thymocytes are shown (C). Horizontal bars represent the median values. Statistical analysis performed (Mann Whitney) *$p<0.05$, **$p<0.01$. Each point represents one mouse.

4.2.13 Increased Proportions of Peripheral T Cells in CCRL1$^{-/-}$ Mice

To assess any role for CCRL1 in the maintenance of the peripheral T cell pool, we examined the populations of T cells in the blood, spleen and inguinal lymph node (LN) of steady-state CCRL1$^{-/-}$ and control mice. Firstly the blood from CCRL1$^{-/-}$ mice and het littermate controls was stained for flow cytometry. TCRβ was used to detect αβ T cells, and then CD4, CD8, CD25 and Foxp3 allowed the subsequent detection of CD4 T cells, CD8 T cells, and Tregs (Figure 57A.) There was a highly significant increase in the proportion of αβ T cells in the blood of CCRL1$^{-/-}$ mice compared to littermate controls (p=<0.0001, het mean: 21.1%, CCRL1$^{-/-}$ mean: 28.5%). Moreover, there was a significant increase in the numbers of αβ T cells/μl blood (p=0.0047), (Figure 57B). The relative proportions of CD4 and CD8 T cells were unchanged in the blood of CCRL1$^{-/-}$ mice compared to controls, however there was a trend for increased numbers of both populations (consistent with the overall trend for increased numbers of αβ T cells) (Figure 57C, Table 25. Although the proportion of αβ T cells was increased in the blood of CCRL1$^{-/-}$ mice, the proportion of Treg was significantly decreased (p=0.0017). The percentage of Treg decreased from a mean of 7.6% in het controls, to 5.3% in CCRL1$^{-/-}$. Despite this difference in proportion, the absolute number of Foxp3^{+} Treg was similar in the peripheral blood of CCRL1$^{-/-}$ and littermate control mice. (Figure 57D, Table 25).

A similar flow cytometric analysis of the spleen was performed whereby splenocytes were stained for TCRβ, CD4, CD8, CD25 and Foxp3 to allow the identification of αβ T cells, CD4 T cells, CD8 T cells, and Foxp3^{+} Treg (Figure 58A). Similar to blood, proportions of αβ T cells were significantly increased in the CCRL1$^{-/-}$ spleen

(p=0.0186), however this increase was not reflected in absolute cell numbers (Figure 58B). The proportion of CD8 T cells was significantly increased in the CCRL1$^{-/-}$ spleen (p=0.0455), and the proportion of CD4 T cells was reciprocally decreased (p=0.0694). Despite this, there was no difference in the absolute number of CD4 or CD8 T cells between the spleen from CCRL1$^{-/-}$ mice and littermate controls (Figure 58C, Table 25). Similarly to the blood, there was a trend for reduced proportions of Treg in the CCRL1$^{-/-}$ spleen, however this was not significant (p=0.1478). The absolute numbers of Treg in the CCRL1$^{-/-}$ spleen were similar to control mice.

The same flow cytometric staining and analysis was performed on cells obtained from the inguinal LN of CCRL1$^{-/-}$ and control mice (Figure 59A). Interestingly, there was no difference in the percentage or absolute number of αβ T cells in the inguinal LN from CCRL1$^{-/-}$ compared to control mice (Figure 59B). Moreover, there was no difference in the proportions or numbers of CD4 or CD8 T cells (Figure 59C). Foxp3^{+} Treg were also present in similar proportions and numbers in the inguinal LN from CCRL1$^{-/-}$ and control mice (Figure 59D, Table 25).

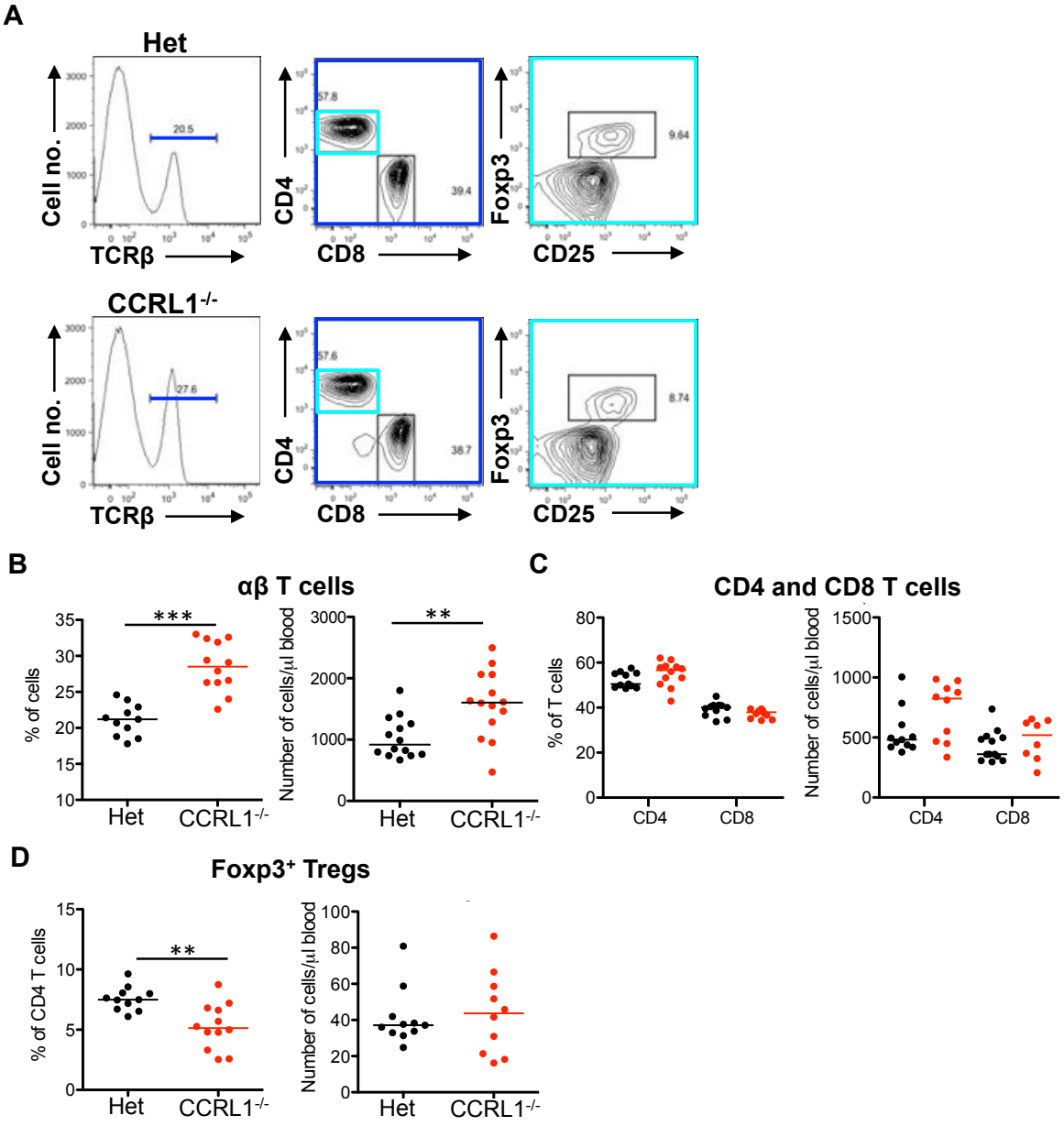

Figure 57. Increased Proportions of T Cells in the Peripheral Blood of CCRL1$^{-/-}$ Mice.

Blood was stained and analysed by flow cytometry to allow the identification of conventional T cells and Tregs. Live lymphocytes were gated prior to the detection of TCRβ^{+} cells (A). The proportions and absolute cell numbers of αβ T cells (B), CD4 and CD8 T cells (B), and Foxp3^{+} Tregs (C) are shown. Horizontal bars represent the median values. Statistical analysis performed (D'Agostino-Pearson followed by t test) ***p<0.01, ***p<0.001* Each point represents one mouse.

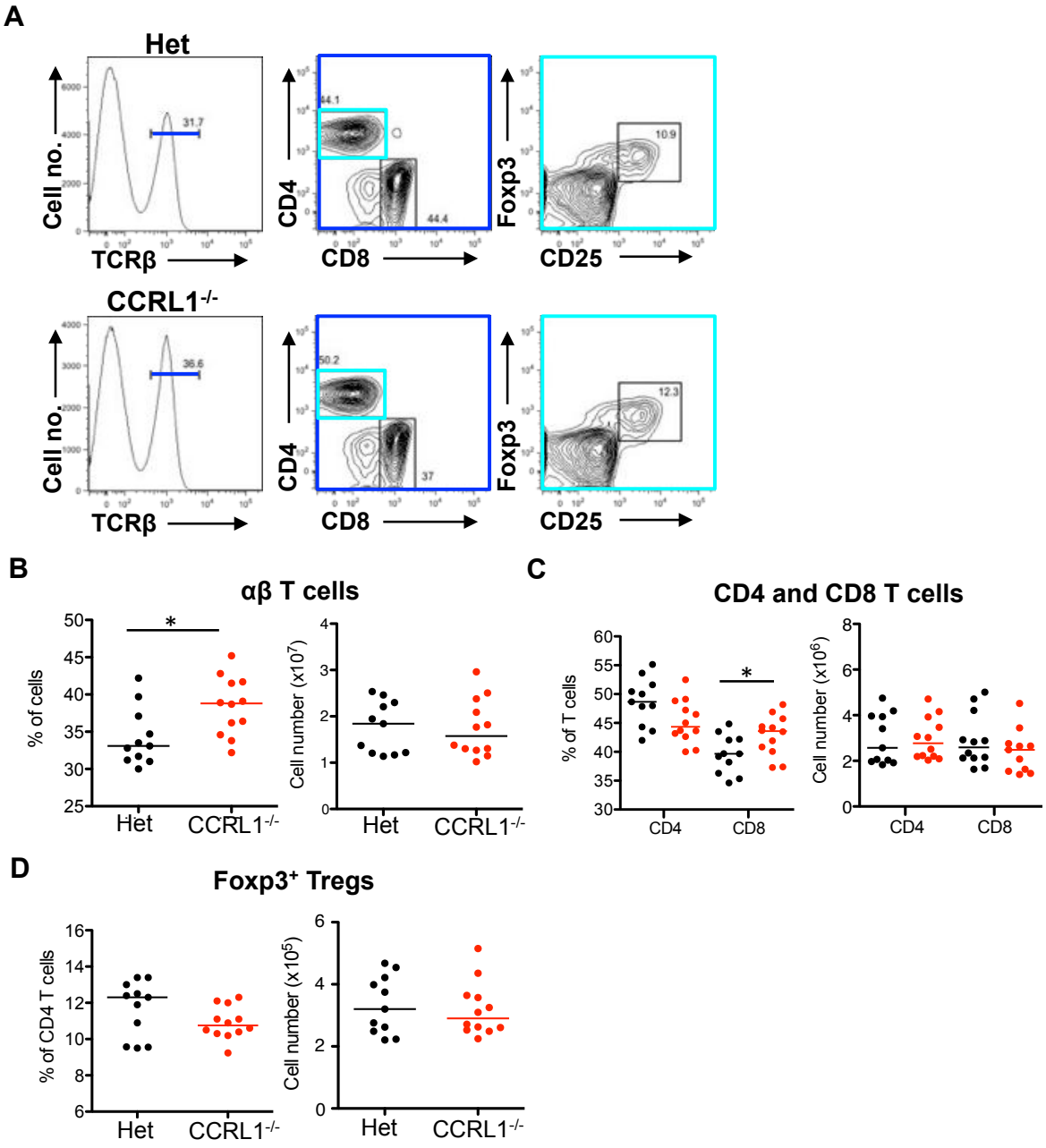

Figure 58. Increased Proportions of T Cells in the Spleen of CCRL1$^{-/-}$ Mice.

Splenocytes were stained and analysed by flow cytometry to allow the identification of conventional T cells and Tregs. Live lymphocytes were gated prior to the detection of TCRβ^{+} cells (A). The proportions and absolute cell numbers of αβ T cells (B), CD4 and CD8 T cells (B), and Foxp3^{+} Tregs (C) are shown. Horizontal bars represent the median values. Statistical analysis performed (D'Agostino-Pearson followed by t test) *$p<0.05$. Each point represents one mouse.

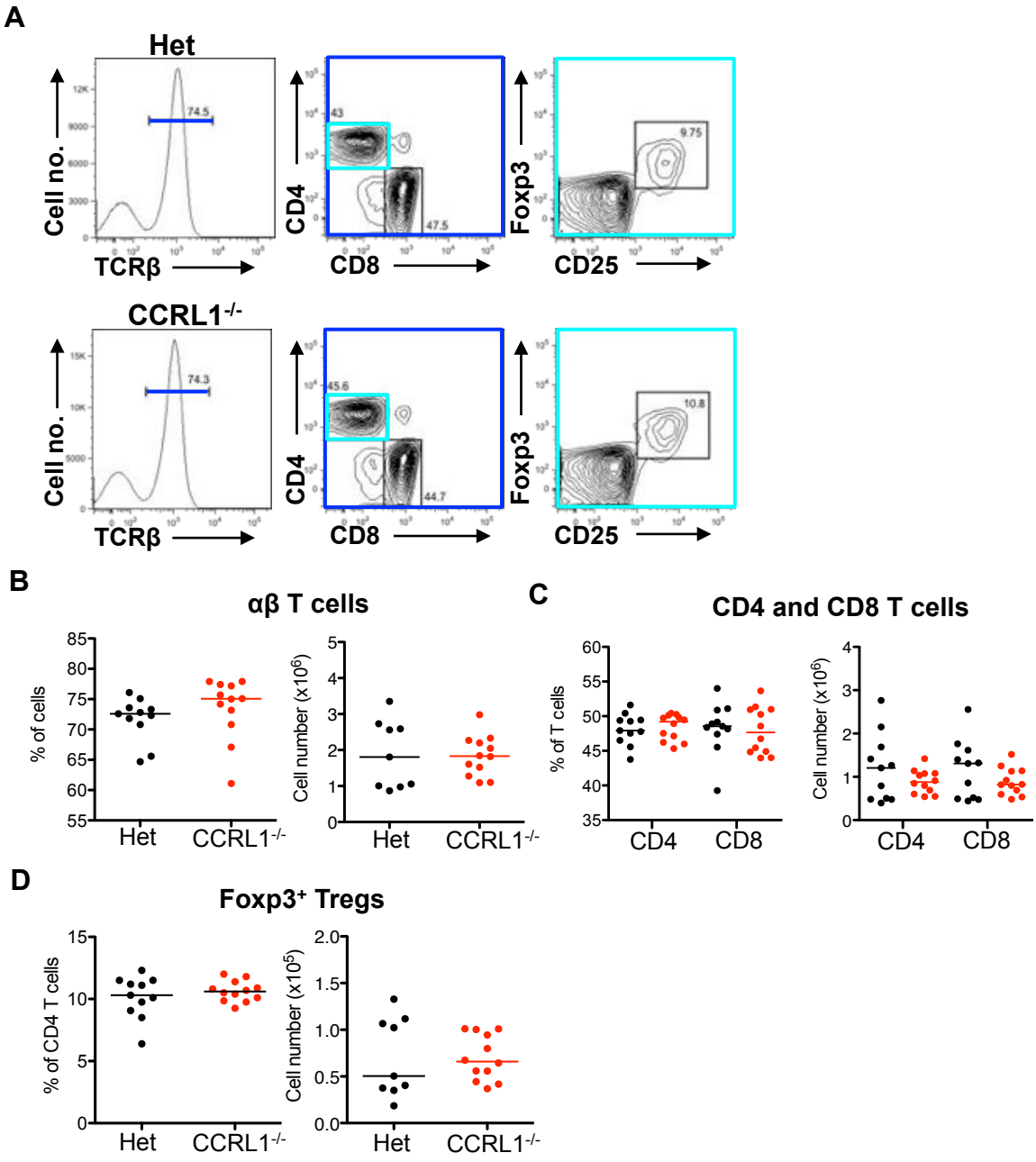

Figure 59. Unaltered Proportions of T Cells in the CCRL1$^{-/-}$ Lymph Node.

Inguinal lymph node cells were stained and analysed by flow cytometry to allow the identification of conventional T cells and Tregs. Live lymphocytes were gated prior to the detection of TCRβ^{+} cells (A). The proportions and absolute cell numbers of αβ T cells (B), CD4 and CD8 T cells (B), and Foxp3^{+} Tregs (C) are shown. Horizontal bars represent the median values. Statistical analysis performed (Mann Whitney). Each point represents one mouse.

4.2.14 Thymic Egress is Not Dependant on CCRL1

Given the increased proportions of αβ T cells in the peripheral blood of CCRL1$^{-/-}$ mice, we compared thymic output between CCRL1$^{-/-}$ mice and littermate controls. This was achieved by crossing CCRL1$^{-/-}$ mice with RAG2pGFP mice to allow the identification of recent thymic emigrants (RTE) by expression of GFP. Expression of GFP was determined on total αβ T cells in blood (Figure 60A), inguinal LN (Figure 60B), and spleen (Figure 60C). No significant differences were found in the proportion of RAG2pGFP^{+} cells between CCRL1$^{-/-}$ mice and littermate controls in blood, lymph node or spleen.

To determine any difference in the egress of specific T cell populations from the thymus, we next identified CD4, CD8 and Foxp3^{+} T cells in the blood by flow cytometry as previously shown (Figure 61A). Expression of RAG2pGFP was determined using blood from a WT (RAG2pGFP negative) mouse as a negative control (not shown). The proportion and number of cells expressing RAG2pGFP are unchanged for CD4, CD8 and Treg cells in the blood (Table 26) (Figure 61B). CD4, CD8 and Treg RTE were identified using the same method in the spleen (Figure 62), and inguinal LN (Figure 63), and similar proportions and numbers of RAG2pGFP^{+} CD4 and CD8 T cells, and Treg were present in both tissues from CCRL1$^{-/-}$ and het littermate controls. These results show similar frequencies of RTE in the blood, spleen and inguinal LN in CCRL1$^{-/-}$ and littermate control mice.

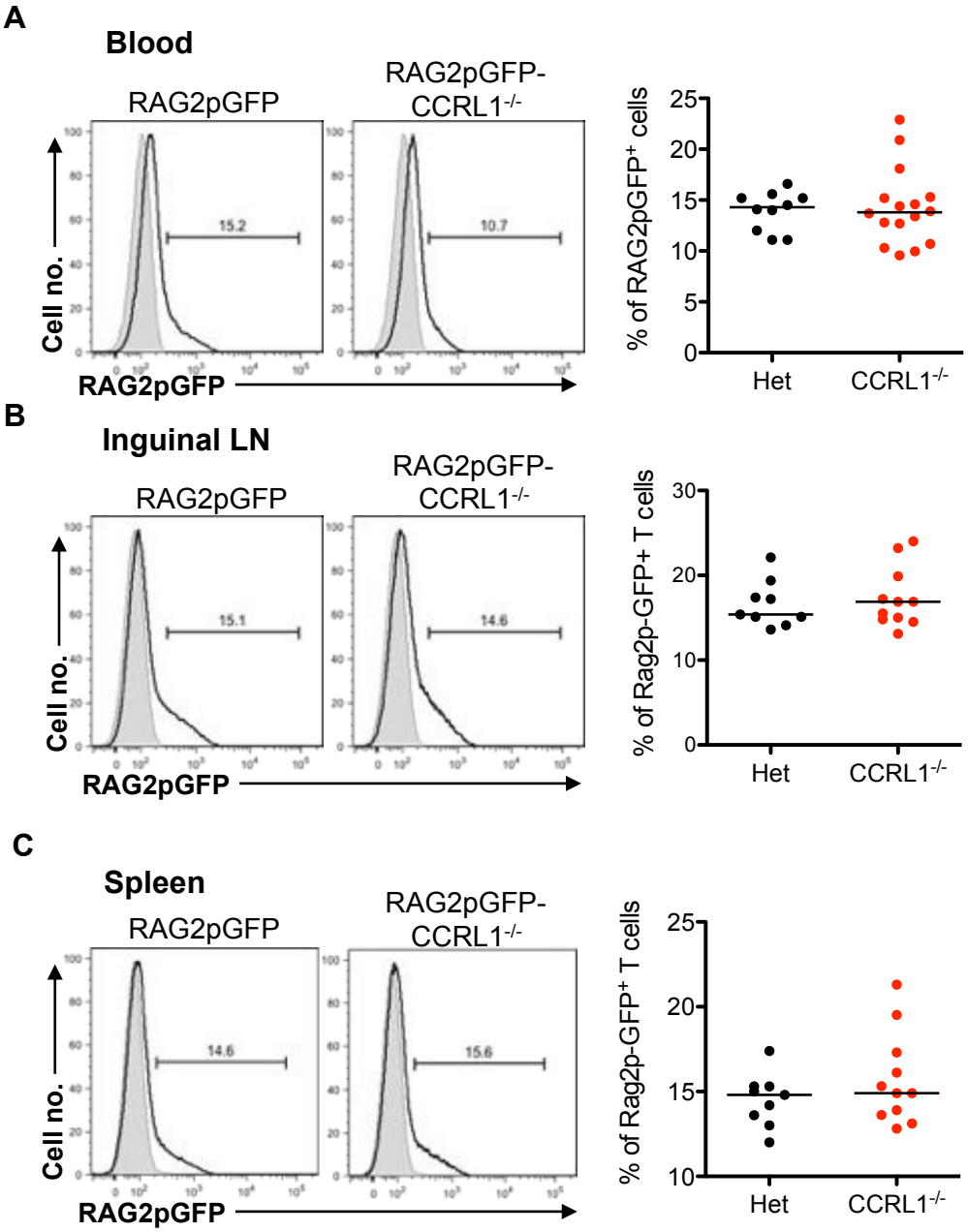

Figure 60. Proportion on RTE in Blood, Lymph Node and Spleen of CCRL1$^{-/-}$ and littermate controls.

Expression of RAG2pGFP was determined on TCRb^{+} T cells from blood (A), inguinal lymph node (B), and spleen (C) using flow cytometry. The proportions of RAG2pGFP^{+} TCRb^{+} T cells were quantitated for each tissue, no significant differences were found between CCRL1$^{-/-}$ mice and littermate controls. Overlaid histograms show GFP expression by cells from WT and RAG2pGFP mice.

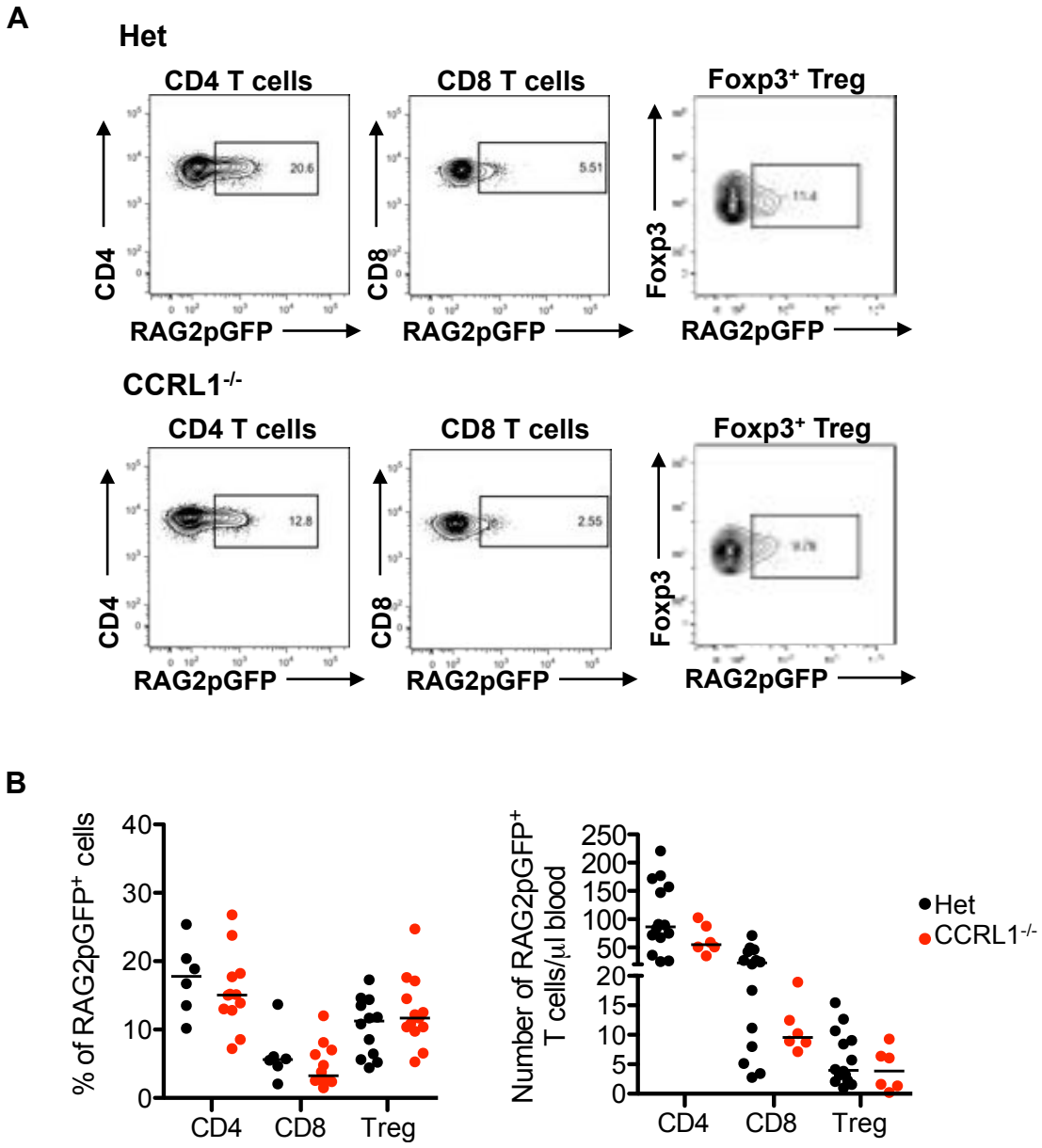

Figure 61. Normal Proportions of RTE in CCRL1$^{-/-}$ Blood.

Blood from CCRL1-RAG2pGFP mice was analysed by flow cytometry to determine the number of GFP^{+} RTE. Live CD3^{+}TCRβ^{+} cells were gated prior to the detection of CD4^{+}, CD8^{+} and Foxp3^{+} T cells (A). The proportion and absolute numbers of GFP^{+} CD4 and CD8 T cells, and Foxp3^{+} Treg are shown (B). Horizontal bars represent the median values. Statistical analysis performed (Mann Whitney). Each point represents one mouse.

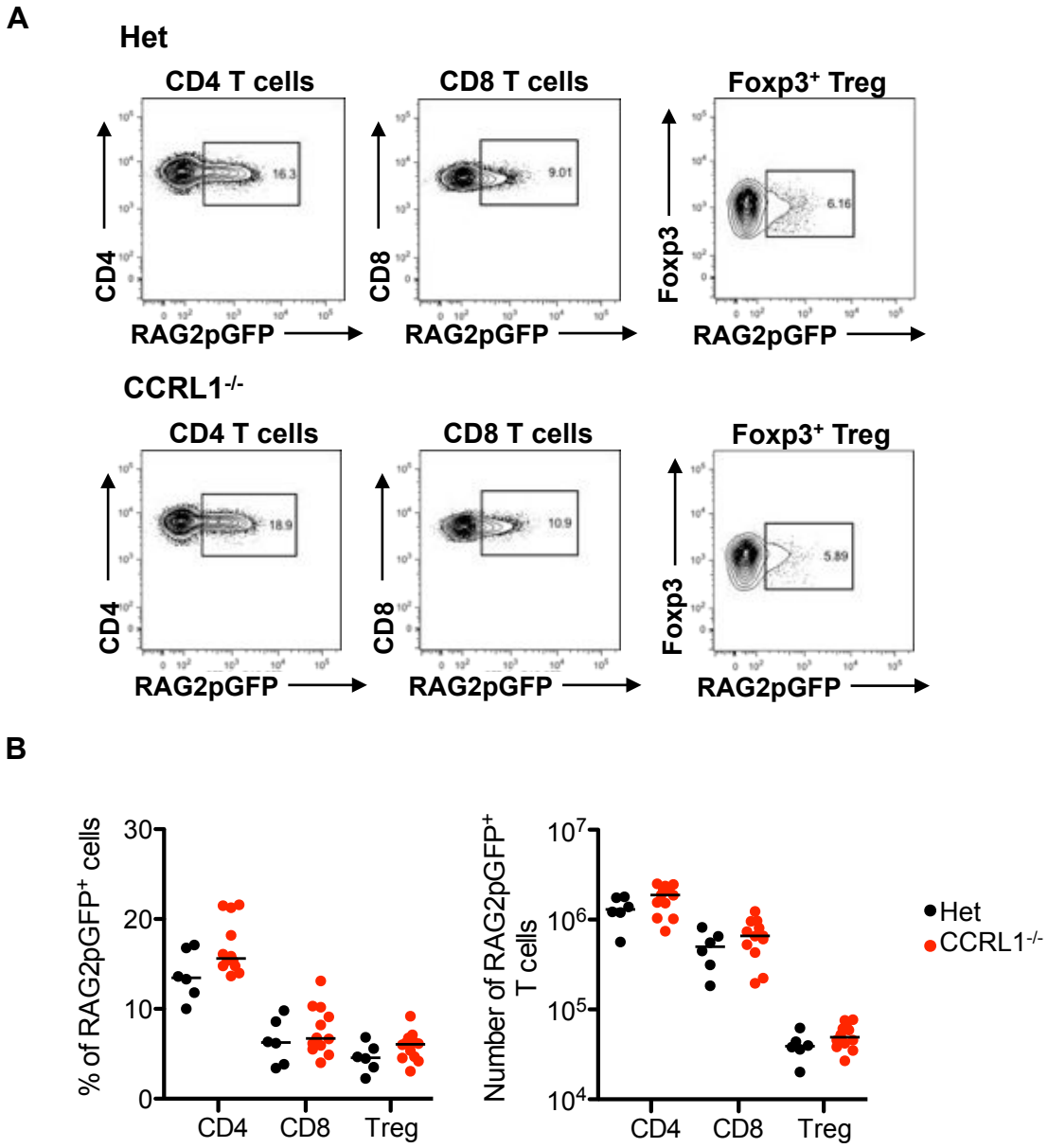

Figure 62. Normal Proportions of RTE in CCRL1$^{-/-}$ Spleen.

Splenocytes from CCRL1-RAG2pGFP mice were analysed by flow cytometry to determine the number of GFP^{+} RTE. Live CD3^{+}TCRβ^{+} cells were gated prior to the detection of CD4^{+}, CD8^{+} and Foxp3^{+} T cells (A). The proportion and absolute number of GFP^{+} CD4 and CD8 T cells, and Foxp3^{+} Treg are shown (B). Horizontal bars represent the median values. Statistical analysis performed (Mann Whitney). Each point represents one mouse.

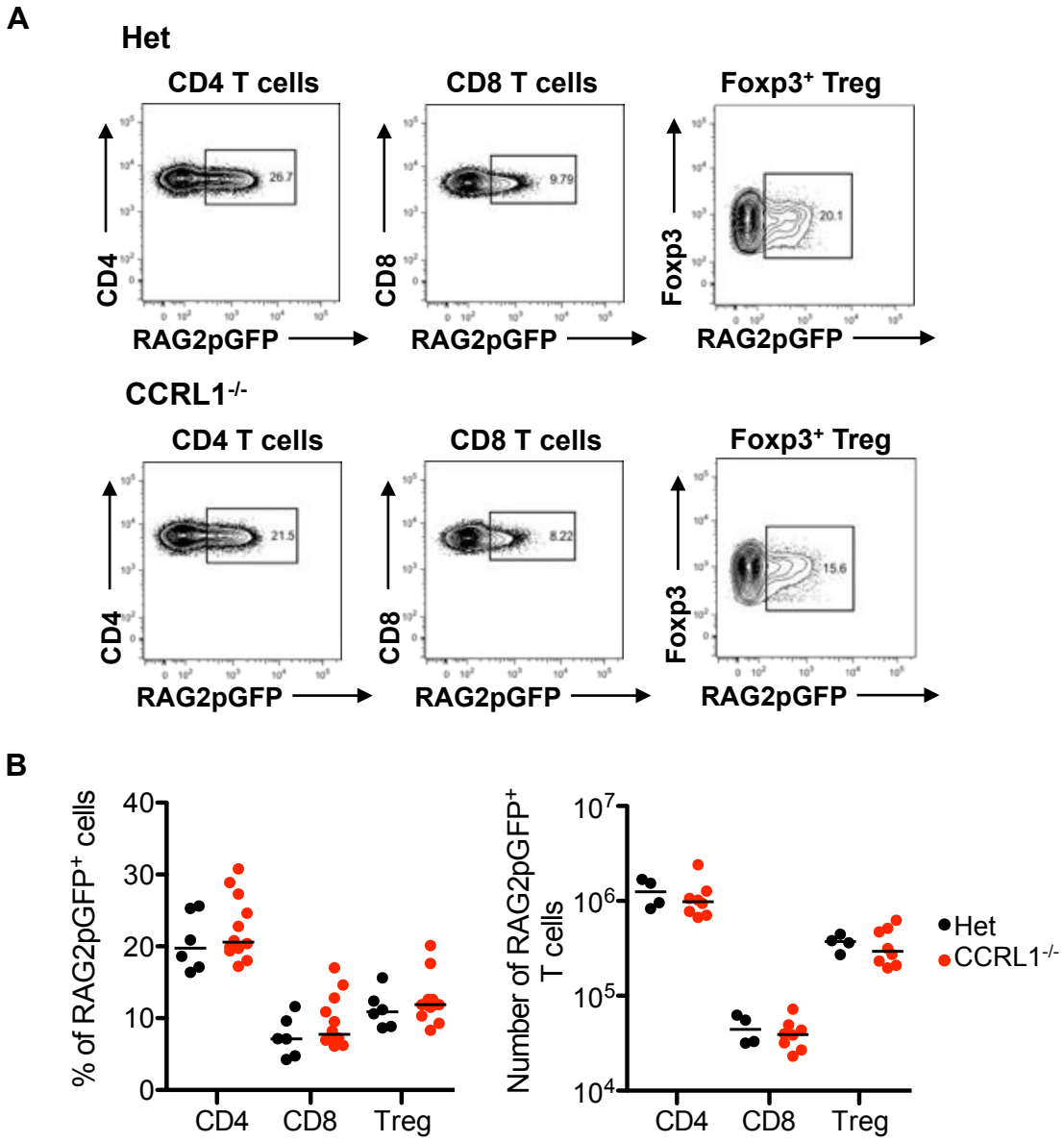

Figure 63. Normal Proportions of RTE in CCRL1$^{-/-}$ Inguinal Lymph Node.

Inguinal lymph nodes from CCRL1-RAG2pGFP mice were analysed by flow cytometry to determine the number of GFP^{+} RTE. Live CD3+TCRβ+ cells were gated prior to the detection of CD4^{+}, CD8^{+} and Foxp3^{+} T cells (A). The proportion and absolute number of GFP^{+} CD4 and CD8 T cells, and Foxp3^{+} Treg are shown (B). Horizontal bars represent the median values. Statistical analysis performed (Mann Whitney). Each point represents one mouse.

Table 25. Statistical Analysis of Peripheral T Cell Populations in the CCRL1-/- Mouse Compared to Littermate Controls

	p values		
	Blood	**Spleen**	**Inguinal LN**
% αβ T cell	***<0.0001***	***0.0186***	0.3251
Number of αβ T cell	***0.0047***	0.9444	0.8981
% CD4 T cell	0.1877	0.0694	0.7286
Number of CD4 T cell	0.0802	0.5279	0.2133
% CD8 T cell	0.1088	***0.0455***	0.8263
Number of CD8 T cell	0.4354	0.5873	0.2318
% Treg	***0.0017***	0.1478	0.4045
Number of Treg	0.7699	0.7037	0.9829

Statistical analysis performed (D'Agostino-Pearson followed by t test), significant p values are highlighted in bold italic type.

Table 26. Statistical Analysis of RAG2pGFP Expression by Peripheral T cell Subsets.

		p values		
		CD4	**CD8**	**Treg**
Proportion	**Blood**	0.4260	0.4824	0.6734
	Spleen	0.0678	0.4260	0.1745
	iLN	0.4260	0.2417	0.3736
Absolute Number	**Blood**	0.2317	0.2011	0.4333
	Spleen	0.1223	0.2417	0.1466
	iLN	0.4606	0.6828	0.8081

Statistical analysis performed (D'Agostino-Pearson followed by Mann Whitney), no statistical differences are present.

4.2.15 Normal Colonisation of the E12 Thymus in the Absence of CCRL1

Progenitor cells are first detected in the murine thymus at E11.5. During pre-vascularisation embryogenesis, progenitor cells migrate to the thymic anlagen from the surrounding mesenchyme (Calderon and Boehm, 2011). At these early developmental stages, CCL21, CCL25 and CXCL12 are expressed by the thymic anlagen and surrounding mesenchyme (Calderon and Boehm, 2011, Liu et al., 2006), and the receptors for these chemokines are expressed by $CD45^+$ cells isolated from the perithymic mesenchyme (Jenkinson et al., 2007a). Combinations of single, double and triple CCR7/CCR9/CXCR4 KO mice have shown the importance of these chemokine-chemokine receptor interactions in the recruitment of progenitor cells to the thymus during pre-vascularisation embryogenesis (Calderon and Boehm, 2011).

We analysed the E12 thymus from $CCRL1^{-/-}$ mice and littermate controls to determine whether CCRL1 played a role in the recruitment of progenitor cells at this early pre-vascular stage. This was achieved by the dissection and digestion of individual thymic lobes from E12 embryos. The resulting cell suspensions were stained for EpCAM and CD45 for flow cytometry, and cells were tallied using counting beads. FACS analysis revealed three populations of cells; $CD45^-EpCAM^+$ TEC, $CD45^+EpCAM^-$ haematopoietic cells, and $CD45^-EpCAM^-$ mesenchymal cells (Figure 64A). The number of haematopoietic cells and TEC were calculated (Figure 64B), and were similar between $CCRL1^{-/-}$ and littermate control thymi (haematopoietic cells p=1.000, TEC p=0.3524. Despite this, the range of $CD45^+$ and $EpCAM^+$ cells was wide, especially in the control group of mice (709-5359 $CD45^+$

cells, 1610-21507 $EpCAM^+$ cells), therefore to take into account any differences in the dissection of the tissue, the $CD45^+$: $EpCAM^+$ ratio was calculated (Figure 64C). This revealed a slightly higher ratio in $CCRL1^{-/-}$ mice, suggesting an increase in the number of $CD45^+$ cells per $EpCAM^+$ cell, however this difference was not statistically significant ($p=0.0667$).

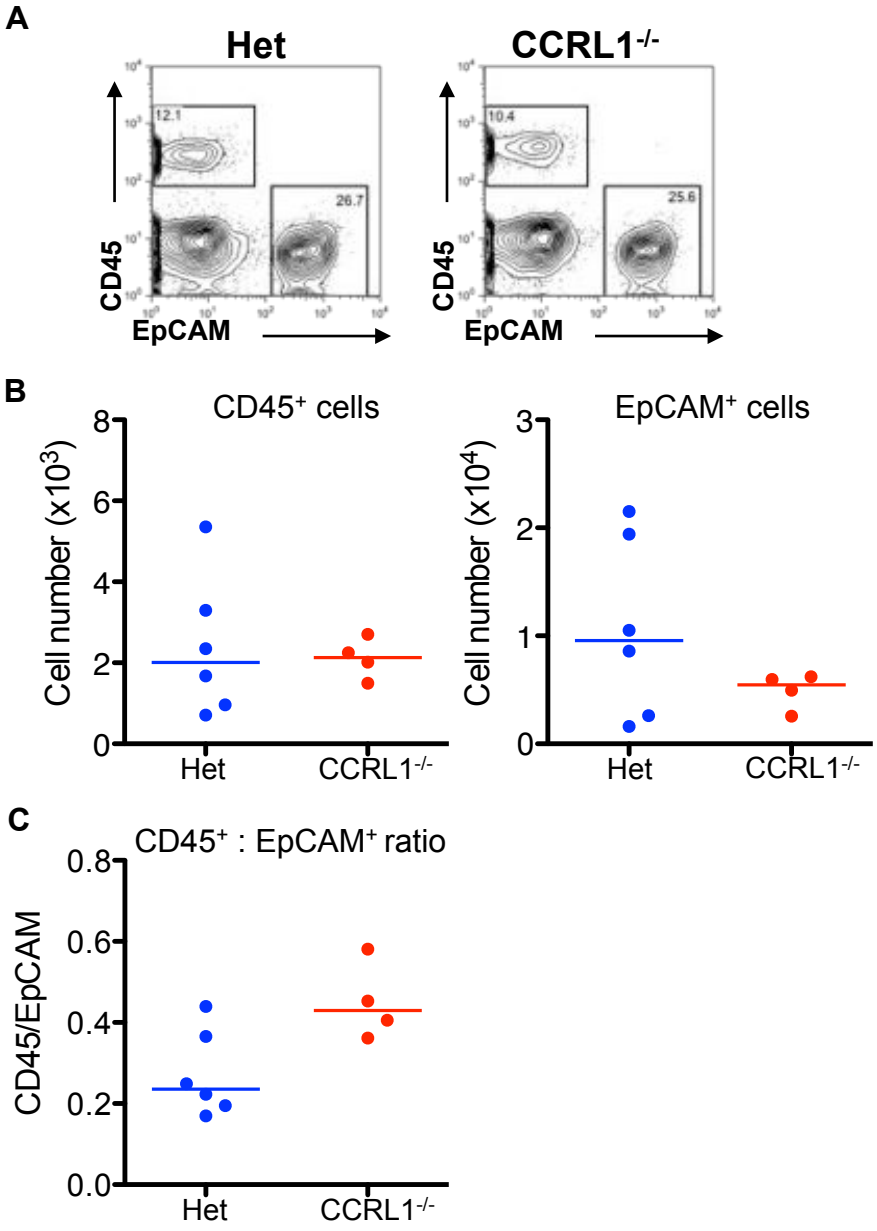

Figure 64. Normal Colonisation of the E12 CCRL1$^{-/-}$ Thymus.

E12 thymic lobes were digested and analysed by flow cytometry to determine the number of EpCAM^{+} and CD45^{+} cells. Live cells were gated prior to the detection of these subsets (A). The number of CD45^{+} and EpCAM^{+} cells are shown (B). The CD45^{+}:EpCAM^{+} ratio was calculated (C). Horizontal bars represent the median values. Statistical analysis performed (Mann Whitney). Each point represents one mouse.

4.2.16 CCRL1 Regulates the Recruitment of Progenitor Cells to Vascularised Embryonic Thymus

Although the vasculature begins to develop in the embryonic thymus at E13.5, it is not functional until E15.5., and at this stage, progenitor cells are recruited to the thymus via vasculature at the CMJ (Liu et al., 2006). Mice deficient in CCR7, CCR9 and CXCR4 have reduced thymus cellularity at E17.5, suggesting a role for these chemokines in the recruitment of progenitor cells by this method (Calderon and Boehm, 2011).

In the previous chapter we showed onset of CCRL1 expression within the embryonic thymus at E13. For this reason we stained sections of E13 WT and CCRL1$^{-/-}$ thymus for CD45, pan-keratin and laminin to observe the organisation of haematopoietic, and epithelial and non-epithelial stromal cells. The WT thymus showed a clear keratin^{+} epithelial cell compartment, completely surrounded by laminin^{+} basal lamina, with CD45^{+} progenitor cells scattered at the periphery and within the tissue (Figure 65A). This distribution of haematopoietic and stromal cells was similar in the CCRL1$^{-/-}$ thymus (Figure 65B).

We analysed the thymus at E14 (pre-vascularisation), E15 (during the transition to functional vasculature), and E17 (post-vascularisation). Thymus from mice at these stages of development were dissected, digested and cells tallied and stained for flow cytometry. As expected, the cellularity of the thymus progressively increased between E14 and E17, however no difference in cellularity was observed between CCRL1$^{-/-}$ and control mice at any age (Figure 66A, Table 27).

Populations of DN thymocytes were identified using the same panel of markers as in the adult thymus. DN thymocytes were identified as $CD45^{+}lineage^{-}$. Lineage markers used were CD3, CD4, CD8, TCRβ, B220, CD11b, CD11c, TER-119, and Ly-G6. Populations of DN1-4 thymocytes were identified based on their expression of CD44 and CD25 (DN1, $CD44^{+}CD25^{-}$, DN2, $CD44^{+}CD25^{+}$, DN3, $CD44^{-}CD25^{+}$, DN4, $CD44^{-}CD25^{-}$). At E14, there was a significant increase in the proportion of DN3 thymocytes in $CCRL1^{-/-}$ thymi ($p=0.0403$). Proportions of DN1, DN2 and DN4 thymocytes were similar between $CCRL1^{-/-}$ and control thymi. Similarly, the number of thymocytes in each DN population are unchanged between E14 $CCRL1^{-/-}$ and control thymi, and no statistical difference was found (Figure 66B, Table 28, Table 29). At E15, there was no difference in the proportion or absolute cell number of DN1-4 thymocytes in $CCRL1^{-/-}$ mice compared to littermate controls (Figure 66C, Table 28, Table 31). Interestingly, at E17, although all proportions of DN thymocytes were unchanged between $CCRL1^{-/-}$ and control mice, there was a significant increase in the number of DN1 thymocytes in the $CCRL1^{-/-}$ thymus ($p=0.0027$) (Table 30, Table 31).

The DN1 population is heterogeneous, consisting of $CD117^{+}$ ETP, and $CD117^{-}$ DN1 thymocytes. To determine whether the increased population of DN1 thymocytes in the E17 $CCRL1^{-/-}$ thymus was a reflection of increased progenitor cells, we analysed the population of ETP. This was achieved by the digestion of embryonic thymic lobes, and subsequent staining for flow cytometry as previously described. ETP were further identified as $CD45^{+}Lineage^{-}CD44^{+}CD25^{-}CD117^{+}$. Consistent with the unaltered DN1 population at E14 and E15, the proportions and numbers of ETP

were unaltered at this developmental stage (Table 32, Figure 67). At E17, there was a significant increase in the proportion ($p=0.0095$), and absolute number ($p=0.0049$) of ETP in the CCRL1$^{-/-}$ thymus compared to littermate controls.

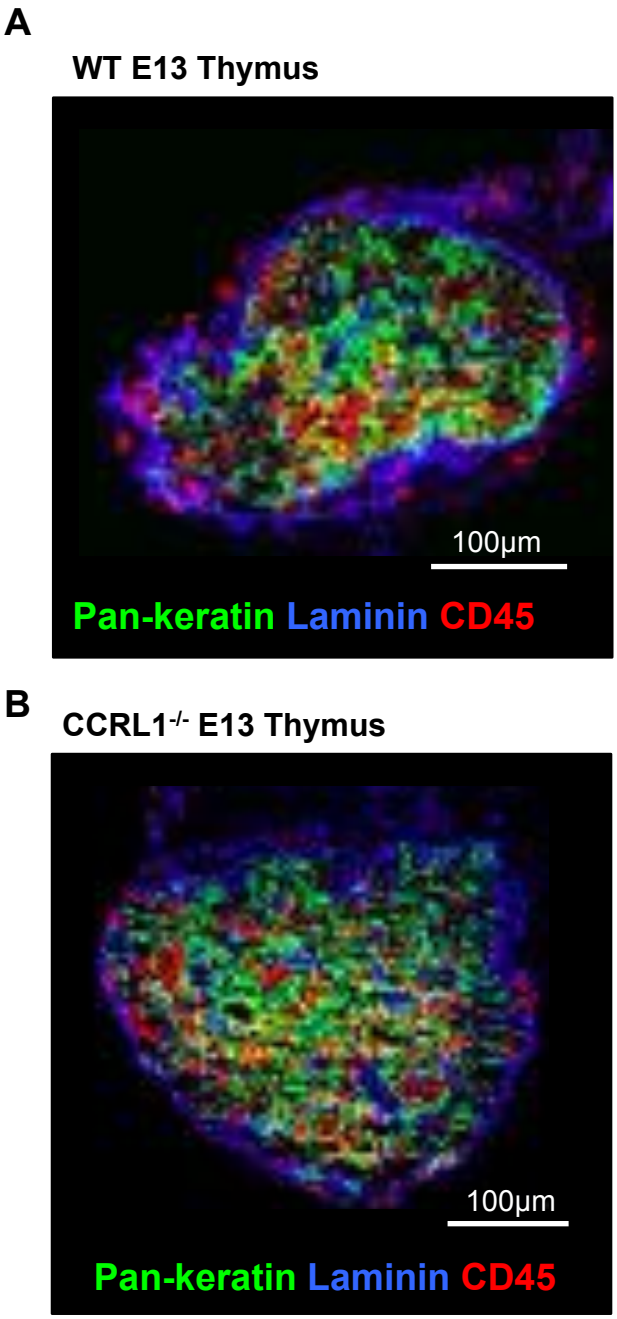

Figure 65. Normal Distribution of Haematopoietic and Stromal Cells in E13 CCRL1$^{-/-}$ Thymus

Cryosections of E13 WT and CCRL1$^{-/-}$ thymus were stained for pan-keratin, laminin and CD45. A similar distribution of these cells is seen in WT (A), and CCRL1$^{-/-}$ (B) thymus. Staining is representative of three mice of each genotype.

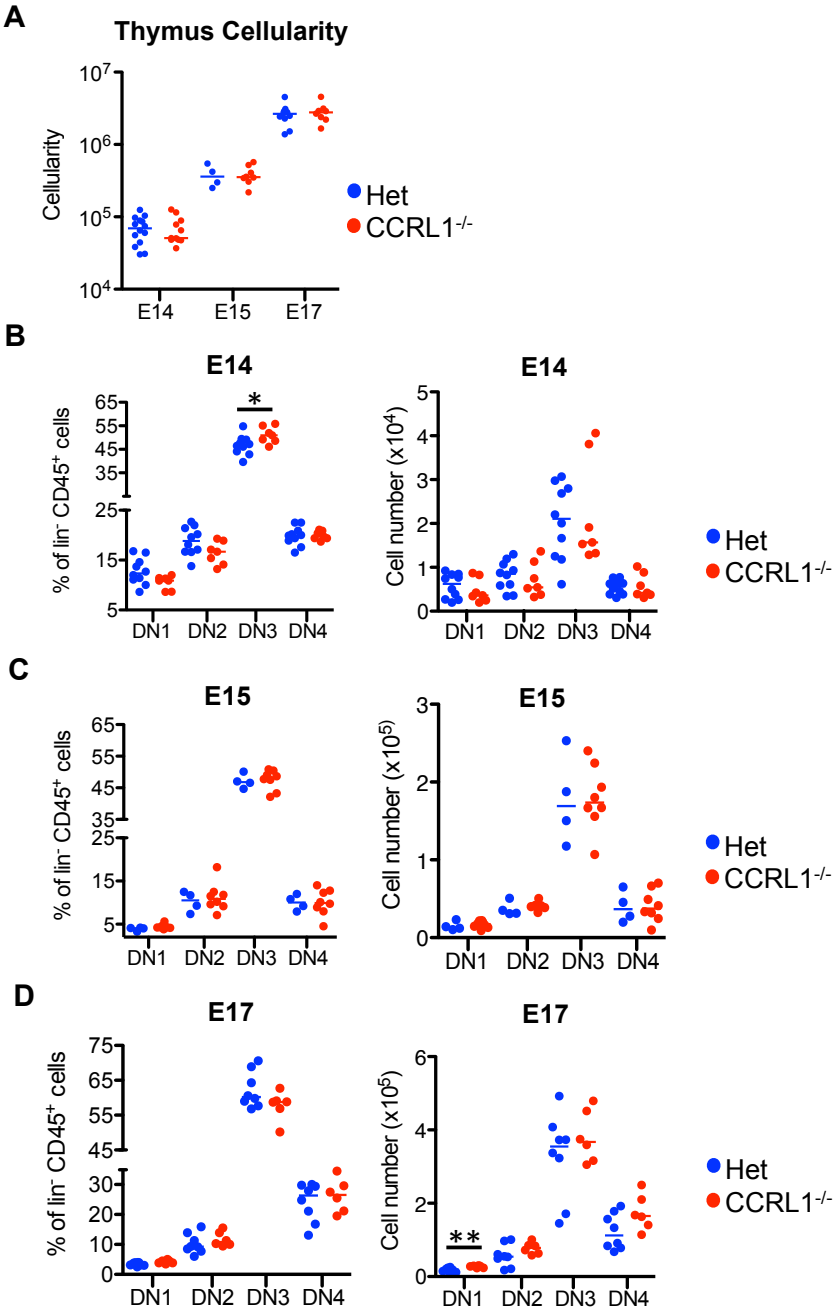

Figure 66. Increased DN1 Thymocytes in the E17 CCRL1$^{-/-}$ Thymus.

E14, E15 and E17 thymic lobes were digested and thymus cellularity tallied (A). Populations of DN thymocytes were analysed by flow cytometry as previously shown in the adult thymus. The proportions and absolute cell numbers of DN1-4 thymocytes are shown at E14 (B), E15 (C), and E17 (D). Horizontal bars represent the median values. Statistical analysis performed (Mann Whitney) *$p<0.05$, **$p<0.01$. Each point represents one mouse.

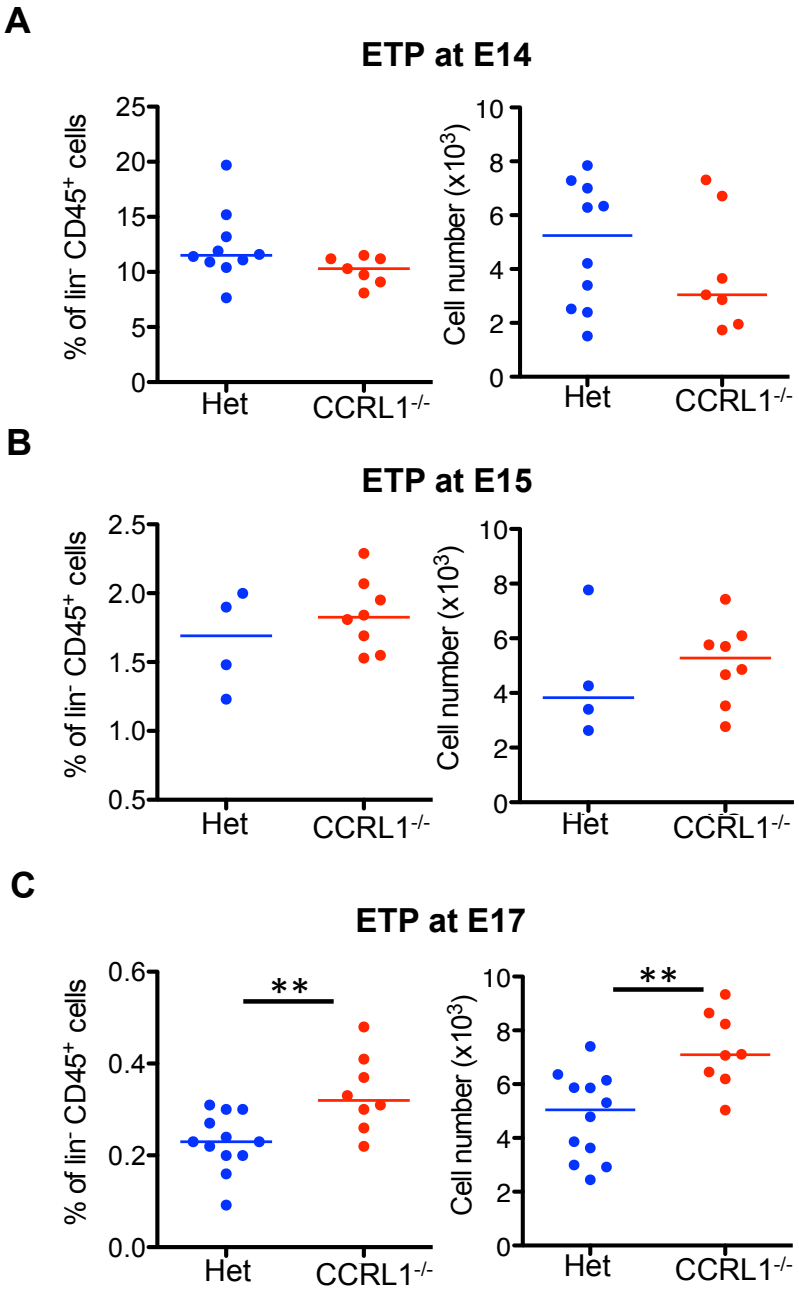

Figure 67. Increased ETP in the E17 CCRL1$^{-/-}$ Thymus.

E14, E15 and E17 thymic lobes were digested and ETP detected by flow cytometry as previously shown in the adult thymus. The proportions and absolute cell numbers of ETP are shown at E14 (B), E15 (C), and E17 (D). Horizontal bars represent the median values. Statistical analysis performed (Mann Whitney) ***p<0.01.* Each point represents one mouse.

Table 27. Thymus Cellularity at E14, E15, and E17

		Median	p value
E14 ($x10^4$)	Het (n=14)	6.96	0.9128
	$CCRL1^{-/-}$ (n=11)	5.08	
E15 ($x10^5$)	Het (n=4)	3.59	0.9333
	$CCRL1^{-/-}$ (n=8)	3.54	
E17 ($x10^5$)	Het (n=12)	2.65	0.6160
	$CCRL1^{-/-}$ (n=8)	2.78	

Median thymus cellularity shown for E14, E15, and E17 $CCRL1^{-/-}$ and het controls. Statistical analysis performed (Mann Whitney).

Table 28. Statistical Analysis of the Proportions of DN Thymocytes from E14, E15 and E17 $CCRL1^{-/-}$ and Littermate Control Thymi

	DN1	DN2	DN3	DN4
E14	0.0784	0.1069	***0.0403***	1.000
E15	0.1091	0.8649	0.5697	0.8081
E17	0.0813	0.2190	0.1812	0.7546

Statistical analysis performed (Mann Whitney). Significant p values highlighted in bold italic type.

Table 29. Proportions of DN Thymocytes in Thymi from E14, E15, and E17 CCRL1$^{-/-}$ and Control Mice.

		DN1			DN2			DN3			DN4		
		Median	25th	75th	Median	25th	75th	Median	25th	75th	Median	25th	75th
E14	Het (n=10)	**12.35**	10.83	15.08	**18.85**	16.68	21.55	**46.85**	43.8	49.18	**19.95**	18.58	21.3
	CCRL1$^{-/-}$ (n=7)	**10.9**	8.65	11.4	**16.7**	14.1	18.9	**51**	48.6	55.1	**19.7**	19.4	20.9
E15	Het (n=4)	**4.12**	3.523	4.23	**10.51**	7.848	12.3	**46.8**	45.18	49.33	**10.01**	8.26	11.7
	CCRL1$^{-/-}$ (n=8)	**4.285**	4.18	4.563	**10.85**	9.27	12.33	**48.15**	44.28	50.05	**9.915**	8.223	12.68
E17	Het (n=8)	**3.485**	3.065	3.915	**9.285**	7.923	13.25	**60.2**	58.03	67.75	**26.35**	17.88	29.7
	CCRL1$^{-/-}$ (n=6)	**4.17**	3.753	4.623	**10.8**	9.87	14.3	**58.75**	55.23	60	**26.5**	20.78	30.83

Data expressed as median (bold type), with 25th and 75th quartiles.

Table 30. Absolute Numbers of DN Thymocytes in Thymi from E14, E15, and E17 CCRL1$^{-/-}$ and Control Mice.

		DN1			DN2			DN3			DN4		
		Median	25th	75th	Median	25th	75th	Median	25th	75th	Median	25th	75th
E14 (x10^4)	Het (n=10)	**6.23**	2.67	8.38	**8.50**	5.28	10.99	**21.05**	12.34	28.44	**5.70**	3.86	6.68
	KO (n=7)	**3.60**	2.46	8.27	**5.42**	3.77	11.30	**15.70**	13.22	38.12	**4.20**	3.77	8.86
E15 (x10^5)	Het (n=4)	**1.31**	1.09	2.08	**3.32**	3.10	4.67	**16.90**	12.58	23.68	**3.65**	2.18	6.02
	KO (n=8)	**1.73**	1.35	2.11	**4.05**	3.87	4.14	**17.36**	15.86	21.67	**3.73**	2.64	6.21
E17 (x10^5)	Het **(**n=8)	**1.88**	1.19	2.25	**5.40**	2.77	8.77	**35.49**	20.93	39.92	**11.23**	7.97	17.31
	KO (n=6)	**2.83**	2.38	2.94	**7.75**	6.15	8.87	**36.71**	31.35	45.86	**16.53**	13.41	22.01

Data expressed as median (bold type), with 25th and 75th quartiles.

Table 31. Statistical Analysis of the Numbers of DN Thymocytes f
and E17 CCRL1$^{-/-}$ and Control Thymi

	DN1	DN2	DN3	
E14	0.4747	0.5362	0.9623	
E15	0.5697	0.2828	0.9333	
E17	***0.0027***	0.1419	0.6620	

Statistical analysis performed (Mann Whitney). Significant p values hig
bold italic type.

Table 32. Statistical Analysis of the ETP Population in E14, E15 a
CCRL1$^{-/-}$ and Control Thymus

	p values	
	Proportion	Absolute Num
E14	0.0878	0.5362
E15	0.4606	0.4606
E17	***0.0095***	***0.0049***

Statistical analysis performed (Mann Whitney). Significant p values hig
in bold italic type.

4.3 Discussion

Given the important role of homeostatic chemokines in intrathymic T cell development and selection, the main aim of this chapter was to investigate the role played by CCRL1, an atypical chemokine receptor that binds CCL19, CCL21 and CCL25. Such work builds on data presented in chapter 3 that define the intrathymic expression patterns of CCRL1, and aims to resolve the current controversy surrounding the role of CCRL1 in thymus function.

4.3.1 CCRL1 Inhibits Thymocyte Migration *In Vitro*

CCRL1 has been shown to scavenge its ligands thereby influencing chemokine bioavailability *in vitro* and *in vivo* (Ulvmar et al., 2014, Heinzel et al., 2007, Comerford et al., 2006, Townson and Nibbs, 2002, Gosling et al., 2000). We have shown CCRL1 is expressed within the thymus and although recent studies have examined the thymic effect of CCRL1 using CCRL1 deficient mice (Bunting et al., 2013, Heinzel et al., 2007), the effect of CCRL1 on thymocyte migration *in vitro* has not been shown.

Our initial experiments aimed to determine the effect of CCRL1 on the migration of thymocytes in response to CCR7 and CCR9 ligands. A transmigration assay was used whereby WT thymocytes migrated through a monolayer of TEP transfected with or without CCRL1 in response to CCL19 or CCL25. We found that CCRL1 inhibited the migration of thymocytes in response to both of these chemokines, consistent with its scavenging function. In addition, at high concentrations of chemokine (20nM CCL19, 180nM CCL25), the number of thymocytes which migrate

across a monolayer of TEP-GFP was reduced. This suggests that CCR7 and CCR9, expressed by thymocytes, are undergoing increased phosphorylation and internalisation leading to receptor desensitisation (Kohout et al., 2004). Interestingly, at these high chemokine concentrations, expression of CCRL1 by TEP cells no longer resulted in reduced thymocyte migration compared to control TEP cells, suggesting that the scavenging ability of CCRL1 had reached its limit. We report CCRL1-mediated inhibition of thymocyte migration in conditions up to 10nM CCL19, and in keeping with this data, Comerford *et al* showed that CCRL1 mediates effective scavenging of 10nM CCL19 *in vitro* (Comerford et al., 2006). Statistical analysis was not performed on our data due to the limited number of repeats (n=2). Although our data is in keeping with reports from the literature, it would be important to repeat the experiment, using an increased number of internal repeats, and also to include a chemokine that is not a ligand of CCRL1 e.g. CXCL12, as a negative control.

4.3.2 Unaltered Thymus Weight and Cellularity in the Absence of CCRL1

Two strains of CCRL1 deficient mice have been generated; CCRL1$^{-/-}$ mice (Comerford et al., 2010), used in the recent publication by Bunting *et al* (Bunting et al., 2013), and homozygous CCRL1-$^{GFP/GFP}$ mice (Heinzel et al., 2007). Early work using CCRL1-$^{GFP/GFP}$ mice revealed a role for this receptor in the homing of DCs to the lymph node, but reported no alterations in thymic function and T cell development (Heinzel et al., 2007). Contrary to this, a recent publication by Bunting *et al* describe severe defects in thymus function of CCRL1$^{-/-}$ mice, including

dramatically increased thymus size and cellularity, resulting in Sjögren's-like pathology in these mice when aged (Bunting et al., 2013).

Given the unclear nature of the role of CCRL1 within the thymus, and our data showing both the expression of CCRL1 within the thymus, and the ability of CCRL1 to inhibit thymocyte migration *in vitro*, we performed our own analysis of thymus function in the absence of CCRL1.

We carried out initial analysis using both strains of CCRL1 deficient mice ($CCRL1^{-/-}$, and $CCRL1\text{-}^{GFP/GFP}$) to monitor any strain-related differences. Initial examination of CCRL1 deficient thymi from either strain revealed no difference in weight or cellularity compared to heterozygous (het) and wild-type (WT) littermate controls. This recapitulates the data shown by Heinzel *et al* but is in contrast to the publication from Bunting *et al,* where increased thymus weight and cellularity of $CCRL1^{-/-}$ mice was reported (Bunting et al., 2013). When comparing the size and cellularity of the $CCRL1^{-/-}$ thymi in our study to that of Bunting *et al*, it is interesting to note that the size and cellularity of the $CCRL1^{-/-}$ thymus is similar in both studies. Surprisingly, it is the thymi of WT mice used by Bunting *et al* which are considerably smaller than the WT thymi used in our study. This prompted a review of the size and cellularity of thymi from WT mice of a similar age in the literature, which revealed thymus weight commonly ranged from approximately 55-70mg, and thymus cellularity frequently ranged from approximately $8x10^7$-$2x10^8$ (Ross et al., 2012, Zlotoff et al., 2010, Krueger et al., 2010, Gossens et al., 2010, Yang et al., 2009, Gray et al., 2007, Hick et al., 2006, Gray et al., 2006, Howard et al., 1999). Data by

Bunting *et al* show an approximate average of 40mg for thymus weight, and $5x10^7$ for thymus cellularity, thus suggesting these control mice had a small thymus in comparison to WT mice used by others in the field and in addition to the WT mice used in our study. For this reason we used $CCRL1^{-/-}$ mice alongside littermate controls in all experiments.

In addition, Bunting *et al* reported increased numbers of mTEC in $CCRL1^{-/-}$ mice, in fitting with the increased thymus size and cellularity they describe. Despite this increased mTEC population, Bunting *et al* show that on a per cell basis, there are more thymocytes per $Aire^+$ mTEC, and propose that this causes defective negative selection, and is the reason for the Sjögren's syndrome-like pathology they observe. We performed our own analysis of the TEC compartment of $CCRL1^{-/-}$ and control mice by flow cytometry. Our analysis determined the proportion and number of total TEC, cTEC, mTEC and $CD80^+Aire^+$ mTEC, and in contrast to Bunting *et al*, found no significant differences in any TEC population compared to littermate controls. Moreover, we show normal cortex and medulla demarcation, and correct positioning of SP and DP thymocytes within these environments. It is important to note that our flow cytometric TEC analysis showed a wide range of absolute cell numbers for all TEC populations. This is most likely due to differing efficiencies in digestion, and would be improved by increasing the number of mice analysed.

4.3.3 CCRL1$^{-/-}$ Mice Have a Normal Programme of T Cell Development

CCR7 and CCR9 are involved in the cortex to medulla migration of thymocytes (Choi et al., 2008, Ueno et al., 2004). This intrathymic migration is vital in order for developing thymocytes to undergo negative selection and further maturation within the medulla. Expression of CCRL1 within the thymus may regulate the bioavailability of CCR7L and CCR9L, and therefore CCR7 and CCR9 dependant processes. Our study used grouped WT and het mice for comparison with CCRL1$^{-/-}$ littermates, to allow a greater number of littermate-controlled mice to be used. Individual WT and het mice can be individually identified on graphical representation of data and show a similar phenotype in all comparisons made.

Our study used flow cytometry to show unchanged proportions and numbers of DP and SP thymocytes, suggesting that this transition does not require CCRL1. Bunting *et al* reported increased proportions of SP4 thymocytes and increased absolute cell numbers of DP, SP4 and SP8 thymocytes, whereas in keeping with our data, Heinzel *et al* reported no differences in these parameters. The overall increase in thymus cellularity reported by Bunting *et al* is likely to account for these differences, however the gating strategy used to detect SP thymocytes differs between our study and the publications by both Heinzel and Bunting *et al*. Our flow cytometric analysis identified SP thymocytes as CD4^{+}CD8^{-}TCRβ^{+} or CD4^{-}CD8^{+}TCRβ^{+} whereas both previous publications did not determine TCRβ expression by SP thymocytes. Gating specifically on TCRβ^{+} cells ensured no contamination within the gate from DP, DN or immature single positive (IPS), all of which express lower levels of TCRβ.

Analysis of the CCRL1$^{-/-}$ thymus by Bunting *et al* showed increased proportions of CD69^{+}CD62L^{-} immature SP4 and SP8 thymocytes. This publication hypothesised that the increased immature thymocyte population they observed was due to impaired post-selection maturation, possibly as a result of altered TEC populations (Bunting et al., 2013). We carried out a similar analysis of SP thymocyte maturation using the same markers, and found no difference in the proportions of immature or mature SP4 or SP8 thymocytes. Additional markers can be used in conjunction with CD69 and CD62L to identify the maturation status of SP thymocytes by flow cytometry, for example Qa2 and CD24 (Weinreich and Hogquist, 2008). However, incorporation of these markers would only be of benefit to further investigate any differences highlighted by our initial use of CD69 and CD62L. In addition to conventional SP thymocyte development we analysed the development of Treg within the CCRL1$^{-/-}$ thymus by flow cytometry. We found no difference in the proportion of CD69^{+}CD25^{+}Foxp3^{-} Treg precursors or CD69^{-}CD25^{+}Foxp3^{+} mature Treg between CCRL1$^{-/-}$ and control thymi, thus providing evidence that CCRL1 is not required for this process.

Previous analysis of DN thymocytes within the CCRL1$^{-/-}$ thymus has yielded contradicting results. Bunting *et al* described decreased proportions of DN3 thymocytes, and increased numbers of DN4 thymocytes, whereas Heinzel *et al* reported no difference in any DN subset. Similar to Heinzel *et al,* our examination of the DN thymocyte population by flow cytometry showed no major differences in the proportion or absolute cell numbers of any DN thymocyte subset. We did find a significant reduction in the number of DN3 thymocytes in female CCRL1$^{-/-}$ thymi

compared to controls, however the absolute cell numbers did not differ greatly, therefore suggesting this difference would not be biologically significant. It is possible that the DN4 population identified by Bunting *et al* included stromal cells, as DN thymocytes were not identified as $CD45^+$ in this particular study, therefore they would be negative for all markers used.

Interestingly, we found increased proportions of early thymic progenitors (ETP) in the $CCRL1^{-/-}$ female thymus. Proportions and absolute cell numbers of ETP were also increased in male thymus but not to a statistically significant level. Previous publications have not determined ETP frequency in the $CCRL1^{-/-}$ thymus, however the recruitment of ETP to the thymus is mediated by CCRL1 ligands (Zlotoff et al., 2010). ETP enter the thymus by vessels at the CMJ, and expression of CCRL1 by TEC at this location may regulate this chemokine-mediated process.

4.3.4 Abnormal Localisation of DN Thymocytes in the Absence of CCRL1

Although we found no difference in the numbers of DN thymocytes, suggesting their development is normal in the absence of CCRL1, we did highlight differences in the localisation of these cells in the $CCRL1^{-/-}$ thymus. The intrathymic migration of DN thymocytes is mediated by CCR9-CCL25 interactions, however, in keeping with our data, this positioning is not crucial for their development (Benz et al., 2004). Staining thymus sections for CD8 and CD25 allowed the quantitation of $CD25^+$ cells in different areas of the thymus. We used CD25 as a marker for DN2 and DN3 thymocytes. It is possible that our analysis may inadvertently include other populations of cells such as $CD25^+$ Treg, although given their location within the

thymic medulla (an area we did not analyse), this is unlikely. Similar to the phenotype described in CCR9$^{-/-}$ mice (Benz et al., 2004), we observed decreased numbers of CD25^{+} cells/mm^{2} in the subcapsular regions of adult and newborn CCRL1$^{-/-}$ thymi. Bunting *et al* also determined the positioning of DN thymocytes within the CCRL1$^{-/-}$ thymus, and showed a different mislocalisation of these cells. Bunting *et al* described a dramatic accumulation of CD25^{+} DN2 thymocytes in the medulla and CMJ, and suggested this was due to low levels of CCL25 throughout the cortex, CMJ and medulla (determined by immunofluorescence) (Bunting et al., 2013). On the other hand, Heinzel *et al* report unaltered homing of DN thymocytes to the SCZ in CCRL1-$^{GFP/GFP}$ mice (Heinzel et al., 2007), however a thorough analysis was not performed in this study. Although we show a significant decrease in the number of CD25^{+} DN thymocytes at the SCZ of CCRL1$^{-/-}$ mice, we did not find a reduction in this population in any other area quantitated. This data does not recapitulate our flow cytometry data, which shows absolute numbers of DN thymocytes are unaltered in CCRL1$^{-/-}$ mice. Future experiments should account for all areas of the thymus, including careful quantitation of the medulla, to resolve this discrepancy.

4.3.5 Normal Levels of CCRL1 Ligand in the CCRL1$^{-/-}$ Thymus

We measured levels of CCRL1 ligand by ELISA, and have shown that levels of CCL19, CCL21 and CCL25 are unchanged in CCRL1 deficient thymi. This suggests any influence that CCRL1 has on chemokine bioavailability is not wide-spread, but is likely to be confined to particular microenvironments. Our ELISA analysis reflects both intracellular stores of chemokine, as well as secreted chemokine. CCRL1 is

only able to regulate levels of extracellular chemokine, therefore it is possible that the high levels of intracellular chemokine have masked any differences between CCRL1$^{-/-}$ and control thymi using this method. An alterative method of tissue processing, which only accounted for extracellular chemokine, would be more informative regarding the influence of CCRL1, however the levels of extracellular chemokine may be below the level of detection if this type of approach was used.

In contrast to our data, Bunting *et al* showed a reduction in total levels of CCL19 and CCL25, measured by ELISA, in the CCRL1$^{-/-}$ thymus, this is an unexpected finding considering the scavenging function of this molecule. When this data was normalised per TEC, Bunting *et al* showed a reduction in CCL19, an increase in CCL21 and unchanged levels of CCL25. It was hypothesised that these differences were due to altered chemokine production by CCRL1 deficient TEC suggesting a role other than chemokine-scavenging for CCRL1 within the thymus (Bunting et al., 2013).

4.3.6 Antigen Presenting Cells in the CCRL1$^{-/-}$ Thymus

Given that thymic DC subsets express CCR9 (Hadeiba et al., 2012), we analysed thymic DC populations by flow cytometry and compared proportions and absolute numbers of cells within each DC population between CCRL1$^{-/-}$ and control thymi. We found no difference in proportions or absolute cell numbers of Sirpα^{-} resident thymic DCs, or migratory thymic pDCs.

Analysis of the Sirpα^{+} migratory thymic DCs revealed increased proportions and absolute cell numbers of this population. The factors involved in the recruitment of this DC subset is not clear, however it is possible that expression of CCR7 and/or CCR9 may be required, as is the case for plasmacytoid DC migration into the thymus (Hadeiba et al., 2012). Further experiments would be necessary to determine the expression of such candidate chemokine receptors by Sirpα^{+} migratory thymic DCs, and to determine if they are correctly positioned within the thymus.

In WT mice, Sirpα^{+} DCs are located in the cortex and perivascular areas - areas that we have shown to express CCRL1. Although we have determined the localisation of total CD11c^{+} DCs within the thymus, and show this is similar between CCRL1$^{-/-}$ and WT mice, staining with additional markers to allow the identification of thymic DC subsets would be beneficial. Moreover, a system to allow the enumeration of thymic DCs in defined areas across the corticomedullary junction, similar to that used by Takahama (Lei et al., 2011), would allow the precise localisation of these cells to be determined.

4.3.7 Populations of Lymphocytes in the Periphery of CCRL1$^{-/-}$ Mice

To determine the extent of thymic reconstitution in the absence of CCRL1, we created irradiation BM chimeras using CCRL1$^{-/-}$ and BoyJ mice to allow the identification of host and donor haematopoietic cells. We show that at 9 weeks post reconstitution, WT mice reconstituted with CCRL1$^{-/-}$ BM have an increased thymus cellularity. It would be important to repeat these experiments, but include two

additional groups of control mice; WT mice reconstituted with WT BM, and CCRL1$^{-/-}$ mice reconstituted with CCRL1$^{-/-}$ BM. These control groups would account for any impact of irradiation, which may be responsible for the differences in thymus cellularity we observed.

To further examine any involvement of CCRL1 in the maintenance of the peripheral T cell pool, we performed a detailed analysis of T cell populations in the blood, spleen and inguinal LN of CCRL1$^{-/-}$ mice compared to littermate controls. This analysis showed increased proportions and numbers of αβ T cells in the blood of CCRL1$^{-/-}$ mice. Interestingly, we found a reduction in the proportion of Foxp3^{+} Treg in the blood of CCRL1$^{-/-}$ mice, however the absolute number of Treg in the blood was unaltered. This could be explained by a slight alteration in the composition of the CD4 T cell subset in terms of conventional CD4 T cell vs. Treg. A reduced proportion of Treg, with unchanged proportion of total CD4 T cells must relate to an increased proportion of conventional CD4 T cells. The reduction in the proportion of Foxp3^{+} Treg in CCRL1$^{-/-}$ mice has not previously been described, and may contribute to the autoimmune pathology described by Bunting *et al* (Bunting et al., 2013), rather than the defective central tolerance that they hypothesise.

The CCRL1$^{-/-}$ spleen showed increased proportions of αβ T cells, however no alterations were seen in Foxp3^{+} Tregs. Analysis of the inguinal LN showed no differences in any T cell subset between CCRL1$^{-/-}$ mice and littermate controls. There are several possibilities for the alterations in T cell populations in different peripheral sites of CCRL1$^{-/-}$ mice. One such reason is likely to be the expression of

CCRL1 within the lymph node (Ulvmar et al., 2014), and the spleen (Appendix, Figure 71). Given the ability of CCRL1 to influence the recruitment of $CCR7^+$ DCs to the lymph node; it is possible that CCRL1 plays a role in the recruitment or egress of cells from any lymphoid tissue where it is expressed. This may result in differential leukocyte populations within the blood, and also within secondary lymphoid tissue.

In addition, the expression of CCRL1 by perivascular TECs may influence the egress of mature thymocytes, which would also impact on the T cell populations within the blood and secondary lymphoid tissue. To address this, we crossed $CCRL1^{-/-}$ mice with RAG2pGFP Tg mice (Boursalian et al., 2004) and determined levels of RAG2pGFP expression by peripheral T cells to identify recent thymic emigrants (RTE). We found no differences in the proportion or absolute number of $RAG2pGFP^+$ CD4 or CD8 conventional T cells, or $Foxp3^+$ Treg in the blood, spleen or inguinal LN of $CCRL1^{-/-}$ and control mice. Bunting *et al* reported increased thymic output in $CCRL1^{-/-}$ mice, determined by increased RTE in the spleen (identified by flow cytometry as $CD3^+CD4^+CD44^-CD69^-CD24^+$), and increased proportions and numbers of $CD4^+CD8^+$ T cells in the spleen. Our FACS analysis of blood and secondary lymphoid tissue always revealed minimal frequencies of DP T cells with no obvious bias for $CCRL1^{-/-}$ mice, consistent with our RTE data. To determine whether the DP T cells observed by Bunting *et al* are immature thymocytes as is proposed, or a staining artefact or doublet cells, it would be important to determine the level of TCRβ expression by these cells. DP thymocytes express lower levels of TCRβ compared to mature SP T cells, therefore if immature T cells egress from the

CCRL1$^{-/-}$ thymus at this relatively early stage of development, surface TCRβ expression may be lower.

4.3.8 The Role of CCRL1 Within the Thymus During Ontogeny

In the previous chapter, we showed expression of CCRL1 within the embryonic thymus from E13 of gestation. In addition, Heinzel *et al* reported that CCRL1$^{-/-}$ mice have normal thymus cellularity at E12.5 and E13.5, while overexpression of CCRL1 by TEC reduces thymus cellularity at E14.5 and E16.5 (Heinzel et al., 2007). Our analysis of the thymus from CCRL1$^{-/-}$ embryos shows no alteration in the number of haematopoietic cells at E12, suggesting that although this initial recruitment relies heavily on chemokines, CCRL1 does not influence this process. This finding is perhaps not surprising given the absence of CCRL1 expression within the thymic anlagen at E12. We also found normal positioning of CD45^{+} cells, and normal stromal cell organisation in the CCRL1$^{-/-}$ thymus at E13, suggesting that although CCRL1 is expressed at this developmental stage, it is not required in these processes.

In addition, we analysed the CCRL1$^{-/-}$ thymus at E14, E15, and E17 (developmental ages where we show high levels of CCRL1 expression within the thymus) and show no difference in the cellularity of the CCRL1$^{-/-}$ thymus at any of these ages compared to littermate controls. At E14 we found a small but statistically significant increase in the percentage of DN3 thymocytes, however this is not reflected in absolute numbers of DN3 thymocytes therefore is unlikely to have biological significance. Interestingly, at E17, we found increased numbers of DN1 thymocytes,

which is reflected in the increased percentages and numbers of ETP, similar to the adult CCRL1$^{-/-}$ thymus. The involvement of chemokines in the recruitment of progenitor cells to the vascularised embryonic thymus has been shown using CCR7/CCR9/CXCR4 triple KO mice, which exhibit reduced thymus cellularity at E17 (Calderon and Boehm, 2011). Our data suggests that CCRL1 influences the CCR7/CCR9 mediated recruitment process of ETPs to the vascularised embryonic thymus, which is most likely due to the perivascular expression of CCRL1 by TECs at the CMJ.

In summary, we show normal thymic function and T cell development in the absence of CCRL1. We show an increased circulating conventional T cell pool, but using RAG2pGFP mice, rule out the involvement of CCRL1 in thymocyte egress. Further studies would be needed to determine the role of CCRL1 on the recruitment of T cells to peripheral lymphoid tissues in an attempt to explain the differences we have highlighted in peripheral lymphoid organs. We suggest a minor role for CCRL1 in the recruitment of progenitor cells to the vascularised embryonic thymus, and provide evidence that this role is maintained in the adult thymus, but to a lesser extent. Overall, this chapter provides a systematic analysis of thymus function in the absence of CCRL1, and in contrast to the recently published data by Bunting *et al*, argues against a major role for CCRL1 in thymus function.

CHAPTER 5: GENERAL DISCUSSION

5.1 Expression and Function of CCRL1 Within the Thymus

CCRL1 binds and scavenges CCL19, CCL21 and CCL25 (Comerford et al., 2006). These chemokines, which also bind the classical chemokine receptors CCR7 and CCR9, mediate the intrathymic migration of thymocytes, which is crucial for their development. The expression of CCRL1 within the thymus may have a functional impact on the regulation of CCR7 and CCR9 dependant processes. This thesis aimed to map CCRL1 expression within the thymus, and to determine any role for this molecule during T cell development using CCRL1 deficient mice.

We have shown expression of CCRL1 within the adult thymus by a high proportion of cTEC, and used immunofluorescence to show the localisation of $CCRL1^{+}$ cTEC at the subcapsular zone. During early T cell development, thymocytes migrate outwards through the cortex to the SCZ. Although the precise mechanisms underlying this migration have not been fully described, CCR9 deficient mice exhibit an accumulation of $CD25^{+}$ DN thymocytes in the subcapsular region, thus showing the requirement for CCR9 during this process (Benz et al., 2004). Similarly to CCR9 deficient mice, we observed an accumulation of $CD25^{+}$ DN thymocytes in the subcapsular region of $CCRL1^{-/-}$ mice. The scavenging action of CCRL1 expression by cTEC may regulate the bioavailability of CCL25 in particular thymic niches, and as a result, may regulate this CCR9 dependant migration. This type of chemokine patterning by CCRL1 has been described in the lymph node, whereby CCRL1 expression by lymphatic endothelial cells in the ceiling of the subcapsular sinus creates functional gradients of CCL21 (Ulvmar et al., 2014). Without a similar quantitative analysis of extracellular CCL25 density in defined thymic regions, it is

not possible to determine whether gradients of this chemokine are regulated by CCRL1.

This thesis also showed expression of CCRL1 by TEC surrounding vasculature at the CMJ. Vessels within this thymic microenvironment are the site of progenitor entry to the thymus (Lind et al., 2001). Several studies using chemokine receptor KO mice have implicated CCR7, CCR9 and CXCR4 in this recruitment process in the embryonic and adult thymus (Calderon and Boehm, 2011, Krueger et al., 2010, Scimone et al., 2006, Liu et al., 2006, Misslitz et al., 2004). We showed increased frequencies of ETP in the adult and E17 embryonic CCRL1$^{-/-}$ thymus, thus suggesting the requirement of CCRL1 in the vascularised thymus to modulate this process. If this is indeed the case, and CCRL1$^{-/-}$ mice have enhanced recruitment of ETP into the thymus, there may be a reciprocal decrease in ETP frequency in the blood. It would therefore be of interest to quantitate the number of ETP in the blood of CCRL1$^{-/-}$ mice using flow cytometry. An alternative explanation for this phenotype may be that ETP do not transit into DN thymocytes as effectively in CCRL1$^{-/-}$ mice, thus accounting for their accumulation, however we show similar proportions and absolute cell numbers of DN thymocytes in the absence of CCRL1 suggesting that this is not the case. We hypothesise that CCRL1 expression by perivascular TEC, may influence the gradients of CCR7 and/or CCR9 ligands at this site, thus regulating the recruitment of ETP, however further experiments would be needed to elucidate the precise mechanism.

Egress of mature T cells from the thymus also occurs at vessels at the CMJ, however this process is heavily dependant on S1P production by neural crest derived pericytes surrounding these vessels (Zachariah and Cyster, 2010). In addition to S1P, CCR7 expression has been implicated in the thymic egress of mature T cells. Neonatal CCR7$^{-/-}$ mice exhibit a reduction in circulating T cells, and moreover, *in vitro* studies show that CCL19 mediates T cell egress in fetal thymic organ cultures, whereas CCL21 does not. (Ueno et al., 2002). Despite this requirement for CCR7 and CCL19 interactions in thymic egress, we found no alteration in the frequency of recent thymic emigrants (RTE) in CCRL1$^{-/-}$ mice using the RAG2pGFP Tg mouse line. It is unknown whether the recruitment of progenitor cells and the export of mature T cells occur via the same blood vessels, or if different vessels would be specialised for each process. Perivascular expression of CCRL1, coupled with the role we have shown for this molecule in the regulation of ETP recruitment, may provide evidence for heterogeneity within the vasculature networks located at the CMJ. If this is the case, it may be possible to use CCRL1 as a marker to distinguish between blood vessels by which ETP are recruited, and mature T cells leave.

We have shown expression of CCRL1 by non-epithelial stromal cells within the thymus. These cells are phenotypically identified as Ly51^{int}podoplanin^{+} and have been shown by others to have high retinoic acid generating activity, and consequently regulate TEC expansion (Sitnik et al., 2012). Expression of CCRL1 by such thymic mesenchyme has not previously been described, and the function of CCRL1 within this population remains unknown. Our study has only identified

CCRL1^{+} mesenchymal cells within the thymus using flow cytometry, thus providing no information about the localisation of these cells. It is likely that the distribution of these cells would be important for their role; therefore it would be necessary to optimise mesenchymal-specific markers for use in immunofluorescence in conjunction with CCRL1-GFP mice.

Our data shows a small population of mTEC that express CCRL1. A well-defined role of mTEC is to express tissue-restricted antigens and mediate negative selection of autoreactive thymocytes (Mathis and Benoist, 2009). CCRL1 expression by mTEC had not been noted in the literature until recently (Ribeiro et al., 2014). In agreement with this publication, we found expression of CCRL1 by CD80^{hi} and CD80^{lo} mTEC. Although Ribeiro *et al* used CCRL1 as a marker to map emergence of TEC populations, the role of CCRL1 expression by mTEC was not addressed. The medullary microenvironment produces CCL19 and CCL21, thus mediating the cortex to medulla migration of SP thymocytes, moreover, the requirement for this environment in the development of invariant NKT (iNKT) and Treg has recently been shown (White et al., 2014, Cowan et al., 2013). We have shown normal SP thymocyte maturation, and unaltered development of nTreg in the absence of CCRL1, thus suggesting that although CCRL1 is expressed by mTEC, it does not influence these mTEC-specific processes.

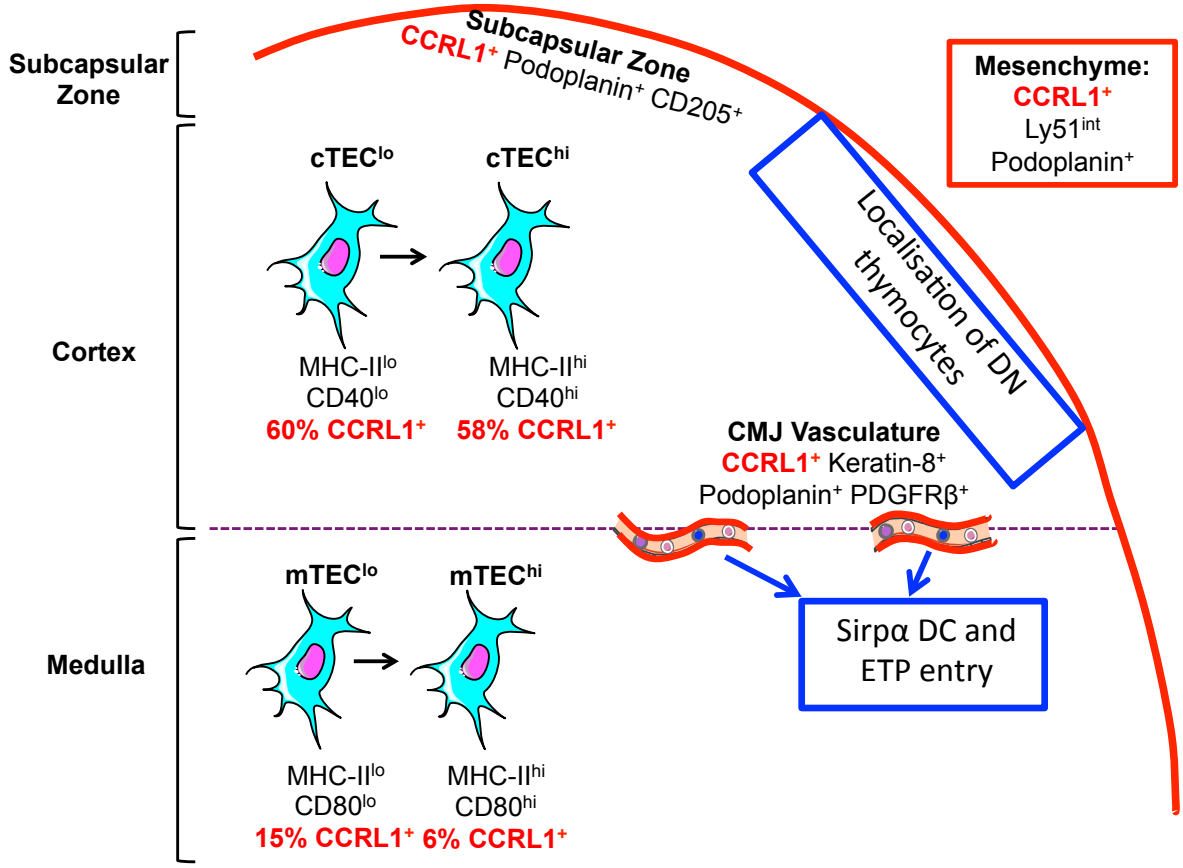

Figure 68. Summary of CCRL1 Expression in the Adult Thymus.

Summary of CCRL1 expression as determined by flow cytometry and immunofluorescence. The population of CCRL1$^+$ mesenchyme has only been detected using flow cytometry, therefore the intrathymic location remains unknown. Role of CCRL1 in the recruitment of ETP and Sirpα$^+$ DCs to the thymus, and the localisation of DN2/3 thymocytes to the SCZ.

We have shown using ELISA that total levels of CCL19, CCL21 and CCL25 are unchanged in the thymus of CCRL1$^{-/-}$ mice compared to littermate controls. As discussed previously, this method will show extracellular chemokine (which CCRL1 is able to scavenge), as well as intracellular stores of chemokine, therefore this method may not be sensitive enough to detect small changes in only the extracellular chemokine compartment. An alterative method to assess chemokine availability would be to stain sections of unfixed thymus for CCL21 and CCL25 and measure the chemokine gradient in areas of the thymus that express CCRL1, as previously shown in the lymph node (Ulvmar et al., 2014). Lack of fixation would limit the detection of intracellular chemokine, thus allowing quantitation of only the extracellular chemokine. This would be useful in providing information regarding the precise location of chemokine gradient patterning, as we could assess the positioning of cells, e.g. SP thymocytes, DCs, in these areas. Although we have shown no gross alteration in the positioning of SP or DP thymocytes, or thymic DCs, a mild mislocalisation of these cells may be apparent when focusing on areas of chemokine gradient disruption. This method worked well in the lymph node, where CCRL1 is only expressed in one microenvironment, however in the thymus we have shown expression of CCRL1 by many stromal cells, which are widely dispersed. Without PFA fixation, detection of CCRL1-GFP would not be possible; therefore it would be difficult to pinpoint specific areas that may be influenced by CCRL1.

Overall, our studies have shown that although many stromal cell populations express CCRL1, absence of this molecule has no major impact on T cell development. This could be due to unknown compensatory mechanisms, for example, CCR7L and CCR9L may bind an additional atypical chemokine receptor (ACKR), which is able to compensate for the lack of CCRL1 in CCRL1$^{-/-}$ mice. One such candidate could be CCRL2, which has been shown to bind CCL19 (Catusse et al., 2010), however the function of this receptor is awaiting further confirmation before being officially categorised as an ACKR.

It is important to note the striking differences between the data shown in this thesis and that reported by Bunting *et al* (Bunting et al., 2013). The reasons for the discrepancy between our findings and those of Bunting *et al* are not clear, however we analysed CCRL1$^{-/-}$ mice alongside littermate controls, thus ruling out the possibility that any potential differences were impacted by differences in animal substrains or their housing and husbandry. Moreover, in agreement in Heinzel *et al* (Heinzel et al., 2007), our analysis of CCRL1 deficient mice, due to homozygous expression of GFP, showed no overt thymus phenotype. Table 33 summarises a comparison of major parameters of thymus function between this thesis, Heinzel *et al*, and Bunting *et al.*

Table 33. Comparison of Results With Published Data.

Parameter	This Thesis	Bunting *et al*	Heinzel *et al*
Thymus Weight	No change	↑	No change
Thymus Cellularity	No change	↑	No change
DN Thymocytes	No change	↓% DN3 ↑number DN4	No change
DP Thymocytes	No change	↑number	No change
SP Thymocytes	No change	↑% SP4 ↑number all SP	No change
SP Maturation	No change	↑$CD69^+CD62L^-$	N/D
ETP	Increased	N/D	N/D
RTE	No change	↑	No change
Thymocyte Positioning	↑DN at SCZ	↑DN at medulla	No change
Thymic DC	↑$Sirp\alpha^+$	N/D	N/D
Chemokine Levels	No change	↓CCL19 and CCL25	N/D
TEC Populations	No change	↑numbers of mTEC	N/D
Autoimmunity	N/D	Yes	N/D

N/D (not determined). Arrows indicate increase or decrease.

5.2 Future Directions

This thesis has mapped CCRL1 expression within the thymus, but has shown that it is dispensable for thymic function. CCRL1 is expressed by epithelial and non-epithelial stromal cells within the thymus, and could be of future use as a marker to help further determine the roles of these stromal populations. Expression analysis could be built upon by including additional non-epithelial cell markers, to further characterise the mesenchymal population using immunofluorescence. Although our data shows that CCRL1 is not required for T cell development, it would be informative to attempt to optimise a method for measuring gradients of CCR7L and CCR9L in the thymus, to confirm its scavenging function *in vivo*. Careful analysis of the positioning of cells, for example DCs and SP thymocytes, in areas of CCRL1 expression may reveal a subtle role for this molecule.

Bunting *et al* reported inflammatory lesions containing T cells, B cells and DCs in the submandibular glands and liver of aged (8-10 month old) CCRL1$^{-/-}$ mice (Bunting et al., 2013). It was hypothesised by Bunting *et al* that this Sjögren's Syndrome-like pathology was due to major thymic perturbations observed in CCRL1$^{-/-}$ mice, which consequently resulted in defective central tolerance and spontaneous autoimmunity. Our study has shown normal thymic function in the absence of CCRL1, thus suggesting defects in central tolerance were an unlikely candidate for the Sjögren's Syndrome described by Bunting *et al.* This prompted us to firstly determine whether CCRL1 was expressed within the salivary gland, as this had not been reported in the literature. We used CCRL1-GFP reporter mice, and showed using immunofluorescence, CCRL1 expression by podoplanin^{+} stromal cells within the

submandibular gland of adult mice (Figure 69) We further explored the role of CCRL1 within the salivary gland, along with collaborators (Joana Dias De Campos and Francesca Barone), by using an inducible model of Sialadenitis (Bombardieri et al., 2012). Briefly, the submandibular gland was cannulated, and replication-defective adenovirus-5 was administered. Over a period of three weeks, this model recapitulates both phenotypic and functional features of Sjögren's Syndrome. Eight days following cannulation, aggregates of T and B cells are visible in the WT salivary glands, however CCRL1$^{-/-}$ salivary glands show mislocalisation of T cells, such that aggregates are not formed, and instead T cells are positioned throughout the tissue (Figure 70). Digestion of these glands and subsequent flow cytometric analysis allowed the identification of CD4^{+}, CD8^{+} and Foxp3^{+} T cells (Figure 71). At day 8 post cannulation, there were significantly higher proportions of CD8 T cells in the salivary gland from CCRL1$^{-/-}$ mice compared to WT (Figure 72). At day 15 post cannulation there were increased absolute numbers of total T cells in the CCRL1$^{-/-}$ salivary gland, however this difference was not apparent from the immunofluorescent staining of the salivary glands at the same time point (Figure 70), therefore further analysis is needed. Although we have shown CCRL1 expression by salivary gland stromal cells, and have shown normal thymic function in CCRL1$^{-/-}$ mice, given the report by Bunting *et al* it would be necessary to generate irradiation BM chimeras to use this model. This would enable us to determine whether the phenotype is due to an absence of CCRL1 expression by stromal or haematopoietic cells.

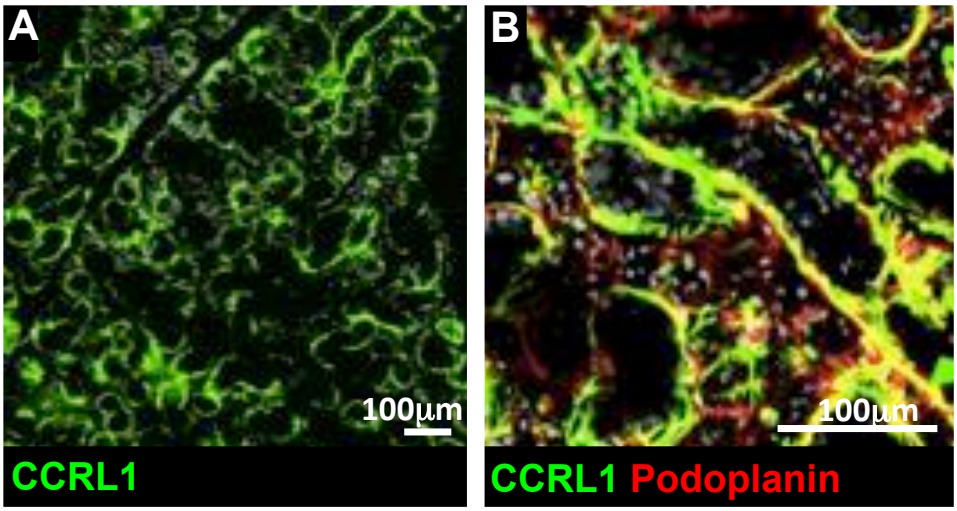

Figure 69. CCRL1 is Expressed by Stromal Cells Within the Salivary Gland.

Submandibular glands from CCRL1-GFP mice were fixed in 2% PFA and frozen. Cryosections were stained for anti-GFP (**A**), and podoplanin (red) (**B**). CCRL1-GFP is detected throughout the tissue, co-staining is visible between CCRL1-GFP and podoplanin.

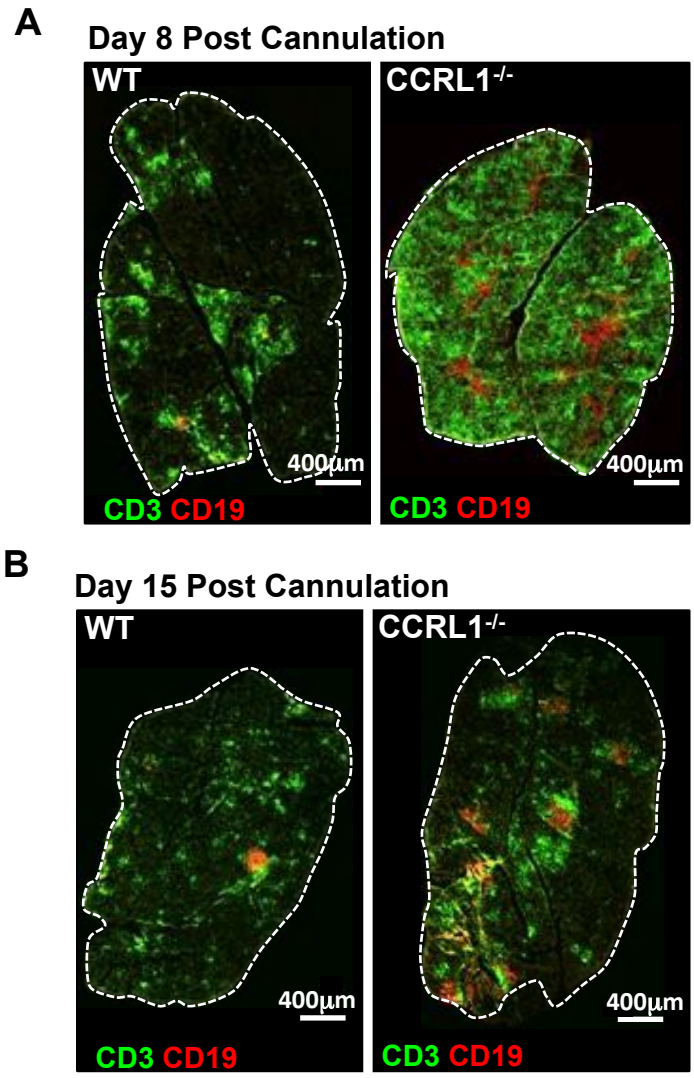

Figure 70. Disrupted Tertiary Lymphoid Structure Formation in CCRL1$^{-/-}$ Salivary Glands Following Cannulation.

The submandibular glands of WT and CCRL1$^{-/-}$ mice were cannulated, and replication-defective adenovirus administered to induce Sjögren's Syndrome pathology. Submandibular glands were harvested 8 (A) and 15 (B) days following cannulation, and were frozen and stained for CD3 and CD19 to show the distribution of T and B cells. At day 8, but not day 15, widespread positioning of CD3^{+} T cells is visible in CCRL1$^{-/-}$ glands.

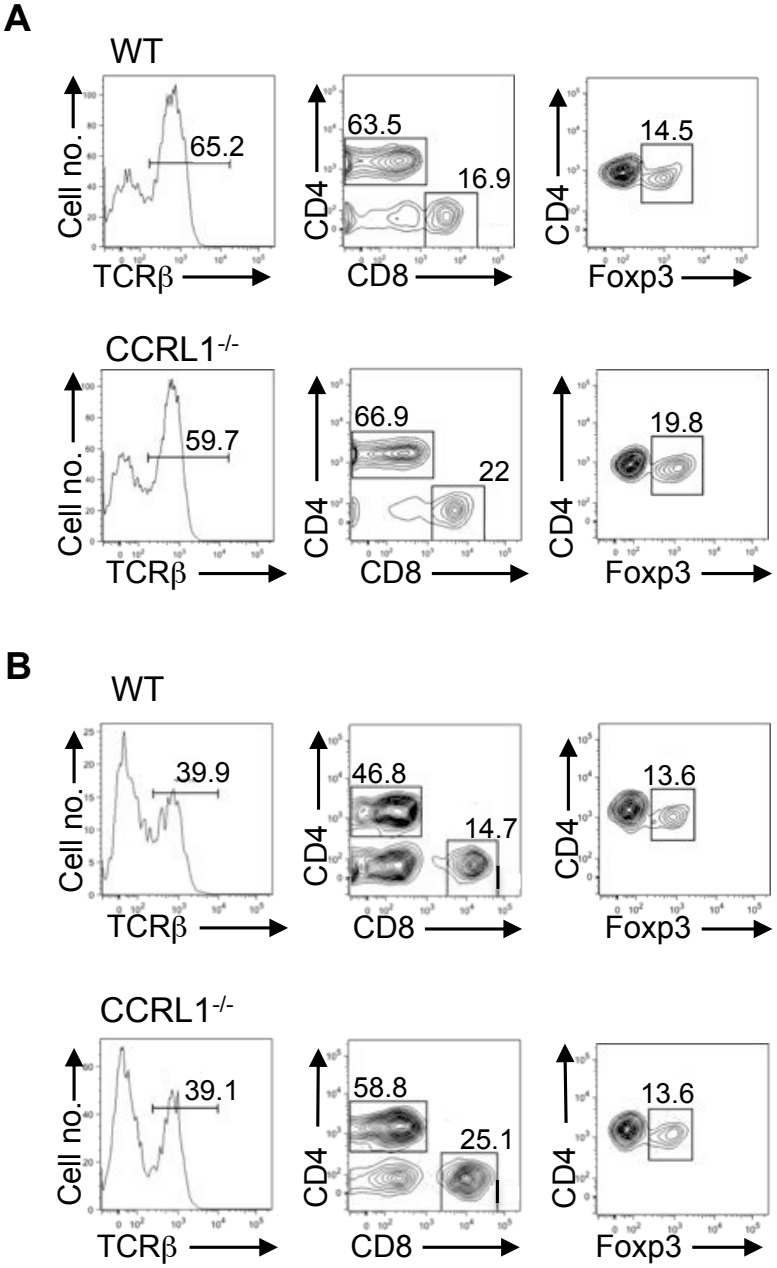

Figure 71. Identification of T cell Subsets in the Salivary Gland Following Cannulation.

The submandibular glands of WT and CCRL1$^{-/-}$ mice were cannulated, and replication-defective adenovirus administered to induce Sjögren's Syndrome pathology. Submandibular glands were harvested 8 (A) and 15 (B) days following cannulation, and were digested and stained for flow cytometry. Representative FACS plots show the identification of total T cells, CD4 T cells, CD8 T cells and Treg. Live CD45^{+} cells were first gated prior to the analysis shown.

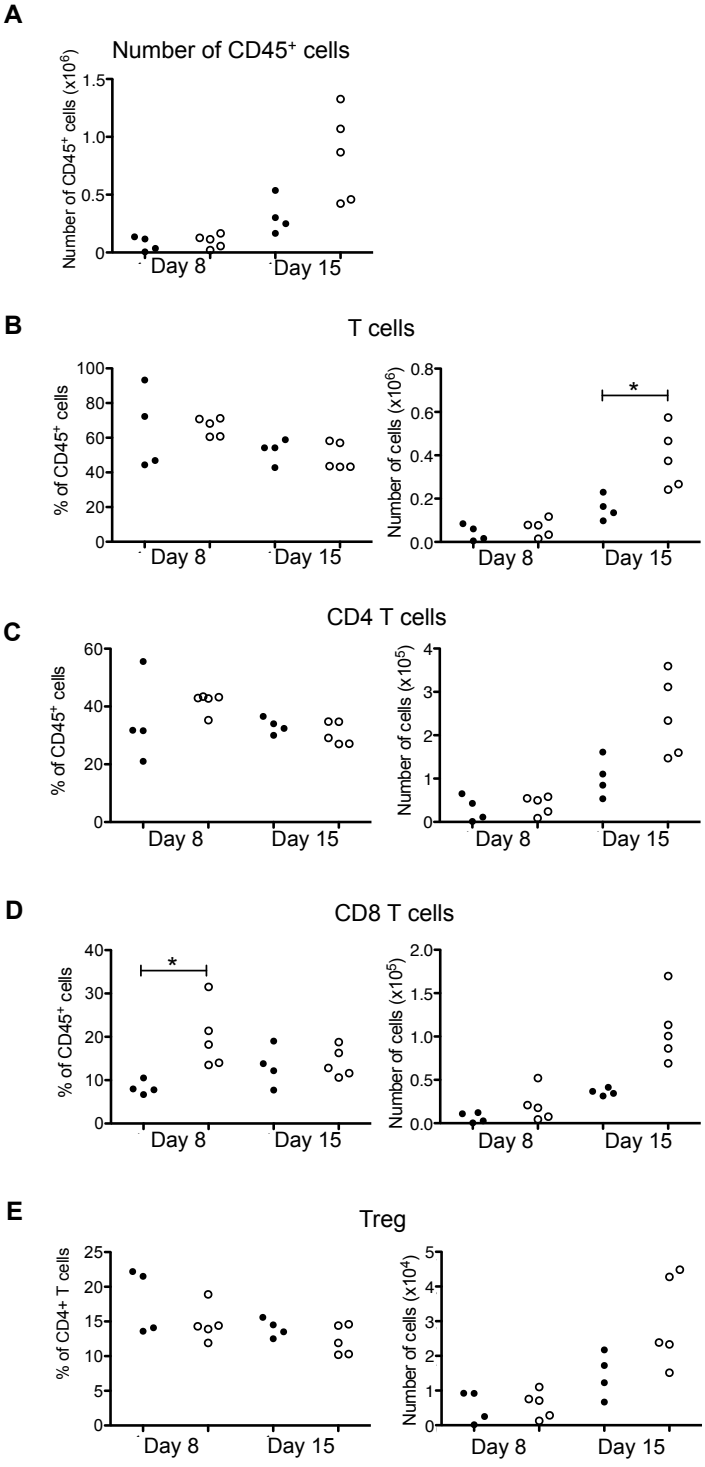

Figure 72.Quantitation of T cells in the Salivary Gland Following Cannulation.

T cell subsets were identified using flow cytometry as previously shown. Proportions of CD45+ cells (A), and proportions and absolute numbers of T cells (B), CD4 T cells (C), CD8 T cells (D), and Treg (E) are shown. Data analysed by Mann Whitney, **p<0.05.*

5.3 Concluding Remarks

In summary, we have shown CCRL1 expression by the majority of cTEC, relatively few mTEC and by a population of mesenchymal cells within the adult thymus. This information would allow the use of CCRL1 as a phenotypic marker to further study heterogeneity within TEC and non-TEC compartments. In addition, we have identified a specific population of $CCRL1^{+}$ TEC which surround vasculature at the CMJ, and have shown data which points towards a role for these cells in the recruitment of progenitor cells to the embryonic and adult thymus.

Importantly, this thesis has contributed to the field of chemokine regulation by atypical chemokine receptors. The publication by Bunting *et al* significantly altered the current understanding of how chemokine-mediated intrathymic T cell development is controlled. The data presented in this thesis helps resolve the discrepancy in the literature by showing that the requirement for CCR7 and CCR9 during thymocyte development does not require CCRL1 mediated regulation of ligand availability.

REFERENCES

AKIRAV, E. M., XU, Y. & RUDDLE, N. H. 2011. Resident B cells regulate thymic expression of myelin oligodendrocyte glycoprotein. *J Neuroimmunol,* 235**,** 33-9.

ALLEN, S. J., CROWN, S. E. & HANDEL, T. M. 2007. Chemokine: receptor structure, interactions, and antagonism. *Annu Rev Immunol,* 25**,** 787-820.

ALLEN, W. E., ZICHA, D., RIDLEY, A. J. & JONES, G. E. 1998. A role for Cdc42 in macrophage chemotaxis. *J Cell Biol,* 141**,** 1147-57.

ALVES, N. L., HUNTINGTON, N. D., RODEWALD, H. R. & DI SANTO, J. P. 2009. Thymic epithelial cells: the multi-tasking framework of the T cell "cradle". *Trends Immunol,* 30**,** 468-74.

ANDERSON, G. & TAKAHAMA, Y. 2012. Thymic epithelial cells: working class heroes for T cell development and repertoire selection. *Trends Immunol,* 33**,** 256-263.

ANDERSON, M. S., VENANZI, E. S., KLEIN, L., CHEN, Z., BERZINS, S. P., TURLEY, S. J., VON BOEHMER, H., BRONSON, R., DIERICH, A., BENOIST, C. & MATHIS, D. 2002. Projection of an immunological self shadow within the thymus by the aire protein. *Science,* 298**,** 1395-401.

BABA, T., NAKAMOTO, Y. & MUKAIDA, N. 2009. Crucial contribution of thymic Sirp alpha+ conventional dendritic cells to central tolerance against blood-borne antigens in a CCR2-dependent manner. *J Immunol,* 183**,** 3053-63.

BACHELERIE, F., GRAHAM, G. J., LOCATI, M., MANTOVANI, A., MURPHY, P. M., NIBBS, R., ROT, A., SOZZANI, S. & THELEN, M. 2014. New nomenclature for atypical chemokine receptors. *Nat Immunol,* 15**,** 207-8.

BAIK, S., JENKINSON, E. J., LANE, P. J., ANDERSON, G. & JENKINSON, W. E. 2013. Generation of both cortical and Aire(+) medullary thymic epithelial compartments from CD205(+) progenitors. *Eur J Immunol,* 43**,** 589-94.

BARGATZE, R. F. & BUTCHER, E. C. 1993. Rapid G protein-regulated activation event involved in lymphocyte binding to high endothelial venules. *J Exp Med,* 178**,** 367-72.

BARONE, F., BOMBARDIERI, M., MANZO, A., BLADES, M. C., MORGAN, P. R., CHALLACOMBE, S. J., VALESINI, G. & PITZALIS, C. 2005. Association of CXCL13 and CCL21 expression with the progressive organization of lymphoid-like structures in Sjogren's syndrome. *Arthritis Rheum,* 52**,** 1773-84.

BASIJI, D. A., ORTYN, W. E., LIANG, L., VENKATACHALAM, V. & MORRISSEY, P. 2007. Cellular image analysis and imaging by flow cytometry. *Clin Lab Med,* 27**,** 653-70, viii.

BASSET, C., HOLTON, J., O'MAHONY, R. & ROITT, I. 2003. Innate immunity and pathogen-host interaction. *Vaccine,* 21 Suppl 2**,** S12-23.

BENSINGER, S. J., BANDEIRA, A., JORDAN, M. S., CATON, A. J. & LAUFER, T. M. 2001. Major histocompatibility complex class II-positive cortical epithelium mediates the selection of CD4(+)25(+) immunoregulatory T cells. *J Exp Med,* 194**,** 427-38.

BENZ, C., HEINZEL, K. & BLEUL, C. C. 2004. Homing of immature thymocytes to the subcapsular microenvironment within the thymus is not an absolute requirement for T cell development. *Eur J Immunol,* 34**,** 3652-63.
BERAHOVICH, R. D., ZABEL, B. A., LEWEN, S., WALTERS, M. J., EBSWORTH, K., WANG, Y., JAEN, J. C. & SCHALL, T. J. 2014. Endothelial expression of CXCR7 and the regulation of systemic CXCL12 levels. *Immunology,* 141**,** 111-22.
BERRES, M. L., TRAUTWEIN, C., ZALDIVAR, M. M., SCHMITZ, P., PAUELS, K., LIRA, S. A., TACKE, F. & WASMUTH, H. E. 2009. The chemokine scavenging receptor D6 limits acute toxic liver injury in vivo. *Biol Chem,* 390**,** 1039-45.
BERZINS, S. P., GODFREY, D. I., MILLER, J. F. & BOYD, R. L. 1999. A central role for thymic emigrants in peripheral T cell homeostasis. *Proc Natl Acad Sci U S A,* 96**,** 9787-91.
BETTELLI, E., CARRIER, Y., GAO, W., KORN, T., STROM, T. B., OUKKA, M., WEINER, H. L. & KUCHROO, V. K. 2006. Reciprocal developmental pathways for the generation of pathogenic effector TH17 and regulatory T cells. *Nature,* 441**,** 235-8.
BLEUL, C. C. & BOEHM, T. 2000. Chemokines define distinct microenvironments in the developing thymus. *Eur J Immunol,* 30**,** 3371-9.
BLUM, J. S., WEARSCH, P. A. & CRESSWELL, P. 2013. Pathways of Antigen Processing. *Annu Rev Immunol*.
BOEHM, T. 2008. Thymus development and function. *Curr Opin Immunol,* 20**,** 178-84.
BOMBARDIERI, M., BARONE, F., LUCCHESI, D., NAYAR, S., VAN DEN BERG, W. B., PROCTOR, G., BUCKLEY, C. D. & PITZALIS, C. 2012. Inducible tertiary lymphoid structures, autoimmunity, and exocrine dysfunction in a novel model of salivary gland inflammation in C57BL/6 mice. *J Immunol,* 189**,** 3767-76.
BOURSALIAN, T. E., GOLOB, J., SOPER, D. M., COOPER, C. J. & FINK, P. J. 2004. Continued maturation of thymic emigrants in the periphery. *Nat Immunol,* 5**,** 418-25.
BRYSON, J. L., GRIFFITH, A. V., HUGHES, B., 3RD, SAITO, F., TAKAHAMA, Y., RICHIE, E. R. & MANLEY, N. R. 2013. Cell-autonomous defects in thymic epithelial cells disrupt endothelial-perivascular cell interactions in the mouse thymus. *PLoS One,* 8**,** e65196.
BUNTING, M. D., COMERFORD, I., SEACH, N., HAMMETT, M. V., ASQUITH, D. L., KORNER, H., BOYD, R. L., NIBBS, R. J. & MCCOLL, S. R. 2013. CCX-CKR deficiency alters thymic stroma impairing thymocyte development and promoting autoimmunity. *Blood,* 121**,** 118-28.
BURNS, J. M., SUMMERS, B. C., WANG, Y., MELIKIAN, A., BERAHOVICH, R., MIAO, Z., PENFOLD, M. E., SUNSHINE, M. J., LITTMAN, D. R., KUO, C. J., WEI, K., MCMASTER, B. E., WRIGHT, K., HOWARD, M. C. & SCHALL, T. J. 2006. A novel chemokine receptor for SDF-1 and I-TAC involved in cell survival, cell adhesion, and tumor development. *J Exp Med,* 203**,** 2201-13.
CABANIOLS, J. P., FAZILLEAU, N., CASROUGE, A., KOURILSKY, P. & KANELLOPOULOS, J. M. 2001. Most alpha/beta T cell receptor diversity is due to terminal deoxynucleotidyl transferase. *J Exp Med,* 194**,** 1385-90.
CALDERON, L. & BOEHM, T. 2011. Three chemokine receptors cooperatively regulate homing of hematopoietic progenitors to the embryonic mouse thymus. *Proc Natl Acad Sci U S A,* 108**,** 7517-22.
CATUSSE, J., LEICK, M., GROCH, M., CLARK, D. J., BUCHNER, M. V., ZIRLIK, K. & BURGER, M. 2010. Role of the atypical chemoattractant receptor CRAM in regulating

CCL19 induced CCR7 responses in B-cell chronic lymphocytic leukemia. *Mol Cancer,* 9**,** 297.
CEDAR, H. & BERGMAN, Y. 2011. Epigenetics of haematopoietic cell development. *Nat Rev Immunol,* 11**,** 478-88.
CHI, A. W., BELL, J. J., ZLOTOFF, D. A. & BHANDOOLA, A. 2009. Untangling the T branch of the hematopoiesis tree. *Curr Opin Immunol,* 21**,** 121-6.
CHOI, Y. I., DUKE-COHAN, J. S., AHMED, W. B., HANDLEY, M. A., MANN, F., EPSTEIN, J. A., CLAYTON, L. K. & REINHERZ, E. L. 2008. PlexinD1 glycoprotein controls migration of positively selected thymocytes into the medulla. *Immunity,* 29**,** 888-98.
CHUNG, C. Y., FUNAMOTO, S. & FIRTEL, R. A. 2001. Signaling pathways controlling cell polarity and chemotaxis. *Trends Biochem Sci,* 26**,** 557-66.
CHUNG, C. Y., LEE, S., BRISCOE, C., ELLSWORTH, C. & FIRTEL, R. A. 2000. Role of Rac in controlling the actin cytoskeleton and chemotaxis in motile cells. *Proc Natl Acad Sci U S A,* 97**,** 5225-30.
COMERFORD, I., MILASTA, S., MORROW, V., MILLIGAN, G. & NIBBS, R. 2006. The chemokine receptor CCX-CKR mediates effective scavenging of CCL19 in vitro. *Eur J Immunol,* 36**,** 1904-16.
COMERFORD, I., NIBBS, R. J., LITCHFIELD, W., BUNTING, M., HARATA-LEE, Y., HAYLOCK-JACOBS, S., FORROW, S., KORNER, H. & MCCOLL, S. R. 2010. The atypical chemokine receptor CCX-CKR scavenges homeostatic chemokines in circulation and tissues and suppresses Th17 responses. *Blood,* 116**,** 4130-40.
COTTON, M. & CLAING, A. 2009. G protein-coupled receptors stimulation and the control of cell migration. *Cell Signal,* 21**,** 1045-53.
COWAN, J. E., PARNELL, S. M., NAKAMURA, K., CAAMANO, J. H., LANE, P. J., JENKINSON, E. J., JENKINSON, W. E. & ANDERSON, G. 2013. The thymic medulla is required for Foxp3+ regulatory but not conventional CD4+ thymocyte development. *J Exp Med,* 210**,** 675-81.
CUROTTO DE LAFAILLE, M. A. & LAFAILLE, J. J. 2009. Natural and adaptive foxp3+ regulatory T cells: more of the same or a division of labor? *Immunity,* 30**,** 626-35.
CUSICK, M. F., LIBBEY, J. E. & FUJINAMI, R. S. 2012. Molecular mimicry as a mechanism of autoimmune disease. *Clin Rev Allergy Immunol,* 42**,** 102-11.
CUTBUSH, M. & MOLLISON, P. L. 1950. The Duffy blood group system. *Heredity (Edinb),* 4**,** 383-9.
DARBONNE, W. C., RICE, G. C., MOHLER, M. A., APPLE, T., HEBERT, C. A., VALENTE, A. J. & BAKER, J. B. 1991. Red blood cells are a sink for interleukin 8, a leukocyte chemotaxin. *J Clin Invest,* 88**,** 1362-9.
DAWSON, T. C., LENTSCH, A. B., WANG, Z., COWHIG, J. E., ROT, A., MAEDA, N. & PEIPER, S. C. 2000. Exaggerated response to endotoxin in mice lacking the Duffy antigen/receptor for chemokines (DARC). *Blood,* 96**,** 1681-4.
DE OBALDIA, M. E., BELL, J. J. & BHANDOOLA, A. 2013. Early T-cell progenitors are the major granulocyte precursors in the adult mouse thymus. *Blood,* 121**,** 64-71.
DELVES, P. J. & ROITT, I. M. 2000. The immune system. First of two parts. *N Engl J Med,* 343**,** 37-49.
DI LIBERTO, D., LOCATI, M., CACCAMO, N., VECCHI, A., MERAVIGLIA, S., SALERNO, A., SIRECI, G., NEBULONI, M., CACERES, N., CARDONA, P. J., DIELI, F. & MANTOVANI, A. 2008. Role of the chemokine decoy receptor D6 in balancing inflammation,

immune activation, and antimicrobial resistance in Mycobacterium tuberculosis infection. *J Exp Med,* 205**,** 2075-84.
DONSKOY, E. & GOLDSCHNEIDER, I. 1992. Thymocytopoiesis is maintained by blood-borne precursors throughout postnatal life. A study in parabiotic mice. *J Immunol,* 148**,** 1604-12.
EHRLICH, L. I., OH, D. Y., WEISSMAN, I. L. & LEWIS, R. S. 2009. Differential contribution of chemotaxis and substrate restriction to segregation of immature and mature thymocytes. *Immunity,* 31**,** 986-98.
FARR, A., NELSON, A. & HOSIER, S. 1992. Characterization of an antigenic determinant preferentially expressed by type I epithelial cells in the murine thymus. *J Histochem Cytochem,* 40**,** 651-64.
FENG, L. Y., OU, Z. L., WU, F. Y., SHEN, Z. Z. & SHAO, Z. M. 2009. Involvement of a novel chemokine decoy receptor CCX-CKR in breast cancer growth, metastasis and patient survival. *Clin Cancer Res,* 15**,** 2962-70.
FINK, P. J. 2013. The biology of recent thymic emigrants. *Annu Rev Immunol,* 31**,** 31-50.
FORSTER, R., DAVALOS-MISSLITZ, A. C. & ROT, A. 2008. CCR7 and its ligands: balancing immunity and tolerance. *Nat Rev Immunol,* 8**,** 362-71.
FOSS, D. L., DONSKOY, E. & GOLDSCHNEIDER, I. 2001. The importation of hematogenous precursors by the thymus is a gated phenomenon in normal adult mice. *J Exp Med,* 193**,** 365-74.
FOSTER, K., SHERIDAN, J., VEIGA-FERNANDES, H., RODERICK, K., PACHNIS, V., ADAMS, R., BLACKBURN, C., KIOUSSIS, D. & COLES, M. 2008. Contribution of neural crest-derived cells in the embryonic and adult thymus. *J Immunol,* 180**,** 3183-9.
FRA, A. M., LOCATI, M., OTERO, K., SIRONI, M., SIGNORELLI, P., MASSARDI, M. L., GOBBI, M., VECCHI, A., SOZZANI, S. & MANTOVANI, A. 2003. Cutting edge: scavenging of inflammatory CC chemokines by the promiscuous putatively silent chemokine receptor D6. *J Immunol,* 170**,** 2279-82.
FROMMER, F. & WAISMAN, A. 2010. B cells participate in thymic negative selection of murine auto-reactive CD4+ T cells. *PLoS One,* 5**,** e15372.
FUERTBAUER, E., ZAUJEC, J., UHRIN, P., RAAB, I., WEBER, M., SCHACHNER, H., BAUER, M., SCHUTZ, G. J., BINDER, B. R., SIXT, M., KERJASCHKI, D. & STOCKINGER, H. 2013. Thymic medullar conduits-associated podoplanin promotes natural regulatory T cells. *Immunol Lett,* 154**,** 31-41.
GALLI, S. J., BORREGAARD, N. & WYNN, T. A. 2011. Phenotypic and functional plasticity of cells of innate immunity: macrophages, mast cells and neutrophils. *Nat Immunol,* 12**,** 1035-44.
GOMMEAUX, J., GREGOIRE, C., NGUESSAN, P., RICHELME, M., MALISSEN, M., GUERDER, S., MALISSEN, B. & CARRIER, A. 2009. Thymus-specific serine protease regulates positive selection of a subset of CD4+ thymocytes. *Eur J Immunol,* 39**,** 956-64.
GOSLING, J., DAIRAGHI, D. J., WANG, Y., HANLEY, M., TALBOT, D., MIAO, Z. & SCHALL, T. J. 2000. Cutting edge: identification of a novel chemokine receptor that binds dendritic cell- and T cell-active chemokines including ELC, SLC, and TECK. *J Immunol,* 164**,** 2851-6.
GOSSENS, K., NAUS, S., HOLLANDER, G. A. & ZILTENER, H. J. 2010. Deficiency of the metalloproteinase-disintegrin ADAM8 is associated with thymic hyper-cellularity. *PLoS One,* 5**,** e12766.

GRAY, D. H., SEACH, N., UENO, T., MILTON, M. K., LISTON, A., LEW, A. M., GOODNOW, C. C. & BOYD, R. L. 2006. Developmental kinetics, turnover, and stimulatory capacity of thymic epithelial cells. *Blood,* 108**,** 3777-85.
GRAY, D. H., TULL, D., UENO, T., SEACH, N., CLASSON, B. J., CHIDGEY, A., MCCONVILLE, M. J. & BOYD, R. L. 2007. A unique thymic fibroblast population revealed by the monoclonal antibody MTS-15. *J Immunol,* 178**,** 4956-65.
GROSSMAN, W. J., VERBSKY, J. W., BARCHET, W., COLONNA, M., ATKINSON, J. P. & LEY, T. J. 2004. Human T regulatory cells can use the perforin pathway to cause autologous target cell death. *Immunity,* 21**,** 589-601.
HADEIBA, H., LAHL, K., EDALATI, A., ODERUP, C., HABTEZION, A., PACHYNSKI, R., NGUYEN, L., GHODSI, A., ADLER, S. & BUTCHER, E. C. 2012. Plasmacytoid dendritic cells transport peripheral antigens to the thymus to promote central tolerance. *Immunity,* 36**,** 438-50.
HANSELL, C. A., HURSON, C. E. & NIBBS, R. J. 2011. DARC and D6: silent partners in chemokine regulation? *Immunology and Cell Biology,* 89**,** 197-206.
HARMAN, B. C., JENKINSON, W. E., PARNELL, S. M., ROSSI, S. W., JENKINSON, E. J. & ANDERSON, G. 2005. T/B lineage choice occurs prior to intrathymic Notch signaling. *Blood,* 106**,** 886-92.
HEINZEL, K., BENZ, C. & BLEUL, C. C. 2007. A silent chemokine receptor regulates steady-state leukocyte homing in vivo. *Proc Natl Acad Sci U S A,* 104**,** 8421-6.
HEWIT, K. D., FRASER, A., NIBBS, R. J. & GRAHAM, G. J. 2014. The N-terminal region of the atypical chemokine receptor ACKR2 is a key determinant of ligand binding. *J Biol Chem*.
HICK, R. W., GRUVER, A. L., VENTEVOGEL, M. S., HAYNES, B. F. & SEMPOWSKI, G. D. 2006. Leptin selectively augments thymopoiesis in leptin deficiency and lipopolysaccharide-induced thymic atrophy. *J Immunol,* 177**,** 169-76.
HJELMSTROM, P., FJELL, J., NAKAGAWA, T., SACCA, R., CUFF, C. A. & RUDDLE, N. H. 2000. Lymphoid tissue homing chemokines are expressed in chronic inflammation. *Am J Pathol,* 156**,** 1133-8.
HORUK, R., CHITNIS, C. E., DARBONNE, W. C., COLBY, T. J., RYBICKI, A., HADLEY, T. J. & MILLER, L. H. 1993. A receptor for the malarial parasite Plasmodium vivax: the erythrocyte chemokine receptor. *Science,* 261**,** 1182-4.
HOU, T., LIANG, D., XU, L., HUANG, X., HUANG, Y. & ZHANG, Y. 2013. Atypical chemokine receptors predict lymph node metastasis and prognosis in patients with cervical squamous cell cancer. *Gynecol Oncol,* 130**,** 181-7.
HOWARD, J. K., LORD, G. M., MATARESE, G., VENDETTI, S., GHATEI, M. A., RITTER, M. A., LECHLER, R. I. & BLOOM, S. R. 1999. Leptin protects mice from starvation-induced lymphoid atrophy and increases thymic cellularity in ob/ob mice. *J Clin Invest,* 104**,** 1051-9.
HUANG, J., GARRETT, K. P., PELAYO, R., ZUNIGA-PFLUCKER, J. C., PETRIE, H. T. & KINCADE, P. W. 2005. Propensity of adult lymphoid progenitors to progress to DN2/3 stage thymocytes with Notch receptor ligation. *J Immunol,* 175**,** 4858-65.
JENKINSON, E. J., JENKINSON, W. E., ROSSI, S. W. & ANDERSON, G. 2006. The thymus and T-cell commitment: the right niche for Notch? *Nat Rev Immunol,* 6**,** 551-5.
JENKINSON, W. E., ROSSI, S. W., PARNELL, S. M., AGACE, W. W., TAKAHAMA, Y., JENKINSON, E. J. & ANDERSON, G. 2007a. Chemokine receptor expression defines heterogeneity in the earliest thymic migrants. *Eur J Immunol,* 37**,** 2090-6.

JENKINSON, W. E., ROSSI, S. W., PARNELL, S. M., JENKINSON, E. J. & ANDERSON, G. 2007b. PDGFRalpha-expressing mesenchyme regulates thymus growth and the availability of intrathymic niches. *Blood,* 109**,** 954-60.

KOHOUT, T. A., NICHOLAS, S. L., PERRY, S. J., REINHART, G., JUNGER, S. & STRUTHERS, R. S. 2004. Differential desensitization, receptor phosphorylation, beta-arrestin recruitment, and ERK1/2 activation by the two endogenous ligands for the CC chemokine receptor 7. *J Biol Chem,* 279**,** 23214-22.

KORN, T., BETTELLI, E., OUKKA, M. & KUCHROO, V. K. 2009. IL-17 and Th17 Cells. *Annu Rev Immunol,* 27**,** 485-517.

KRUEGER, A., WILLENZON, S., LYSZKIEWICZ, M., KREMMER, E. & FORSTER, R. 2010. CC chemokine receptor 7 and 9 double-deficient hematopoietic progenitors are severely impaired in seeding the adult thymus. *Blood,* 115**,** 1906-12.

KUMAR, H., KAWAI, T. & AKIRA, S. 2009. Toll-like receptors and innate immunity. *Biochem Biophys Res Commun,* 388**,** 621-5.

LAX, S., ROSS, E. A., WHITE, A., MARSHALL, J. L., JENKINSON, W. E., ISACKE, C. M., HUSO, D. L., CUNNINGHAM, A. F., ANDERSON, G. & BUCKLEY, C. D. 2012. CD248 expression on mesenchymal stromal cells is required for post-natal and infection-dependent thymus remodelling and regeneration. *FEBS Open Bio,* 2**,** 187-90.

LEE, J. S., FREVERT, C. W., WURFEL, M. M., PEIPER, S. C., WONG, V. A., BALLMAN, K. K., RUZINSKI, J. T., RHIM, J. S., MARTIN, T. R. & GOODMAN, R. B. 2003. Duffy antigen facilitates movement of chemokine across the endothelium in vitro and promotes neutrophil transmigration in vitro and in vivo. *J Immunol,* 170**,** 5244-51.

LEI, Y., RIPEN, A. M., ISHIMARU, N., OHIGASHI, I., NAGASAWA, T., JEKER, L. T., BOSL, M. R., HOLLANDER, G. A., HAYASHI, Y., MALEFYT RDE, W., NITTA, T. & TAKAHAMA, Y. 2011. Aire-dependent production of XCL1 mediates medullary accumulation of thymic dendritic cells and contributes to regulatory T cell development. *J Exp Med,* 208**,** 383-94.

LEPIQUE, A. P., PALENCIA, S., IRJALA, H. & PETRIE, H. T. 2003. Characterization of vascular adhesion molecules that may facilitate progenitor homing in the post-natal mouse thymus. *Clin Dev Immunol,* 10**,** 27-33.

LI, J., LI, Y., YAO, J. Y., JIN, R., ZHU, M. Z., QIAN, X. P., ZHANG, J., FU, Y. X., WU, L., ZHANG, Y. & CHEN, W. F. 2007. Developmental pathway of CD4+CD8- medullary thymocytes during mouse ontogeny and its defect in Aire-/- mice. *Proc Natl Acad Sci U S A,* 104**,** 18175-80.

LIND, E. F., PROCKOP, S. E., PORRITT, H. E. & PETRIE, H. T. 2001. Mapping precursor movement through the postnatal thymus reveals specific microenvironments supporting defined stages of early lymphoid development. *J Exp Med,* 194**,** 127-34.

LIU, C., SAITO, F., LIU, Z., LEI, Y., UEHARA, S., LOVE, P., LIPP, M., KONDO, S., MANLEY, N. & TAKAHAMA, Y. 2006. Coordination between CCR7- and CCR9-mediated chemokine signals in prevascular fetal thymus colonization. *Blood,* 108**,** 2531-9.

LOVE, P. E. & BHANDOOLA, A. 2011. Signal integration and crosstalk during thymocyte migration and emigration. *Nature Reviews Immunology,* 11**,** 469-477.

LUCHE, H., ARDOUIN, L., TEO, P., SEE, P., HENRI, S., MERAD, M., GINHOUX, F. & MALISSEN, B. 2011. The earliest intrathymic precursors of CD8alpha(+) thymic

dendritic cells correspond to myeloid-type double-negative 1c cells. *Eur J Immunol,* 41**,** 2165-75.
MATHIS, D. & BENOIST, C. 2009. Aire. *Annu Rev Immunol,* 27**,** 287-312.
MCKIMMIE, C. S., SINGH, M. D., HEWIT, K., LOPEZ-FRANCO, O., LE BROCQ, M., ROSE-JOHN, S., LEE, K. M., BAKER, A. H., WHEAT, R., BLACKBOURN, D. J., NIBBS, R. J. & GRAHAM, G. J. 2013. An analysis of the function and expression of D6 on lymphatic endothelial cells. *Blood,* 121**,** 3768-77.
MEDZHITOV, R. & JANEWAY, C., JR. 2000. Innate immune recognition: mechanisms and pathways. *Immunol Rev,* 173**,** 89-97.
MIKKOLA, H. K. & ORKIN, S. H. 2006. The journey of developing hematopoietic stem cells. *Development,* 133**,** 3733-44.
MILLARD, T. H., SHARP, S. J. & MACHESKY, L. M. 2004. Signalling to actin assembly via the WASP (Wiskott-Aldrich syndrome protein)-family proteins and the Arp2/3 complex. *Biochem J,* 380**,** 1-17.
MILLER, J. F. 1961. Immunological function of the thymus. *Lancet,* 2**,** 748-9.
MILLER, J. F. 1962. Effect of Neonatal Thymectomy on the Immunological Responsiveness of the Mouse. *Proc R Soc Lond B Biol Sci,* 156**,** 415-428.
MILLER, L. H., MASON, S. J., DVORAK, J. A., MCGINNISS, M. H. & ROTHMAN, I. K. 1975. Erythrocyte receptors for (Plasmodium knowlesi) malaria: Duffy blood group determinants. *Science,* 189**,** 561-3.
MISSLITZ, A., PABST, O., HINTZEN, G., OHL, L., KREMMER, E., PETRIE, H. T. & FORSTER, R. 2004. Thymic T cell development and progenitor localization depend on CCR7. *J Exp Med,* 200**,** 481-91.
MOMBAERTS, P., IACOMINI, J., JOHNSON, R. S., HERRUP, K., TONEGAWA, S. & PAPAIOANNOU, V. E. 1992. RAG-1-deficient mice have no mature B and T lymphocytes. *Cell,* 68**,** 869-77.
MORI, S., NAKANO, H., ARITOMI, K., WANG, C. R., GUNN, M. D. & KAKIUCHI, T. 2001. Mice lacking expression of the chemokines CCL21-ser and CCL19 (plt mice) demonstrate delayed but enhanced T cell immune responses. *J Exp Med,* 193**,** 207-18.
MULLER, S. M., STOLT, C. C., TERSZOWSKI, G., BLUM, C., AMAGAI, T., KESSARIS, N., IANNARELLI, P., RICHARDSON, W. D., WEGNER, M. & RODEWALD, H. R. 2008. Neural crest origin of perivascular mesenchyme in the adult thymus. *J Immunol,* 180**,** 5344-51.
MULLER, S. M., TERSZOWSKI, G., BLUM, C., HALLER, C., ANQUEZ, V., KUSCHERT, S., CARMELIET, P., AUGUSTIN, H. G. & RODEWALD, H. R. 2005. Gene targeting of VEGF-A in thymus epithelium disrupts thymus blood vessel architecture. *Proc Natl Acad Sci U S A,* 102**,** 10587-92.
NAGIRA, M., IMAI, T., HIESHIMA, K., KUSUDA, J., RIDANPAA, M., TAKAGI, S., NISHIMURA, M., KAKIZAKI, M., NOMIYAMA, H. & YOSHIE, O. 1997. Molecular cloning of a novel human CC chemokine secondary lymphoid-tissue chemokine that is a potent chemoattractant for lymphocytes and mapped to chromosome 9p13. *J Biol Chem,* 272**,** 19518-24.
NAKAGAWA, T., ROTH, W., WONG, P., NELSON, A., FARR, A., DEUSSING, J., VILLADANGOS, J. A., PLOEGH, H., PETERS, C. & RUDENSKY, A. Y. 1998. Cathepsin L: critical role in Ii degradation and CD4 T cell selection in the thymus. *Science,* 280**,** 450-3.

NEDJIC, J., AICHINGER, M., EMMERICH, J., MIZUSHIMA, N. & KLEIN, L. 2008. Autophagy in thymic epithelium shapes the T-cell repertoire and is essential for tolerance. *Nature,* 455**,** 396-400.

NEMAZEE, D. 2006. Receptor editing in lymphocyte development and central tolerance. *Nat Rev Immunol,* 6**,** 728-40.

NIBBS, R. J. & GRAHAM, G. J. 2013. Immune regulation by atypical chemokine receptors. *Nat Rev Immunol,* 13**,** 815-29.

NIBBS, R. J., WYLIE, S. M., PRAGNELL, I. B. & GRAHAM, G. J. 1997a. Cloning and characterization of a novel murine beta chemokine receptor, D6. Comparison to three other related macrophage inflammatory protein-1alpha receptors, CCR-1, CCR-3, and CCR-5. *J Biol Chem,* 272**,** 12495-504.

NIBBS, R. J., WYLIE, S. M., YANG, J., LANDAU, N. R. & GRAHAM, G. J. 1997b. Cloning and characterization of a novel promiscuous human beta-chemokine receptor D6. *J Biol Chem,* 272**,** 32078-83.

NITTA, T., MURATA, S., SASAKI, K., FUJII, H., RIPEN, A. M., ISHIMARU, N., KOYASU, S., TANAKA, K. & TAKAHAMA, Y. 2010. Thymoproteasome shapes immunocompetent repertoire of CD8+ T cells. *Immunity,* 32**,** 29-40.

ODAKA, C. 2009. Localization of mesenchymal cells in adult mouse thymus: their abnormal distribution in mice with disorganization of thymic medullary epithelium. *J Histochem Cytochem,* 57**,** 373-82.

OHIGASHI, I., ZUKLYS, S., SAKATA, M., MAYER, C. E., ZHANYBEKOVA, S., MURATA, S., TANAKA, K., HOLLANDER, G. A. & TAKAHAMA, Y. 2013. Aire-expressing thymic medullary epithelial cells originate from beta5t-expressing progenitor cells. *Proc Natl Acad Sci U S A,* 110**,** 9885-90.

OLDHAM, W. M. & HAMM, H. E. 2008. Heterotrimeric G protein activation by G-protein-coupled receptors. *Nat Rev Mol Cell Biol,* 9**,** 60-71.

PERERA, J., MENG, L., MENG, F. & HUANG, H. 2013. Autoreactive thymic B cells are efficient antigen-presenting cells of cognate self-antigens for T cell negative selection. *Proc Natl Acad Sci U S A,* 110**,** 17011-6.

PETRIE, H. T. & ZUNIGA-PFLUCKER, J. C. 2007. Zoned out: functional mapping of stromal signaling microenvironments in the thymus. *Annu Rev Immunol,* 25**,** 649-79.

PLOTKIN, J., PROCKOP, S. E., LEPIQUE, A. & PETRIE, H. T. 2003. Critical role for CXCR4 signaling in progenitor localization and T cell differentiation in the postnatal thymus. *J Immunol,* 171**,** 4521-7.

PORRITT, H. E., RUMFELT, L. L., TABRIZIFARD, S., SCHMITT, T. M., ZUNIGA-PFLUCKER, J. C. & PETRIE, H. T. 2004. Heterogeneity among DN1 prothymocytes reveals multiple progenitors with different capacities to generate T cell and non-T cell lineages. *Immunity,* 20**,** 735-45.

PRUENSTER, M., MUDDE, L., BOMBOSI, P., DIMITROVA, S., ZSAK, M., MIDDLETON, J., RICHMOND, A., GRAHAM, G. J., SEGERER, S., NIBBS, R. J. & ROT, A. 2009. The Duffy antigen receptor for chemokines transports chemokines and supports their promigratory activity. *Nat Immunol,* 10**,** 101-8.

RADTKE, F., MACDONALD, H. R. & TACCHINI-COTTIER, F. 2013. Regulation of innate and adaptive immunity by Notch. *Nat Rev Immunol,* 13**,** 427-37.

RADTKE, F., WILSON, A., STARK, G., BAUER, M., VAN MEERWIJK, J., MACDONALD, H. R. & AGUET, M. 1999. Deficient T cell fate specification in mice with an induced inactivation of Notch1. *Immunity,* 10**,** 547-58.

REHM, A., ANAGNOSTOPOULOS, I., GERLACH, K., BROEMER, M., SCHEIDEREIT, C., JOHRENS, K., HUBLER, M., HETZER, R., STEIN, H., LIPP, M., DORKEN, B. & HOPKEN, U. E. 2009. Identification of a chemokine receptor profile characteristic for mediastinal large B-cell lymphoma. *Int J Cancer,* 125**,** 2367-74.

REIF, K., OKKENHAUG, K., SASAKI, T., PENNINGER, J. M., VANHAESEBROECK, B. & CYSTER, J. G. 2004. Cutting edge: differential roles for phosphoinositide 3-kinases, p110gamma and p110delta, in lymphocyte chemotaxis and homing. *J Immunol,* 173**,** 2236-40.

RIBEIRO, A. R., MEIRELES, C., RODRIGUES, P. M. & ALVES, N. L. 2014. The intermediate expression of CCRL1 reveals novel subpopulations of medullary thymic epithelial cells that emerge in the postnatal thymus. *Eur J Immunol*.

RIBEIRO, A. R., RODRIGUES, P. M., MEIRELES, C., DI SANTO, J. P. & ALVES, N. L. 2013. Thymocyte Selection Regulates the Homeostasis of IL-7-Expressing Thymic Cortical Epithelial Cells In Vivo. *Journal of Immunology,* 191**,** 1200-1209.

RODE, I. & BOEHM, T. 2012. Regenerative capacity of adult cortical thymic epithelial cells. *Proc Natl Acad Sci U S A,* 109**,** 3463-8.

ROLINK, A. G., MASSA, S., BALCIUNAITE, G. & CEREDIG, R. 2006. Early lymphocyte development in bone marrow and thymus. *Swiss Med Wkly,* 136**,** 679-83.

ROLINK, A. G., MASSA, S., BALCIUNAITE, G. & CEREDIG, R. 2007. Early lymphocyte development in bone marrow and thymus. *Swiss Med Wkly,* 137 Suppl 155**,** 20S-24S.

ROSS, E. A., COUGHLAN, R. E., FLORES-LANGARICA, A., LAX, S., NICHOLSON, J., DESANTI, G. E., MARSHALL, J. L., BOBAT, S., HITCHCOCK, J., WHITE, A., JENKINSON, W. E., KHAN, M., HENDERSON, I. R., LAVERY, G. G., BUCKLEY, C. D., ANDERSON, G. & CUNNINGHAM, A. F. 2012. Thymic function is maintained during Salmonella-induced atrophy and recovery. *J Immunol,* 189**,** 4266-74.

ROSSI, D. & ZLOTNIK, A. 2000. The biology of chemokines and their receptors. *Annu Rev Immunol,* 18**,** 217-42.

ROSSI, S. W., JENKINSON, W. E., ANDERSON, G. & JENKINSON, E. J. 2006. Clonal analysis reveals a common progenitor for thymic cortical and medullary epithelium. *Nature,* 441**,** 988-91.

ROT, A. 1992. Endothelial cell binding of NAP-1/IL-8: role in neutrophil emigration. *Immunol Today,* 13**,** 291-4.

SANCHEZ-MARTIN, L., SANCHEZ-MATEOS, P. & CABANAS, C. 2013. CXCR7 impact on CXCL12 biology and disease. *Trends Mol Med,* 19**,** 12-22.

SCHUMANN, K., LAMMERMANN, T., BRUCKNER, M., LEGLER, D. F., POLLEUX, J., SPATZ, J. P., SCHULER, G., FORSTER, R., LUTZ, M. B., SOROKIN, L. & SIXT, M. 2010. Immobilized chemokine fields and soluble chemokine gradients cooperatively shape migration patterns of dendritic cells. *Immunity,* 32**,** 703-13.

SCHWARZ, K., GAUSS, G. H., LUDWIG, L., PANNICKE, U., LI, Z., LINDNER, D., FRIEDRICH, W., SEGER, R. A., HANSEN-HAGGE, T. E., DESIDERIO, S., LIEBER, M. R. & BARTRAM, C. R. 1996. RAG mutations in human B cell-negative SCID. *Science,* 274**,** 97-9.

SCHWEICKART, V. L., EPP, A., RAPORT, C. J. & GRAY, P. W. 2000. CCR11 is a functional receptor for the monocyte chemoattractant protein family of chemokines. *J Biol Chem,* 275**,** 9550-6.
SCIMONE, M. L., AIFANTIS, I., APOSTOLOU, I., VON BOEHMER, H. & VON ANDRIAN, U. H. 2006. A multistep adhesion cascade for lymphoid progenitor cell homing to the thymus. *Proc Natl Acad Sci U S A,* 103**,** 7006-11.
SCOLLAY, R. & GODFREY, D. I. 1995. Thymic emigration: conveyor belts or lucky dips? *Immunol Today,* 16**,** 268-73; discussion 273-4.
SERWOLD, T., EHRLICH, L. I. & WEISSMAN, I. L. 2009. Reductive isolation from bone marrow and blood implicates common lymphoid progenitors as the major source of thymopoiesis. *Blood,* 113**,** 807-15.
SHEN, H. Q., LU, M., IKAWA, T., MASUDA, K., OHMURA, K., MINATO, N., KATSURA, Y. & KAWAMOTO, H. 2003. T/NK bipotent progenitors in the thymus retain the potential to generate dendritic cells. *J Immunol,* 171**,** 3401-6.
SHITARA, S., HARA, T., LIANG, B., WAGATSUMA, K., ZUKLYS, S., HOLLANDER, G. A., NAKASE, H., CHIBA, T., TANI-ICHI, S. & IKUTA, K. 2013. IL-7 produced by thymic epithelial cells plays a major role in the development of thymocytes and TCRgammadelta+ intraepithelial lymphocytes. *J Immunol,* 190**,** 6173-9.
SITNIK, K. M., KOTARSKY, K., WHITE, A. J., JENKINSON, W. E., ANDERSON, G. & AGACE, W. W. 2012. Mesenchymal cells regulate retinoic acid receptor-dependent cortical thymic epithelial cell homeostasis. *J Immunol,* 188**,** 4801-9.
STEIN, J. V., ROT, A., LUO, Y., NARASIMHASWAMY, M., NAKANO, H., GUNN, M. D., MATSUZAWA, A., QUACKENBUSH, E. J., DORF, M. E. & VON ANDRIAN, U. H. 2000. The CC chemokine thymus-derived chemotactic agent 4 (TCA-4, secondary lymphoid tissue chemokine, 6Ckine, exodus-2) triggers lymphocyte function-associated antigen 1-mediated arrest of rolling T lymphocytes in peripheral lymph node high endothelial venules. *J Exp Med,* 191**,** 61-76.
TAGHON, T., YUI, M. A. & ROTHENBERG, E. V. 2007. Mast cell lineage diversion of T lineage precursors by the essential T cell transcription factor GATA-3. *Nat Immunol,* 8**,** 845-55.
TAKAHAMA, Y. 2006. Journey through the thymus: stromal guides for T-cell development and selection. *Nat Rev Immunol,* 6**,** 127-35.
TAKAMATSU, H., OKUNO, T. & KUMANOGOH, A. 2010. Regulation of immune cell responses by semaphorins and their receptors. *Cell Mol Immunol,* 7**,** 83-8.
TAKATSUKA, S., SEKIGUCHI, A., TOKUNAGA, M., FUJIMOTO, A. & CHIBA, J. 2011. Generation of a panel of monoclonal antibodies against atypical chemokine receptor CCX-CKR by DNA immunization. *J Pharmacol Toxicol Methods,* 63**,** 250-7.
TANAKA, Y., ADAMS, D. H. & SHAW, S. 1993a. Proteoglycans on endothelial cells present adhesion-inducing cytokines to leukocytes. *Immunol Today,* 14**,** 111-5.
TANAKA, Y., MAMALAKI, C., STOCKINGER, B. & KIOUSSIS, D. 1993b. In vitro negative selection of alpha beta T cell receptor transgenic thymocytes by conditionally immortalized thymic cortical epithelial cell lines and dendritic cells. *Eur J Immunol,* 23**,** 2614-21.
TANG, Q. & BLUESTONE, J. A. 2008. The Foxp3+ regulatory T cell: a jack of all trades, master of regulation. *Nat Immunol,* 9**,** 239-44.

THORNTON, A. M. & SHEVACH, E. M. 2000. Suppressor effector function of CD4+CD25+ immunoregulatory T cells is antigen nonspecific. *J Immunol,* 164**,** 183-90.
TOURNAMILLE, C., COLIN, Y., CARTRON, J. P. & LE VAN KIM, C. 1995. Disruption of a GATA motif in the Duffy gene promoter abolishes erythroid gene expression in Duffy-negative individuals. *Nat Genet,* 10**,** 224-8.
TOURNAMILLE, C., LE VAN KIM, C., GANE, P., BLANCHARD, D., PROUDFOOT, A. E., CARTRON, J. P. & COLIN, Y. 1997. Close association of the first and fourth extracellular domains of the Duffy antigen/receptor for chemokines by a disulfide bond is required for ligand binding. *J Biol Chem,* 272**,** 16274-80.
TOWNSON, J. R. & NIBBS, R. J. 2002. Characterization of mouse CCX-CKR, a receptor for the lymphocyte-attracting chemokines TECK/mCCL25, SLC/mCCL21 and MIP-3beta/mCCL19: comparison to human CCX-CKR. *Eur J Immunol,* 32**,** 1230-41.
TURNER, S. J., DOHERTY, P. C., MCCLUSKEY, J. & ROSSJOHN, J. 2006. Structural determinants of T-cell receptor bias in immunity. *Nat Rev Immunol,* 6**,** 883-94.
UENO, T., HARA, K., WILLIS, M. S., MALIN, M. A., HOPKEN, U. E., GRAY, D. H., MATSUSHIMA, K., LIPP, M., SPRINGER, T. A., BOYD, R. L., YOSHIE, O. & TAKAHAMA, Y. 2002. Role for CCR7 ligands in the emigration of newly generated T lymphocytes from the neonatal thymus. *Immunity,* 16**,** 205-18.
UENO, T., SAITO, F., GRAY, D. H., KUSE, S., HIESHIMA, K., NAKANO, H., KAKIUCHI, T., LIPP, M., BOYD, R. L. & TAKAHAMA, Y. 2004. CCR7 signals are essential for cortex-medulla migration of developing thymocytes. *J Exp Med,* 200**,** 493-505.
ULVMAR, M. H., HUB, E. & ROT, A. 2011. Atypical chemokine receptors. *Exp Cell Res,* 317**,** 556-68.
ULVMAR, M. H., WERTH, K., BRAUN, A., KELAY, P., HUB, E., ELLER, K., CHAN, L., LUCAS, B., NOVITZKY-BASSO, I., NAKAMURA, K., RULICKE, T., NIBBS, R. J., WORBS, T., FORSTER, R. & ROT, A. 2014. The atypical chemokine receptor CCRL1 shapes functional CCL21 gradients in lymph nodes. *Nat Immunol*.
VINET, J., VAN ZWAM, M., DIJKSTRA, I. M., BROUWER, N., VAN WEERING, H. R., WATTS, A., MEIJER, M., FOKKENS, M. R., KANNAN, V., VERZIJL, D., VISCHER, H. F., SMIT, M. J., LEURS, R., BIBER, K. & BODDEKE, H. W. 2013. Inhibition of CXCR3-mediated chemotaxis by the human chemokine receptor-like protein CCX-CKR. *Br J Pharmacol,* 168**,** 1375-87.
VIRET, C., LAMARE, C., GUIRAUD, M., FAZILLEAU, N., BOUR, A., MALISSEN, B., CARRIER, A. & GUERDER, S. 2011. Thymus-specific serine protease contributes to the diversification of the functional endogenous CD4 T cell receptor repertoire. *J Exp Med,* 208**,** 3-11.
WALTERS, S. N., WEBSTER, K. E., DALEY, S. & GREY, S. T. 2014. A Role for Intrathymic B Cells in the Generation of Natural Regulatory T Cells. *J Immunol*.
WARD, S. G. 2006. T lymphocytes on the move: chemokines, PI 3-kinase and beyond. *Trends Immunol,* 27**,** 80-7.
WATANABE, K., PENFOLD, M. E., MATSUDA, A., OHYANAGI, N., KANEKO, K., MIYABE, Y., MATSUMOTO, K., SCHALL, T. J., MIYASAKA, N. & NANKI, T. 2010. Pathogenic role of CXCR7 in rheumatoid arthritis. *Arthritis Rheum,* 62**,** 3211-20.
WATANABE, N., WANG, Y. H., LEE, H. K., ITO, T., WANG, Y. H., CAO, W. & LIU, Y. J. 2005. Hassall's corpuscles instruct dendritic cells to induce CD4+CD25+ regulatory T cells in human thymus. *Nature,* 436**,** 1181-5.

WATTS, A. O., VERKAAR, F., VAN DER LEE, M. M., TIMMERMAN, C. A., KUIJER, M., VAN OFFENBEEK, J., VAN LITH, L. H., SMIT, M. J., LEURS, R., ZAMAN, G. J. & VISCHER, H. F. 2013. beta-Arrestin recruitment and G protein signaling by the atypical human chemokine decoy receptor CCX-CKR. *J Biol Chem,* 288**,** 7169-81.

WEINREICH, M. A. & HOGQUIST, K. A. 2008. Thymic emigration: when and how T cells leave home. *J Immunol,* 181**,** 2265-70.

WHITE, A. J., JENKINSON, W. E., COWAN, J. E., PARNELL, S. M., BACON, A., JONES, N. D., JENKINSON, E. J. & ANDERSON, G. 2014. An essential role for medullary thymic epithelial cells during the intrathymic development of invariant NKT cells. *J Immunol,* 192**,** 2659-66.

WHITEHEAD, G. S., WANG, T., DEGRAFF, L. M., CARD, J. W., LIRA, S. A., GRAHAM, G. J. & COOK, D. N. 2007. The chemokine receptor D6 has opposing effects on allergic inflammation and airway reactivity. *Am J Respir Crit Care Med,* 175**,** 243-9.

YANG, H., YOUM, Y. H. & DIXIT, V. D. 2009. Inhibition of thymic adipogenesis by caloric restriction is coupled with reduction in age-related thymic involution. *J Immunol,* 183**,** 3040-52.

ZACHARIAH, M. A. & CYSTER, J. G. 2010. Neural crest-derived pericytes promote egress of mature thymocytes at the corticomedullary junction. *Science,* 328**,** 1129-35.

ZENG, X. H., OU, Z. L., YU, K. D., FENG, L. Y., YIN, W. J., LI, J., SHEN, Z. Z. & SHAO, Z. M. 2011. Coexpression of atypical chemokine binders (ACBs) in breast cancer predicts better outcomes. *Breast Cancer Res Treat,* 125**,** 715-27.

ZHANG, N. & BEVAN, M. J. 2011. CD8(+) T cells: foot soldiers of the immune system. *Immunity,* 35**,** 161-8.

ZHAO, Y., MANGALMURTI, N. S., XIONG, Z., PRAKASH, B., GUO, F., STOLZ, D. B. & LEE, J. S. 2011. Duffy antigen receptor for chemokines mediates chemokine endocytosis through a macropinocytosis-like process in endothelial cells. *PLoS One,* 6**,** e29624.

ZHOU, L., CHONG, M. M. & LITTMAN, D. R. 2009. Plasticity of CD4+ T cell lineage differentiation. *Immunity,* 30**,** 646-55.

ZHU, Z., SUN, Z., WANG, Z., GUO, P., ZHENG, X. & XU, H. 2013. Prognostic impact of atypical chemokine receptor expression in patients with gastric cancer. *J Surg Res,* 183**,** 177-83.

ZLOTOFF, D. A., SAMBANDAM, A., LOGAN, T. D., BELL, J. J., SCHWARZ, B. A. & BHANDOOLA, A. 2010. CCR7 and CCR9 together recruit hematopoietic progenitors to the adult thymus. *Blood,* 115**,** 1897-905.

APPENIX

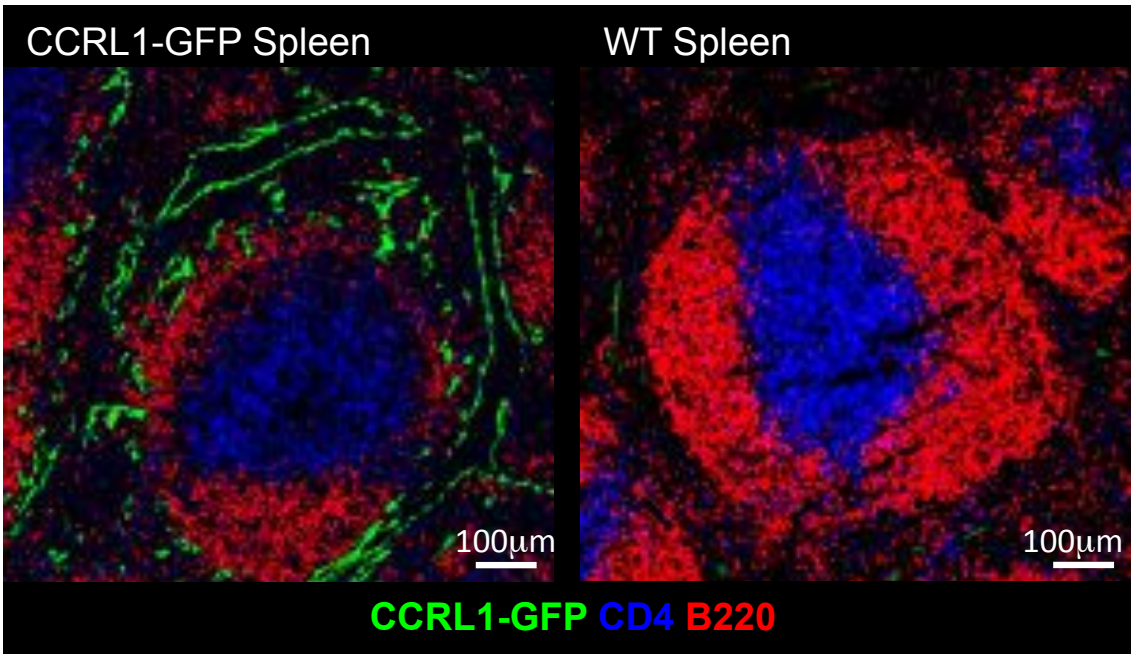

Figure 71. CCRL1 Expression Within the Spleen.

Adult CCRL1-GFP and WT spleen were fixed in 4% PFA and then frozen. Cryosections were stained for CD4 and B220. CCRL1-GFP expression (green) is readily observed by cells at the marginal zone. No GFP^+ cells are detected in the WT spleen.